

UC San Diego

UC San Diego Electronic Theses and Dissertations

Title

Design and optimization of polymeric silole and boronate photoluminescent probes for improved explosives detection applications

Permalink

<https://escholarship.org/uc/item/1h44z419>

Author

Sanchez, Jason C.

Publication Date

2008

Peer reviewed|Thesis/dissertation

UNIVERSITY OF CALIFORNIA, SAN DIEGO

**Design and Optimization of Polymeric Silole and Boronate Photoluminescent
Probes for Improved Explosives Detection Applications**

A Dissertation submitted in partial satisfaction of the requirements for the degree
Doctor of Philosophy

in

Chemistry

by

Jason C. Sanchez

Committee in charge:

Professor William C. Trogler, Chair
Professor Seth Cohen
Professor David Hendrickson
Professor Andrew Kummel
Professor Yuhwa Lo

2008

Copyright©

Jason C. Sanchez, 2008

All rights reserved

The dissertation of Jason C. Sanchez is approved, and it is acceptable in quality and form for publication on microfilm.

Chair

University of California, San Diego

2008

DEDICATION

For my wife Erin who brings true happiness to my life and is a constant reminder of how lucky I really am. For our baby boy that she carries inside her, no need for self-motivation now!

For my parents who continue to make life easy for us and set a positive example for our family. For my sisters who find a way everyday to make me a proud brother.

For my grandparents who give more than they have, take less than they should, and understand the meaning family.

TABLE OF CONTENTS

Signature Page.....	iii
Dedication.....	iv
Table of Contents.....	v
List of Symbols and Abbreviations.....	xiii
List of Figures.....	xviii
List of Schemes.....	xxv
List of Tables.....	xxii
Acknowledgements.....	xxx
Vita, publications, and patents.....	xxxiii
Abstract of the Dissertation.....	xxxvi
Chapter I Review of Polycarbosilanes, Catalytic Hydrosilylation, and Current Explosives Detection Applications.....	1
1.1 Polycarbosilanes.....	2
1.1.1 Electronic Properties of Silicon.....	2
1.1.2 Synthesis of Polycarbosilanes.....	3
1.1.3 Electronic Delocalization in Polycarbosilanes.....	5
1.2 Hydrosilylation Catalysts and Mechanisms.....	5
1.3 Poly(silyl-vinylene)s.....	11
1.3.1 Optimization of Reaction Conditions.....	11
1.3.2 Photoactive Polymers.....	14

1.3.3 Catalyst Modification.....	14
1.3.4 Applications.....	17
1.4 Polysiloles.....	18
1.4.1 Introduction to Siloles.....	18
1.4.2 Polymerization Methods.....	19
1.5 Explosives Detection Using Luminescent Sensors.....	20
1.5.1 Targeted Explosive Analytes.....	20
1.5.2 Improving Sensor Properties.....	22
1.5.2.1 Particle Sampling.....	24
1.5.3 Luminescent Polymer Sensors.....	25
1.6 Objectives of the Dissertation.....	28
1.7 Acknowledgements.....	31
1.8 References.....	32
 Chapter II Synthesis, Characterization, and Evaluation 1,1-Tetraphenylsilole- and 1,1-Silafluorene-vinylene Polymers for Explosives Detection.....	 41
2.1 Abstract.....	42
2.2 Introduction.....	44
2.3 Results and Discussion.....	48
2.3.1 Model Compounds.....	48
2.3.2 Polymerizations.....	52
2.3.3 Photoluminescence.....	54
2.3.3.1 Solution-phase Photoluminescence.....	54

2.3.3.2 Solid-state Photoluminescence.....	56
2.3.3.3 Solution-phase Quantum Efficiencies of Fluorescence.....	59
2.3.4 Explosives Detection by Fluorescence Quenching.....	60
2.3.4.1 Solution-phase Stern–Volmer Analysis.....	60
2.3.4.2 Probing Explosive Analyte Binding by ²⁹ Si NMR.....	62
2.3.4.3 Surface Detection of Explosive Particulates.....	74
2.3.4.4 Theoretical Calculations.....	78
2.3.4.5 Detection Interferents.....	81
2.4 Conclusions.....	82
2.5 Experimental.....	83
2.5.1 General Synthetic Techniques.....	83
2.5.2 ²⁹ Si NMR Data.....	84
2.5.3 X-ray Crystal Structure Determination.....	85
2.5.4 Theoretical Methods.....	86
2.5.5 Solid-state Explosives Detection.....	87
2.5.6 Synthesis of 1,1-diethynylsilafluorene (DESF).....	88
2.5.7 Synthesis of Methyl(tetraphenyl)silole-vinylene Trimer.....	89
2.5.8 Synthesis of Methyl(tetraphenyl)silole-silafluorene-vinylene Cotrimer.....	89
2.5.9 Synthesis of Methylsilafluorene-vinylene Trimer.....	90
2.5.10 Synthesis of Poly(tetraphenyl)silole-vinylene.....	90
2.5.11 Synthesis of Poly(tetraphenyl)silole-silafluorene-vinylene.....	91
2.5.12 Synthesis of Poly(silafluorene-vinylene).....	91

2.5.13 Synthesis of 1-methyl-1-vinyl(tetraphenyl)silole.....	92
2.5.14 Synthesis of 1-methyl-1-vinylsilafuorene.....	92
2.6 Acknowledgements.....	94
2.7 Appendix.....	95
2.8 References.....	99
Chapter III Divinylbenzene Bridged Silole and Silafuorene Polymers. Improved Applications to Surface Imaging of Explosive Particulates.....	105
3.1 Abstract.....	106
3.2 Introduction.....	107
3.3 Results and Discussion.....	111
3.3.1 Model Compounds.....	111
3.3.2 Catalyst Optimization and Polymerization.....	117
3.3.3 Photoluminescence.....	119
3.3.3.1 Solution-phase Photoluminescence and Quantum Efficiencies.....	119
3.3.3.2 Solid-state Photoluminescence.....	122
3.3.4 Explosives Detection by Fluorescence Quenching.....	124
3.3.4.1 Surface Detection of Explosive Particulates.....	124
3.3.4.2 Solid-state Stern–Volmer Analysis.....	129
3.3.4.3 Detection Interferents.....	132
3.4 Conclusions.....	133
3.5 Experimental.....	133
3.5.1 General Synthetic Techniques.....	133
3.5.2 X-ray Crystal Structure Determination.....	134

3.5.3 Synthesis of 1-methyl-1- <i>trans</i> (2-trimethylsilyl)ethenyl-2,3,4,5-(tetraphenyl)silole.....	135
3.5.4 Synthesis of 1,4-di(1-methyl-1- <i>trans</i> -ethenyl-2,3,4,5-(tetraphenyl)silole)benzene.....	136
3.5.5 Synthesis of 1,4-di(1-methyl-1- <i>trans</i> -ethenyl-silafluorene)benzene.....	136
3.5.6 Synthesis of Poly((tetraphenyl)silole-phenylenedivinylene).....	137
3.5.7 Synthesis of Poly(silafluorene-phenylenedivinylene).....	138
3.5.8 Synthesis of 1,1-dihydrido-4,5,8,9-bis(triptycene)silafluorene.....	138
3.6 Acknowledgements.....	140
3.7 Appendix.....	141
3.8 References.....	142
 Chapter IV Efficient Blue Emitting Silafluorene-fluorene Conjugated Copolymers for Increased Explosives Detection Sensitivity.....	 146
4.1 Abstract.....	147
4.2 Introduction.....	148
4.3 Results and Discussion.....	152
4.3.1 Synthesis and Structural Characterization.....	152
4.3.2 Photophysical Properties.....	154
4.3.3 Explosives Detection.....	160
4.4 Conclusions.....	174
4.5 Experimental.....	175
4.5.1 General Synthetic Techniques.....	175
4.5.2 Solid-state Explosives Detection.....	176

4.5.3 Synthesis of 2,7-di(1-methyl-1- <i>trans</i> -ethenyl-silafluorene)- 9 <i>H</i> -fluorene.....	178
4.5.4 Synthesis of 2,7-di(1-methyl-1- <i>trans</i> -ethenyl-silafluorene)-9,9- dimethyl-9 <i>H</i> -fluorene.....	179
4.5.5 Synthesis of 2,7-di(1-methyl-1- <i>trans</i> -ethenyl-silafluorene)-9,9'- spirobifluorene.....	179
4.5.6 Synthesis of Poly(silafluorene-(9 <i>H</i> -fluorene)divinylene).....	180
4.5.7 Synthesis of Poly(silafluorene-(9,9-dimethyl-9 <i>H</i> -fluorene)divinylene).....	181
4.5.8 Synthesis of Poly(silafluorene-(9,9'-spirobifluorene)divinylene).....	181
4.6 Acknowledgements.....	183
4.7 References.....	184
Chapter V Selective Detection of Explosives Using a “Turn-on” Fluorescence Mechanism.....	
5.1 Abstract.....	189
5.2 Introduction.....	191
5.3 Results and Discussion.....	196
5.3.1 Detection of Nitramine and Nitrate Esters.....	196
5.3.1.1 Two-step Detection System.....	196
5.3.1.2 Three-step Tandem Sensor.....	200
5.3.2 Single Step Selective Detection of Nitrate Esters.....	206
5.3.2.1 Model Compound.....	206
5.3.2.2 Explosives Detection.....	208
5.3.2.3 Mechanism of Turn-on Fluorescence Response.....	212
5.4 Conclusions.....	219

5.5 Experimental.....	220
5.5.1 General Synthetic Techniques.....	220
5.5.2 Methods and Reagents.....	221
5.5.3 Solid-state Explosives Detection.....	222
5.5.3.1 Turn-on Fluorescence Detection with 2,3-diaminonaphthalene.....	222
5.5.3.2 Turn-on Fluorescence Detection with PSF1.....	223
5.5.4 Synthesis of 2,7-di(1-methyl-1- <i>trans</i> -ethenyl-silafluorene)fluorenone.....	225
5.6 Acknowledgements.....	226
5.7 References.....	227
Chapter VI Synthesis of Polyfluoran for the Detection of Vapor Phase Hydrogen Peroxide. Application as a Turn-on Fluorescence Sensor for Organic Peroxide Explosives.....	230
6.1 Abstract.....	231
6.2 Introduction.....	232
6.3 Results and Discussion.....	236
6.3.1 Synthesis and Characterization.....	236
6.3.2 Detection of Hydrogen Peroxide.....	239
6.4 Conclusions.....	251
6.5 Experimental.....	252
6.5.1 General Synthetic Techniques.....	252
6.5.2 Periodic Acid Test for Cis-diols.....	253
6.5.3 Peroxide Detection.....	253
6.5.4 Synthesis of 3,9-dip-tolyl-2,4,8,10-tetraoxa-3,9-diboraspiro	

[5.5]undecane.....	254
6.5.5 Synthesis of Poly-3□,6□-bis(1,3,2- dioxaborinane)fluoran.....	255
6.6 Acknowledgements.....	256
6.7 Appendix.....	257
6.8 References.....	260
Chapter VII Dissertation Summary, Conclusions, and Proposed Future Work.....	263
7.1 Summary of Hydrosilylation Polymerization.....	264
7.2 Summary of Explosives Detection.....	268
7.3 Conclusions.....	270
7.4 Future Work.....	271

LIST OF SYMBOLS AND ABBREVIATIONS

Å	Ångström	cm ⁻¹	wavenumber
[A]	Analyte concentration	cm ⁻²	per centimeter squared
ACE	acetone	cm ⁻³	per centimeter cubed
ACN	acetonitrile	°	degree
AFM	Atomic Force Microscopy	Δ	delta, heat, or change
AgIO ₃	silver iodate	δ	chemical shift; ppm
AIBN	2,2'-Azobisisobutyronitrile	CL-20	2,4,6,8,10,12-hexanitro- 2,4,6,8,10,12- hexaazaisowurtzitane
AIE	aggregated induced emission	C-4	plastic explosive composition using RDX as its main explosive component
AN	ammonium nitrate		
AgNO ₃	silver nitrate		
a.u.	arbitrary units	D	diameter
br	broad	d	doublet or days
BQ	benzoquinone	DAN	2,3-diaminonaphthalene
C	carbon	DC peroxide	dicumyl peroxide
°C	degree Celsius	dd	doublet of doublets
calcd	calculated	DDNP	diazodinitrophenol
CCDC	Cambridge Crystallographic Data Centre	DEB	diethynylbenzene
CDCl ₃	deuterated chloroform	Δ	delta
cm	centimeter	decomp	decomposition

DFT	density functional theory	GPC	gel permeation chromatography
DMSO	dimethylsulfoxide	h	hour
DNB	dinitrobenzene	H	hydrogen
DNT	dinitrotoluene	H ₂ O	water
e ⁻	electron	H ₂ O ₂	hydrogen peroxide
ε	molar extinction coefficient; M ⁻¹ cm ⁻¹	H ₂ PtCl ₆	chloroplatinic acid
ε _{max}	molar extinction coefficient at wavelength of maximum absorption; M ⁻¹ cm ⁻¹	HMTD	hexamethylene triperoxide diamine
η	viscosity (cP)	HMX	cyclotetramethylene-tetranitramine
EGDN	dinitroethylene glycol	HOMO	highest occupied molecular orbital
EPA	Environmental Protection Agency	Hz	hertz, s ⁻¹
eq	equivalents	I	fluorescence intensity
EtOH	ethanol	I ₀	initial fluorescence intensity
Et ₂ O	diethyl ether	IED	improvised explosive device
eV	Electron-Volt (1 eV = 1.6·10 ⁻¹⁹ Joules)	IMS	ion mobility spectrometry, ion mobility spectrometer
Φ	fluorescence quantum yield	∞	infinity
Φ _{rel}	relative fluorescence quantum yield	INEPT	insensitive nuclei enhanced by polarization transfer
fg	femtogram	IR	infrared (spectroscopy or radiation)
g	gram	J	coupling constant; Hz
		k	reaction rate constant; s ⁻¹

K	Kelvin	m	multiplet
K_a	association constant	m^3	cubic meter
K_{SV}	Stern-Volmer constant	MCL	maximum contaminant level
kHz	kilohertz	MeOH	methanol
kJ	kilojoules	mg	milligram
KOH	potassium hydroxide	μg	microgram
λ	wavelength, lambda	μs	microsecond
λ_{abs}	wavelength of absorption, lambda	MHz	megahertz
λ_{em}	wavelength of emission, lambda	min	minutes
λ_{ex}	wavelength of excitation, lambda	MIP	molecularly imprinted polymer
λ_{flu}	wavelength of fluorescence, lambda	μL	microliter
L	liter	mL	milliliter
LED	light emitting diode	μm	micrometer
ln	natural log	μM	micromolar
LUMO	lowest unoccupied molecular orbital	mM	millimolar
M	molar; mol L^{-1}	μmol	micromole
M_w	weight-averaged molecular weight	mmol	millimole
M_N	number-averaged molecular weight	mol	mole, $6.022 \cdot 10^{23}$
		MP	melting point
		ms	millisecond
		n	degree of polymerization

NaOH	sodium hydroxide	ppb	parts per billion
NB	nitrobenzene	PPE	poly(<i>p</i> -phenylenethynylene)
ng	nanogram	ppm	parts per million
nm	nanometer	PN	potassium nitrate
NM	nitromethane	ppt	parts per trillion
NMR	nuclear magnetic resonance	ppth	parts per thousand
ns	nanosecond	PPV	poly(<i>p</i> -phenylenevinylene)
OLED	organic light emitting diode	P_{vap}	vapor pressure (Torr)
ONC	octanitrocubane	[Q]	concentration of quencher
OSHA	Occupational Safety and Health Administration	R^2	coefficient of determination
PA	picric acid	RDX	cyclotrimethylene trinitramine
PDI	polydispersity index	ROS	reactive oxygen species
π	pi; bond or orbital	rt	room temperature
π^*	pi-star; anti-bonding π orbital	ρ	density (g cm^{-3})
PETN	pentaerythritol tetranitrate	σ	sigma; bond or orbital
pg	picogram	σ^*	sigma-star; anti-bonding σ orbital
pH	$\text{pH} = -\log[\text{H}^+]$	s	singlet or seconds
Ph	phenyl	Si	silicon
PL	photoluminescence	SN	sodium nitrate
PLED	polymer light emitting diode	SOMO	singly occupied molecular orbital
		spnmr	single pulse delay NMR

t	time
T	Tesla
T ₁	spin-lattice relaxation time
TATB	1,3,5-triamino-2,4,6-trinitrobenzene
TATP	triacetone triperoxide
Tetryl	2,4,6-trinitrophenyl-N-methylnitramine
THF	tetrahydrofuran
TLC	thin-line chromatography
TMS	trimethylsilyl or trimethylsilane
TNB	trinitrobenzene
TNG	trinitroglycerin
TNT	trinitrotoluene
TTT	tris-(trinitromethyl)triazine
UV	ultra-violet
UV-A	ultra-violet (254 nm)
UV-B	ultra-violet (302 nm)
UV-C	ultra-violet (360 nm)
UV-vis	ultra-violet – visible radiation
ν	wave number, cm ⁻¹
w:v	weight:volume; g solute per 100 mL solvent

LIST OF FIGURES

Chapter I

Figure 1-1.	Backbone structure for silane and carbosilane polymers.....	4
Figure 1-2.	Possible stereo-isomers produced by the hydrosilylation of alkynes.....	6
Figure 1-3.	A modified Chalk-Harrod mechanism for hydrosilylation.....	7
Figure 1-4.	Mechanism for group 9 metal catalyzed hydrosilylation. Proposed intermediates for <i>cis-trans</i> isomerization.....	8
Figure 1-5.	Ruthenium catalyzed hydrosilylation of primary silanes featuring a silylene intermediate.....	9
Figure 1-6.	Early transition metal metallocene hydrosilylation mechanism including a slow σ -bond metathesis.....	10
Figure 1-7.	Structure of a silylene-spaced vinylarene dendritic fluorescent dye.....	16
Figure 1-8.	Chemical structure of metallacyclopentadiene core units.....	17
Figure 1-9.	Synthesis of 1,1-polymetalloles.....	18
Figure 1-10.	Comparison between the internal bond angles of secondary silole and silane monomers.....	19
Figure 1-11.	Chemical structure and classification of common targeted explosive analytes.....	21
Figure 1-12.	Conjugated fluorescent polymers for explosives detection.....	26

Chapter II

Figure 2-1.	Conjugated fluorescent polymers for explosives detection.....	45
Figure 2-2.	^1H NMR spectrum of methylsilafluorene-vinylene trimer.....	50

Figure 2-3.	Thermal ellipsoid plot of methyl(tetraphenyl)silole-vinylene trimer....	51
Figure 2-4.	Chemical structures of (tetraphenyl)silole- and silafluorene-vinylene polymers.....	52
Figure 2-5.	Structural comparison of silole polymers.....	54
Figure 2-6.	UV-vis and fluorescence spectra of model trimers compared with polymers.....	56
Figure 2-7.	Depiction of the orbital overlap between the vinylene bridge and LUMO of the silacyclopentadiene ring.....	57
Figure 2-8.	Solid-state photoluminescence data for polymers.....	58
Figure 2-9.	Structures of common high explosives categorized by functional group class.....	60
Figure 2-10.	^{29}Si NMR of methylsilafluorene-vinylene trimer.....	64
Figure 2-11.	^{29}Si NMR chemical shifts for the outer Si atoms of methylsilafluorene-vinylene trimer at 20 °C when exposed to 33 equivalents of different Lewis base analytes.....	65
Figure 2-12.	Correlation between Lewis basicity and the change in peak position of methylsilafluorene-vinylene trimer in the ^{29}Si NMR upon addition of a series of analytes.....	66
Figure 2-13.	Superimposed ^{29}Si NMR spectra of the outer Si atoms in methylsilafluorene-vinylene trimer when exposed to increasing equivalents of acetonitrile at 20 °C.....	67
Figure 2-14.	Plot of chemical shift dependence of the peripheral Si atoms of methylsilafluorene-vinylene trimer on the equivalents of ACN added and a Scatchard plot.....	69
Figure 2-15.	UV-vis spectra of methylsilafluorene-vinylene trimer on addition of Lewis base analytes.....	70
Figure 2-16.	<i>Ab initio</i> DFT calculations on methylsilafluorene-vinylene trimer and TNT at the B3LYP/6-31G* level.....	72
Figure 2-17.	^{29}Si NMR spectra of methylsilafluorene-vinylene trimer on addition of TNT.....	73

Figure 2-18.	Image of fluorescence quenching image of poly(silafluorene-vinylene) by solid-particulates of RDX.....	76
Figure 2-19.	Frontier orbital energy correlation diagram for model trimers with various explosive analytes.....	79
Figure 2-20.	Frontier orbital density figures for TNT and RDX.....	97
Figure 2-21.	Frontier orbital density figures for HMX and PETN.....	98
Figure 2-22.	Frontier orbital density figures for model trimers.....	98

Chapter III

Figure 3-1.	Chemical structures of silicon-containing vinylene polymers.....	108
Figure 3-2.	Thermal ellipsoid plot of 1-methyl-1- <i>trans</i> (2-trimethylsilyl)ethenyl-2,3,4,5-(tetraphenyl)silole.....	112
Figure 3-3.	Thermal ellipsoid plot of 1,4-di(1-methyl-1- <i>trans</i> -ethenyl-2,3,4,5-(tetraphenyl)silole)benzene.....	113
Figure 3-4.	Thermal ellipsoid plot of 1,4-di(1-methyl-1- <i>trans</i> -ethenyl-silafluorene)benzene.....	114
Figure 3-5.	Chemical structure of 1,1-dihydrido-4,5,8,9-bis(triptycene)silafluorene.....	115
Figure 3-6.	Superimposed crystal structures of 1,4-di(1-methyl-1- <i>trans</i> -ethenyl-2,3,4,5-(tetraphenyl)silole)benzene and 1,4-di(1-methyl-1- <i>trans</i> -ethenyl-silafluorene)benzene.....	116
Figure 3-7.	UV-vis and fluorescence spectra of siloles and silafluorenes.....	121
Figure 3-8.	Solid-state fluorescence emission spectra for siloles and silafluorenes.....	123
Figure 3-9.	Examples of fluorescence quenching detection of various explosive solid-particulates.....	126
Figure 3-10.	Schematic representation of explosive analyte binding events with poly(silafluorene-phenylenedivinylene).....	128

Figure 3-11.	Solid-state fluorescence quenching of polymers by TNT on silica TLC plates.....	130
---------------------	---	-----

Chapter IV

Figure 4-1.	Absorption and photoemission spectra of dimers and polymers.....	156
Figure 4-2.	Solid-state photoemission spectra on TLC plates and quartz plates.....	158
Figure 4-3.	Examples of fluorescence quenching of polymer thin-film by solid-particulates of various explosives.....	163
Figure 4-4.	Solid-state fluorescence quenching behavior of poly(silafluorene-(9 <i>H</i> -fluorene)divinylene) on silica TLC plates in the presence of various explosives.....	165
Figure 4-5.	Solid-state fluorescence quenching behavior of poly(silafluorene-(9,9-dimethyl-9 <i>H</i> -fluorene)divinylene) on silica TLC plates in the presence of various explosives.....	168
Figure 4-6.	Solid-state fluorescence quenching behavior of poly(silafluorene-(9,9'-spirobifluorene)divinylene) on silica TLC plates in the presence of various explosives.....	169
Figure 4-7.	Qualitative energy level diagram comparing the emitting state energies of polymers with the LUMO energies of RDX, PETN and TNT.....	171
Figure 4-8.	Structures of poly(silafluorene-vinylene) and poly(silafluorene-phenylenedivinylene).....	173

Chapter V

Figure 5-1.	Pathway for fluorimetric detection of nitrate and nitrite in biological systems using 2,3-diaminonaphthalene (DAN).....	195
Figure 5-2.	Chemical structures of the targeted explosives.....	197
Figure 5-3.	Release of nitrite from RDX upon α -hydride extraction by a hydroxide base.....	198

Figure 5-4.	Turn-on fluorescence detection of RDX using the two-step process.....	200
Figure 5-5.	Turn-on fluorescence detection of five successive fingerprints of C-4.....	201
Figure 5-6.	Turn-on fluorescence detection of five successive fingerprints of PE-4.....	201
Figure 5-7.	Side-by-side comparison of two-step turn-on sensor with fluorescence quenching sensor.....	203
Figure 5-8.	Formation of Meisenheimer complex on hydroxide nucleophilic attack of nitroaromatic compounds.....	204
Figure 5-9.	Example of three-step sensor for selective explosives detection.....	205
Figure 5-10.	Chemical structures of fluorenyl polymer and model dimers.....	207
Figure 5-11.	Absorption and photoemission spectra of fluorenone dimer.....	208
Figure 5-12.	Example of the time-dependent turn-off/turn-on selective detection of production line PETN.....	209
Figure 5-13.	Example of detection selectivity for TNT and PETN.....	210
Figure 5-14.	Time-dependent solution phase fluorescence quenching behavior of fluorene dimer upon exposure to UV light in the presence of various analytes.....	211
Figure 5-15.	Time-dependent solution phase fluorescence quenching behavior of fluorene dimer on continuous exposure to UV light in the presence of various analytes.....	213
Figure 5-16.	IR data showing the thin-film photooxidation of fluorene dimer under UV light in the presence of oxygen.....	214
Figure 5-17.	Time-dependent solution phase fluorescence quenching plots of protected and unprotected fluorene dimers upon exposure to UV light.....	215
Figure 5-18.	Time-dependent solution phase fluorescence quenching plots of fluorene dimer upon exposure to UV light in the	

	presence of various analytes.....	217
Figure 5-19.	Proposed mechanism for the selective oxidation of fluorene by PETN.....	218

Chapter VI

Figure 6-1.	Chemical structures of TATP and HMTD.....	233
Figure 6-2.	Fluorescence response of polyfluoran to 2.9 ppm of H ₂ O ₂ vapor after 220 min.....	239
Figure 6-3.	Fluorescence trace of polyfluoran exposed to various vapor concentrations of H ₂ O ₂	240
Figure 6-4.	First order kinetics plot of the fluorescence response of polyfluoran exposed to various concentrations of H ₂ O ₂	242
Figure 6-5.	Images of the fluorescence response of polyfluoran to various concentrations of H ₂ O ₂ vapor.....	243
Figure 6-6.	Fluorescence response of polyfluoran to UV light over a 5 h period.....	244
Figure 6-7.	Comparison of fluorescence response between polyfluoran and the fluoran monomer on exposure to H ₂ O ₂ , UV light, and ambient conditions.....	245
Figure 6-8.	Correlation between the concentration of H ₂ O ₂ and the time to reach I _∞	246
Figure 6-9.	Correlation between the concentration of H ₂ O ₂ and the time to reach 3σ of the fluorescence response noise.....	247
Figure 6-10.	Images of the fluorescence response of polyfluoran to various solution concentrations of H ₂ O ₂ and interferents.....	250
Figure 6-11.	Fluorescence response of polyfluoran to ambient conditions.....	257
Figure 6-12.	¹ H NMR spectrum of model dimer.....	258
Figure 6-13.	¹³ C NMR spectrum of model dimer.....	259

Chapter VII

Figure 7-1. Depiction of the orbital overlap between the vinylene spacer and the silicon center along the backbone of polymetallacyclopentadiene-vinylene.....267

LIST OF SCHEMES

Chapter I

- Scheme 1-1.** Platinum catalyzed hydrosilylation of bis(dimethylsilyl)acetylene with 1,4-diethynylbenzene.....12
- Scheme 1-2.** Platinum catalyzed hydrosilylation of bis-silanes with dialkynes.....13
- Scheme 1-3.** Platinum catalyzed hydrosilylation of diethynylsilanes with secondary silanes.....13
- Scheme 1-4.** Self-hydrosilylation of diethylethynylsilane.....14

Chapter II

- Scheme 2-1.** Synthetic routes to the trimeric model compounds.....49

Chapter III

- Scheme 3-1.** Hydrosilylation of trimethylsilylacetylene by 1-hydrido-1-methyl-(tetraphenyl)silole using H_2PtCl_6111
- Scheme 3-2.** Synthesis of model dimers by catalytic hydrosilylation.....113
- Scheme 3-3.** Synthesis of polymers by catalytic hydrosilylation.....117

Chapter IV

- Scheme 4-1.** Synthesis of fluorene polymers by catalytic hydrosilylation.....152
- Scheme 4-2.** Synthesis of model dimers by catalytic hydrosilylation.....154

Chapter VI

- Scheme 6-1.** Selective oxidation of 3,6-bis(pinacolatoboron)fluoran by H_2O_2 forming the fluorescein fluorophore.....235

Scheme 6-2.	Synthesis of model dimer by double transesterification.....	237
Scheme 6-3.	Synthesis of polyfluoran by double transesterification.....	238

Chapter VII

Scheme 7-1.	A summary of the catalytic hydrosilylation of 1,1-dihydridometalloles with various diethynylaryl comonomers.....	265
--------------------	---	-----

LIST OF TABLES

Chapter I

Table 1-1.	Properties of targeted explosive analytes.....	23
-------------------	--	----

Chapter II

Table 2-1.	Results of catalytic hydrosilylation syntheses.....	53
Table 2-2.	Summary of photoluminescence data for monomers, trimers, and polymers.....	55
Table 2-3.	Summary of Stern-Volmer constants (K_{sv}) for polymer fluorescence quenching with explosive analytes.....	61
Table 2-4.	^{29}Si NMR results for methylsilafluorene-vinylene trimer.....	63
Table 2-5.	Chemical shifts of the peripheral Si atoms of methylsilafluorene-vinylene trimer in the presence of increasing equivalents of ACN at 20 °C.....	68
Table 2-6.	Solid-state detection limits (ng cm^{-2}) for trace explosives by fluorescence quenching of sprayed-on films of polymers.....	75
Table 2-7.	HOMO and LUMO energies calculated for the various explosives and trimers at the B3LYP/6-31G* level of theory.....	77
Table 2-8.	Summary of X-ray crystallographic data for methyl(tetraphenyl)silole-vinylene trimer.....	95
Table 2-9.	Tabulated HOMO and LUMO energies calculated for various explosives and at the B3LYP/6-311+G** level of theory.....	96

Chapter III

Table 3-1.	Polymerization results for polymers prepared by catalytic hydrosilylation with various catalysts in toluene for 24 h.....	118
-------------------	---	-----

Table 3-2.	Summary of photoluminescence data for monomers, dimers, and polymers.....	120
Table 3-3.	Summary of solid-state detection limits (ng cm ⁻²) for various explosives by fluorescence quenching.....	127
Table 3-4.	Summary of solid-state Stern-Volmer constants (K _{SV}).....	131
Table 3-5.	Summary of X-ray crystallographic data for model compounds.....	141

Chapter IV

Table 4-1.	Molecular weights for fluorene polymers prepared by catalytic hydrosilylation.....	153
Table 4-2.	Photoluminescence data for silafluorene-fluorene dimers and copolymers.....	155
Table 4-3.	Summary of chemical structure and selected physical properties of explosive analytes.....	161
Table 4-4.	Summary of solid-state detection limits for various explosives by fluorescence quenching.....	164
Table 4-5.	Summary of solid-state Stern–Volmer constants.....	167
Table 4-6.	Comparison of photoluminescent properties and sensor response of silafluorene based polymers synthesized by catalytic hydrosilylation.....	172

Chapter V

Table 5-1.	A list of some common explosive mixtures and their components....	193
Table 5-2.	Vapor pressure and detection limits of the different classes of explosives.....	199

Chapter VI

Table 6-1.	Properties of organic peroxide based explosives compared with TNT.....	234
-------------------	--	-----

Table 6-2.	Summary of polyfluoran fluorescence responses on exposure to H ₂ O ₂ vapor.....	241
Table 6-3.	Time-dependent detection limits of H ₂ O ₂ vapor by polyfluoran at various exposure times.....	248

Chapter VII

Table 7-1.	Photoluminescence and molecular weight results from the hydrosilylation polymerization of various 2,3,4,5-tetraphenylsilole and silafluorene copolymers.....	266
Table 7-2.	Summary of explosives detection by fluorescence quenching of silole and silafluorene based polymers.....	269

ACKNOWLEDGEMENTS

I want to thank my advisor Professor Bill Trogler for taking me into his lab and mentoring me for the past four years. He has a wealth of knowledge to offer and I have enjoyed our conversations on chemistry as well as sports. It was also an honor to work with Dr. Sarah Toal, who showed me what was required to become a successful chemist. I am grateful to the Trogler lab members, current and past, of whom I have had endless conversations and good laughs.

It was a pleasure to work with both Dr. Anthony Mrse and Dr. Antonio DiPasquale. Their knowledge and input is evident throughout this dissertation.

Without my friends here at UCSD, this process would have been a lot less enjoyable. Thank you Chris and Seth for the late nights and endless weekends watching and debating sports. We had a good run here! Thanks also to the rest of the softball and flag football entourage; a necessary escape from the lab vortex.

I must acknowledge my undergraduate mentors, Professor Mike Elliott and Professor Nancy Levinger, at Colorado State University who made me realize that chemistry is my passion.

Chapter One, in part, is a reprint of the material as it appears in the following paper: Sanchez, J. C.; Trogler, W. C. "Hydrosilylation of Dienes as a Route to Functional Polymers Delocalized Through Silicon" *Macromol. Chem. Phys. (Special Article Series)* **2008**, in press.

Chapter Two, in part, is a reprint of the material as it appears in the following paper: Sanchez, J. C.; DiPasquale, A. G.; Rheingold, A. L.; Trogler, W. C. "Synthesis, Luminescent Properties, and Explosives Sensing with 1,1-Tetraphenylsilole- and 1,1-

Silafluorene-vinylene Polymers” *Chem. Mater.* **2007**, *19*, 6459–6470. The crystallographic information file (CIF) for compounds **1** and **3** is available on the internet at pubs.acs.org as “Supporting Information” to these publications.

Chapter Three, in part, is a reprint of the material as it appears in the following paper: Sanchez, J. C.; Urbas, S. A.; Toal, S. J.; DiPasquale, A. G.; Rheingold, A. L.; Trogler, W. C. “Catalytic Hydrosilylation Routes to Divinylbenzene Bridged Silole and Silafluorene Polymers. Applications to Surface Imaging of Explosive Particulates” *Macromolecules* **2008**, *41*, 1237-1245. The crystallographic information file (CIF) for compounds **1-3** is available on the internet at pubs.acs.org as “Supporting Information” to this publication.

Chapter Four, in part, is a reprint of the material as it appears in the following paper: Sanchez, J. C.; Trogler, W. C. “Efficient Blue Emitting Silafluorene-fluorene Conjugated Copolymers: Selective Turn-off/turn-on Detection of Explosives” *J. Mater. Chem.* **2008**, DOI: 10.1039/b802623h.

Chapter Five, in part, is a reprint of the material as it appears in the following papers: Sanchez, J. C.; Toal, S. J.; Wang, Z.; Dugan, R. E.; Trogler, W. C. “Selective Detection of Trace Nitroaromatic, Nitramine and Nitrate Ester Explosive Residues Using a Three-step Fluorimetric Sensing Process: A Tandem Turn-off, Turn-on Sensor” *J. Foren. Sci.* **2007**, *52*, 1308–1313 and Sanchez, J. C.; Trogler, W. C. “Efficient Blue Emitting Silafluorene-fluorene Conjugated Copolymers: Selective Turn-off/Turn-on Detection of Explosives” *J. Mater. Chem.* **2008**, DOI: 10.1039/b802623h.

Chapter Six, in part, is a reprint of the material as it appears in the following papers: Sanchez, J. C.; Trogler, W. C. “Polymerization of a Boronate Functionalized

Fluorophore by Double Transesterification. Applications to Fluorescence Detection of Hydrogen Peroxide Vapor” *J. Mater. Chem.*, submitted 2008.

VITA

- 2004 B.S., Honors, Chemistry, Colorado State University
- 2004 GEM Fellow
- 2004 – 2005 Teaching Assistant, Department of Chemistry and Biochemistry,
University of California, San Diego
- 2005 – 2008 National Science Foundation Graduate Research Fellow
- 2006 M.S., Chemistry, University of California, San Diego
- 2008 Ph.D., Chemistry, University of California, San Diego

PUBLICATIONS

Sanchez, J. C.; Trogler, W. C. “Hydrosilylation of Diynes as a Route to Functional Polymers Delocalized Through Silicon” *Macromol. Chem. Phys. (Special Article Series)* **2008**, in press.

Sanchez, J. C.; Trogler, W. C. “Polymerization of a Boronate Functionalized Fluorophore by Double Transesterification. Applications to Fluorescence Detection of Hydrogen Peroxide Vapor” *J. Mater. Chem.*, submitted 2008.

Sanchez, J. C.; Trogler, W. C. “Efficient Blue Emitting Silafluorene-fluorene Conjugated Copolymers: Selective Turn-off/Turn-on Detection of Explosives” *J. Mater. Chem.* **2008**, DOI: 10.1039/b802623h. **(Highlighted by Chemical Technology and C&EN)**

Sanchez, J. C.; Urbas, S. A.; Toal, S. J.; DiPasquale, A. G.; Rheingold, A. L.; Trogler, W. C. “Catalytic Hydrosilylation Routes to Divinylbenzene Bridged Silole and Silafluorene Polymers. Applications to Surface Imaging of Explosive Particulates” *Macromolecules* **2008**, *41*, 1237-1245.

Sanchez, J. C.; DiPasquale, A. G.; Rheingold, A. L.; Trogler, W. C. “Synthesis, Luminescent Properties, and Explosives Sensing with 1,1-Tetraphenylsilole- and 1,1-Silafluorene-vinylene Polymers” *Chem. Mater.* **2007**, *19*, 6459–6470. **(Highlighted by ACS as ‘Noteworthy Chemistry’ 28 January 2008)**

Sanchez, J. C.; Toal, S. J.; Wang, Z.; Dugan, R. E.; Trogler, W. C. “Selective Detection of trace Nitroaromatic, Nitramine and Nitrate Ester Explosive Residues Using a Three-step Fluorimetric Sensing Process: A Tandem Turn-off, Turn-on Sensor” *J. Foren. Sci.* **2007**, *52*, 1308–1313.

Toal, S. J.; Sanchez, J. C.; Dugan, R. E.; Trogler, W. C. “Visual Detection of Trace Nitroaromatic Explosive Residue Using Photoluminescent Metallolene-containing Polymers” *J. Foren. Sci.* **2007**, *52*, 79-83.

PATENTS

Trogler, W. C.; Sanchez, J. C. "Detection of Hydrogen Peroxide Vapors by a Turn-on Fluorescence Response Initiated by an Oxidative Depolymerization of a Boronate Functionalized Fluorophore" provisional patent filed **2008** (No. SD2008-279).

Trogler, W. C.; Sanchez, J. C.; Toal, S. J.; Zheng, W. "Detection of Nitro- and Nitrate-containing Compounds" European Patent WO2008005096, January 10, **2008**.

Trogler, W. C.; Urbas, S. A.; Toal, S. J.; Sanchez, J. C. "Inorganic Polymers and use of Inorganic Polymers for Detecting Nitroaromatic Compounds" European Patent WO2007024227, March 1, **2007**.

Trogler, W. C.; Sanchez, J. C. "Fluorescence Detection of Nitrogen-containing High Explosives and Blue Organic LED" provisional patent filed **2007** (No. SD2007-074).

Trogler, W. C.; Sanchez, J. C. "Detection of Explosive Particulates by Fluorescence Quenching of Blue-emitting Polymers and Selectivity Through Oxidation Control" provisional patent filed **2007** (No. SD2008-023).

ABSTRACT OF THE DISSERTATION

Design and Optimization of Polymeric Silole and Boronate Photoluminescent Probes for Improved Explosives Detection Applications

by

Jason C. Sanchez

Doctor of Philosophy in Chemistry

University of California, San Diego, 2008

Professor William C. Trogler, Chair

Hydrosilylation of silole and silafluorene fluorophores is an effective polymerization tool for the synthesis of σ^* - π/π^* delocalized structures. Improvements in molecular weights (4000-20 000), reaction conditions (0-50 °C), and functional group variety were obtained for 1,1-polysilole and 1,1-polysilafluorene materials. The polymers were screened for their ability to detect organic based explosives by a fluorescence quenching mechanism. The explosives screened include the nitroaromatic-based explosives TNT, DNT, PA, and Tetryl, the nitramine-based explosives RDX and HMX, the nitrate ester-based explosives PETN, TNG, and

EGDN, and the organic peroxide-based explosives TATP and HMTD. Explosive particulates were targeted to increase the sensitivity of detection for low volatility explosives. Detection limits as low as 1 pg cm^{-2} were obtained by the optimization of the polymers properties. Sensitivity is gained by tuning the frontier molecular orbital band gap to better match the LUMO energies of the explosive analytes. The excited state electron transfer process is also improved by Lewis acid/base interactions between the nitro groups of the explosives and the silacycle core of the silole and silafluorene fluorophores.

Sensors target the specific chemical functionalities of nitramine and nitrate ester based explosives for fluorescence imaging. Nitramine and nitrate ester based explosives can be detected selectively through the release of nitrite by an α -hydride abstraction and a subsequent acid-catalyzed triazotization with 2,3-diaminaphthalene. The naphthotriazole product is visibly fluorescent as a thin-film providing a turn-on fluorescence signal. Nitrate ester-based explosives can be specifically targeted using a turn-on fluorescence response from the oxo-anion specific oxidation of unprotected fluorene units in polysilafluorene-divinylene fluorene. Both turn-on fluorescence sensors can be used in tandem with the fluorescence quenching sensors to provide selective explosives detection assays based on a fluorescence signal response.

Organic peroxide based explosives are targeted through a selective oxidative depolymerization of a boronate-based polymer. The polymer is synthesized by a double transesterification polymerization driven by formation of a stable six-member bis-boronate polymer with fluoran repeat units in the backbone. After exposure to

hydrogen peroxide, which can be formed from the UV decomposition of TATP and HMTD, the polymer undergoes a selective oxidative deprotection of the boronate functionalities forming a highly luminescent fluorescein. Detection limits of 3 ppb over an 8 h period are achieved through observation of the turn-on fluorescence response.

CHAPTER I

Review of Polycarbosilanes, Catalytic Hydrosilylation, and Current Explosives Detection Applications

1.1 POLYCARBOSILANES

Polycarbosilanes are an important class of functional materials with desirable physiochemical properties.¹ These hybrid materials are defined by silicon atoms in the backbone of both aliphatic and olefinic carbon oligomers and polymers, which improves physical properties such as thermal stability,² solubility,³ and processability,⁴ and lowering their toxicity.⁵ These functional materials have found use as semiconductors,⁶ ceramic precursors,⁷ fire retardants,⁸ and hybrid elastomeric components.⁹ The non-polar character and strength of the Si-C bond in polycarbosilanes imparts a resistance to depolymerization and photodegradation as compared to polysilanes (Si-Si coupled polymers).¹⁰ The inert polycarbosilane framework also permits post-polymerization functionalization. This feature is crucial for applications in thin-film monolayer assemblies and for nanoparticle derivativization.

1.1.1 Electronic Properties of Silicon

Although silicon and carbon are isoelectronic, the larger covalent radius and reduced electronegativity of silicon spawns unique electronic features in polycarbosilanes. These include increased bond polarity with heteroatoms, such as oxygen and halogens, as well as empty d-orbitals and Si-C σ^* orbitals.¹¹ These empty valence orbitals can participate in back-bonding and promote lone pair delocalization with adjacent atoms, such as nitrogen and oxygen. Delocalization also facilitates electronic communication along the polymer backbone. An unusual σ -delocalized

electronic structure is found in silicon coupled oligo and polysilanes.¹ This unique orbital interaction has been characterized spectroscopically and is supported by several theoretical models including the free electron model, the Sandorfly model, density functional theory, and band theory.¹² Delocalization through σ -bonds distinguishes silicon-coupled polymeric materials from saturated carbon based polymers and suggests that silicon might be used to bridge conjugated organic systems while still incorporating the desired physiochemical properties of the silicon atom. This has enabled advancements in silicon containing materials for photoresists,¹³ photo- and electroluminescent materials,¹⁴ and conducting materials.¹⁵ The presence of photo-active properties in aliphatic carbosilane polymers adds a functional electronic dimension to otherwise typically inert materials.

1.1.2 Synthesis of Polycarbosilanes

Polycarbosilanes were first synthesized by Kipping et al. in the 1920's using alkali metal polycondensation of diphenyldichlorosilane to form cyclic and oligomeric polysilanes.¹⁶ These materials are conventionally referred to as 'polysilanes' because they incorporate a Si-Si backbone with pendant alkyl groups bounded to Si. Since silicon and carbon are the main components, they are classified as "carbosilanes" (Figure 1-1). Burkard synthesized the first well characterized polysilanes in 1949.¹⁷ These materials were found to be intractable, which limited applications. The results discouraged research in this area until the late 1960's when Kumada and Tamao¹⁸ along with Boberski^{12k} synthesized a series of linear polydimethyl silanes. Soluble and

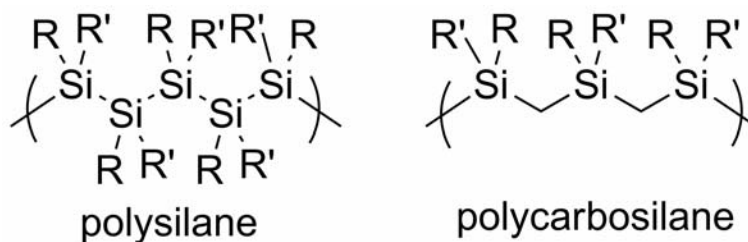


Figure 1-1. Backbone structure for silane and carbosilane polymers.

processable polysilanes were further developed in West's lab during the 1970's.¹⁹ It was not until the recent development of catalytic dehydrogenative coupling of Si-H bonds that linear polysilanes became an important class of functional polymers.²⁰ However, dehydrogenative coupling of silanes remains limited to a small class of silanes and functional groups.²¹ It was often noted that the weak Si-Si bonds in the backbone of the polymeric materials produced an easily photodegradable framework.^{1,22}

At the time when polysilanes were being pushed aside as viable functional materials due to their insolubility, peroxide catalyzed hydrosilylation of alkenes was pioneered by Sommer in 1947.²³ This approach was predicated on the formation of a silicon-carbon skeleton (polycarbosilanes) that would incorporate the desirable physiochemical properties of the silicon atom in an organic polymer. Transition metal catalyzed hydrosilylation was developed by Speier in 1957,²⁴ promoting a widespread interest in the synthesis of polycarbosilanes as functional materials. Hydrosilylation could be catalyzed by many metals, thereby producing a diverse library of chemo- and regio-selective reaction conditions which has since become the favored method for silicon-carbon bond formation.²⁵

1.1.3 Electronic Delocalization in Polycarbosilanes

Electronic delocalization in saturated polycarbosilanes lies between that observed in polysilanes and polyethylene.²⁶ The unique σ - σ^* conjugation found in polysilanes is interrupted by the introduction of methylene spacers in polycarbosilanes. Increasing the saturated carbon chain length in the polysilane framework rapidly decreases conjugation. In alternating aliphatic silicon-carbon backbones, like those produced by hydrosilylation of α,ω -dienes, conjugation is minimal. To increase delocalization and thereby access optically active polymers, hydrosilylation of diynes was used to create silyl-vinyl polymers. Unique conjugation properties were seen between the σ orbital of the silicon atoms and the π orbitals of the carbon-vinylene bonds.²⁷ This chapter focuses on the use of catalytic hydrosilylation of diynes for the synthesis of new functional materials.

1.2 HYDROSILYLATION CATALYSTS AND MECHANISMS

Hydrosilylation refers to the oxidative addition of a Si-H bond across an alkene or alkyne forming a Si-C bond. Hydrosilylation is selective toward carbon-carbon multiple bonds, tolerating functional groups such as ester, nitriles, amines, amides, nitro, ketone, ether, phosphate, sulfide, and sulfones, just to name a few.²⁸ Hydrosilylation of alkynes may produce several isomers including *trans* (*E*), *cis* (*Z*), and geminal products resulting from β -1,2 (syn and anti) and α -2,1 additions (Figure 1-2).²⁹ The selectivity toward these products depends on sterics, kinetic control, and the specific catalyst used. Over the years, many metals have been examined as

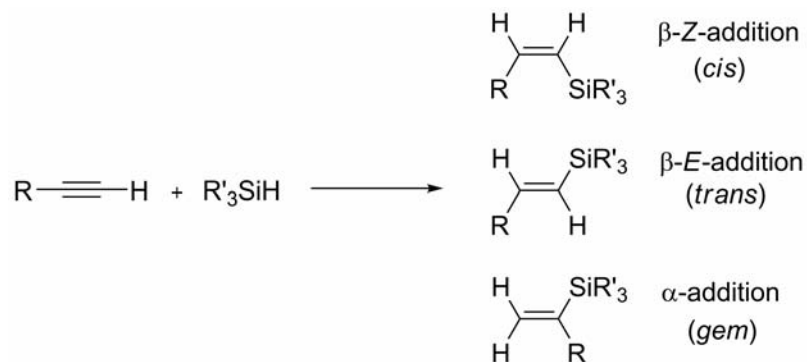


Figure 1-2. Possible stereo-isomers produced by the hydrosilylation of alkynes.

effective hydrosilylation catalysts. Among the most popular are platinum, palladium, rhodium, and nickel. Hexachloroplatinic(IV) acid (Speier's catalyst) is the catalyst of choice for most hydrosilylation reactions.^{24,30} This heterogeneous catalyst is activated through the formation of platinum(0) clusters that provide a platform for oxidative addition of the Si-H bond. Other platinum catalysts, such as Karstedt's catalyst³¹ and platinum phosphine derivatives, are also effective, and involve platinum(0) species.³² However, the reactivity of these catalysts decreases with increasing ligand substitution at the metal center. Palladium complexes are not as reactive as their platinum counterparts, but tend to be more stereo-selective.³³ Rhodium catalysts, including Wilkinson's catalyst ($\text{RhCl}(\text{PPh}_3)_3$), are effective for the hydrosilylation of both alkynes and alkenes. Although these catalysts can control the regio- and stereo-isomers formed, reactions proceed slowly for most substrates.³⁴ Other catalysts used include cobalt,³⁵ ruthenium,³⁶ osmium,^{28d} chromium,³⁷ molybdenum,³⁸ tungsten,³⁹ copper,⁴⁰ iron,⁴¹ and actinides.⁴²

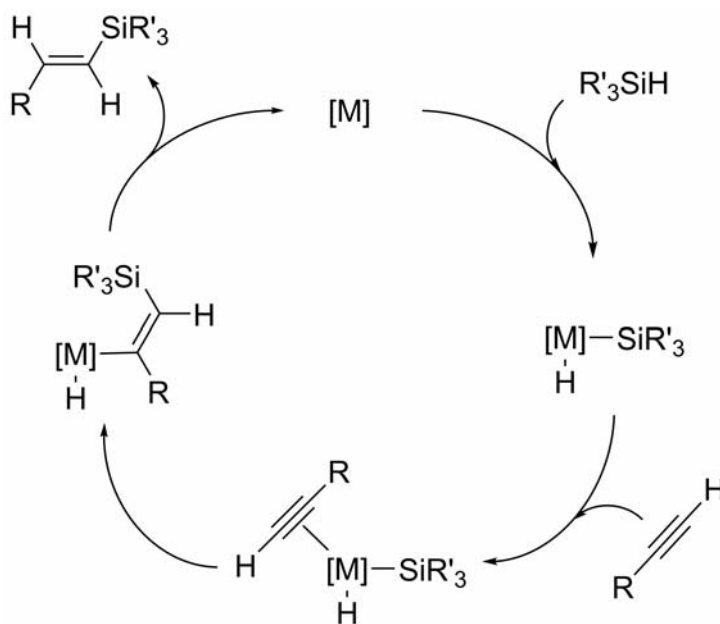


Figure 1-3. A modified Chalk-Harrod mechanism for hydrosilylation.

Since Speier's discovery of the platinum catalyzed hydrosilylation, several mechanisms have been proposed. For platinum catalysts, the first widely accepted mechanism was proposed by Chalk and Harrod in 1965.⁴³ Subsequent analysis of the reaction intermediates present during the hydrosilylation of both alkenes and alkynes led to the modified Chalk-Harrod mechanism, which describes the migratory olefin insertion into the metal-silyl bond rather than into the metal-hydride bond (Figure 1-3).⁴⁴ The reaction follows a typical catalytic pathway beginning with oxidative addition of a silylhydride, subsequent coordination of the alkene or alkyne, an insertion of the olefin into the Pt-Si bond, and finally a reductive elimination of product. Rhodium and other group 9 transition metal catalysts proceed by a similar Chalk-Harrod oxidative addition mechanism with some differences. Olefin insertion is directed to the Rh-Si bond and reductive elimination follows a series of isomerization

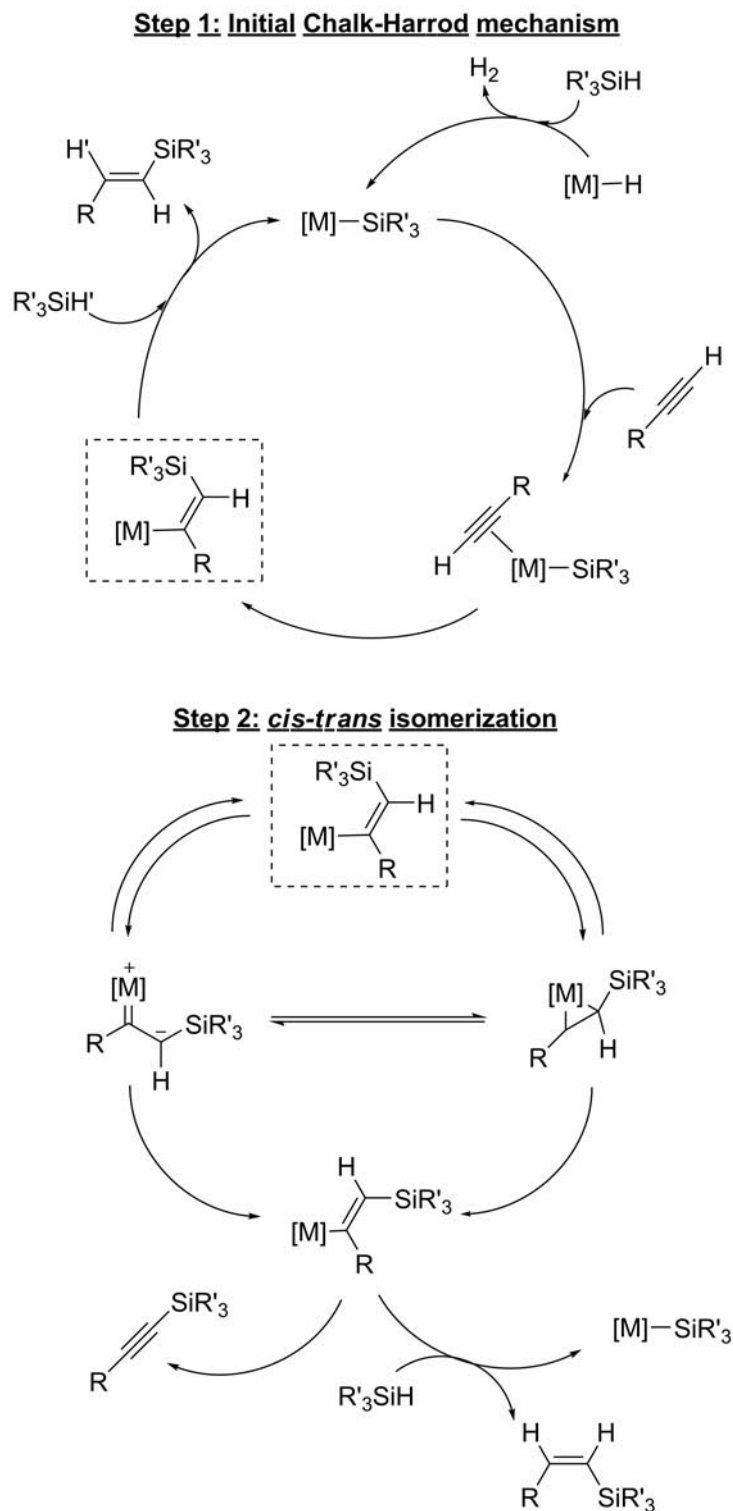


Figure 1-4. Mechanism for group 9 metal catalyzed hydrosilylation. Proposed intermediates for *cis-trans* isomerization.

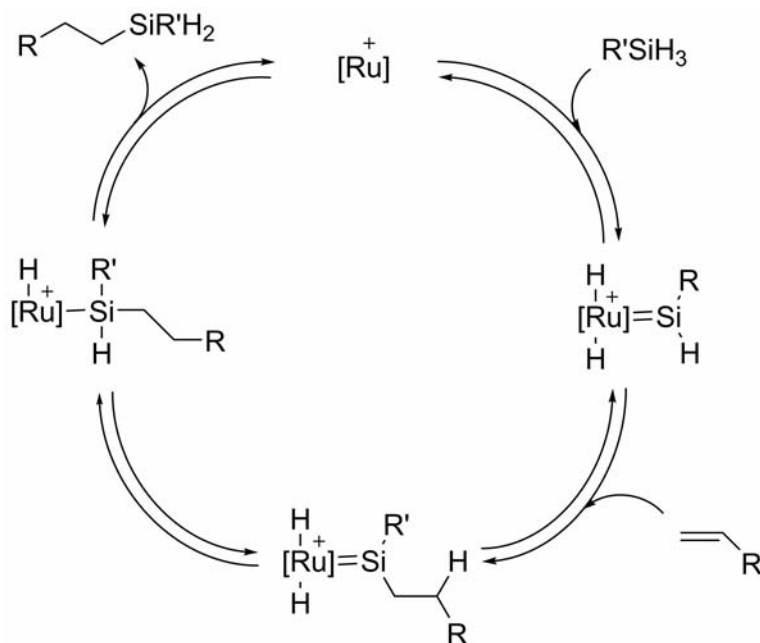


Figure 1-5. Ruthenium catalyzed hydrosilylation of primary silanes featuring a silylene intermediate.

steps that are controlled by sterics, the electronic nature of the silane, and the stability of the formed metal carbene or metallacyclopropane intermediates (Figure 1-4).⁴⁵ In this case, isomerization of the olefin inserted intermediate is limited and the stereochemistry of addition is initially determined by sterics of the ancillary ligands.

The mechanism proposed for hydrosilylation by ruthenium-based catalysts involves a silylene intermediate.⁴⁶ This is initiated by the activation of two Si-H bonds (Figure 1-5). The mechanism is similar to a hydroboration reaction where the insertion of the alkene does not occur between a metal-hydride or metal-silylide but with the activated Si-H bond of the silylene. This unique mechanism promotes the hydrosilylation of sterically restricted substrates, selectivity towards monosubstituted silanes, the absence of unsaturated products, and anti-Markovnikov regio-chemistry.

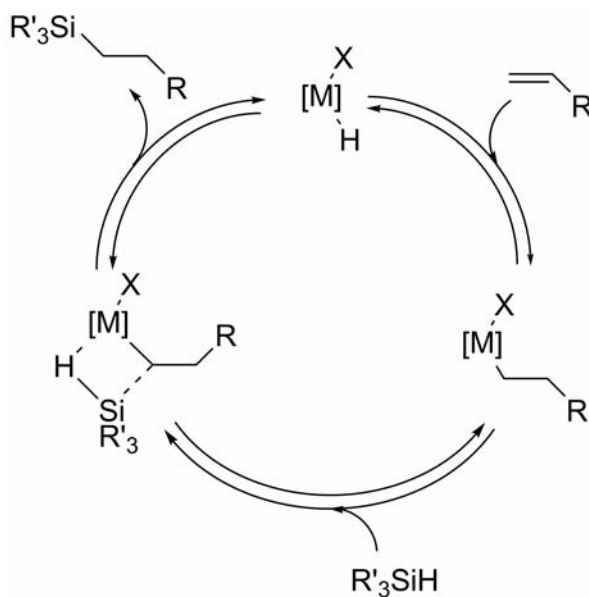


Figure 1-6. Early transition metal metallocene hydrosilylation mechanism including a slow σ -bond metathesis.

Early transition metal metallocene catalysts also are thought to initially proceed via the Chalk-Harrod mechanism. The proposed mechanism involves a fast olefin insertion into the metal-hydride bond followed by a slow σ -bond metathesis reaction with the silane (Figure 1-6).⁴⁷ Iron based catalysts promote hydrosilylation by first coordinating the olefin and then undergoing a typical Chalk-Harrod hydrosilylation mechanism through which $Fe(0)$ is the active species.⁴⁸ Iron offers a cheaper and non-toxic alternative to the precious heavy metals typically used for hydrosilylation. However, the iron-catalyzed reaction is substrate specific and has only been studied with primary silanes.

The versatility of catalytic hydrosilylation makes it attractive for the production of chemically complex functional materials. Catalysts and substrates can be varied to control stereo-chemistry. Recent studies have focused on delocalized

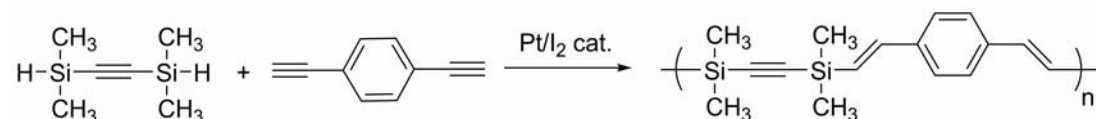
polycarbosilane materials prepared by double hydrosilylation of diynes to produce silyl-vinylene polymeric materials. These copolymers show enhanced delocalization through the bridging silicon atoms to yield functional hybrid materials for photolithography, electroluminescence, and sensing applications.

1.3 POLY(SILYL-VINYLENE)S

Hydrosilylation of alkynes has become a favored approach to the formation of alternating silyl-vinylene based polymers. These materials have applications as photoresists, cross-linkable prepolymers, ceramic precursors, electron transporting materials, and photo luminescent and optoelectronic materials. Many of these properties arise from the unique $\sigma^*-\pi$ delocalization observed along the polymer backbone.

1.3.1 Optimization of Reaction Conditions

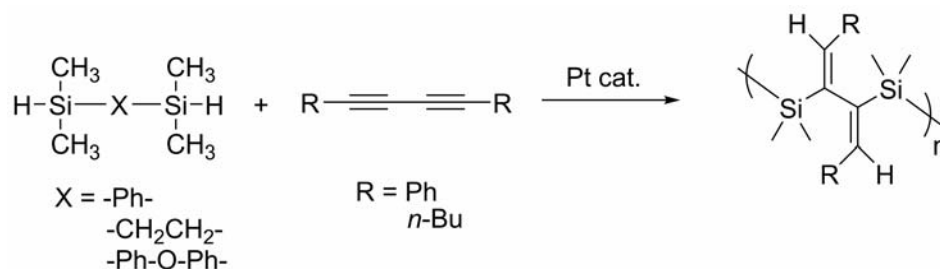
The kinetics for hydrosilylation of alkynes are highly favored over alkenes; however, stereo-chemistry is more difficult to control. Factors that affect the synthesis of stereo-regular polymers include the catalyst structure, kinetics, sterics, and electronic nature of the silyl-hydride. As is typical in highly delocalized systems, the *trans*-isomer is the desired stereo-chemistry. This provides the best orbital overlap between comonomers as compared to *cis*- and geminal isomers. Much effort has been placed into optimizing the reaction conditions through catalyst modifications, reaction times, temperatures, and comonomer optimization. Keller et al. reported the use of



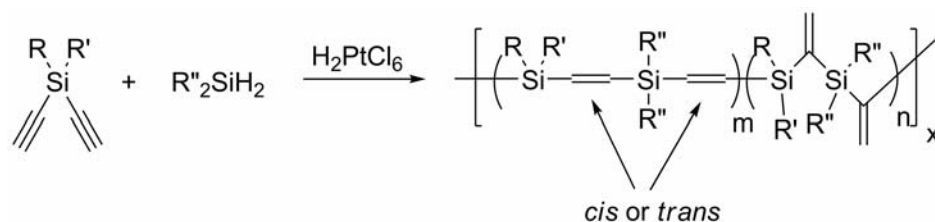
Scheme 1-1. Platinum catalyzed hydrosilylation of bis(dimethylsilyl)acetylene with 1,4-diethynylbenzene.

bis(dimethylsilyl)acetylene as the comonomer for catalytic hydrosilylation polymerization with 1,4-diethynylbenzene (Scheme 1-1).⁴⁹ Speier's platinum catalyst was used and continues to be used as an effective heterogeneous catalyst for hydrosilylation polymerization. It was noticed that under moderate reaction temperatures, only *trans* products were formed. The acetylene spacer between bulky silyl groups was found inert to the polyaddition reactions. This was the first example of the use of steric hindrance to control the hydrosilylation reactivity. More recent studies by Hensler et al. have been devoted to the hydrosilylation of 1,3-diynes (Scheme 1-2).⁵⁰ The increased steric freedom in these systems creates a pathway for the formation of many isomers. Through the use of model reactions, it was determined that *E,E*-2,3 products were the most common, yielding either silane substituted polyvinylenes or unique polycarbosilanes with the silane monomers interrupted by two α -vinylidene functionalities. Through careful choice of aryl spacers between bis-silanes, cross-linked polymers may also be obtained.⁵¹

Luneva et al. noticed that similar copolymers could be made by placing the ethynyl functionalities directly on one of the silane comonomers (Scheme 1-3).⁵² This allowed for higher reaction temperatures to be used to generate stereo-regular *trans*-poly(silyl-vinylene)s due to the close proximity of the ethynyl groups sterically

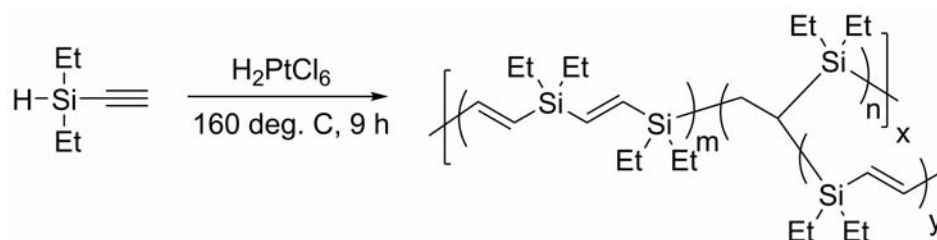


Scheme 1-2. Platinum catalyzed hydrosilylation of bis-silanes with dialkynes.



Scheme 1-3. Platinum catalyzed hydrosilylation of diethynylsilanes with secondary silanes.

directing formation of the desired product. This employed both kinetic control and stoichiometric regulation of reactant concentrations to produce high molecular weight polymers. Barton et al. extended this approach idea by creating a silane monomer that incorporated both the Si-H and ethynyl functionalities.^{7c} Self-hydrosilylation minimized undesirable byproducts. Barton also noticed that at high temperatures (>160 °C) chain branching occurred due to cross-polymerization of the terminal Si-H bonds with the vinylene spacers (Scheme 1-4). Although this is problematic for linear, conducting polymer applications, it illustrates the versatility of hydrosilylation polymerization to produce cross-linked macromolecular and dendritic structures.



Scheme 1-4. Self-hydrosilylation of diethylethynylsilane.

1.3.2 Photoactive Polymers

Because of the relative ease of hydrosilylation polymerization, interest arose in synthesizing photo-active polymers. Shim et al. utilized phenylene-vinylene frameworks to produce UV-blue emitting polymers.⁵³ It was noticed that by using 1,4-diethynylbenzene as the comonomer, α -alkylidene (gem) linkages were produced along with the typical *trans*-alkene products. This apparently resulted from the steric freedom of the ethynyl groups as compared to previous studies. Further work using self-hydrosilylation of silane substituted phenylacetylenes shows that the degree of regio-regularity can be controlled by sterics.^{7b} The photo-absorption and luminescence spectra of the silylenephenylenevinylene polymers synthesized by Shim et al. show increased delocalization in the *trans*-only products, as compared to the mixed *cis-trans* polymers even though molecular weights are compromised to a degree.

1.3.3 Catalyst Modification

Speier's catalyst was generally used for the preceding polyaddition reactions. It is easily removed from the reaction matrix by simple filtration. However, Nishihara et al. showed that catalytic hydrosilylation polymerization can be regio- and stereo-

controlled through catalyst modification.⁵⁴ It was found that Wilkinson's catalyst could be used to create both *trans*- and *cis*-isomers depending on the sequence of monomer addition as well as the reaction temperature. Using the principles of steric control characterized in the previous studies, they obtained high molecular weight, regio-regular polymers with a variety of diethynyl substituted aryl monomers. The use of bis-silane aryl comonomers in conjunction with the bis-ethynyl aryl comonomers allowed them to achieve high molecular weights while selectively synthesizing either all *trans*- or all *cis*-vinylene products. Masuda et al. further characterized the photochemistry of these polymers and found that both the *trans*- and *cis*-isomers show similar absorption and emission wavelengths.⁵⁵ However, the quantum efficiency of fluorescence for the *trans*-isomer is much higher (~2-10 times greater) than for the *cis*-isomer. Under UV irradiation, the *cis*-isomer photoisomerizes to the all *trans*-product, revealing the expected increase in photoluminescence quantum efficiency as well as demonstrating Si-C bond stability under UV irradiation. These polymers show promise as electroluminescent materials, without requiring the dopants typically necessary with current technology.

Until this point, molecular weights for hydrosilylation of dialkynes resulted in moderate (<20 000) molecular weights. Recent work by Takeuchi et al. has shown palladium as an effective hydrosilylation catalyst.⁵⁶ Palladium is selective for hydrosilylation of alkynes over alkenes, minimizing the cross-linked dendritic byproducts that may be observed with other catalysts. This selectivity results in an

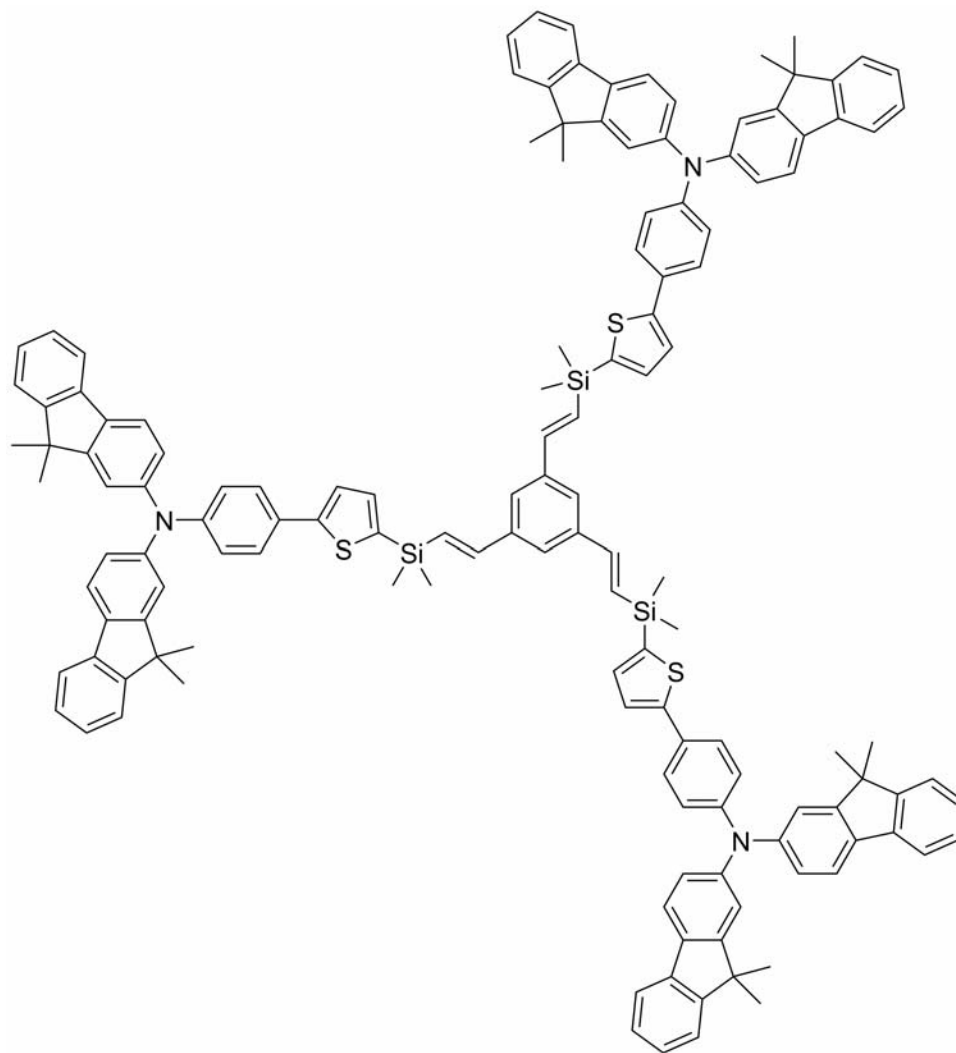


Figure 1-7. Structure of a silylene-spaced vinylarene dendritic fluorescent dye.

increase in the molecular weights of these polymers to ~50 000. However, stereoselectivity is diminished, with both *cis* and *trans* products observed. Although this can be problematic for photoluminescence applications and for the formation of optically pure polymers, it can be advantageous for synthesizing delocalized silylenevinylene polymers with pendant vinyl groups for cross-polymerization or further functionalization.

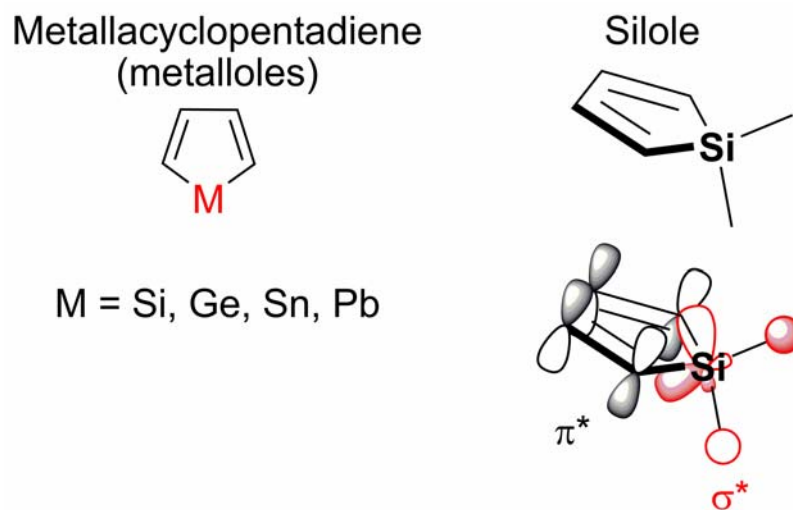


Figure 1-8. Chemical structure of metallacyclopentadiene core units. Orbital overlap between the σ^* (silyl) and the π^* (butadiene) fragments decrease the frontier molecular orbital bandgap energy creating electron transporting and luminescent properties.

1.3.4 Applications

Catalytic hydrosilylation as a one-step process for preparing vinylene based polymers, has led to several new applications. For example, Ko et al. have used catalytic hydrosilylation to create three-dimensional first generation dendritic fluorescent dyes (Figure 1-7).⁵⁷ Moisture stable hyperbranched polysilylenevinylenes with pendant ethynyl groups have been prepared as light and heat cross-linkable prepolymers.^{2,58} Catalyst tuning has also afforded photoactivated curing and patterning of preceramic polymer films.⁵⁹

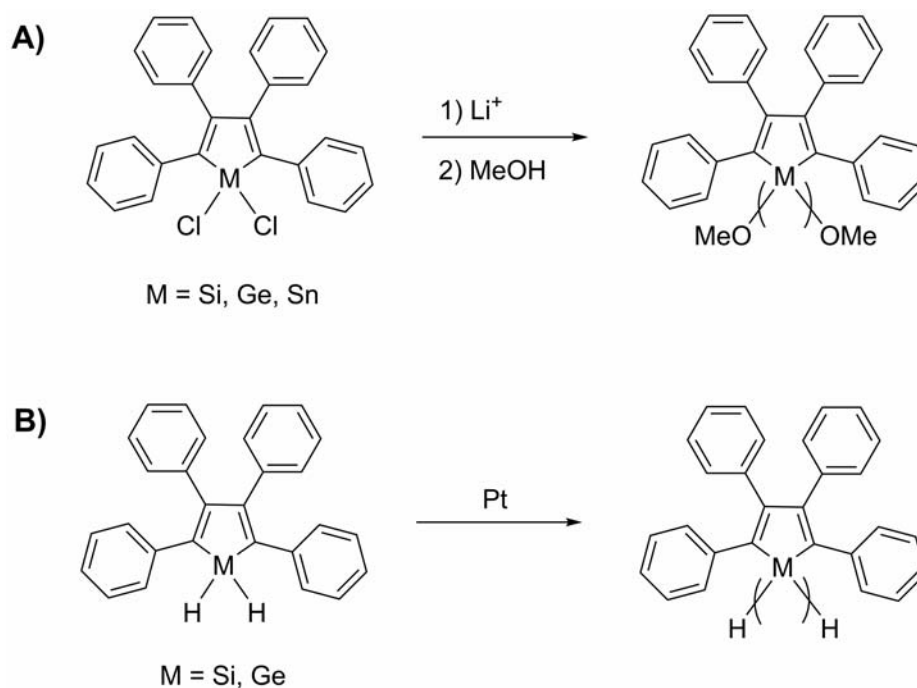


Figure 1-9. Synthesis of 1,1-polymetalloles by A) Stoichiometric Wurtz coupling and B) Catalytic dehydrocoupling.

1.4 POLYSILOLES

1.4.1 Introduction to Siloles

Hydrosilylation of alkynes has been explored as a polymerization technique for synthesizing tunable polymers in light emitting devices, organic charge carrier materials, and luminescent sensors. One way to increase the efficiency and effectiveness for these applications is to use cyclic silanes (silacycles) to manipulate the frontier molecular orbitals of the silane comonomer, thereby gaining visible fluorescence and electron-transporting properties.⁶⁰ The core structure of these modified silanes consists of a metallacyclopentadiene (metallole) heterocyclic unit (Figure 1-8). Many studies have shown that the unique luminescent properties of these molecules arise from overlap between the σ^* orbital of the bridgehead silyl group and

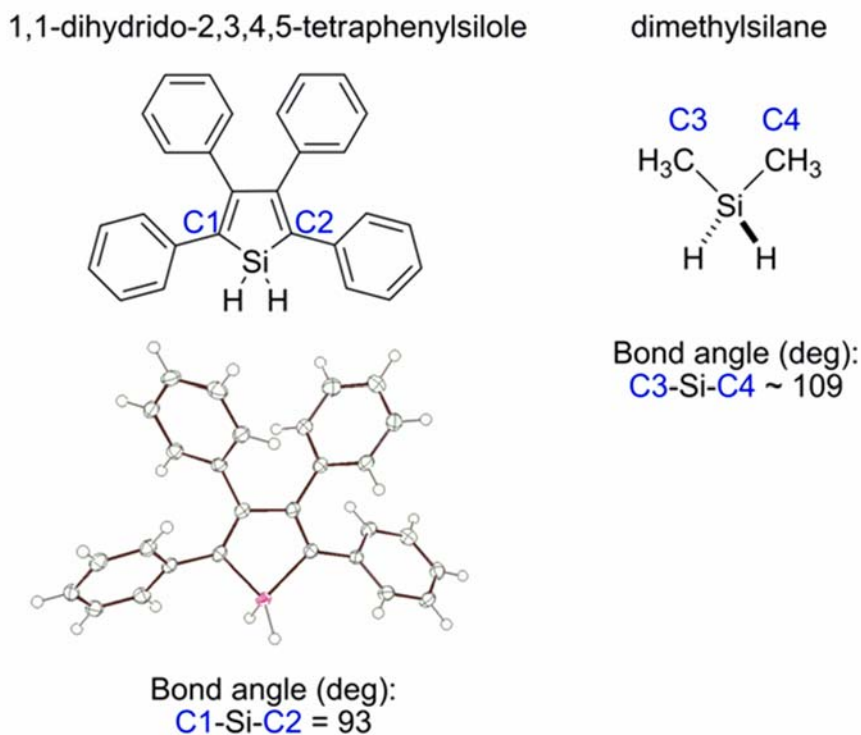


Figure 1-10. Comparison between the internal bond angles of secondary silole and silane monomers.

the π^* orbitals of the butadiene moiety.⁶¹ The σ -orbital contribution to this delocalized system is similar to the unique σ -conjugation seen in polysilanes. This unusual conjugation is present in all group 14 metalloid containing metallacyclopentadiene moieties other than carbon. This dissertation will focus on using hydrosilylation of conjugated diynes to build delocalized luminescence polymers containing silacyclopentadienes (siloles).

1.4.2 Polymerization Methods

Most previous polymerization methods target coupling the butadiene portion of the silacyclopentadiene framework.⁶² However, substitutions to this region of the

silacycle can significantly alter the electronic properties of the material and usually result in the formation of rigid polymers that are limiting in their thin-film photoluminescent and conducting properties. To avoid this, both stoichiometric Wurtz coupling and catalytic dehydrocoupling polymerization techniques have been used to create Si-Si linked polymetalloles (Figure 1-9).^{60b,63} However, these materials are low molecular weight oligomers and may yield cyclic products under the harsh reaction conditions. This was once thought to be a result of steric hindrance surrounding this silicon center, preventing effective coordination to the metal dehydrocoupling catalyst center. However, the internal angle of the metallacyclopentadiene is actually smaller than that seen in silane analogues (Figure 1-10).⁶³ Although sterics may play a role due to the large ligand framework typically observed in 2,3,4,5-tetraphenylsilole and the short bond distance observed in dehydrocoupled silole polymers, the steric availability of the silicon center for oxidative addition to metal centers prompted our interest in hydrosilylation as a possible polymerization technique.

1.5 EXPLOSIVES DETECTION USING LUMINESCENT SENSORS

1.5.1 Targeted Explosives and Applications

Reliable detection of trace explosive materials has become a focal point in security screening methods.⁶⁴ Applications such as minefield remediation,⁶⁵ crime scene investigations,⁶⁶ and counter-terrorism activities (e.g., facility protection and personnel, baggage, and cargo screening⁶⁷) are areas of concern. These applications attempt to target a wide variety of explosive materials, the most common of which can

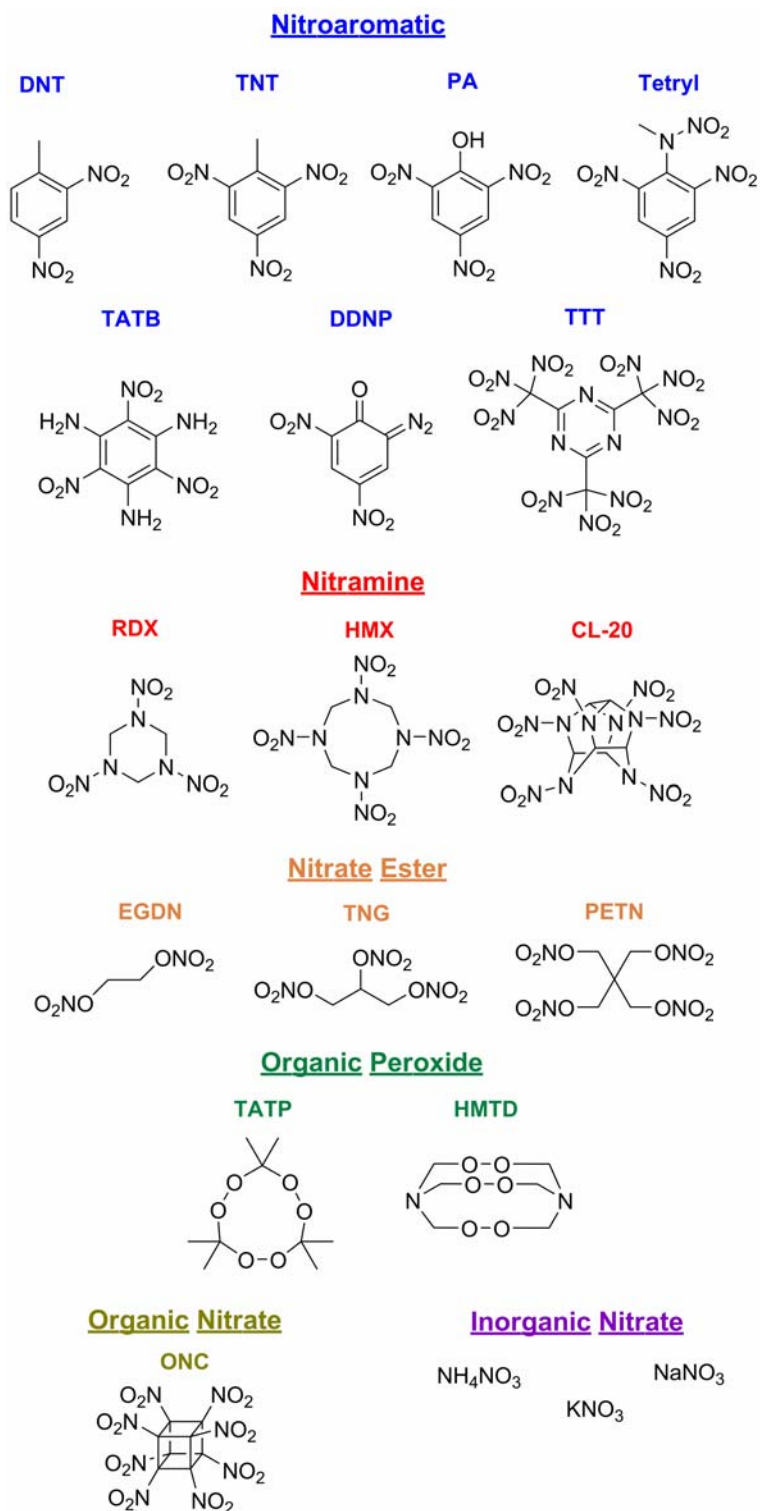


Figure 1-11. Chemical structure and classification of common targeted explosive analytes.

be categorized by their key chemical functional groups (Figure 1-11). Although there are more than 250 known explosive materials,⁶⁸ sensor technologies are focused on the most commonly used organic nitrate-, organic peroxide-, and nitrate salt-based explosives. These compounds are typically the most readily available, easily synthesized, shock sensitive, or easily packaged explosives (Table 1-1). Common explosives, such as 2,4,6-trinitrotoluene (TNT), make up the bulk of antipersonnel land mines found in 62 countries around the world.^{65,67} The quantity of hidden land mines, ammunition bunkers, and improvised explosive devices (IED) continues to increase in areas of civil unrest. Other targeted organic and nitrate based explosives include 2,4-dinitrotoluene (DNT), picric acid (PA), 2,4,6-trinitrophenyl-N-methylnitramine (Tetryl), 1,3,5-triamino-2,4,6-trinitrobenzene (TATB), diazodinitrophenol (DDNP), tris-(trinitromethyl)triazine (TTT), cyclotrimethylenetrinitramine (RDX), cyclotetramethylene-tetranitramine (HMX), 2,4,6,8,10,12-hexanitro-2,4,6,8,10,12-hexaazaisowurtzitane (CL-20), dinitroethylene glycol (EGDN), trinitroglycerin (TNG), pentaerythritol tetranitrate (PETN), triacetone triperoxide (TATP), hexamethylene triperoxide diamine (HMTD), octanitrocubane (ONC), ammonium nitrate (AN), potassium nitrate (PN), and sodium nitrate (SN).

1.5.2 Improving Sensor Properties

In addition to better sensitivity for a greater range of common explosives, advances in the detection of suspicious materials for their explosives content are needed in the areas of cost efficiency, sensitivity, selectivity, portability and speed of

Table 1-1. Properties of targeted explosive analytes.

Explosive	Explosive Category	MP (°C)	P _{vap} (Torr)	Detonation velocity (m s ⁻¹)
DNT	secondary	67-70	1.1×10^{-4}	7000
TNT	secondary	80	5.8×10^{-6}	6850
PA	secondary	123	5.8×10^{-9}	7900
Tetryl	secondary	130	5.7×10^{-9}	7570
TATB	secondary	350	<i>na</i>	7350
DDNP	primary	<i>na</i>	<i>na</i>	6900
TTT	secondary	91-92	<i>na</i>	<i>na</i>
RDX	secondary	206	4.6×10^{-9}	8750
HMX	secondary	276-286	8.0×10^{-11}	9110
CL-20	secondary	<i>na</i>	<i>na</i>	9650
EGDN	secondary	-22	2.8×10^{-2}	<i>na</i>
TNG	secondary	13	4.4×10^{-4}	7750
PETN	secondary	141	1.4×10^{-8}	8400
TATP	primary	91	<i>na</i>	5300
HMTD	primary	75 (dec.)	<i>na</i>	4500
ONC	secondary	<i>na</i>	<i>na</i>	10 100
AN	tertiary	170	<i>na</i>	5300
PN	tertiary	334	<i>na</i>	<i>na</i>
SN	tertiary	307	<i>na</i>	<i>na</i>

the signal analysis.⁶⁸ Current technology typically addresses one or two of these issues using instrumental or spectroscopic methods for vapor phase or bulk detection.⁶⁹ Yet, no current method successfully incorporates all the features listed above. Constraints hindering the advancement of these technologies include the limited sample size

available for analysis, interferences, numerous vapor pressures and other physical properties of the targeted explosives, and deliberate concealment of the explosive material prior to use.⁶⁵ Most current methods that achieve good sensitivity do so through vapor phase sample analysis. However, vapor sampling may be limited by the low volatility of many explosives at room temperature (Table 1-1). Nitroaromatic explosives such as TNT have moderate vapor pressures but at low surface concentrations the vapor concentration of TNT is significantly less than its equilibrium vapor pressure.⁷⁰ Explosives, such as RDX and HMX, have substantially lower vapor pressures, which is typical of most organic nitrate based explosives, making vapor detection of these compounds difficult.⁷¹ Packaging may lower effective vapor pressures of even the most volatile explosive materials by a factor of 1000.^{64,65} Only the highest vapor pressure explosives, or taggants such as dinitroethylene glycol (EDGN) and 2,3-dimethyl-2,3-dinitrobutane (DMNB), respectively, can be reliably detected by vapor methods.⁷² It is rare than an explosive or explosive mixture is not encapsulated in a sealed casing or are bound by plasticizers, both of which block the escape of vapors.

1.5.2.1 Particle Sampling

Sensitivity towards less volatile or encapsulated explosives has been improved, from a practical standpoint, through standoff detection⁷³ and direct analysis of explosive particulates through solid-phase generators and analysis.⁷⁴ It is well documented that the handling of explosive materials can leave microgram quantities of

explosive residues on subjects and transport vehicles.⁷⁵ In addition, explosives with low vapor pressures can persist on hair follicles for days and after repeated washings upon exposure or handling of the material.⁷⁶ By targeting particulate residue rather than the vapor form of the explosives, pre-concentration sampling issues can be avoided.

To date, nearly all instrumental characterization methods have been investigated for their applicability as explosive sensors.⁷⁷ These methods can be classified as electrochemical sensors, mass sensors, optical sensors, and biosensors. Approaches have been adapted for both bulk and trace detection to analyze suspicious materials, personnel, and cargo. However, adaptation of these techniques into low cost, low power devices that provide both rapid data analysis and portability has been limited.

1.5.3 Luminescent Polymer Sensors

As mentioned above, an alternative to vapor sampling is the chemical analysis of solid particulates that remain after the handling of explosive materials.⁷⁸ Common methods that utilize particulate sampling include both colorimetric and fluorescence sensors, which take advantage of human visual processing power, rather than instrumental evaluation.⁷⁹⁻⁸¹ One promising technology uses conjugated photoluminescent polymers to rapidly detect explosive vapors. The use of fluorescent polymers for the detection of explosive vapors and particulates has been adapted for both instrumental and visual imaging approaches (Figure 1-12).⁸¹ Detection limits in

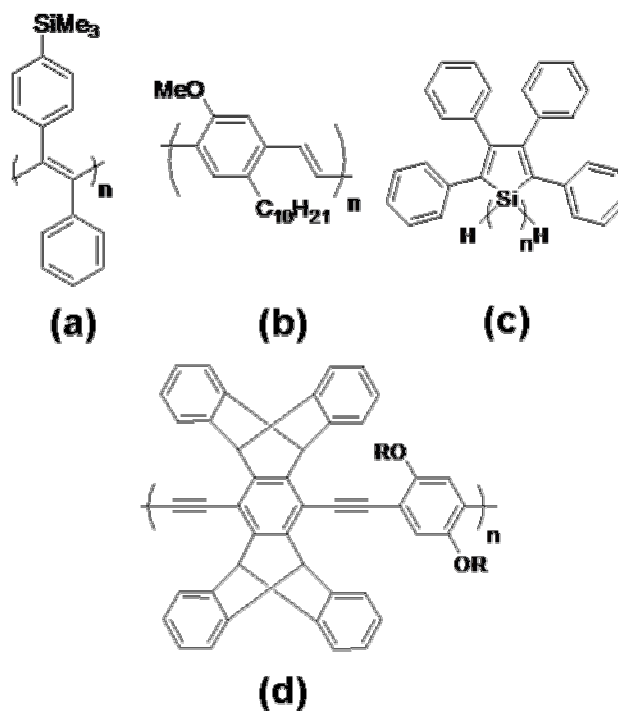


Figure 1-12. Conjugated fluorescent polymers for explosives detection: (a) polyacetylene PTMSDPA, (b) poly(*p*-phenylenevinylene) DP10-PPV, (c) 1,1-poly(tetraphenyl)silole, (d) poly(*p*-phenylene-ethynylene).

the parts-per-trillion (ppt) level and femtogram amounts have been achieved with a fluorescence quenching mechanism. However, this approach has been limited to the detection of volatile explosives such as TNT while signal response is typically evaluated by spectroscopic methods. These luminescent materials use an amplified fluorescence quenching pathway to detect vapors of highly oxidizing explosives. Poly(tetraphenyl)siloles, in particular, have the advantage of visual analysis, ease of synthesis, and their ability to semi-selectively bind explosive analytes (Figure 1-12c).⁸² Previous reports have demonstrated the ability of 1,1-poly(tetraphenyl)silole to image trace particulates of explosive materials in the solid-state.^{82,83} However, no single polymer has been able to detect the entire range of common high explosives by

a fluorescence quenching mechanism, in part due the broad range of reduction potentials found among explosive materials.

Luminescent polymers offer rapid response times, low detection limits, intuitive interpretation, and cost efficient solutions. The properties of luminescent polymers can be altered by tuning the HOMO and LUMO energy levels through chemical modification of the polymer backbone and the degree of π -conjugation.⁸⁴ By extending the conjugation length, properties such as electron-hole mobility, emission wavelength, crystal packing (excimer emission) and amplified chemosensor response can be altered. In order to optimize detection sensitivity, new polymers are required with increased fluorescence quantum yields. It is also important to match the excited state energy to the LUMO energy of a broad class of explosive in order to promote rapid electron transfer and efficient quenching of the fluorescence pathway. Yet the emission energy should remain low enough to be visible for non-instrumental detection.

The challenge for current development of effective explosives sensors lies in the demand for a single low cost, portable sensor that provides all the desired conveniences while offering a rapid and easily evaluated response with high sensitivity and selectivity. The use of fluorescence as a detection mechanism inherently includes many of these features. The challenge is to manipulate the fluorophore materials to achieve simultaneous selective detection of explosive particulates, including the very difficult to detect organic peroxide based explosives,⁸⁵ while improving sensitivity and signal analysis.

1.6 OBJECTIVES OF THE DISSERTATION

The objective of the research presented herein is to develop an understanding of the fluorescence based explosives detection process from a chemical and electronic point of view and to use that knowledge to develop new photo-luminescent sensors that improve on the sensitivity and selectivity of current methods. The present work focuses on the use of luminescent metallole fluorophores to simplify the synthetic process, thereby creating a much more economic sensor than the current technology. This simplification does not inhibit sophisticated chemical design from being integrated into the sensor technology.

Chapter Two offers a new polymerization route to delocalized 1,1-silole- and 1,1-silafluorene-vinylene polymers. Catalytic hydrosilylation improves the molecular weight, reaction conditions, and polymer strength over those obtained through dehydrocoupling. The polymers are screened for their ability to detect explosive particulates with detection limits reaching 200 pg cm^{-2} . Conclusions are made regarding the effects that frontier molecular orbital energy matching between sensor and analyte as well as analyte binding have on the overall detection efficiency of these sensors.

Chapter Three builds on the knowledge gained from Chapter 2 through modifications to the fluorophore bandgap by introducing a phenylene-divinylene spacer between metallole units in the polymer framework. Red-shifting the emission allows for better visualization of the polymer thin-film. Larger spatial gaps between silole and silafluorene units create better analyte binding at the silacycle centers and

improve the polymer molecular weight during synthesis. Detection limits reaching 100 pg cm^{-2} are achieved with these improvements. A solid-state Stern-Volmer analysis is also introduced as a new method for quantifying the detection of explosive particulates.

Chapter Four examines the improvements in sensor sensitivity gained by increasing the quantum efficiencies of the polymer materials. Fluorescence quantum efficiencies were increased using a fluorenylene-divinylene co-monomer in the silafluorene polymer structure. Detection limits of 1 pg cm^{-2} were achieved using these new highly emissive polymers. Detection was improved based on the ability to better visualize the polymer thin-film luminescence. The amount of polymer used during the detection process was also minimized, creating a more cost effective sensor.

Chapter Five introduces two new turn-on fluorescence sensors for the selective detection of nitramine and nitrate ester based explosives. The first sensor targets the release of nitrite from nitramine- and nitrate ester-based explosives, forming a luminescent naphthotriazole complex. This can be combined with the luminescent polymer sensors to form a three step selective sensing method. The second sensor builds upon the technology observed in Chapter 4 to introduce a single polymer material that incorporates both a turn-off and turn-on fluorescence mechanism for the selective detection of nitrate ester based explosives. This sensory material is the first example, to our knowledge, of a single polymer selectively detecting multiple classes of explosives using both a turn-off and turn-on fluorescence mechanism.

Chapter Six presents double transesterification as a pathway for the polymerization of a boronic ester functionalized fluoran. This polymer was designed and evaluated for the detection of hydrogen peroxide vapors. These vapors can be produced from organic peroxide based explosives by UV decomposition. Detection works through the oxidative depolymerization of the boronate backbone resulting in the production of a highly luminescent fluorescein compound. Detection limits of 3 ppb over an 8 h period are observed. This is one of only two effective vapor phase hydrogen peroxide sensors that do not require a complex solution phase detection process.

Chapter Seven summarizes the finding in this dissertation and offers insight into future improvements that can be made to fluorescent sensory technology.

1.7 ACKNOWLEDGEMENTS

This chapter, in part, is a reprint of the material as it appears in the following paper: Sanchez, J. C.; Trogler, W. C. “Hydrosilylation of Diynes as a Route to Functional Polymers Delocalized Through Silicon” *Macromol. Chem. Phys. (Special Article Series)* **2008**, in press.

1.8 REFERENCES

- (1) (a) Abd-El-Aziz, A. S., Carraher Jr., C. E., Pittman Jr., C. U., Zeldin, M., Eds. In *Macromolecules Containing Metal and Metal-Like Elements*; J. Wiley & Sons: 2005; Vol. 4. (b) Ohshita, J. *Yuki Gosei Kagaku Kyokaiishi* **2001**, *59*, 11–22. (c) Jones, R. G., Ando, W., Chojnowski, J., Eds. In *Silicon-containing polymers*; Kluwer Academic Publishers: 2000. (d) Mark, J. E.; Allcock, H. R.; West, R. In *Inorganic Polymers*, Prentice Hall: New Jersey, 1992. (e) Miller, R. D.; Michl, J. *Chem. Rev.* **1989**, *89*, 1359–1410. (f) Zeldin, M., Wynne, K. J., Allcock, H. R., Eds. In *Inorganic and Organometallic Polymers: Macromolecules Containing Silicon, Phosphorus, and other Inorganic Elements*; 1988. (g) Rochow, E. G. In *Silicon and Silicones*; Springer-Verlag: Berlin, 1987; p 99. (h) West, R. *J. Organomet. Chem.* **1986**, *300*, 327–346. (i) Tacke, R. In *Organosilicon and Bioorganosilicon Chemistry: Structure, Bonding, and Synthetic Application*; Sakurai, H., Ed.; J. Wiley: New York, 1985. (j) Weber, W. P. In *Silicon Reagents for Organic Synthesis*; Springer: Berlin, 1983. (k) Mark, J. E.; Kato, J. K. *J. Polym. Sci., Polym. Symp.* **1976**, *54*, 217–225. (l) Bruins, P. F. In *Silicon Technology*; J. Wiley: New York, 1970; p 38. (m) Noll, W. In *Chemistry and Technology of Silicones*; Academic: New York, 1968; p 113.
- (2) Xiao, Y.; Wong, R. A.; Son, D. Y. *Macromolecules* **2000**, *33*, 7232–7234.
- (3) Ohshita, J.; Kunai, A. *Acta Polym.* **1998**, *49*, 379–403.
- (4) Kim, H. K.; Ryu, M.-K.; Kim, K.-D.; Lee, S.-M.; Cho, S.-W.; Park, J.-W. *Macromolecules* **1998**, *31*, 1114–1123.
- (5) Kircheldorf, H. R., Ed. In *Silicon in Polymer Synthesis*; Springer: Berlin, 1996.
- (6) (a) Jung, S. H.; Kim, H. K.; Kim, S. H.; Kim, Y. H.; Jeoung, S. C.; Kim, D. *Macromolecules* **2000**, *33*, 9277–9288. (b) Ohshita, J.; Takada, A.; Kai, H.; Kunai, A.; Komaguchi, K.; Shiotani, M.; Adachi, A.; Sakamaki, K.; Okita, K.; Harima, Y.; Kunugi, Y.; Yamashita, K.; Ishikawa, M. *Organometallics* **2000**, *19*, 4492–4498. (c) Fang, M. C.; Watanabe, A.; Matsuda, M. *Macromolecules* **1996**, *29*, 6807–6813. (d) Kunai, A.; Ueda, T.; Horata, K.; Toyoda, E.; Nagamoto, I.; Ohshita, J.; Ishikawa, M. *Organometallics* **1996**, *15*, 2000–2008. (e) Tanaka, K.; Ago, H.; Yamabe, T.; Ishikawa, M.; Ueda, T. *Organometallics* **1994**, *13*, 3496–3501. (f) Ohshita, J.; Watanabe, T.; Kanaya, D.; Ohsaki, H.; Ishikawa, M.; Ago, H.; Tanaka, K.; Yamabe, T. *Organometallics* **1994**, *13*, 5002–5012.
- (7) (a) Haberecht, J.; Nesper, R.; Grützmacher, H. *Chem. Mater.* **2005**, *17*, 2340–2347. (b) Kim, D. S.; Shim, S. C. *J. Polym. Sci., A: Polym. Chem.* **1999**, *37*,

- 2263–2273. (c) Pang, Y.; Ijadi-Maghsoodi, S.; Barton, T. J. *Macromolecules* **1993**, *26*, 5671–5675. (d) Whitmarsh, C. K.; Interrante, L. V. *Organometallics* **1991**, *10*, 1336–1344. (e) Seyferth, D.; Sobon, C. A.; Borm, J. *New J. Chem.* **1990**, *14*, 545–547. (f) West, R. In *Ultrastructure Processing of Ceramics, Glasses and Composites*; Hench, L. L., Ulrich, D. R., Eds.; Wiley: New York, 1984; p 235. (g) Yajima, S.; Hayashi, J.; Omori, M. *Chem. Lett.* **1975**, 931–934.
- (8) (a) Lligadas, G.; Ronda, J. C.; Galià, M.; Cádiz, V. *Biomacromolecules* **2006**, *7*, 2420–2426. (b) Devaux, E.; Rochery, M.; Bourbigot, S. *Fire Mater.* **2002**, *26*, 149–154.
- (9) (a) Yoon, K.; Son, D. Y. *Macromolecules* **1999**, *32*, 5210–5216. (b) Lewis, L. N.; Stein, J.; Gao, Y.; Colborn, R. E.; Hutchins, G. *Platinum Met. Rev.* **1997**, *41*, 66–75.
- (10) Mazumder, B. In *Silicon and Its Compounds*; Science Publishers Inc.: Enfield, 2000.
- (11) (a) Pawlenko, S. In *Organosilicon Chemistry*; Walter de Gruyter: New York, 1986; p 109. (b) Bazant, V.; Chvalovsky, V.; Rathousky, J. In *Organosilicon Compounds*; Academic: New York, 1965; Vol. 1.
- (12) (a) Seki, K.; Mori, T.; Inokuchi, H.; Murano, K. *Bull. Chem. Soc. Jpn.* **1988**, *61*, 351–358. (b) Mintmire, J. W.; Ortiz, J. V. *Macromolecules* **1988**, *21*, 1189–1191. (c) Nelson, J. T.; Pietro, W. J. *J. Phys. Chem.* **1988**, *92*, 1365–1371. (d) Takeda, K.; Fujino, M.; Seki, K.; Inokuchi, H. *Phys. Rev. B* **1987**, *36*, 8129–8137. (e) Bigelow, R. W.; McGrane, K. M. *J. Polym. Sci., Polym. Phys. Ed.* **1986**, *24*, 1233–1245. (f) Takeda, K.; Teramae, H.; Matsumoto, N. *J. Am. Chem. Soc.* **1986**, *108*, 8186–8190. (g) Herman, A.; Dreczewski, B.; Wojnowski, W. *Chem. Phys.* **1985**, *98*, 475. (h) Herman, A.; Dreczewski, B.; Wojnowski, W. *J. Organomet. Chem.* **1983**, *251*, 7–14. (i) Verwoerd, W. S. *J. Comput. Chem.* **1982**, *3*, 445–450. (j) Allerd, A. L.; Ernst, C. A.; Ratner, M. A. In *Homoatomic Rings, Chains and Macromolecules of Main-Group Elements*; Rheingold, A. L., Ed.; Elsevier: New York, 1977; p 307. (k) Boberski, W. G.; Allerd, A. L. *J. Organomet. Chem.* **1975**, *88*, 65–72. (l) Pitt, C. G.; Bursey, M. M.; Rogerson, P. F. *J. Am. Chem. Soc.* **1970**, *92*, 519–522.
- (13) Miller, R. D.; MacDonald, S. A. *J. Imaging Sci.* **1987**, *31*, 43–46.
- (14) (a) Michl, J.; Downing, J. W.; Karatsu, T.; Klingensmith, K. A.; Wallraff, G. M.; Miller, R. D. In *Inorganic and Organometallic Polymers, ACS Symposium Series 360*; Zeldin, M., Wynne, K., Allcock, H., Eds.; American Chemical Society: Washington DC, 1988; Chap. 5, p 61. (b) Harrah, L. A.; Zeigler, J.

- Macromolecules* **1987**, *20*, 2037–2039. (c) Todesco, R. V.; Kamat, P. V. *Macromolecules* **1986**, *19*, 196–200. (d) Trefonas, P.; West, R.; Miller, R. D.; Hofer, D. *J. Polym. Sci., Polym. Lett. Ed.* **1983**, *21*, 823–829.
- (15) (a) Samuel, L. M.; Sanda, P. N.; Miller, R. D. *Chem. Phys. Lett.* **1989**, *159*, 227–230. (b) Abkowitz, M.; Stolka, M. *Philos. Mag. Lett.* **1988**, *58*, 239–245. (c) Kepler, R. G.; Zeigler, J. M.; Harrah, L. A.; Kurtz, S. R. *Phys. Rev. B* **1987**, *35*, 2818–2822. (d) Fujino, M. *Chem. Phys. Lett.* **1987**, *136*, 451–453. (e) Stolka, M.; Yuh, H.-J.; McGrane, K.; Pai, D. M. *J. Polym. Sci., Part A: Polym. Chem.* **1987**, *25*, 823–827.
- (16) Kipping, F. S. *J. Chem. Soc.* **1924**, *125*, 2291–2297.
- (17) Burkhard, C. A. *J. Am. Chem. Soc.* **1949**, *71*, 963–964.
- (18) Kumada, M.; Tamao, K. *Adv. Organometal. Chem.* **1968**, *6*, 19.
- (19) (a) West, R. *Pure Appl. Chem.* **1982**, *54*, 1041–1050. (b) West, R.; Carberry, E. *Science* **1975**, *189*, 179–186.
- (20) (a) Harrod, J. F. *Coord. Chem. Rev.* **2000**, *206-207*, 493–531. (b) Grimmond, B. J.; Corey, J. Y. *Organometallics* **2000**, *19*, 3776–3783. (c) Reichl, J. A.; Berry, D. H. *Adv. Organomet. Chem.* **1998**, *43*, 197–265. (d) Gauvin, F.; Harrod, J. F.; Woo, H. G. *Adv. Organomet. Chem.* **1998**, *42*, 363–405. (e) Tilley, T. D. *Acc. Chem. Res.* **1993**, *26*, 22–29.
- (21) (a) Rosenberg, L.; Kobus, D. N. *J. Organomet. Chem.* **2003**, *685*, 107–112. (b) Peulecke, N.; Thomas, D.; Baumann, W.; Fischer, C.; Rosenthal, U. *Tetrahedron Lett.* **1997**, *38*, 6655–6656. (c) Imori, T.; Woo, H.-G.; Walzer, J. F.; Tilley, T. D. *Chem. Mater.* **1993**, *5*, 1487–1492.
- (22) (a) Trefonas, P.; Miller, R.; West, R. *J. Am. Chem. Soc.* **1985**, *107*, 2737–2742. (b) Schnabel, W.; Kuvi, J. In *Aspects of Degradation and Stabilization of Polymers*; Jellinek, H. H. G., Ed.; Elsevier: New York, 1978; p 202.
- (23) Sommer, L. H.; Pietrusza, E. W.; Whitmore, F. C. *J. Am. Chem. Soc.* **1947**, *69*, 188.
- (24) Speier, J. L.; Webster, J. A.; Barnes, G. H. *J. Am. Chem. Soc.* **1957**, *79*, 974–979.
- (25) Marciniec, B. In *Applied Homogenous Catalysis with Organometallic Compounds*, 2nd ed.; Cornils, B., Herrmann, W. A., Eds.; Wiley-VCH: Weinheim, 2002; Vol. 1, Chap. 2.6.

- (26) (a) Sakurai, Y.; Yoshimura, D.; Ishii, H.; Ouchi, Y.; Isaka, H.; Teramae, H.; Matsumoto, N.; Hasegawa, S.; Ueno, N.; Seki, K. *J. Phys. Chem. B* **2001**, *105*, 5626–5629. (b) Isaka, H.; Teramae, H.; Fujiki, M.; Matsumoto, N. *Macromolecules* **1995**, *28*, 4733–4735.
- (27) (a) Ohshita, J.; Kunai, A. *Acta Polym.* **1998**, *49*, 379–403. (b) Kunai, A.; Toyoda, E.; Nagamoto, I.; Horio, T.; Ishikawa, M. *Organometallics* **1996**, *15*, 75–83. (c) Ohshita, J.; Kanaya, D.; Watanabe, T.; Ishikawa, M. *J. Organomet. Chem.* **1995**, *489*, 165–173. (d) Ohshita, J.; Matsuguchi, A.; Furumori, K.; Hong, R.-F.; Ishikawa, M. *Macromolecules* **1992**, *25*, 2134–2140. (e) Corriu, R. J. P.; Gerbler, P.; Guérin, C.; Henner, B. J. L.; Jean, A.; Mutin, P. H. *Organometallics* **1992**, *11*, 2507–2513. (f) Wu, H. J.; Interrante, L. V. *Macromolecules* **1992**, *25*, 1840–1841. (g) Hu, S. S.; Weber, W. P. *Polym. Bull.* **1989**, *21*, 133–140.
- (28) (a) Marciniac, B. *Silicon Chem.* **2002**, *1*, 155–175. (b) Ojima, I. In *The Chemistry of Organic Silicon Compounds*; Rappoport, Z., Apologia, Y., Eds.; Wiley: New York, 1998; Vol. 2, Chap. 29. (c) Marciniac, B., Ed. In *Comprehensive Handbook on Hydrosilylation*; Pergamum Press: Oxford, 1992. (d) Ojima, I. In *The Chemistry of Organic Silicon Compounds*; Pataki, S., Rappoport, Z., Eds.; Wiley: New York, 1989; Chap. 25.
- (29) (a) Trost, B. M.; Ball, Z. T. *Synthesis* **2005**, *6*, 853–887. (b) Brunner, H. *Angew. Chem. Int. Ed.* **2004**, *43*, 2749–2750. (c) Chauhan, M.; Hauck, B. J.; Keller, L. P.; Boudjouk, P. *J. Organomet. Chem.* **2002**, *645*, 1–13. (d) Ojima, I.; Li, Z.; Zhu, J. In *The Chemistry of Organic Silicon Compounds*; Rappoport, Z., Apologia, Y., Eds.; Wiley: Chi Chester, England, 1998; Vol. 2, p 1687. (e) Fleming, I.; Dunogues, J.; Smithers, R. *Org. React.* **1989**, *37*, 57–575.
- (30) Speier, J. L. *Adv. Organomet. Chem.* **1979**, *17*, 407–447.
- (31) Carlstadt, B. D., 1973, *U. S. Patent* 3,775,452.
- (32) Watanabe, H.; Asami, M.; Nagai, Y. *J. Organomet. Chem.* **1980**, *195*, 363–373.
- (33) (a) Tietze, L. F.; Ila, H.; Bell, H. P. *Chem. Rev.* **2004**, *104*, 3453–3516. (b) LaPointe, A. M.; Rix, F. C.; Brookhart, M. *J. Am. Chem. Soc.* **1997**, *119*, 906–917.

- (34) (a) Mori, A.; Takahisa, E.; Kajiro, H.; Hirabayashi, K.; Nishihara, Y.; Hiyama, T. *Chem. Lett.* **1998**, *5*, 443–444. (b) Calhoun, A. D.; Lung, K. R.; Nile, T. A.; Stokes, L. L.; Smith, S. C. *Transition Met. Chem.* **1983**, *8*, 365–368.
- (35) Chalk, A. J.; Harrod, J. F. *Adv. Organomet. Chem.* **1968**, *6*, 119–170.
- (36) (a) Matsuda, T.; Kadowaki, S.; Murakami, M. *Chem. Commun.* **2007**, *25*, 2627–2629. (b) Menozzi, C.; Dalko, P. I.; Cossy, J. *J. Org. Chem.* **2005**, *70*, 10717–10719. (c) Glaser, P. B.; Tilley, D. *J. Am. Chem. Soc.* **2003**, *125*, 13640–13641. (d) Trost, B. M.; Ball, Z. T. *J. Am. Chem. Soc.* **2001**, *123*, 12726–12727. (e) Brockmann, M.; tom Dieck, H.; Kleinwächter, I. *J. Organomet. Chem.* **1986**, *309*, 345–353. (f) Marciniak, B.; Guliński, J. *J. Organomet. Chem.* **1983**, *253*, 349–362. (g) Marciniak, B.; Guliński, J. *J. Mol. Catal.* **1980**, *10*, 123–126.
- (37) (a) Özkar, S.; Akhmedov, V. M.; Kayran, C. *J. Organomet. Chem.* **1997**, *533*, 103–108. (b) Abdalqader, W. F.; Chmielewski, D. M.; Grevels, F. W.; Özkar, S.; Peynircioglu, N. B. *Organometallics* **1996**, *15*, 604–614. (c) Abdalqader, W.; Özkar, S.; Peynircioglu, N. B. *Z. Naturforsch* **1993**, *48B*, 539–540. (d) Kotzian, M.; Kreiter, C. G.; Michael, G.; Özkar, S. *Chem. Ber.* **1983**, *116*, 3637–3658.
- (38) (a) Fernandes, A. C.; Fernandes, R.; Romão, C. C.; Royo, B. *Chem. Commun.* **2005**, *2*, 213–214. (b) Keinan, E.; Perez, D. *J. Org. Chem.* **1987**, *52*, 2576–2580.
- (39) (a) Watanabe, T.; Hashimoto, H.; Tobita, H. *J. Am. Chem. Soc.* **2006**, *128*, 2176–2177. (b) Watanabe, T.; Hashimoto, H.; Tobita, H. *Angew. Chem., Int. Ed.* **2004**, *43*, 218–221.
- (40) (a) Díez-González, S.; Kaur, H.; Zinn, F. K.; Stevens, E. D.; Nolan, S. P. *J. Org. Chem.* **2005**, *70*, 4784–4796. (b) Lee, D.-L.; Yun, J. *Tetrahedron Lett.* **2004**, *45*, 5415–5417. (c) Lipshutz, B. H.; Noson, K.; Chrisman, W. *J. Am. Chem. Soc.* **2001**, *123*, 12917–12918. (d) Chen, J.-X.; Daeuble, J. F.; Stryker, J. M. *Tetrahedron* **2000**, *56*, 2789–2798.
- (41) (a) Schroeder, M. A.; Wrighton, M. S. *J. Am. Chem. Soc.* **1976**, *98*, 551–558. (b) Schroeder, M. A.; Wrighton, M. S. *J. Organomet. Chem.* **1977**, *128*, 345–358. (c) Archer, A. M.; Bouwkamp, M. W.; Cortez, M.-P.; Lobkovsky, E.; Chirik, P. J. *Organometallics* **2006**, *25*, 4269–4278. (d) Nishiyama, H.; Furuta, A. *Chem. Commun.* **2007**, 760–762.
- (42) Barnea, E.; Eisen, M. S. *Coord. Chem. Rev.* **2006**, *250*, 855–899.

- (43) (a) Chalk, A. J.; Harrod, J. F. *J. Am. Chem. Soc.* **1967**, *89*, 1640–1647. (b) Chalk, A. J.; Harrod, J. F. *J. Am. Chem. Soc.* **1965**, *87*, 16–21. (c) Harrod, J. F.; Chalk, A. J. *J. Am. Chem. Soc.* **1965**, *87*, 1133–1135.
- (44) Duckett, S. B.; Perutz, R. H. *Organometallics* **1992**, *11*, 90–98.
- (45) (a) Jun, C. H.; Crabtree, R. H. *J. Organomet. Chem.* **1993**, *447*, 177–187. (b) Ojima, I.; Clos, N.; Donovan, R. J.; Ingallina, P. *Organometallics* **1990**, *9*, 3127–3133.
- (46) Glaser, P. B.; Tilley, T. D. *J. Am. Chem. Soc.* **2003**, *125*, 13640–13641.
- (47) (a) Gountchev, T. I.; Tilley, T. D. *Organometallics* **1999**, *18*, 5661–5667. (b) Kesti, M. R.; Waymouth, R. M. *Organometallics* **1992**, *11*, 1095–1103.
- (48) Bart, S. C.; Lobkovsky, E.; Chirik, P. J. *J. Am. Chem. Soc.* **2004**, *126*, 13794–13807.
- (49) Son, D. Y.; Bucca, D.; Keller, T. M. *Tetrahedron Lett.* **1996**, *37*, 1579–1582.
- (50) Perry, R. J.; Karageorgis, M.; Hensler, J. *Macromolecules* **2007**, *40*, 3929–3938.
- (51) Kobayashi, T.; Hayashi, T.; Tanaka, M. *Chem. Lett.* **1998**, 763–764.
- (52) Korshak, V. V.; Sladkov, A. M.; Luneva, L. K. *Izv. Akad. Nauk SSSR, Otd. Khim. Nauk* **1962**, 2251–2253.
- (53) Kim, D. S.; Shim, S. C. *J. Polym. Sci., A: Polym. Chem.* **1999**, *37*, 2933–2940.
- (54) Mori, A.; Takahisa, E.; Kajiro, H.; Nishihara, Y. *Macromolecules* **2000**, *33*, 1115–1116.
- (55) Sumiya, K.-I.; Kwak, G.; Sanda, F.; Masuda, T. *J. Polym. Sci., Part A: Polym. Chem.* **2004**, *42*, 2774–2783.
- (56) Yamashita, H.; de Leon, M. S.; Channasanon, S.; Suzuki, Y.; Uchimaru, Y.; Takeuchi, K. *Polymer* **2003**, *44*, 7089–7093.
- (57) (a) Son, H.-J.; Han, W.-S.; Kim, H.; Kim, C.; Ko, J.; Lee, C.; Kang, S. O. *Organometallics* **2006**, *25*, 766–774. (b) Lee, T.; Jung, I.; Song, K. H.; Baik, C.; Kim, S.; Kim, D.; Kang, S. O.; Ko, J. *Organometallics* **2004**, *23*, 4184–4191.

- (58) Kwak, G.; Masuda, T. *Macromol. Rapid. Commun.* **2002**, *23*, 68–72.
- (59) (a) Guo, A.; Fry, B. E.; Neckers, D. C. *Chem. Mater.* **1998**, *10*, 531–536. (b) Fry, B. E.; Guo, A.; Neckers, D. C. *J. Organomet. Chem.* **1997**, *538*, 151–162. (c) Fry, B. E.; Neckers, D. C. *Macromolecules* **1996**, *29*, 5306–5312. (d) Lewis, F. D.; Salvi, G. D. *Inorg. Chem.* **1995**, *34*, 3182–3189.
- (60) (a) Yamaguchi, S.; Endo, T.; Uchida, M.; Izumizawa, T.; Furukawa, K.; Tamao, K. *Chem. Eur. J.* **2000**, *6*, 1683–1692. (b) Sohn, H.; Huddleston, R. R.; Powell, D. R.; West, R. *J. Am. Chem. Soc.* **1999**, *121*, 2935–2936. (c) Xu, Y.; Fujino, T.; Naito, H.; Dohmaru, T.; Oka, K.; Sohn, H.; West, R. *Jpn. J. Appl. Phys.* **1999**, *38*, 6915–6918. (d) Tamao, K.; Uchida, M.; Izumizawa, T.; Furukawa, K.; Yamaguchi, S. *J. Am. Chem. Soc.* **1996**, *118*, 11974–11975.
- (61) (a) Yu, G.; Yin, S.; Liu, Y.; Chen, J.; Xu, X.; Sun, X.; Ma, D.; Zhan, X.; Peng, Q.; Shuai, Z.; Tang, B.; Zhu, D.; Fang, W.; Luo, Y. *J. Am. Chem. Soc.* **2005**, *127*, 6335–6346. (b) West, R.; Sohn, H.; Powell, D. R.; Mueller, T.; Apeloig, Y. *Angew. Chem., Int. Ed. Engl.* **1996**, *35*, 1002–1004. (c) Yamaguchi, Y. *Synthetic Met.* **1996**, *82*, 149–153. (d) West, R.; Sohn, H.; Bankwitz, U.; Calabrese, J.; Apeloig, Y.; Mueller, T. *J. Am. Chem. Soc.* **1995**, *117*, 11608–11609. (e) Khabashesku, V. N.; Balaji, V.; Boganov, S. E.; Nefedov, O. M.; Michl, J. *J. Am. Chem. Soc.* **1994**, *116*, 320–329.
- (62) (a) Chen, J.; Cao, Y. *Macromol. Rapid. Commun.* **2007**, *28*, 1714–1742. (b) Hissler, M.; Dyer, P. W.; Réau, R. *Coord. Chem. Rev.* **2003**, *244*, 1–44. (c) Yamaguchi, S.; Tamao, K. *J. Organomet. Chem.* **2002**, *653*, 223–228.
- (63) Toal, S. J.; Sohn, H.; Zakarov, L. N.; Kassel, W. S.; Golen, J. A.; Rheingold, A. L.; Trogler, W. C. *Organometallics* **2005**, *24*, 3081–3087.
- (64) (a) Moore, D. S. *Rev. Sci. Instrum.* **2004**, *75*, 2499–2512. (b) Singh, S. *J. Hazard. Mater.* **2007**, *144*, 15–28.
- (65) Steinfeld, J. I.; Wormhoudt, J. *Annu. Rev. Phys. Chem.* **1998**, *49*, 203–232.
- (66) Smith, K. D.; McCord, B. R.; McCrehan, W. A.; Mount, K.; Rowe, W. F. *J. Foren. Sci.* **1999**, *44*, 789–794.
- (67) Rouhi, A. M. *Chem. Eng. News.* **1997**, *75*, 14–22.
- (68) Federal Register, 67, No. 81, 20864–20866 (2002).
- (69) (a) Hakansson, K.; Coorey, R. V.; Zubarev, R. A.; Talrose, V. L.; Hakansson, P. *J. Mass. Spectrom.* **2000**, *35*, 337–346. (b) Smith, K. D.; McCord, B. R.;

- McCrehan, W. A.; Mount, K.; Rowe, W. F. *J. Foren. Sci.* **1999**, *44*, 789–794. (c) Sylvia, J. M.; Janni, J. A.; Klein, J. D.; Spencer, K. M. *Anal. Chem.* **2000**, *72*, 5834–5840. (d) Popov, I. A.; Chen, H.; Kharybin, O. N.; Nikolaev, E. N.; Cooks, R. G. *Chem. Commun.* **2005**, *15*, 1953–1955. (e) Kolla, P. *Anal. Chem.* **1995**, *67*, 184A–189A. (f) XPRAY Field Test Kit available from Mistral Group, Web URL: http://www.mistralgroup.com/SEC_explosives.asp.
- (70) Trogler, W. C. In *Electronic Noses & Sensors for the Detection of Explosives*; Gardner, J. W., Yinon, J., Eds.; Kluwer Academic Publishers: 2004; p 39.
- (71) Mostak, P. In *Vapour and Trace Detection of Explosives for Anti-terrorism Purposes*; Krausa, M., Reznev, A. A., Eds.; Kluwer Academic Publishers: 2004; p 23.
- (72) Davidson, W. R.; Stott, W. R.; Sleeman, R.; Akery, A. K. *Proc. SPIE* **1994**, *2092*, 108–119.
- (73) (a) Hansen, H. J. *Proc. IEEE* **2007**, *95*, 1691–1704. (b) Gottfried, J. L.; De Lucia, F. C., Jr.; Munson, C. A.; Miziolek, A. W. *J. Anal. At. Spectrom.* **2008**, *23*, 205–216.
- (74) (a) Davies, J. P.; Hallowell, S. F.; Hoglund, D. E. *Proc. SPIE* **1994**, *2092*, 137–144. (b) Elias, L. *J. Test. Eval.* **1994**, *22*, 280–281. (c) Neudorfl, P.; McCooeye, M. A.; Elias, L. In *Proc. Int. Symp. Anal. Detect. Expl.*, 4th, London; Yinon, J., Ed.; Kluwer: Dordrecht, 1992; pp 373–384.
- (75) (a) Yinon, J.; Zitrin, S. In *Modern Methods and Applications in Analysis of Explosives*; Wiley: Chichester, 1993. (b) Gresham, G. L.; Davies, J. P.; Goodrich, L. D.; Blackwood, L.G.; Liu, B. Y.; Thimsen, D.; Yoo, S. H. *Proc. SPIE* **1994**, *2276*, 34–44.
- (76) Oxley, J. C.; Smith, J. L.; Kirschenbaum, L. J.; Marimnganti, S. *J. Foren. Sci.* **2007**, *52*, 1291–1296.
- (77) (a) Moore, D. S. Los Alamos Report LAUR-03-1665 (2003). (b) Yinon, J. *Trends Analyt. Chem.* **2002**, *21*, 292–301. (c) Bruschini, C. ExploStudy, Final Report, Ecole Polytechnique Federale de Lausanne, Web URL: <http://diwww.epfl.ch/lami/detec/> (2001). (d) Urbansky, E. T. *Crit. Rev. Anal. Chem.* **2000**, *30*, 311–343. (e) Yinon, J. In *Forensic and Environmental Detection of Explosives*; Wiley: Chichester, 1999. (g) Nyden, M. R. *A Technical Assessment of Portable Explosives Vapor Detection Devices*, NII Rep. 300-89; NIST: Gaithersburg, MD, 1990. (h) Yinon, J. *Crit. Rev. Anal. Chem.* **1977**, *7*, 1–35.

- (78) Committee on Assessment of Security Technologies for Transportation, Opportunities to Improve Airport Passenger Screening with Mass Spectrometry (National Academy of Sciences, Washington, D.C., 2003).
- (79) Plexus Scientific Corporation. <http://www.plexsci.com/expray.shtml> (27 Nov 2006).
- (80) (a) Wampler, S. Lawrence Livermore National Laboratory. <http://www-cms.llnl.gov/s-t/elite.html> (27 Nov 2006). (b) Dynes, R. C. *President's Report; Report 16(6)*: May 2006.
- (81) (a) McQuade, D. T.; Pullen, A. E.; Swager, T. M. *Chem. Rev.* **2000**, *100*, 2537–2574. (b) Toal, S. J.; Trogler, W. C. *J. Mater. Chem.* **2006**, *16*, 2871–2883. (c) Liu, Y.; Mills, R.; Boncella, J.; Schanze, K. *Langmuir* **2001**, *17*, 7452–7455. (d) Chang, C.; Chao, C.; Huang, J. H.; Li, A.; Hsu, C.; Lin, M.; Hsieh, B.; Su, A. *Synth. Met.* **2004**, *144*, 297–301.
- (82) (a) Toal, S. J.; Jones, K. A.; Magde, D.; Trogler, W. C. *J. Am. Chem. Soc.* **2005**, *127*, 11661–11665. (b) Toal, S. J.; Magde, D.; Trogler, W. C. *Chem. Comm.* **2005**, *43*, 5465–5467. (c) Sohn, H.; Sailor, M. J.; Douglas, M.; Trogler, W. C. *J. Am. Chem. Soc.* **2003**, *123*, 3821–3830. (d) Sohn, H.; Calhoun, R. M.; Sailor, M. J.; Trogler, W. C. *Angew. Chem., Int. Ed. Engl.* **2001**, *40*, 2104–2105.
- (83) Toal, S. J.; Sanchez, J. C.; Dugan, R. E.; Trogler, W. C. *J. Foren. Sci.* **2007**, *52*, 79–83.
- (84) Seki, K.; Furuyama, T.; Kawasumi, T.; Sakurai, Y.; Ishii, H.; Kajikawa, K.; Ouchi, Y.; Masuda, T. *J. Phys. Chem. B* **1997**, *101*, 9165–9169.
- (85) Schulte-Ladbeck, R.; Vogel, M.; Karst, U. *Anal. Bioanal. Chem.* **2006**, *386*, 559–565.

CHAPTER II

Synthesis, Characterization, and Evaluation 1,1-Tetraphenylsilole- and 1,1-Silafluorene-vinylene Polymers for Explosives Detection

2.1 ABSTRACT

The syntheses, spectroscopic characterizations, and fluorescence quenching efficiencies of polymers and copolymers containing (tetraphenyl)silole- or silafluorene-vinylene repeat units are reported. These materials were prepared by catalytic hydrosilylation reactions between appropriate monomeric metallole alkynes and hydrides. Trimeric model compounds methyl(tetraphenyl)silole-vinylene trimer (**1**), methyl(tetraphenyl)silole-silafluorene-vinylene cotrimer (**2**) and methylsilafluorene-vinylene trimer (**3**) were synthesized to provide detailed structural and spectroscopic characteristics of the polymer backbone and to assess the extent of delocalization in the luminescent excited-state. Poly((tetraphenyl)silole-vinylene) (**4**), poly((tetraphenyl)silole-silafluorene-vinylene) (**5**) and poly(silafluorene-vinylene) (**6**) maintain a regio-regular *trans*-vinylene Si-C backbone with possible ground state σ^* - π and excited state σ^* - π^* conjugation through the vinylene bridge between metallole units. Fluorescence spectra of the polymers show a ~ 13 nm (1030 - 550 cm^{-1}) bathochromic shift in λ_{flu} from their respective model compounds. Molecular weights (M_n) for these polymers and copolymers are in the range of 4000-4500. Detection of nitroaromatic explosives by solution-phase fluorescence quenching of polymers **4-6** was observed with Stern-Volmer constants in the range of 400~20 000 for TNT, DNT, and picric acid (PA). A surface detection method for the analysis of solid particulates of TNT, DNT, PA, RDX, HMX, Tetryl, TNG and PETN is also described for silafluorene containing polymers. Polymer **6** exhibited detection for all the preceding types of explosive residues with a 200 pg cm^{-2} detection limit for Tetryl. Polymers **4**

and **5** only exhibited luminescence quenching with nitroaromatic explosives, revealing that the excited-state energy of the sensor plays a key role in the fluorescence detection of explosives.

2.2 INTRODUCTION

Reliable detection of trace explosive materials has become a focal point in security screening methods. Applications such as minefield remediation,¹ crime scene investigations,² and counter-terrorism activities (e.g., facility protection and personnel, baggage, and cargo screening³) are areas of concern. Instrumental techniques include gas chromatography coupled with mass spectrometry,⁴ gas chromatography-electron capture detection,² surface-enhanced Raman spectroscopy,⁵ mass spectrometry,⁶ X-ray imaging, nuclear quadrupole resonance, thermal and fast neutron analysis, and ion mobility spectrometry.⁷ Approaches have been adapted for both bulk and trace detection methods to analyze suspicious materials, personnel, and cargo. Cost, complexity, and robust portability are problematic for many of these methods.

Conventional spectroscopic and imaging techniques typically employ bulk or vapor phase sampling. As described in a previous report,⁸ vapor sampling may be limited by the low volatility of many explosives at room temperature. Nitroaromatic explosives such as TNT have moderate vapor pressures (7×10^{-6} Torr at room temperature), but at low surface concentrations the vapor concentration of TNT is significantly less than its equilibrium vapor pressure.⁹ Explosives, such as RDX and HMX, have substantially lower vapor pressures (5×10^{-9} and 8×10^{-11} Torr, respectively), which makes vapor detection of these compounds difficult.¹⁰

An alternative to vapor sampling is the chemical analysis of solid particulates that remain after the handling of explosive materials.¹¹ This includes colorimetric and fluorescence sensing devices that take advantage of human visual processing power,

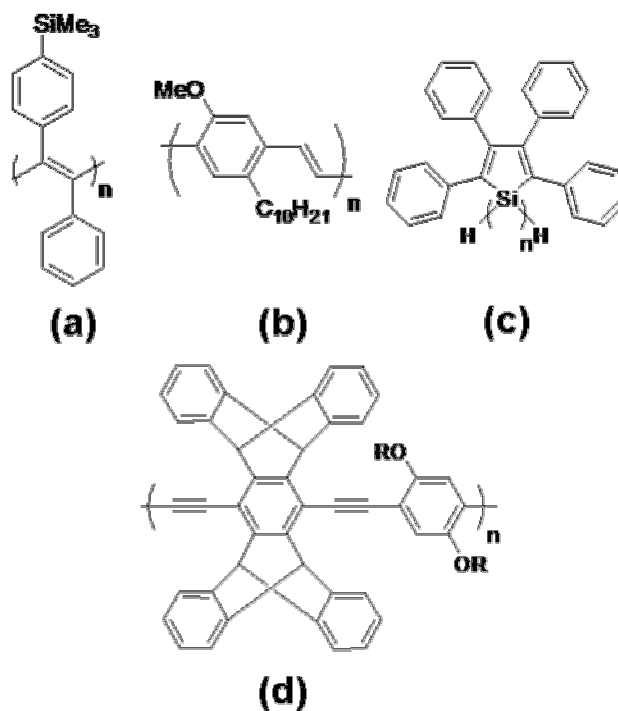


Figure 2-1. Conjugated fluorescent polymers for explosives detection: (a) polyacetylene PTMSDPA, (b) poly(*p*-phenylenevinylene) DP10-PPV, (c) 1,1-poly(tetraphenyl)silole, (d) poly(*p*-phenylene-ethynylene).

rather than instrumental evaluation.¹²⁻¹⁴ The use of fluorescent polymers for the detection of explosive vapors and particulates has been adapted for both instrumental and visual imaging approaches (Figure 2-1).¹⁴ Poly(tetraphenyl)siloles, in particular, have the advantage of ease of synthesis and their ability to semi-selectively bind explosive analytes (Figure 2-1c).¹⁵ Previous reports have demonstrated the ability of 1,1-poly(tetraphenyl)silole to image trace particulates of explosive materials in the solid-state.^{15d,8} However, no single polymer has been able to detect the entire range of common high explosives by a fluorescence quenching mechanism, in part due the broad range of reduction potentials found among explosive materials. The use of a wide band-gap polymer should create optimal energy overlap with a more extensive

collection of explosive materials. However, there remain relatively few examples of stable conjugated polymers that emit in the UV-blue region of the spectrum.¹⁶

Siloles, such as silicon-containing 2,3,4,5-(tetraphenyl)silacyclopentadienes, are highly luminescent in the solid-state.¹⁷ Their unique photo-electronic properties arise from conjugation between the σ^* orbitals of the bridging silicon and the π^* orbital of the metallole butadiene fragment.¹⁸ Silafluorene derivatives possess similar core electronic features but their biphenyl framework increases the band-gap energy, allowing for UV-blue emission. Both metalloles have been studied as electron-transporting materials,¹⁹ OLED materials²⁰ and inorganic polymer sensors.^{15,8} Typical synthetic routes to metallole polymers include Suzuki,²¹ Sonogashira,²² and various coupling reactions^{20a,23} through positions on the aromatic systems. There are only a few examples of metallole polymerization in the 1,1 positions (dehydrocoupling and Wurtz coupling) and only one claim of polysilafluorene, which is Si-Si coupled in the 1,1 positions.²⁴ Polymerization via the 1,1 positions is attractive because fluorescent properties of the metallole ring will not be altered significantly and the coiled polymer structures obtained may prevent π -stacking and self-quenching in thin-film applications. This synthetic approach also requires fewer steps and may provide soluble polymers as a result of the flexible structure. Although Si-Si coupled polymers containing (tetraphenyl)silole have been prepared,²³ 1,1-silafluorene polymers have not been studied due to the tendency of 1,1-dihydridosilafluorene to yield cyclic structures.^{20a,b}

Conjugated organic poly(vinylene)s have been investigated extensively as electron-transporting materials and electroluminescent materials.²⁵ It would be desirable to prepare metallole-vinylene polymers that incorporate conjugation between metallole centers. Hydrosilylation is a technique often used in silane chemistry to form silicon-vinylene functionalities.²⁶ Addition of the Si-H bond across a carbon-carbon triple bond yields a vinylene product, that extends the conjugation and diminished the band-gap in the polymeric material.²⁷ An attractive feature of polycarbosilanes is the presence of a strong Si-C backbone, as compared to the weaker Si-Si backbone in poly(tetraphenyl)silole.

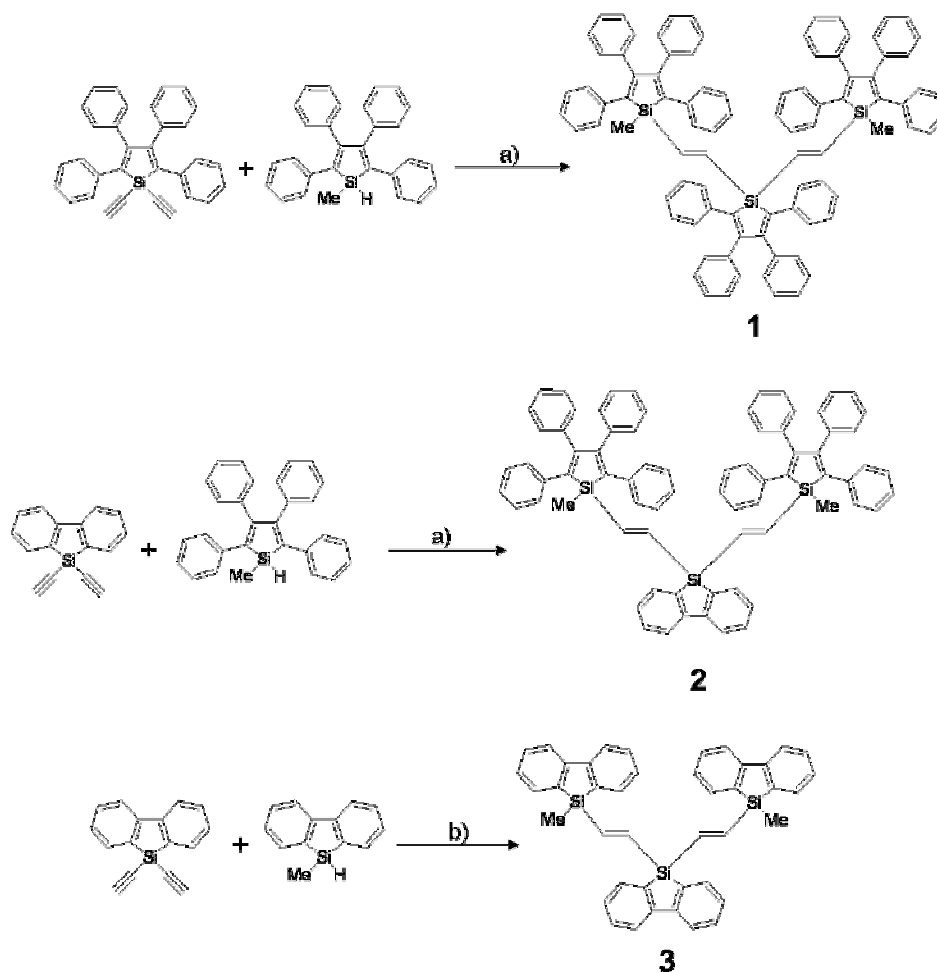
This chapter reports the synthesis of poly((tetraphenyl)silole-vinylene), a poly((tetraphenyl)silole-silafluorene-vinylene) and poly(silafluorene-vinylene) by catalytic hydrosilylation. This method provides a facile synthetic route to regio-regular polymers that retain the inherent electronic properties of the monomers, yet incorporate partial delocalization as evidenced by a bathochromic shift in the fluorescence spectra. These polymers include 2,3,4,5-(tetraphenyl)silole and silafluorene moieties directly conjugated through bridging vinylenes by $\sigma^*-\pi/\pi^*$ conjugation. This provides one of the first examples of polymerization of silafluorene in the 1,1-position yielding a UV-blue emitting material. In addition, a new method for the surface detection of TNT, DNT, picric acid (PA), RDX, HMX, Tetryl, TNG and PETN particulates by an amplified fluorescence quenching pathway is described. Visual detection limits down to the picogram level were achieved. This method allows for efficient sampling of high priority, low volatility explosives such as RDX, HMX

and PETN. *Ab initio* density functional theory (DFT) calculations were used to probe energetic properties of the donor and acceptor on the detection process. In addition, ^{29}Si NMR spectra provided evidence for Lewis acid-base interactions between basic oxygen atoms of the high explosive molecules and the Si atom of the silacycle chromophore. Poly(silafluorene-vinylene) provides the best energy matching and analyte binding for the explosives studied and proves to be an effective luminescent sensor for both nitroaromatics and the nitrate ester-nitramine classes of explosives.

2.3 RESULTS AND DISCUSSION

2.3.1 Model Compounds

Structural characterization of metallole polymers can be challenging because of peak broadening in the ^1H NMR spectrum, irregular stereochemistry, and the lack of spectroscopically distinct terminal groups. In an effort to gain insight into the structure and reactivity of new metallole-vinylene polymers, model trimeric complexes were first synthesized. As seen in Scheme 2-1, trimers **1-3** were prepared using combinations of various monomers. Yields and analytical purities after several precipitations were good. Elemental analysis of even the highly crystalline materials yielded slightly low carbon analyses, presumably due to the formation of silicon carbide in the combustion analysis. This problem was greater in the polymers for which ^{29}Si NMR spectra (*vide infra*) also revealed Lewis acidic character, which leads to entrainment of water. ^1H NMR spectra are included in the supplementary material to demonstrate purity and entrapped water.



Scheme 2-1. Synthetic routes to the trimeric model compounds. a) H_2PtCl_6 , toluene, 70°C , 3 h; b) H_2PtCl_6 , toluene, 50°C , 2 h.

Analysis of the reaction mixture at varying temperatures revealed a high selectivity for hydrosilylation over dehydrocoupling at lower reaction temperatures. The use of thermal control to minimize the dehydrocoupling pathway has been demonstrated previously.²³ Hydrosilylation may also produce both *cis*- and *trans*-products, depending on the steric bulk surrounding the ethynyl functionality. It was important to confirm the stereochemistry in the model compounds, so that the regio-regularity of the key polymerization step was defined. In the case of the silafluorene

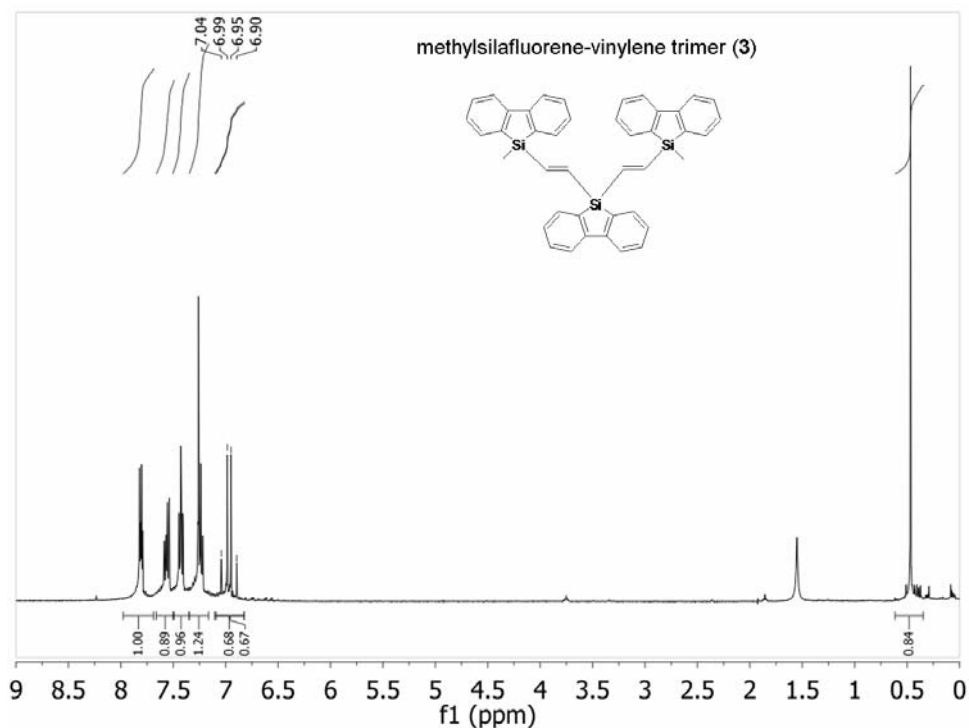


Figure 2-2. ^1H NMR spectrum of **3**.

trimer **3**, ^1H NMR characterization revealed a *trans*-product (Figure 2-2). Doublets representing the vinylene hydrogens appear at 7.02 ppm and 6.93 ppm in the ^1H NMR spectrum. Coupling constants of 22.2 and 22.8 Hz, respectively, are close to the 19 Hz observed for silane substituted *trans*-vinylene products.²⁸ This result was promising because previous attempts to polymerize secondary silanes by hydrosilylation of simple aryl acetylenes failed to provide regio-regular products due to the low steric hindrance around the silicon atom.²⁹ By placing the ethynyl functionalities directly on the silafluorene, hydrosilylation proceeded exclusively (>98% by NMR) to *trans*-product.

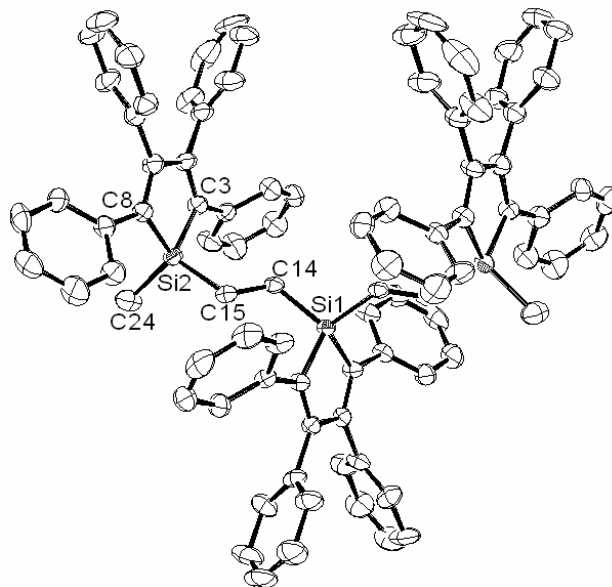


Figure 2-3. Thermal ellipsoid plot of **1** at the 50% probability level. Hydrogen atoms were excluded for clarity. Selected bond lengths, (Å): C14-C15 1.309(3); and angles, (deg): Si2-C15-C14 127.1(2), C15-C14-Si1 124.1(2), C8-Si2-C3 92.55(11), C24-Si2-C15 107.64(12).

Trimers **1** and **2** were more difficult to characterize by NMR spectroscopy because of overlap between the vinylic hydrogens and the phenyl proton resonances. However, the more sterically hindered (tetraphenyl)silole should have an even greater preference for the *trans*-product than silafluorene. An attempt to obtain X-ray quality crystals for the trimers proved unsuccessful for the silafluorene containing trimers **2** and **3** but successful for trimer **1**. The structure reveals a *trans*-only product (Figure 2-3). Yields obtained after recrystallization only slightly decreased from 73% to 68%, showing that the crystals indeed contain the predominant isomer. The vinylene moiety C14-C15 has a bond length of 1.309(3) Å, which is typical for carbon-carbon double bonds. The torsion angles for Si2-C15-C14 and C15-C14-Si1 are 127.1(2)° and 124.1(2)°, respectively. The former is slightly higher presumably due to steric

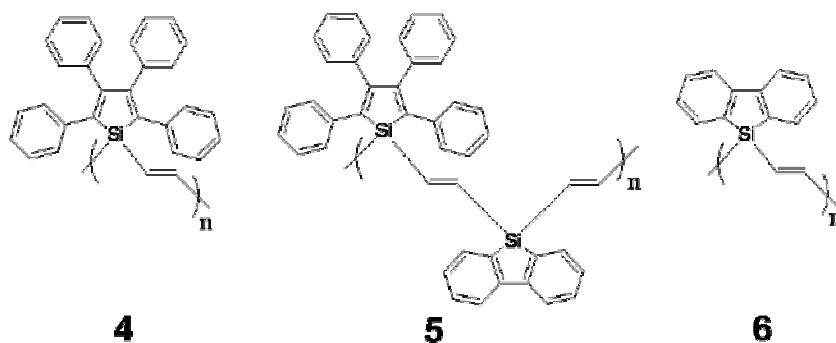


Figure 2-4. Chemical structures of (tetraphenyl)silole- and silafluorene-vinylene polymers.

interactions between the phenyl substituents of the outer two silole moieties. The internal torsion angle for C8-Si2-C3 is $92.55(11)^\circ$, which is close to a typical value of $93.21(6)^\circ$ observed for silacyclopentadienes.²³ These strained silacycles expose the silicon center to attack by Lewis bases, which will prove to be an important feature for the binding of explosive analytes. Since both 1,1-diethynyl(tetraphenyl)silole (DEsilole) and 1,1-diethynylsilafluorene (DESF) sterically direct *cis*-addition during hydrosilylation, it was concluded that trimer **2** was structurally similar.

2.3.2 Polymerizations

With spectroscopic and structural evidence from the model compounds showing that hydrosilylation affords a regio-regular *trans*-product in good yield, polymers **4-6** were synthesized under similar conditions using 1,1-diethynyl functionalized monomers (Figure 2-4). Reaction progress was monitored by ^1H NMR spectroscopy. Polymerization was complete in all cases after 24 h at 70°C or 48 h at 50°C . However, increased molecular weights are observed for reactions at 70°C . The

Table 2-1. Results of catalytic hydrosilylation syntheses of polymers **4-6**.

Polymer	Yield (%) ^a	M _w (GPC)	(M _w /M _n) ^b	n
4	73	4000	1.15	10
5	71	4500	1.24	8
6	66	4300	1.37	21
Poly(tetraphenyl)silole	88	1500	1.1	4

^a Calculated after 3 precipitations from methanol; ^b Calculated by GPC.

polymers are soluble in common organic solvents including dichloromethane, toluene, tetrahydrofuran and ethyl acetate. Low molecular weight oligomers, which are present as minor byproducts, may be removed by repeated precipitations from methanol.

Molecular weights were determined by GPC (Table 2-1). The molecular weights of polymers **4-6** are slightly higher than those observed for poly(tetraphenyl)silole.²³ They also incorporate a Si-C backbone rather than a Si-Si backbone, whose bonds differ in strength by $\sim 150 \text{ kJ mol}^{-1}$. These polymers are expected to adopt a helical structure similar to poly(tetraphenyl)silole (Figure 2-5). Both polymers **4** and **6** have a more open structure than poly(tetraphenyl)silole. The phenyl substituents around the silacyclopentadiene frame of polymer **4** hinder access to the silicon centers. However, the more porous structure of polymer **6** may allow for effective analyte binding to the Lewis acidic silicon atom.

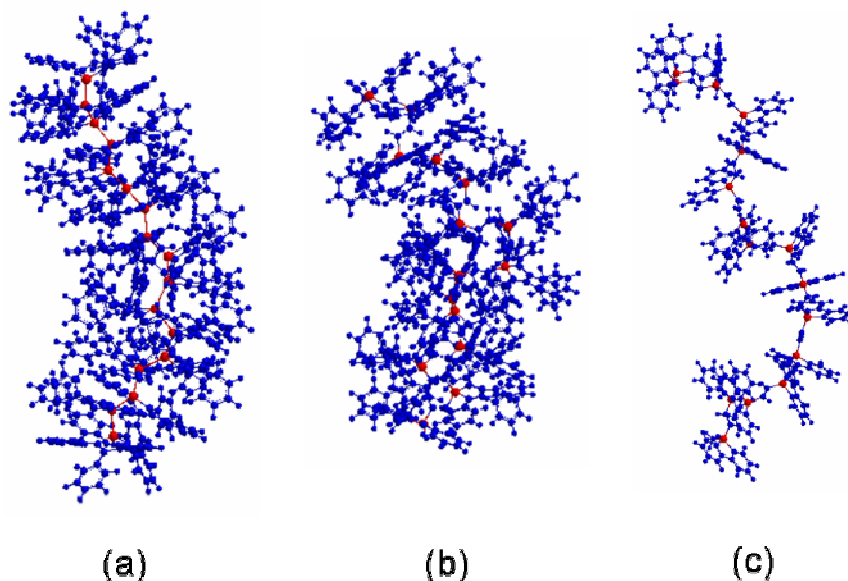


Figure 2-5. Structural comparison of (a) poly(tetraphenyl)silole $n = 17$; (b) **4** $n = 15$; (c) **6** $n = 16$. Red atoms represent the silicon backbone. Polymer structures were simulated using Molecular Mechanics on Chem3D Ultra 9.0.

2.3.3 Photoluminescence

2.3.3.1 Solution-phase Photoluminescence

Photoluminescence (PL) data was collected on the monomer, trimer, and polymer materials synthesized in this study (Table 2-2). Polymers **4-6** exhibited a ~ 13 nm ($1030\text{-}550\text{ cm}^{-1}$) bathochromic shift in λ_{flu} from their analogous trimer complexes **1-3** along with broadening toward the low energy side of the emission band (Figure 2-6). These features suggest an increase in delocalization through the backbone with increasing chain length. Delocalization is more commonly observed in rigid phenylene-type polymers where bridging alkynyl functionalities allow for a high degree of conjugation between monomer units.³⁰ However, similar delocalization is seen in poly(tetraphenyl)silole where a red-shift in fluorescence is a result of $\sigma\text{-}\sigma^*$

Table 2-2. Summary of photoluminescence data for monomers, trimers, and polymers.

Metallole	λ_{abs} (nm) ^a	ϵ_{max} (L mol ⁻¹ cm ⁻¹) ^b	Solution λ_{flu} (nm) ^a	Thin-film λ_{flu} (nm) ^c	Φ_{flu} ^d (%)
DEsilole	305, 390	7500	490	485	0.13
DESF	291, 324	7700	356	365	24
1	304, 388	18 000 ^e	480	487	0.40
2	296, 381	9400 ^e	478	483	0.30
3	290	20 400 ^e	349	357	6.1
4	304, 389	2900	493	490	1.0
5	297, 390	1800	492	486	2.0
6	294	6300	362	376	4.3

^a UV-vis and fluorescence taken in toluene; ^b Absorptivities are calculated per mole of metalloid; ^c Emission maximum for thin layer of fluorophore absorbed onto TLC plate; ^d Quantum yield of fluorescence $\pm 30\%$, relative to 9,10-diphenylanthracene³¹ in toluene; ^e Absorptivities per metallole are 1/3rd the reported value.

conjugation of the Si-Si backbone.²³ In the present case, the vinylene bridge of polymers **4-6** allows partial $\sigma^*(\text{Si-C})-\pi(\text{vinylene})$ conjugation along the backbone in the ground state and $\sigma^*(\text{Si-C})-\pi^*(\text{vinylene})$ conjugation in the lowest excited state (Figure 2-7). The crystal structure of **1** reveals a RMS out-of-plane angle between the two vinylene bridges of 76.7°. This orientation, with respect to the face of the silole ring, is such that the π -orbitals involved in the carbon-carbon double bond are directed toward the σ^* and π^* orbitals of the silole ring. Orbital overlap thereby allows for delocalization throughout the polymer via the bridging vinylene. This is supported by density functional theory (DFT) calculations presented later. Polymer **5** shows an emission band at 492 nm, which is similar to polymer **4** and characteristic of (tetraphenyl)silole emission. The lack of emission from the silafluorene moiety of

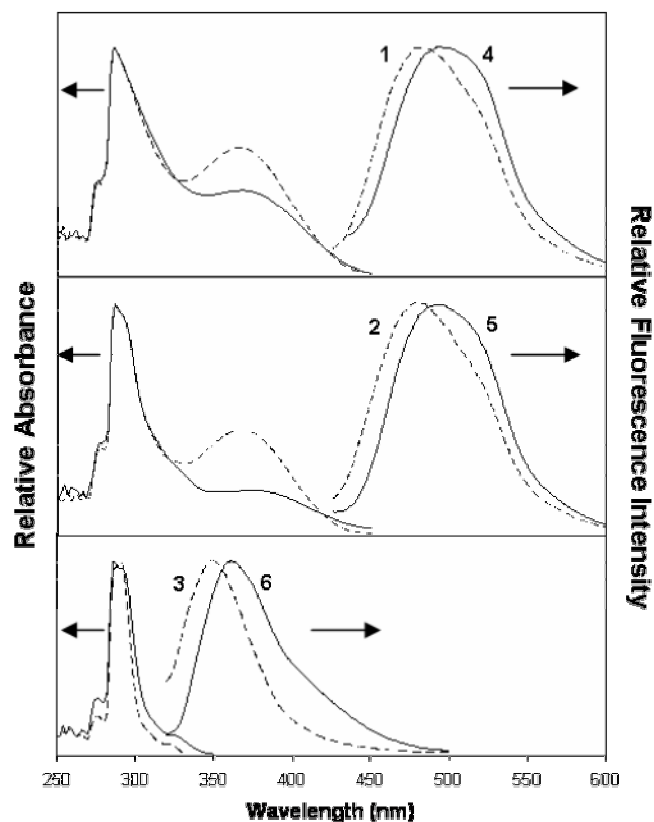


Figure 2-6. UV-vis and fluorescence spectra of model trimers **1-3** (dotted lines) as compared with polymers **4-6** (solid lines) showing a bathochromic emission shift for the polymers.

polymer **5** also suggests the presence of electronic communication through the polymer chain. It is typical for (tetraphenyl)siloles, which have a lower LUMO than silafluorenes, to act as sinks for excitons in delocalized copolymer systems.³¹

2.3.3.2 Solid-state Photoluminescence

Solid-state PL data was collected to determine the effect of aggregation during thin-film explosives detection studies. Two different techniques were used. The first method involved spin-casting toluene solutions of the materials onto quartz discs.³²

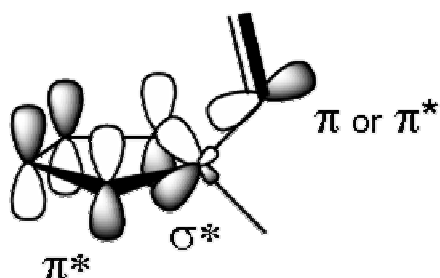


Figure 2-7. Depiction of the orbital overlap between the vinylene bridge and LUMO of the silacyclopentadiene ring. Structural orientation is based on the crystal structure data of trimer **1**. Phenyl rings and hydrogens are omitted for clarity. The π^* (butadiene)- σ^* (Si) orbital overlap forms the LUMO of the silole moiety. The π orbital of the vinylene bridge overlaps with the silole LUMO accounting for ground state orientation in **1**. In the excited state overlap of the π^* vinylene orbital with the silole LUMO is observed in the DFT calculations (supplementary material LUMO figure e) and accounts for red shifting of the emission spectra in metallole polymers **4-6**.

This technique has widely used for solid-state fluorescence characterization of functional polymeric materials. Quartz provides a smooth, UV-transparent surface and the emission spectrum of the film reflects polymer stacking effects. However, this method requires a high solubility of the polymer in appropriate volatility solvents, high molecular weights for casting uniform films, large amounts of sample, and is expensive and time-consuming.³³ The second method employs absorption of the polymer dissolved in CHCl_3 (4.0 mg mL^{-1}) spotted onto the silica gel of a thin-layer chromatography (TLC) plate. This technique was used by Tang et al. to more conveniently analyze the solid-state PL properties of various (tetraphenyl)siloles with good reproducibility.³⁴ The silica surface is porous and adsorption may alter the packing properties of more rigid polymers, such as **7**. Both methods were studied to

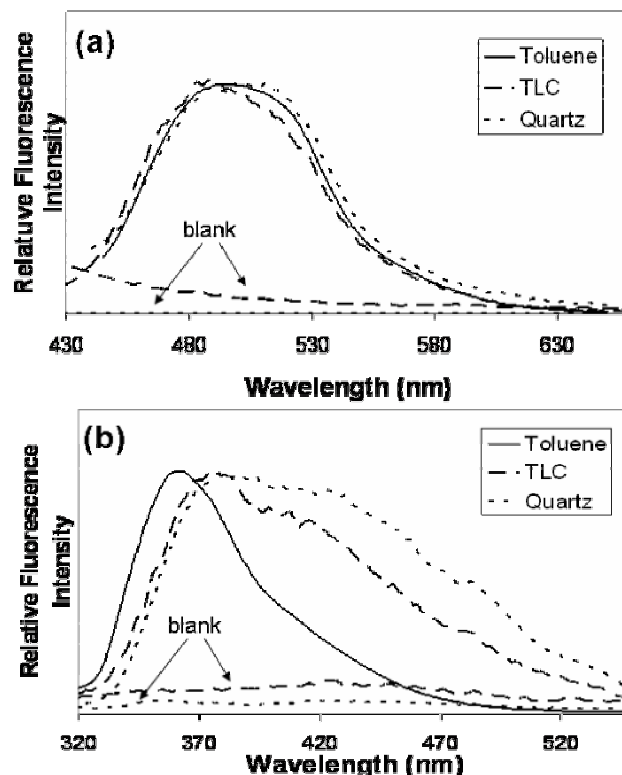


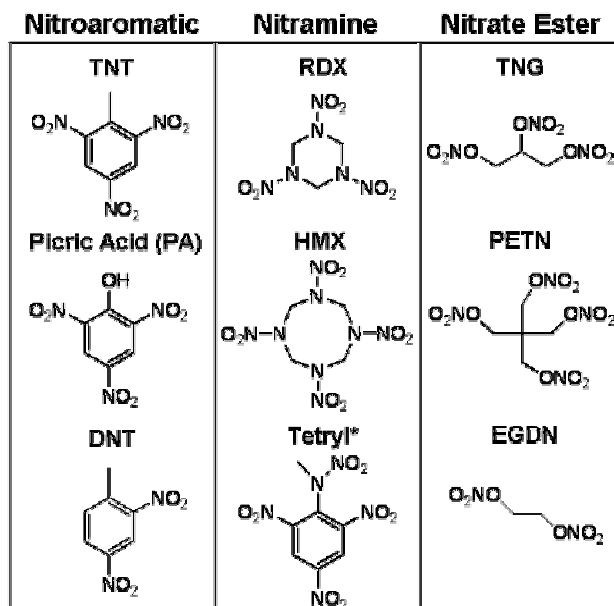
Figure 2-8. Solid-state photoluminescence data for polymers **4** (a) and **5** (b) collected on silica TLC plates and quartz discs. Data for a blank TLC plate and a blank quartz disc are shown.

gain insight into the solid-state spectral properties. Figure 2-8 compares these different approaches with the solution-phase fluorescence spectra of polymers **4** and **6**. Polymer **4** shows no significant change in λ_{flu} for each substrate used. This suggests that there is minimal inter-chain electronic communication in the solid-state and that the TLC method is a useful and spectroscopically reliable method for measuring the solid-state PL properties of (tetraphenyl)silole polymers. However, the emission spectrum of polymer **6** shows an increasing bathochromic shift from solution to TLC to quartz substrates. This suggests that the packing of the more rigid silafluorene framework becomes more ordered in the solid state. This is likely the result of inter-chain π - π

stacking interactions that lead to red-shifted excimer emission. While not unexpected, this trend will need to be taken into consideration when choosing substrates for explosives detection applications.

2.3.3.3 Solution-phase Quantum Efficiencies of Fluorescence

Solution-phase quantum yields of fluorescence (Φ_{flu}) increased for polymers **4** and **5** from their analogous trimer complexes **1** and **2** (Table 2-2). This supports the hypothesis that the polymers adopt more rigid, coiled structures. The trimers and polymers synthesized from the (tetraphenyl)silole monomer exhibit an increased Φ_{flu} through steric crowding, which is expected to hinder phenyl ring rotation. This phenomenon has been extensively documented by the observed aggregated induced emission (AIE) of precipitated silole nanoparticles.³⁵ The emission quantum efficiency of polymer **6** decreased slightly from trimer **3**. Even with a slight decrease in Φ_{flu} , **3** and **6** exhibit quantum efficiencies several orders of magnitude higher than (tetraphenyl)silole counterparts in the solution phase. This may be attributed to structural rigidity of the silafluorene moiety, which reduces the number of non-radiative decay pathways. The addition of the vinylene bridges into the polymer may also contribute to the good quantum yields of fluorescence.³⁶ The lack of reliable reference materials prevents the calculation of absolute solid-state quantum yields for most polymeric materials.³⁷ When compared to poly(tetraphenyl)silole, polymers **4-6** also exhibit an overall increase in the relative solid state fluorescence quantum efficiencies. This along with exciton delocalization along the polymer backbone is an



*May also be classified as nitroaromatic

Figure 2-9. Structures of common high explosives categorized by functional group class.

important characteristic for fluorescence sensing applications. More efficient luminescence effectively reduces background interferences during detection. It also requires less material to be used, decreasing the overall cost of the detection. Delocalization of excitons throughout a conjugated polymer improves sensing by amplified fluorescence quenching of entire polymer chains by a single analyte molecule.^{14a}

2.3.4 Explosives Detection by Fluorescence Quenching

2.3.4.1 Solution-phase Stern-Volmer Analysis

The widely used high explosives contain nitroaromatic, nitrate ester, and nitramine functionalities (Figure 2-9). Detection of these explosives requires targeting

Table 2-3. Summary of Stern-Volmer constants (K_{sv}) for polymer fluorescence quenching with explosive analytes reported in M^{-1} in toluene solution. Detection of RDX was not observed for polymers **4-6**.

Polymer	TNT	DNT	PA
4	10 500	4300	16 400
5	9900	4100	15 600
6	10 200	5500	20 100
Poly(tetraphenyl)silole ^a	4300	2400	11 000

^a ref. (22).

a specific chemical or physical property. Detection by amplified fluorescence quenching presumably involves electron transfer from the polymer fluorophore to the lowest unoccupied molecular orbital (LUMO) of the explosive materials. In this study, solution-phase Stern-Volmer quenching studies were initially carried out for **4-6** in toluene solvent to characterize the fluorescence quenching efficiency of several common explosive materials (2,4,6-trinitrotoluene (TNT), picric acid (PA), 2,6-dinitrotoluene (DNT) and cyclotrimethylenetrinitramine (RDX)). The Stern-Volmer constant is calculated using Equation 1.

$$(I_0/I) - 1 = K_{sv} [A] \quad (1)$$

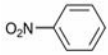
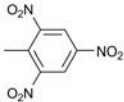
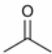
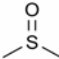

Polymers **4-6** exhibit linear Stern-Volmer plots for the explosives studied at concentrations below 3.0×10^{-4} M. The Stern-Volmer constants are summarized in

Table 2-3. These constants are a quantitative measure of explosives detection efficiency. Data for poly(tetraphenyl)silole is included in the table for comparison. Polymers **4-6** show a higher quenching efficiency than obtained with poly(tetraphenyl)silole. This may be due to enhanced amplified quenching expected for the higher molecular weight polymers. In addition, improved conjugation throughout the backbone of the polymer may increase the quenching. RDX was not detectable in solution within the noise limits of the fluorimeter.

2.3.4.2 Probing Explosive Analyte Binding by ^{29}Si NMR

The high Stern-Volmer quenching constants observed for the detection of nitroaromatic explosives prompted us to investigate solution polymer-analyte interactions using ^{29}Si NMR. Strained silacycles have found use as effective Lewis acid catalysts.³⁸ The rigid nature of the metallacyclopentadiene unit and the small internal C-Si-C angle of these systems ($\sim 90^\circ$) make them candidate Lewis acids. Even though π - π interactions may facilitate association of some aromatic explosives with the polymer, the nitro-groups on the periphery of most common explosive materials have the potential to act as Lewis base donors. We hypothesized that the silicon centers in the silole and silafluorene based polymers may bind the nitro-containing explosives, through the lone pairs of the nitro groups, during thin-film detection studies in the solid state. This helps explain the low detection limits observed and the general effectiveness of silole and silafluorene polymers. ^{29}Si NMR spectroscopy is ideally suited to identify substrate/analyte interactions through the use of NMR

Table 2-4. ^{29}Si NMR results for **3**. Spectra taken in benzene- d_6 with 27 equivalents of analyte.

Analyte	Structure	Lewis basicity $-\Delta H^\circ_{\text{BF}_3}$ (kJ mol^{-1})	$\Delta_{\text{outer Si}}$ (ppm)	$\Delta_{\text{inner Si}}$ (ppm)
NB		35.79	0.028(1)	0.080(3)
TNT		—	0.103(1)	0.133(2)
ACE		76.03	0.375(2)	0.466(4)
NM	$-\text{NO}_2$	37.63	0.564(4)	0.517(4)
DMSO		105.3	0.613(2)	0.688(4)
THF		90.40	0.630(3)	0.687(5)
ACN	$-\text{C}\equiv\text{N}$	60.39	0.797(1)	-0.383(4)

observable parameters such as chemical shift and relaxation time.³⁹ The model trimer complex **3**, provides a well characterized structural representation of polymer **6**. A series of Lewis base analytes were chosen to supply a range of Lewis basicities. The analytes include dimethylsulfoxide (DMSO), nitrobenzene (NB), nitromethane (NM), acetonitrile (ACN), acetone (ACE), tetrahydrofuran (THF) and 2,4,6-trinitrotoluene (TNT). The chemical structure and Lewis basicities, referenced to BF_3 as the Lewis acid,⁴⁰ for these analytes are found in Table 2-4. NM was used as a model for nitro-aliphatic based explosives such as RDX and PETN. NB and TNT represent the

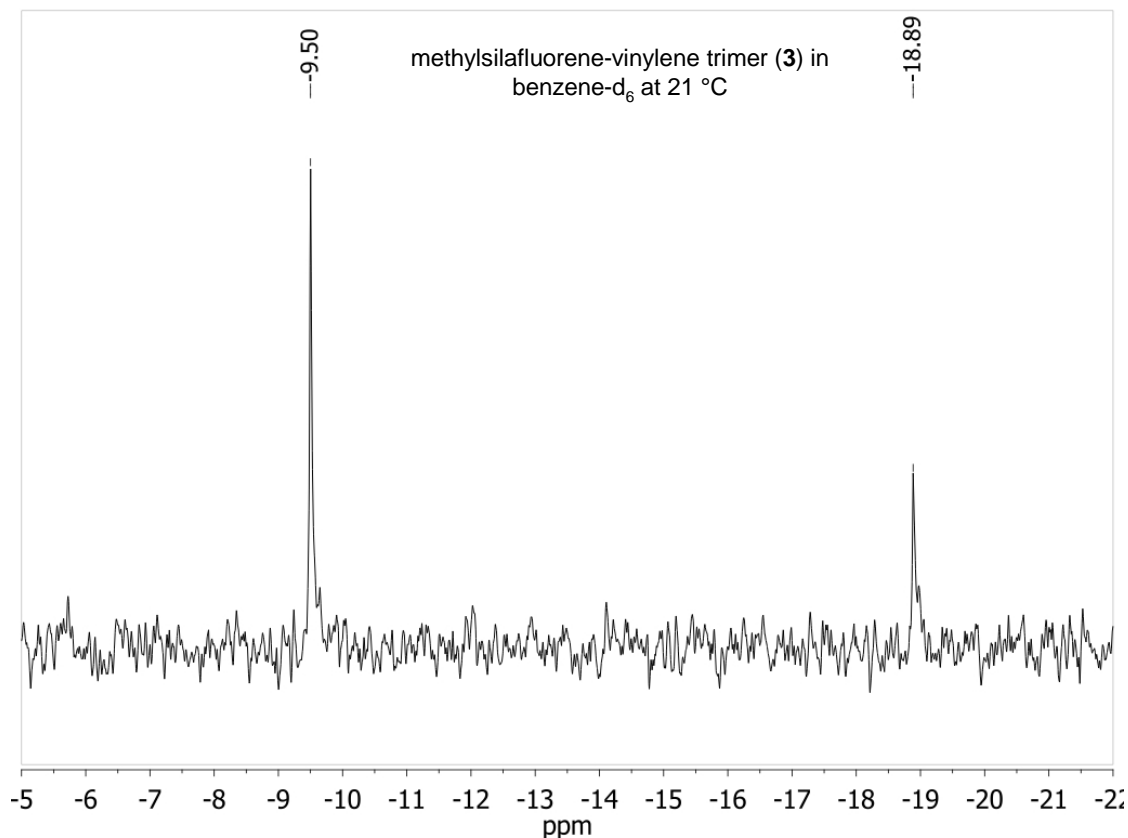


Figure 2-10. ^{29}Si NMR of **3**.

aromatic based nitro explosives.

The ^{29}Si NMR of **3** reveals two peaks that correspond to the peripheral silicon centers and the single central silicon center of **3** (Figure 2-10). These peaks are up-field from the TMS resonance at -9.50 ppm and -18.9 ppm, respectively. Figure 2-11 shows the ^{29}Si NMR spectra acquired in benzene-d₆ expanded around the resonance observed for the peripheral silicon centers of **3** with and without the addition of analytes. All spectra were acquired using ^1H decoupling during acquisition only and were referenced to TMS (tetramethylsilane) at 0 ppm. TMS, itself a weak Lewis acid, was contained in an internal capillary to prevent interaction with the analytes. The

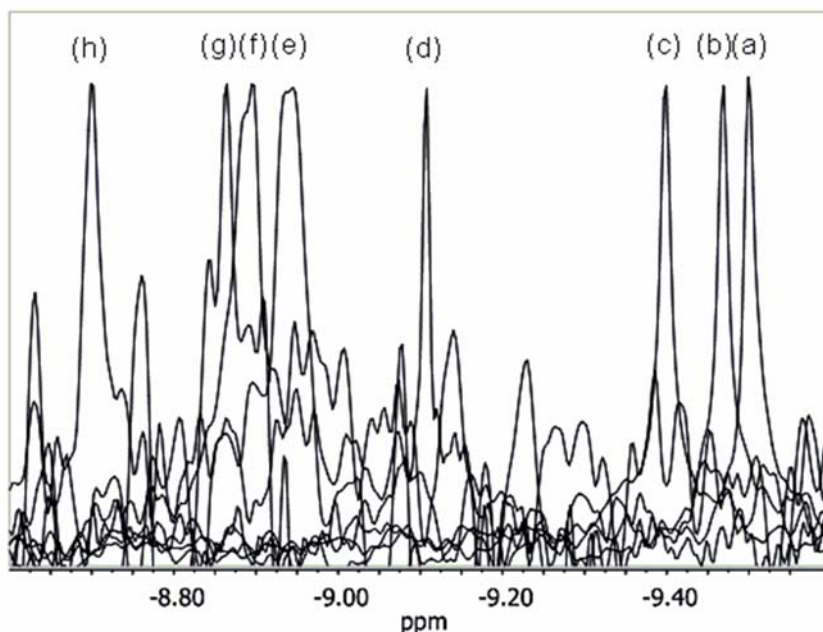


Figure 2-11. ^{29}Si NMR chemical shifts for the outer Si atoms of **3** at 20 °C when exposed to 33 equivalents of (a) No analyte; (b) NB; (c) TNT; (d); ACE; (e) NM; (f) DMSO; (g) THF; (h) ACN. Spectra taken in benzene- d_6 .

observed shifts are down-field and are within a range of ~ 1 ppm. This finding is consistent with previous ^{29}Si NMR studies analyzing Lewis base displacement in rigid-rod silane polymers.⁴¹

Table 2-4 lists changes in ^{29}Si NMR chemical shifts (Δ) for both the central and peripheral silicon resonances of **3** in the presence of the Lewis base analytes. The changes in shifts are reported from single Lorentzian fits to the NMR data using the Simplex algorithms available in Origin 8 (see Experimental). Errors are reported at the 95% confidence level (2σ). Distinct shifts occur in the ^{29}Si NMR resonances for both the silicon centers of **3** when exposed to TNT. This supports the hypothesis that nitro- and nitrate-containing organic explosives can bind to these silicon-containing

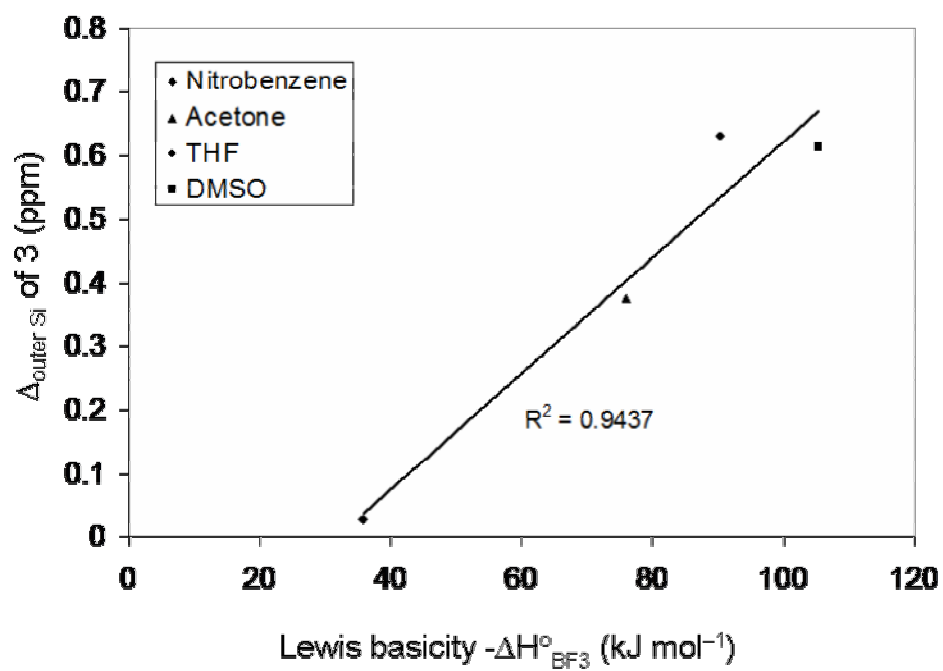


Figure 2-12. Correlation between Lewis basicity and the change in peak position of the peripheral Si atoms of **3** in the ²⁹Si NMR upon addition of a series of analytes (33 equivalents).

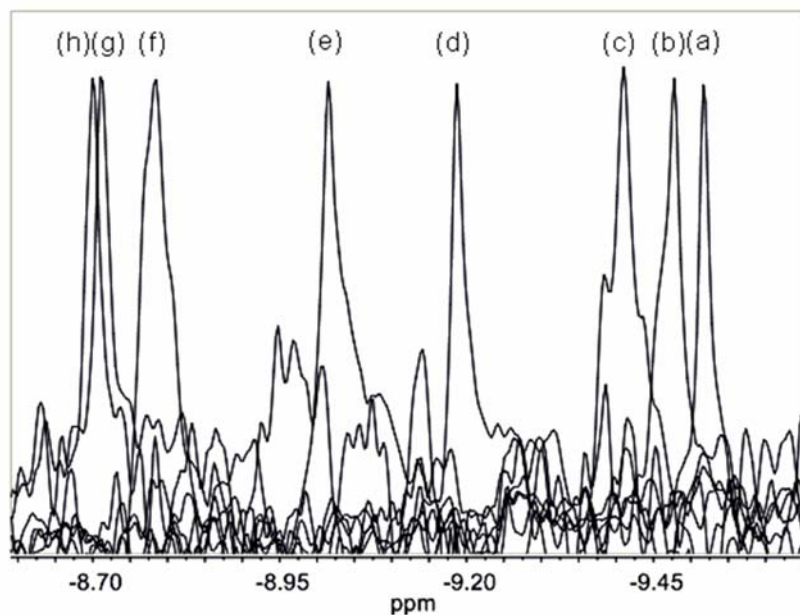


Figure 2-13. Superimposed ^{29}Si NMR spectra of the outer Si atoms in **3** when exposed to increasing equivalents of acetonitrile at 20 °C. (a) No acetonitrile; (b) 3 equivalents; (c) 9 equivalents; (d) 15 equivalents; (e) 21 equivalents; (f) 27 equivalents; (g) 33 equivalents; (h) 39 equivalents.

polymers. This weak donor acceptor interaction could provide an efficient pathway for electron transfer quenching of the excited state of silacycle containing polymers.

While a general correlation is observed between Lewis basicity and chemical shift for NB, ACE, DMSO, and THF (Figure 2-12), the data obtained for NM and ACN indicate that the correlation may be complicated by additional effects. ACN is the least sterically restricted and may have better access to the Si centers. This could explain the largest shift difference (Δ) of 0.797(1) ppm noticed for this analyte. In addition, ACN is the only Lewis base in this study with nitrogen lone pairs.

Evidence of Lewis acid-base interactions in these strained silacycle systems can also be seen through analyte titration. Figure 2-13 shows the chemical shifts for

Table 2-5. Chemical shifts of the peripheral Si atoms of **3** in the presence of increasing equivalents of ACN at 20 °C.

Equivalents of ACN	$\delta_{\text{outer Si}}$ (ppm)
0	-9.5182(5)
3	-9.4747(9)
9	-9.411(2)
15	-9.190(1)
21	-9.023(2)
27	-8.785(1)
33	-8.705(1)
39	-8.714(2)

the peripheral silicon centers of **3** when exposed to increasing equivalents of ACN. The ^{29}Si NMR resonance shifts continually down-field on addition of ACN until a threshold is reached at around 33 added equivalents (Table 2-5). An association constant (K_a) of 0.12 M^{-1} was calculated for the binding of ACN to the peripheral silicon centers of **3** using the Scatchard method (Equation 2, Figure 2-14).^{42,43}

$$\Delta\delta/[A]_0 = -K_a\Delta\delta + K_a\Delta\delta_{\text{max}} \quad (2)$$

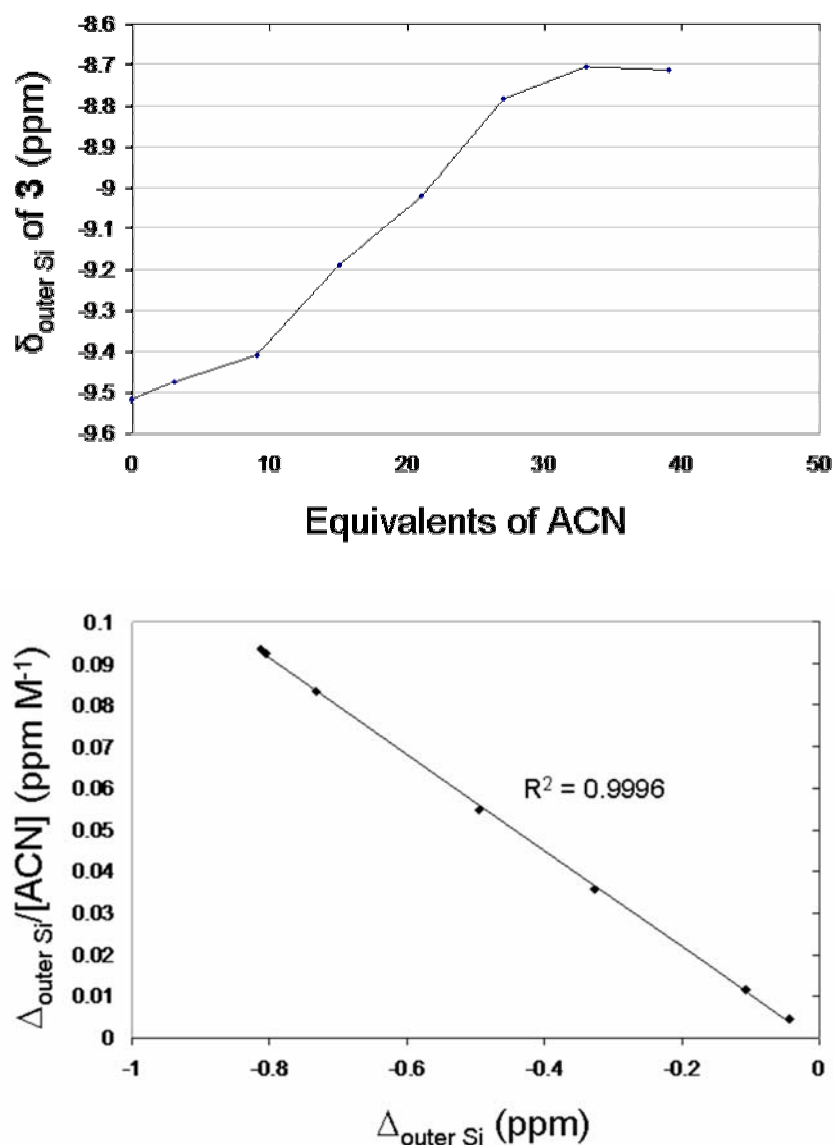


Figure 2-14. TOP: Plot of chemical shift dependence of the peripheral Si atoms of **3** on the equivalents of ACN added. BOTTOM: Scatchard plot showing binding interactions between ACN and **3** based on ^{29}Si NMR data. The gradient is equal to $-K_a$.

ACN shows the largest effect on the ^{29}Si NMR resonances, providing an upper limit for K_a in this study. Further support of substrate/analyte binding was revealed through NMR relaxation studies. Spin-lattice relaxation times (T_1) of 5.86(3) s and 4.83(4) s

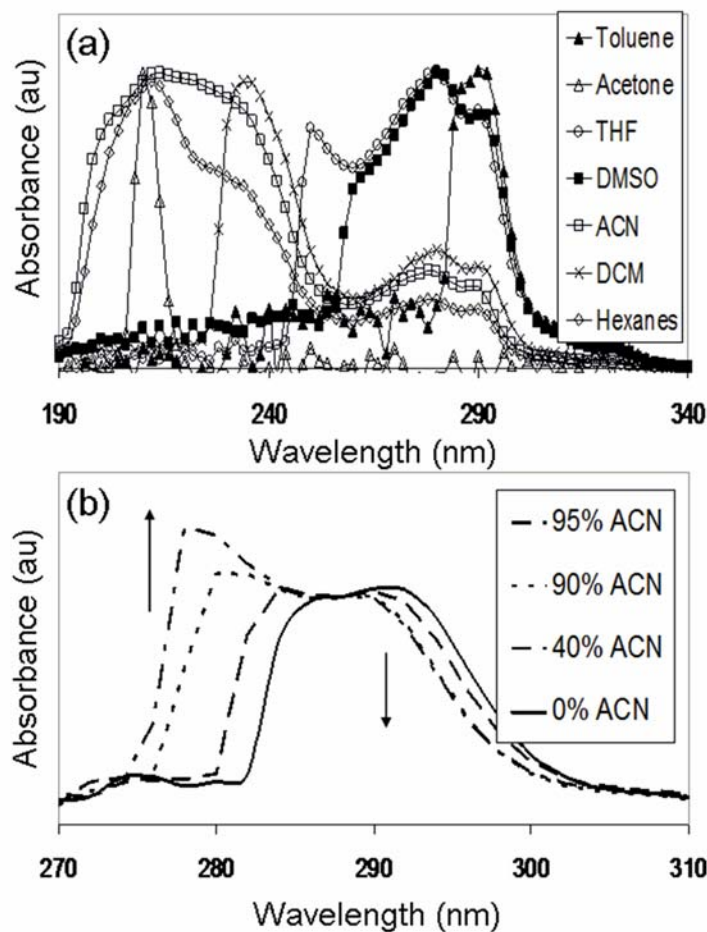


Figure 2-15. UV-vis spectra of **3**. (a) Spectra individually taken in 100% of given solvent. DCM = dichloromethane; (b) Spectra taken in toluene with increasing percentages of ACN.

were measured for ACN by ^1H NMR in benzene- d_6 at 20 °C in the absence and presence of **2**, respectively. The significant change in T_1 values indicates a binding event between ACN and **3**.^{42b,44} The viscosity (η) of both solutions at 20 °C as measured were identical (0.688(3) cP), indicating no major change occurred in the solution properties affecting T_1 (Equation 3).

$$\eta_1/\eta_2 = (t_1\rho_1)/(t_2\rho_2) \quad (3)$$

Low temperature studies were performed with the intention to observe isolated populations of bound and unbound states. However, these studies were complicated by low temperature insolubility and the physical properties of the solvents and analytes used. The binding studies were also carried out in dichloromethane- d_2 to determine the extent of ring current effects that toluene- d_8 may have had on the chemical environment of silicon centers. The peaks shift for 33 equivalents of acetone in dichloromethane- d_2 lowered to 0.270(6) ppm from 0.3068(9) ppm in toluene- d_8 at room temperature and to 0.248(1) ppm from 0.436(1) ppm in toluene- d_8 at -50 °C, indicating a small but observable solvent effect as well as a small but expected temperature dependence.

Binding of an analyte to the silicon center of these fluorescent molecules might also cause a change in the absorption spectra, since the lowest excited state involves the π^* orbital of the metallole ring. UV-vis spectra were measured in a range of solvents. Several solvents used in the ^{29}Si NMR study (NM and NB) could not be investigated due to their strong UV absorption. Figure 2-15a shows the spectra of the silafluorene trimer in a variety of solvents. It is clear that the solvent has a distinct effect on the absorption properties of the silafluorene trimer. For example, the spectra reveal a blue shift in λ_{msx} of 80, 56, and 12 nm for ACN, dichloromethane (DCM), and DMSO, respectively. The isosbestic point obtained on addition of UV transparent ACN (Figure 2-15b) further suggests an equilibrium binding process. The UV spectra

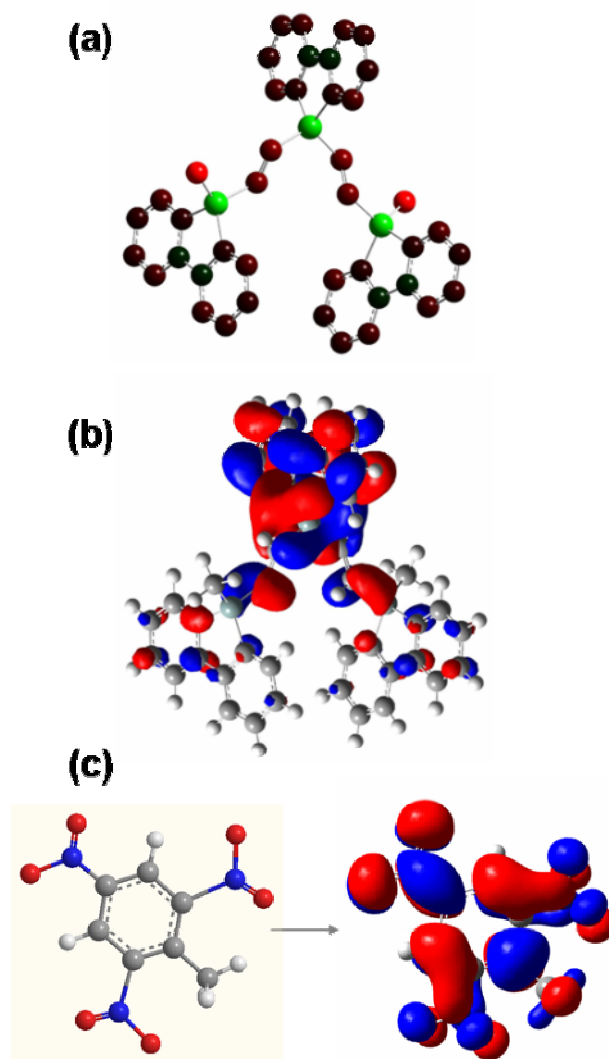


Figure 2-16. *Ab initio* DFT calculations on trimer **3** and TNT at the B3LYP/6-31G* level. (a) Electrostatic potentials for **3**. Colors range from -0.668 to $+0.668$ with green denoting the electron deficient regions and red denoting the electron rich regions. (b) Lowest unoccupied molecular orbital (LUMO) of **3**. (c) LUMO of TNT.

of **3** in DMSO (dielectric constant = 47) and THF (dielectric constant = 7.6) are found to be very similar. This suggests that solvatochromism is not a major contributing factor to the spectral shifts observed.

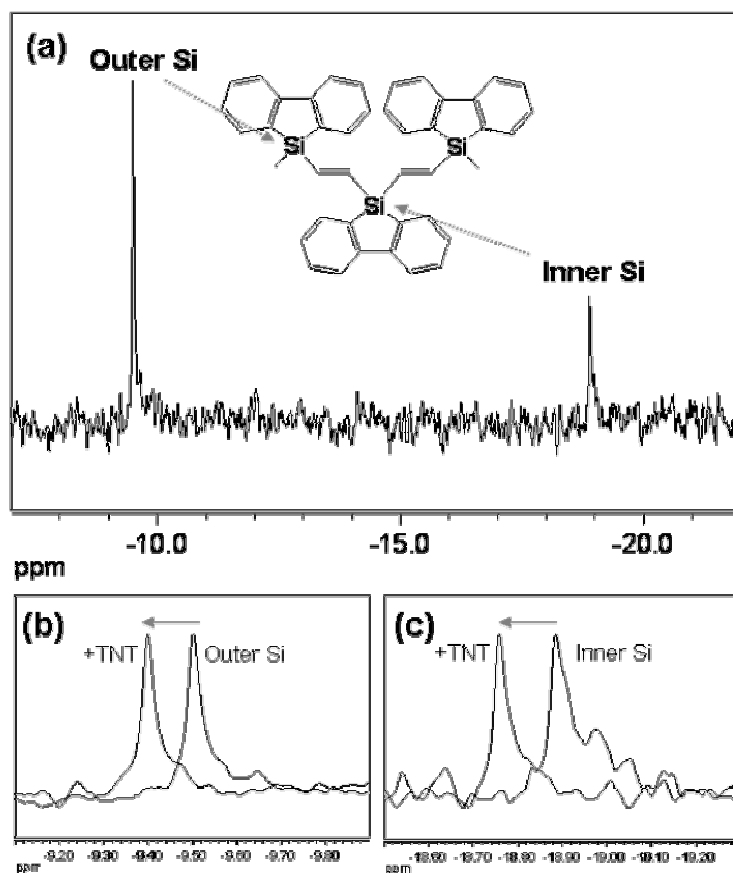


Figure 2-17. ^{29}Si NMR spectra of trimer **3**. Spectra taken in d_6 -benzene at a concentration of 100 mg mL^{-1} . TMS was used as an internal capillary standard referenced to 0 ppm. (a) Both peaks corresponding to the different silicon environments. (b) A downfield shift of the outer Si peak upon exposure to 12 eq. of TNT. (c) A downfield shift of the inner Si peak on exposure to 12 eq. of TNT.

The electrostatic potential (Mulliken charges) modeled by *ab initio* DFT calculations for trimer **3** shows a positive charge distribution centered on the silicon atoms (Figure 2-16). The $^1\text{SOMO}$ was calculated to model the excited-state orbital from which the electron is transferred from the polymer sensor to the analyte. A static quenching model, which implies pre-association of the explosive analyte, has been established through previous fluorescence quenching lifetime studies.^{15c} Figure 2-16 depicts the molecular orbital density of the LUMO for trimer **3** and the LUMO for

TNT. The LUMO of **3** resides primarily on or near the central silicon. The LUMO for TNT is localized on the aromatic system and the nitro oxygen atoms. Thus, a ground-state Lewis acid-base interaction between nitro groups of TNT and the silicon centers of trimer **3** facilitates orbital overlap between the two and provides an efficient inner-sphere pathway for electron-transfer quenching of the excited-state (Figure 2-17). Even though trimer **3** effectively binds the explosive analytes and can be used as an explosives sensor, the advantage of using polymers is two-fold. Delocalization in conjugated polymers allows for amplified detection at any point along the polymer chain.⁴⁵ Also, extended conjugation red shifts the emission toward visible solid-state luminescence in polymer **6**. This is important in thin-film imaging applications by visible fluorescence.

2.3.4.3 Surface Detection of Explosive Particulates

Given the limited practical applicability of solution-phase explosives detection, we explored a surface sensing method for imaging trace explosives particulates using thin-films of polymers **4-6**. A detailed procedure for this method can be found in the experimental section. Detection limits for this method are reported in ng cm^{-2} to emphasize the quantity of explosive deposited in the given area. The explosives studied by this detection method were expanded to include cyclotetramethylene-tetranitramine (HMX), 2,4,6-trinitrophenyl-N-methylnitramine (Tetryl), trinitroglycerin (TNG), and pentaerythritol tetranitrate (PETN). Dinitroethylene glycol (EGDN) and the explosives taggant 2,3-dimethyl-2,3-dinitrobutane (DMNB) are too

Table 2-6. Solid-state detection limits (ng cm^{-2}) for trace explosives by fluorescence quenching of sprayed-on films of polymers **4-6**. Dash represents no detection at 64 ng cm^{-2} level.

Explosive	P_{vap} (Torr) at 25 °C	4		5		6	
		Porcelain	Filter Paper	Porcelain	Filter Paper	Porcelain	Filter Paper
Tetryl	5.7×10^{-9}	0.3	1	1	1	2	0.2
TNT	5.8×10^{-6}	0.6	2	0.6	0.6	2	0.3
PA	5.8×10^{-9}	2	2	16	2	3	2
RDX	4.6×10^{-9}	—	—	—	32	16	2
PETN	1.4×10^{-8}	—	—	—	—	16	2
DNT	1.1×10^{-4}	32	3	2	3	16	2
HMX	8.0×10^{-11}	—	—	—	—	32	3
TNG	4.4×10^{-4}	—	—	—	—	—	3

volatile ($P_{\text{vap}} = 2.8 \times 10^{-2}$ Torr and 2.1×10^{-3} Torr, respectively) to be detected at a 64 ng cm^{-2} limit using this surface detection method due to their rapid evaporation.

The results of the surface detection study are seen in Table 2-6. As expected, polymer **4** only undergoes quenching by nitroaromatic explosives. However, copolymer **5** is able to detect both RDX and nitroaromatic explosives when illuminated at 254 nm, but not upon illumination at 360 nm. Polymer **6** detects the entire range of explosives at much lower detection limits than either polymer **4** or **5**. A photograph of the solid-state detection of RDX using polymer **6** is seen in Figure 2-18. Even though RDX is unable to effectively quench the luminescence of polymer **6** in solution, it very efficiently quenches the polymer luminescence in the solid state with a detection limit of 2 ng cm^{-2} . This suggests that the close proximity of polymer and analyte in solid-state detection studies facilitates the excited-state electron transfer

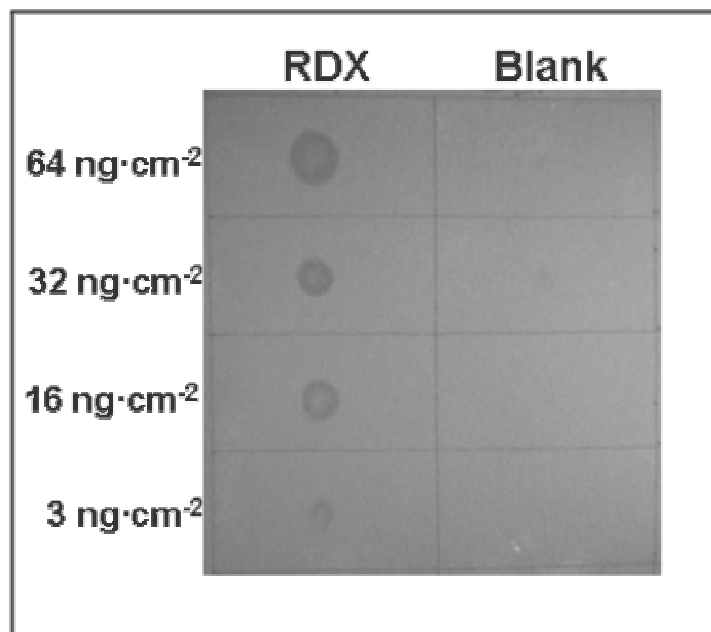


Figure 2-18. Fluorescence quenching of polymer **6** by solid-particulates of RDX in a thin film on filter paper as observed using a Sony 2.0 megapixel digital camera as a black and white image (right) under continuous UV irradiation (254 nm).

process, resulting in improved detection of non-nitroaromatic explosives. Weak Lewis acid-base interactions may help orient the explosive-metallolite moieties for efficient excited-state electron transfer in the solid solution film studies, but would be much less important in quenching experiments performed in very dilute solutions. The detection of a large range of trace explosive particles by UV-blue emitting polymer **6** reveals that effective energy matching through frontier molecular orbital tuning is another factor to consider when designing a polymeric sensors.⁴⁶ Typically, non-conjugated explosive materials, which make up the majority of nitrate ester and nitramine based explosives, have more negative reduction potentials than conjugated aromatic explosive materials, rendering them difficult to detect by fluorescence quenching. Polymer **6** exhibits a wider band-gap, as seen by its UV-blue emission

Table 2-7. HOMO and LUMO energies calculated for the various explosives and trimers **1** and **3** at the B3LYP/6-31G* level of theory. Values in parentheses are the calculated ¹SOMO energies and corresponding band-gaps.

Compound	LUMO (eV)	HOMO (eV)	Band-gap (eV)
Octanitrocubane	-4.463	-9.823	5.361
Tetryl	-3.918	-8.109	4.109
Picric Acid	-3.891	-8.218	4.327
TNT	-3.483	-8.435	4.952
PETN	-3.075	-8.707	5.633
CL-20	-3.020	-8.816	5.796
DNT	-2.966	-8.109	5.143
HMX	-2.721	-8.299	5.578
RDX	-2.531	-8.245	5.714
TNG	-2.476	-9.088	6.612
EGDN	-2.122	-8.898	6.775
DMNB	-2.068	-8.027	5.959
TATP	0.354	-6.340	6.694
HMTD	0.680	-6.313	6.993
1	-1.741 (-2.159)	-5.252	3.511 (3.093)
3	-1.116 (-1.942)	-5.769	4.653 (3.827)

band, as compared to polymers **4** and **5**. This produces a better redox driving force with a wider range of explosives.

2.3.4.4 Theoretical Calculations

To see whether the electron accepting ability of the explosive analyte correlated with ease of detection, theoretical calculations at the B3LYP/6-31G* level of theory were used to determine the HOMO and LUMO energies for the optimized structures of the explosive analytes. The frontier molecular orbital energies as well as the ¹SOMO of trimers **1** and **3** were also calculated to model the energy of the polymer donor **4** and **6**. The calculated band-gap energies of the explosives were found to agree well with the first absorptions observed in the UV-vis spectra and the calculated LUMO energies correlate well with measured redox potentials for TNT, RDX and HMX.⁴⁷ Delocalization within the trimers was observed in the calculations by comparing band-gap energies with previous calculations on the monomer.⁴⁸ For example, the band-gap for trimer **3** is 4.65 eV while the band-gap for the silafluorene monomer is 4.97 eV. The ¹SOMO energies of the polymers should be slightly lower in energy (0.1 eV) than those calculated for the trimers due to further delocalization, as observed in the red-shifted UV-vis and fluorescence spectra. Table 2-7 lists the results for the calculated HOMO and LUMO energies for each explosive studied, as well as the ¹SOMO of **1** and **3**. The explosives are tabulated in descending order of LUMO energies. These energy levels are expected to represent the relative ease of transferring an electron to each explosive in the fluorescence quenching process.

The excited-state energies of **1** and **3** were plotted on the same scale as the molecular orbital calculations for the explosives (Figure 2-19). The ¹SOMO energies for the trimers lie within the range of LUMO energies of the explosive analytes

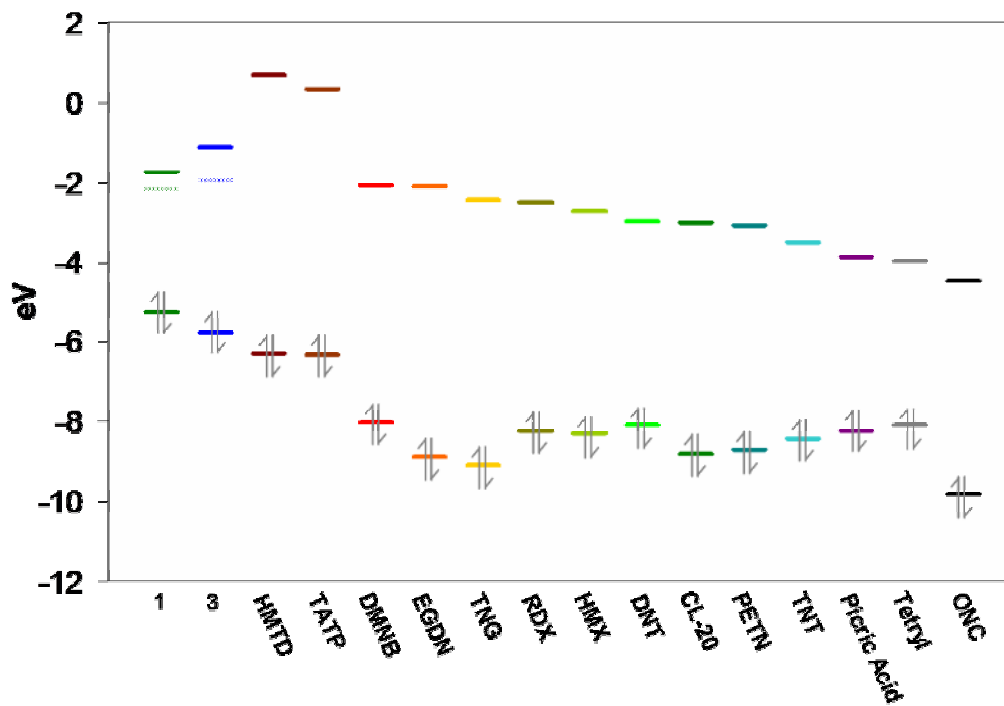


Figure 2-19. Frontier orbital energy correlation diagram for model trimers **1** and **3** with various explosive analytes. Models **1** and **3**: bottom lines represent the HOMO energies; top lines represent the LUMO energies; the middle lines (broken) represent the singlet excited-state energies (1 SOMO) calculated with spin polarization. This is the orbital energy from which the excited-state electron transfer process takes place. Explosives: bottom lines represent the HOMO energies; top lines represent the LUMO energies.

detected. Trimer **3** is at a higher energy and thus maintains a better driving force for electron transfer to the explosives than trimer **1**. The trend observed in the detection limits for all the explosives parallels the LUMO energy of each explosive in remarkably good agreement. This good correlation between theoretical and experimental results supports the conclusion that the LUMO energy of explosive analytes is an important factor in the fluorescence quenching process.

The highly delocalized nitroaromatic explosives generally have lower LUMO energies and are detected much better by fluorescence quenching sensors than aliphatic nitro and nitrate based explosives. PETN is an exception to the perfect correlation with LUMO energies. It has comparable LUMO energies to DNT, HMX and RDX. Using the calculated LUMO energy for PETN, it would be expected that both (tetraphenyl)silole and silafluorene polymers would be able to detect this explosive. In practice, only polymer **6** is able to detect PETN at nanogram levels. This result suggests that while frontier orbital energy matching is a dominant factor, it is not the only variable that determines explosives detection in the solid-state. The high volatility of EGDN and DMNB prevented their detection even though their calculated LUMO energies lie slightly below those calculated for the trimers. Other high priority explosives such as triacetone triperoxide (TATP), hexamethylene triperoxide diamine (HMTD), 2,4,6,8,10,12-hexanitro-2,4,6,8,10,12-hexaazaisowurtzitane (CL-20)⁴⁹ and octanitrocubane (ONC)⁵⁰ were calculated and are included in the plot of Figure 2-19. The difficulty in obtaining analytical samples and shock sensitivity of these explosives prevented direct analysis. However, the calculations strongly suggest that the LUMO energies for peroxide based explosives are far too high to act as effective electron acceptors for a photo-induced electron transfer process using typical fluorescent polymers. However, the LUMO energies for CL-20 and ONC fall well within the range of detectable explosives using polymers **4-6**. It would be predicted that CL-20 would be detected at limit range of about 1-5 ng cm⁻². The highly sensitive ONC

explosive has the lowest calculated LUMO energy and therefore is predicted to be the easiest explosive for detection, based purely on energetic considerations.

2.3.4.5 Detection Interferents

Selectivity and insensitivity to common interferents are other important considerations when developing an explosive sensing polymer. Polymers **4-6** as well as poly(tetraphenyl)silole show no change in luminescence when exposed to common organic solvents such as THF, toluene, and methanol. Benzophenone and benzoquinone are typically analyzed for their effectiveness as redox interferents in the detection of explosives by fluorescence quenching. Pentiptycene-derived polymers show some sensitivity towards these interferents.³⁷ Polymers **4** and **5**, as well as poly(tetraphenyl)silole, show no response to benzophenone. However, polymer **6** is quenched by benzophenone particulates down to 3 ng cm⁻². This further supports the hypothesis that both reduction potentials and electronic overlap play an important role in the thin-film fluorescence quenching mechanism. Polymer **6** has a wider band-gap than the (tetraphenyl)silole-containing polymers, thus increasing its ability to detect a wider range of electron accepting materials. Also, the lone pairs that reside on the carbonyls of benzophenone and benzoquinone may effectively bind as Lewis bases to the strained silacycle containing polymer. Future studies will focus on improving molecular recognition aspects so-as-to increase selectivity and sensitivity towards specific classes of explosives.

2.4 CONCLUSIONS

New silole- and silafluorene-vinylene polymers **4-6** have been synthesized for use as fluorescent chemosensors for the detection of high explosives. Crystal structure analysis of model trimer complexes and fluorescence emission comparisons between polymers and trimers show a regio-regular *trans*-product conjugated through the silicon vinylene bonds. The high quantum efficiencies (especially for polymer **6**), partial conjugation through the backbone and multiple analyte binding mechanisms yield high Stern-Volmer quenching constants for nitroaromatic explosives such as TNT, DNT and PA in solution.

The open structure of polymer **6** as compared to polymers **4** and **5** allows for Lewis acid-base interactions of analytes with the silacycle ring. Using ^{29}Si NMR as a probe for sensor-to-analyte interactions between silafluorene containing materials and explosive analytes, we have shown that lone pairs on both oxygen and nitrogen atoms can bind to the silicon centers through a Lewis acid-base interaction enhanced by the ring strain in the silacycle. Further evidence for these binding events was provided by spin-lattice relaxation times and UV-vis spectroscopy.

The high-energy band-gap of **6** allows for the detection of a wider range of explosive materials, including the important high explosives RDX, HMX, TNG, and PETN in the solid state. Theoretical calculations show that LUMO energies of explosives closely follow the observed detection limits obtained with these silicon containing polymers. By tuning the band-gap of the fluorescent sensors, relative detection sensitivities can be predicted based on matching the excited-state energies

with the LUMO energies of the explosives. Solid-state detection of explosive particulates using silafluorene-containing polymer **6** provides very low detection limits by a rapid, simple sensing method. Optimizing the energy overlap and thereby lowering the activation energy barrier for the electron transfer process between the explosive analytes and the sensing polymer appears to be a crucial factor. Polymers **4-6** also show promise as a new generation of conjugated and stable organometallic polymers for blue emitting optical electronic materials.

2.5 EXPERIMENTAL

2.5.1 General Synthetic Techniques

Caution: TNT and picric acid are high explosives and should be handled only in small quantities. Picric acid also forms shock sensitive compounds with heavy metals. Purchased explosive standards were handled as dilute solutions to eliminate an explosion hazard. All synthetic manipulations were carried out under an atmosphere of dry argon gas using standard Schlenk techniques. Dry solvents were purchased from Aldrich Chemical Co. Inc. and used after purification with an MBraun Auto Solvent Purification System. Spectroscopic grade toluene from Fisher Scientific was used for the fluorescence measurements. Monomers, 1,1-dihydrido(tetraphenyl)silole, 1,1-dihydridosilafluorene, 2,2'-dibromobiphenyl, 1,1-diethynyl-(tetraphenyl)silole, 1-methyl-1-hydrido(tetraphenyl)silole, 1-methyl-1-hydridosilafluorene and 1,1-dichlorosilafluorene were synthesized by literature procedures.^{24,34,51-54} All other reagents were purchased from Aldrich Chemical Co. and

used as received. Picric acid and DNT were purchased from Aldrich Chemical Co. and recrystallized from ethanol and methanol, respectively. TNT was prepared from DNT⁵⁵ and recrystallized from toluene. RDX, HMX, Tetryl, TNG and PETN were purchased as 1 mg mL⁻¹ analytical standards in acetonitrile from Cerilliant®.

NMR data were collected with the use of a Varian Unity 300 or 500 MHz spectrometer (300.1 MHz for ¹H, 77.5 MHz for ¹³C, and 99.4 MHz for ²⁹Si NMR). Infrared spectra were obtained with the use of a Nicolet Magna-IRTM Spectrometer 550. GPC-RI data were obtained with the use of a Viscotek GPCmax VE 2001 GPC and a Viscotek VE 3580 refractive index detector calibrated with polystyrene standards. Fluorescence emission and excitation spectra were recorded with the use of a Perkin-Elmer Luminescence Spectrometer LS 50B. UV-vis spectra were obtained with the use of a Hewlett-Packard 8452A diode array spectrometer.

2.5.2 ²⁹Si NMR Data

²⁹Si NMR data were collected using a Varian Mercury Plus spectrometer and 9.4 T superconducting magnet (399.911 MHz for ¹H and 79.450 MHz for ²⁹Si NMR). The solution-state ²⁹Si NMR spectra were recorded using an internal tetramethylsilane (TMS) reference, separated from the sample matrix using a tapered glass insert (Wilmad part WGS-5BL.) Chemical shifts were measured relative to the TMS reference (0 ppm) in all cases. ²⁹Si NMR spectra were acquired using single pulse then acquire experiment (spnmr) with proton decoupling during the acquisition period only. The pulse delay was set 5 s and a pulse time of 7.5 μs was used ($\pi/4$ was measured as

15 μ s for **3** in benzene- d_6 .) T_1 was not measured for any of the ^{29}Si sites. Typical acquisition times were 3 h. 1 Hz of exponential line-broadening was applied to the data during processing. The ^{29}Si NMR data were fitted using the Lorentz equation in Origin8 (Equation 4).

$$y = y_0 + [(2A/\pi) (w/(4(x-x_c)^2 + w^2))] \quad (4)$$

Error analysis was performed at a confidence level of 95% using 2σ for the calculated x_0 . ^1H T_1 measurements were performed on samples using an inversion-recovery pulse sequence and VNMR-native processing algorithms. Data for T_1 analysis were taken at 20 °C in benzene- d_6 .

2.5.3 X-ray Crystal Structure Determination

Diffraction intensity data were collected with a Bruker P4/CCD Smart Apex CCD diffractometer at 100 K. Compound **1** diffracted very weakly limiting data to about 1.0 Å resolution. The correctness of the centrosymmetric assignment was based on the clear presence of two-fold rotational symmetry. The structure was solved by direct methods, completed by subsequent difference Fourier syntheses, and refined by full matrix least-squares procedures on F^2 . SADABS absorption corrections were applied to all data. All non-hydrogen atoms were refined with anisotropic displacement coefficients. All H atoms were found on the difference maps and refined with isotropic thermal parameters. All software and sources of scattering factors are

contained in the SHELXTL (5.10) program package (G.Sheldrick, Bruker XRD, Madison, WI). Compound **1** was solved in space group C2/c with an R(F) = 6.9% with 28422 reflections measured. A complete crystal structure analysis can be found in the crystallographic information file (CIF) in the supporting information.

2.5.4 Theoretical Methods

Geometries were optimized and vibrational analyses were performed at the density functional (DFT) level of theory using the 6-31G* basis set.⁵⁶ The hybrid B3LYP functional was employed, which combines Becke's gradient-corrected exchange functional⁵⁷ with gradient-corrected correlation functional of Lee, Yang and Parr.⁵⁸ The vibrational analyses were used to confirm the nature of the stationary points, and the unscaled vibrational frequencies were used to compute thermal contributions to enthalpies. Excited-state energy calculations on **1** and **3** were carried out using TD-DFT methods on previously optimized ground-state structures.⁵⁹ All calculations were carried out with the Gaussian 03 suite of programs.⁶⁰

2.5.5 Solid-state Explosives Detection

Solutions of the high explosives RDX, HMX, Tetryl, PETN, and TNG were prepared directly from dilute analytical standards purchased from Cerilliant®. The explosive solutions were spotted onto Whatman® filter paper at the desired concentration level using a glass microsyringe. A solvent blank was spotted next to each explosive as a control. All depositions were prepared from a 5 µL volume,

producing a spot of ~ 1 cm in diameter, to ensure consistent analysis. Detection limits are reported in ng cm^{-2} to emphasize the quantity of explosive materials deposited. Upon solvent evaporation, the substrate is airbrushed at a rate of 0.5 mL s^{-1} with a 0.5 mg mL^{-1} solution (1:1, toluene:acetone) of the desired polymer. The addition of toluene facilitates the transient dissolution of explosive analytes to insure effective mixing with the polymers upon drying. Polymers **4** and **5** were visualized using a blacklight ($\lambda_{\text{em}} = 365 \text{ nm}$) as the excitation source and identified by their yellow-green luminescence. A blue luminescence was observed for polymer **6** using a UV-C light source ($\lambda_{\text{em}} = 254 \text{ nm}$). Similar detection limits for the high explosive analytes were observed using polymer **6** illuminated by a UV-B ($\lambda_{\text{em}} = 302 \text{ nm}$) light source. Detection studies were performed for each explosive at trace contamination levels of 64, 32, 16, 8, 3, 2, 1, 0.6 and 0.3 ng cm^{-2} . In the case of Tetryl, several dilutions were necessary in order to reach the detection limit.

Illuminated samples were examined by an independent observer to determine if quenching was visually discernible. A double-blind test was carried out using two spots of the explosive material at each concentration, which were spotted randomly onto three locations along with solvent blanks. The independent observer was unaware where the solvent control and explosive spots were distributed. Dark spots in the luminescent film indicate quenching of the polymer by the analyte. Detection limits are reported as the lowest amount of explosive necessary for the independent observer to observe quenching visually and accurately ($>95\%$) in the correct locations. A summary of the detection limits is reported in Table 2-6. Different sampling surfaces,

such as glass and porcelain, were also tested. Similar detection limits were observed for polymers **4** and **5** on these surfaces. Detection limits for polymer **6** decreased for the white porcelain surface. The smooth and shiny surface scattered the UV-C light producing a reflection with a similar color as the emitting polymer. This affected the ability to observe quenching at low explosive concentrations. On filter paper, where reflected light was less problematic, polymer **6** had the lowest detection limits for all explosives studied.

2.5.6 Synthesis of 1,1-diethynylsilafluorene (DESF)

To a dry THF solution of 1,1-dichlorosilafluorene (1.0 g, 4.0 mmol) was slowly added ethynylmagnesium bromide (0.5 M in THF, 16 mL, 8 mmol). The solution was stirred at room temperature for 2 h. The light brown solution was filtered and evaporated to dryness. The light brown solid was purified by sublimation (90-110 °C, 0.2 Torr) to afford a white crystalline solid (640 mg, 70%). Selected data; MP: 139-141 °C; ¹H NMR (300.134 MHz, CDCl₃): δ 7.80 (dd, 4H, PhH), 7.50 (td, 2H, PhH), 7.35 (td, 2H, PhH); 2.60 (s, 2H, -C≡CH); ¹³C {H} NMR (75.403 MHz, CDCl₃): δ 148.62, 133.83, 132.13, 131.60, 128.71, 121.49, 96.91, 82.04; ²⁹Si NMR (71.548 MHz, inversed gated decoupling, CDCl₃): δ -51.2 (s, silafluorene); IR (KBr): ν_{C=C} = 2028 cm⁻¹, ν_{C-H} = 3244 cm⁻¹; CH calcd for C₁₆H₁₀Si: C 80.3, H 4.63; Found: C 80.8, H 4.43.

2.5.7 Synthesis of 1,1'-(1E,1'E)-2,2'-(2,3,4,5-tetraphenyl-1H-silole-1,1'-diyl)bis(ethene-2,1-diyl)bis(1-methyl-2,3,4,5-tetraphenyl-1H-silole) (methyl(tetraphenyl)silole-vinylene trimer) (1)

To a dry toluene (8 mL) solution of 1,1-diethynyl(tetraphenyl)silole (200 mg, 0.46 mmol) and 1-methyl-1-hydrido(tetraphenyl)silole (378 mg, 0.92 mmol) was added H_2PtCl_6 (1 mg, 0.003 mmol). The solution was stirred at 70 °C for 3 h. The orange solution was then filtered and the solvent removed by vacuum. The brown residue was precipitated from 1 mL of THF with 10 mL of MeOH to afford a yellow powder (395 mg, 70%), which was recrystallized from benzene. Selected data; MP: 243-246 °C; ^1H NMR (300.134 MHz, CDCl_3): δ 6.76-7.06 (br, 64H, PhH, $-\text{HC}=\text{CH}-$), 0.508 (s, 6H, $-\text{CH}_3$); ^{29}Si NMR (71.548 MHz, inverse gated decoupling, CDCl_3): δ -2.66 (s, silafluorene); CH calcd for $\text{C}_{90}\text{H}_{70}\text{Si}_3$: C 87.5, H 5.71; Found: C 87.3, H 6.04.

2.5.8 Synthesis of 5,5-bis((E)-2-(1-methyl-2,3,4,5-tetraphenyl-1H-silol-1-yl)vinyl)-5H-dibenzo[b,d]silole (methyl(tetraphenyl)silole-silafluorene-vinylene cotrimer) (2)

To a dry toluene (8 mL) solution of 1 (150 mg, 0.65 mmol) and 1-methyl-1-hydrido(tetraphenyl)silole (522 mg, 1.3 mmol) was added H_2PtCl_6 (1 mg, 0.003 mmol). The solution was stirred at 70 °C for 3 h. The orange solution was then filtered and the solvent was removed by vacuum. The brown residue was precipitated from 1 mL of THF with 10 mL of MeOH to afford a light yellow powder (430 mg, 64%). Selected data; MP: 120 °C (decomp.); ^1H NMR (300.134 MHz, CDCl_3): δ 7.84 (dd,

4H, PhH), 7.45 (td, 2H, PhH), 6.76-7.06 (br, 46H, PhH, -HC=CH-), 0.502 (s, 6H, -CH₃); ²⁹Si NMR (71.548 MHz, inversed gated decoupling, CDCl₃): δ -2.66 (s, silafluorene); CH calcd for C₇₄H₅₈Si₃•2.0H₂O: C 83.3, H 5.85; Found: C 83.5, H 6.03.

2.5.9 Synthesis of 5,5'-(1E,1'E)-2,2'-(5H-dibenzo[b,d]silole-5,5-diyl)bis(ethene-2,1-diyl)bis(5-methyl-5H-dibenzo[b,d]silole) (methylsilafluorene-vinylene trimer) (3)

To a dry toluene (8 mL) solution of 1 (150 mg, 0.65 mmol) and 1-methyl-1-hydridosilafluorene (256 mg, 1.3 mmol) was added H₂PtCl₆ (1 mg, 0.003 mmol). The solution was stirred at 50 °C for 2 h. The orange solution was then filtered and the solvent removed under vacuum. The brown residue was precipitated from 1 mL of THF with 10 mL of MeOH to afford a white powder (270 mg, 66%). Selected data; MP: 70 °C (decomp.); ¹H NMR (300.134 MHz, CDCl₃): δ 7.81 (br, 12H, PhH), 7.56 (br, 6H, PhH), 7.42 (br, 6H, PhH), 6.80 (dd, 4H, -HC=CH-, J = 22 Hz), 0.472 (s, 6H, -CH₃); ²⁹Si NMR (71.548 MHz, inversed gated decoupling, CDCl₃): δ 1.18 (center Si), -9.44 (endgroups); CH calcd for C₄₂H₃₄Si₃•H₂O: C 78.7, H 5.66; Found: C 79.1, H 5.93.

2.5.10 Synthesis of poly(tetraphenylsilole-vinylene) (PSV) (4)

To a dry toluene (3 mL) solution of 1,1-diethynyl(tetraphenyl)silole (100 mg, 0.23 mmol) and 1,1-dihydrido(tetraphenyl)silole (89 mg, 0.23 mmol) was added H₂PtCl₆ (1 mg, 0.003 mmol). The solution was stirred at 80 °C for 24 h. The orange solution was filtered and the solvent removed by vacuum evaporation. The brown

residue was precipitated from 1 mL of THF with 10 mL of MeOH to afford a yellow powder (138 mg, 73%). Selected data; ^1H NMR (300.134 MHz, CDCl_3): δ 6.20-8.10 (br, PhH, $-\text{HC}=\text{CH}-$), 2.61 (s, 2H, $-\text{C}\equiv\text{C}-\text{H}$, terminal); ^{29}Si NMR (71.548 MHz, inversed gated decoupling, CDCl_3): δ 6.0 (weak signal); CH calcd for $\text{C}_{30}\text{H}_{22}\text{Si}\cdot 1.5\text{H}_2\text{O}$: C 82.4, H 5.76; Found: C 82.9, H 5.78.

2.5.11 Synthesis of poly(tetraphenylsilole-silafluorene-vinylene) (5)

To a dry toluene (3 mL) solution of 1 (100 mg, 0.43 mmol) and 1,1-dihydrido(tetraphenyl)silole (168 mg, 0.43 mmol) was added H_2PtCl_6 (1 mg, 0.003 mmol). The solution was stirred at 80 °C for 24 h. The orange solution was then filtered and the solvent removed under vacuum. The brown residue was precipitated from 1 mL of THF with 10 mL of MeOH to afford a light yellow powder (190 mg, 71%). Selected data; ^1H NMR (300.134 MHz, CDCl_3): δ 5.60-8.20 (br, PhH, $-\text{HC}=\text{CH}-$), 2.56 (s, 2H, $-\text{C}\equiv\text{CH}$, terminal); ^{29}Si NMR (71.548 MHz, inversed gated decoupling, CDCl_3): δ 6.0 (weak signal); CH calcd for $\text{C}_{44}\text{H}_{32}\text{Si}_2\cdot\text{H}_2\text{O}$: C 83.3, H 5.40; Found: C 83.4, H 5.94.

2.5.12 Synthesis of poly(silafluorene-vinylene) (PSFV) (6)

To a dry toluene (3 mL) solution of 1 (100 mg, 0.43 mmol) and 1,1-dihydridosilafluorene (79 mg, 0.43 mmol) was added H_2PtCl_6 (1 mg, 0.003 mmol). The solution was stirred at 80 °C for 24 h. The orange solution was then filtered and the solvent removed under vacuum. The brown residue was precipitated from 1 mL of

THF with 10 mL of MeOH to afford a yellow powder (118 mg, 66%). Selected data; ^1H NMR (300.134 MHz, CDCl_3): δ 5.80-8.50 (br, PhH, $-\text{HC}=\text{CH}-$), 2.55 (s, 2H, $-\text{C}\equiv\text{CH}$, terminal); ^{29}Si NMR (71.548 MHz, inverse gated decoupling, CDCl_3): δ 6.0 (weak signal); CH calcd for $\text{C}_{13}\text{H}_{10}\text{Si}\cdot 0.5\text{H}_2\text{O}$: C 76.7, H 5.45; Found: C 77.2, H 5.09.

2.5.13 Synthesis of 1-methyl-1-vinyl(tetraphenyl)silole (7)

Diphenylacetylene (10 g, 56 mmol) and chopped lithium wire (62 mmol) in dry THF (40 mL) were stirred overnight under argon. The dark green reaction was cannulated into a solution of methylvinylchlorosilane (4 mL, 31 mmol) and dry THF (90 mL) and stirred for 2 h at room temperature and then refluxed for 5 h. The reaction was quenched with sat. NH_4Cl and the organic solvent was removed by evaporation under vacuum. Extraction and crystallization in ether afforded yellow crystals (6.9 g, 59%). Selected Data; MP: 73-74 °C (Lit: 77-78 °C)⁶¹; ^1H NMR (300.133 MHz, CDCl_3): δ 6.80-7.15 (br. m, 20H, PhH), 6.37 (dd, 1H, $\text{SiCH}=\text{C}$), 6.19 (dd, 1H, $-\text{C}=\text{CH}_2$), 5.97 (dd, 1H, $-\text{C}=\text{CH}_2$), 0.589 (s, 3H, $-\text{CH}_3$); $^{13}\text{C}\{\text{H}\}$ NMR (75.403 MHz, CDCl_3): δ 155.34, 140.23, 139.73, 139.04, 136.38, 133.86, 130.17, 129.25, 128.12, 127.71, 126.53, 125.87, -6.34; ^{29}Si NMR (99.36 MHz, INEPT, CDCl_3 , TMS (δ 0.0)): δ -1.95 (s, silole); CH calcd for $\text{C}_{31}\text{H}_{26}\text{Si}$: C 87.2, H 6.14; Found: C 87.1, H 6.24 .

2.5.14 Synthesis of 1-methyl-1-vinylsilfluorene (8)

To a dry ethereal solution of 2,2'-dibromobiphenyl (5.0 g, 16 mmol) was slowly added n-BuLi (1.6 M in hexanes, 21 mL, 33 mmol) at -78 °C. The solution was

stirred at -78 °C for 10 min and then at room temperature overnight. To the cloudy yellow-green solution was added methylvinylchlorosilafluorene (2.08 mL, 16 mmol) at -78 °C. The solution was stirred for 20 min then stirred overnight at room temperature. The cloudy white reaction mixture was quenched with NH₄Cl and extracted with ether. The organics were dried over MgSO₄ and evaporated to dryness. The light yellow solid was recrystallized in hexanes to afford white crystals (1.8 g, 51%). Selected data; MP: 58-60 °C; ¹H NMR (300.134 MHz, CDCl₃): δ 7.85 (d, 2H, PhH), 7.64 (d, 2H, PhH), 7.46 (t, 2H, PhH), 7.30 (t, 2H, PhH), 6.26 (dd, 1H, SiCH=), 6.15 (dd, 1H, =CH₂), 5.97 (dd, 1H, =CH₂), 0.542 (s, 3H, -CH₃); ¹³C{H} NMR (75.403 MHz, CDCl₃): δ 148.49, 137.41, 135.53, 134.31, 133.45, 130.65, 127.73, 121.18, -5.46; ²⁹Si NMR (71.548 MHz, inverse gated decoupling, CDCl₃): δ -8.52 (s, silafluorene); CH calcd for C₁₅H₁₄Si: C 81.0, H 6.35; Found: C 80.9, H 6.81.

2.6 ACKNOWLEDGEMENTS

This chapter, in part, is a reprint of the material as it appears in the following paper: Sanchez, J. C.; DiPasquale, A. G.; Rheingold, A. L.; Trogler, W. C. “Synthesis, Luminescent Properties, and Explosives Sensing with 1,1-Tetraphenylsilole- and 1,1-Silafluorene-vinylene Polymers” *Chem. Mater.* **2007**, *19*, 6459–6470. The crystallographic information file (CIF) for compounds **1** and **3** is available on the internet at pubs.acs.org as “Supporting Information” to these publications.

2.7 APPENDIX

Table 2-8. Summary of X-ray Crystallographic Data for compound **3**.

3	
Formula	C ₁₃₂ H ₁₁₂ Si ₃
Formula weight	1782.49
Space group	C2/c
<i>a</i> , Å	22.059(3)
<i>b</i> , Å	15.588(2)
<i>c</i> , Å	34.607(5)
α , deg	90
β , deg	108.167(2)
γ , deg	90
<i>V</i> , Å ³	11307(3)
<i>Z</i> , <i>Z'</i>	4, 0.5
Crystal color, habit	yellow, block
ρ (calc), g cm ⁻³	1.047
μ (MoK α), mm ⁻¹	0.089
Temp, K	100(2)
Reflections measured	28422
Reflections ind.	9767 [R _{int} =0.0611]
R(F) (<i>I</i> > 2 σ (<i>I</i>)) ^a	0.0688
R(ω F ²) (<i>I</i> > 2 σ (<i>I</i>)) ^b	0.1771

^a R = $\sum ||F_o| - |F_c|| / \sum |F_o|$; ^b R(ω F²) = $\{\sum [\omega(F_o^2 - F_c^2)^2] / \sum [\omega(F_o^2)^2]\}^{1/2}$;
 $\omega = 1 / [\sigma^2(F_o^2) + (aP)^2 + bP]$, P = $[2F_c^2 + \max(F_o, 0)] / 3$

Table 2-9. Tabulated HOMO and LUMO energies calculated for various explosives and at the B3LYP/6-311+G** level of theory.

Compound	LUMO (eV)	HOMO (eV)	Band-gap (eV)
Tetryl	-4.327	-8.544	4.218
Picric Acid	-4.299	-8.599	4.299
TNT	-3.891	-8.816	4.925
PETN	-3.565	-9.197	5.633
DNT	-3.401	-8.435	5.034
HMX	-3.102	-8.707	5.605
RDX	-3.020	-8.626	5.605
TNG	-2.966	-9.524	6.588
EGDN	-2.639	-9.360	6.721
DMNB	-2.531	-8.435	5.905
TATP	-0.109	-6.694	6.585
HMTD	-0.136	-6.721	6.585

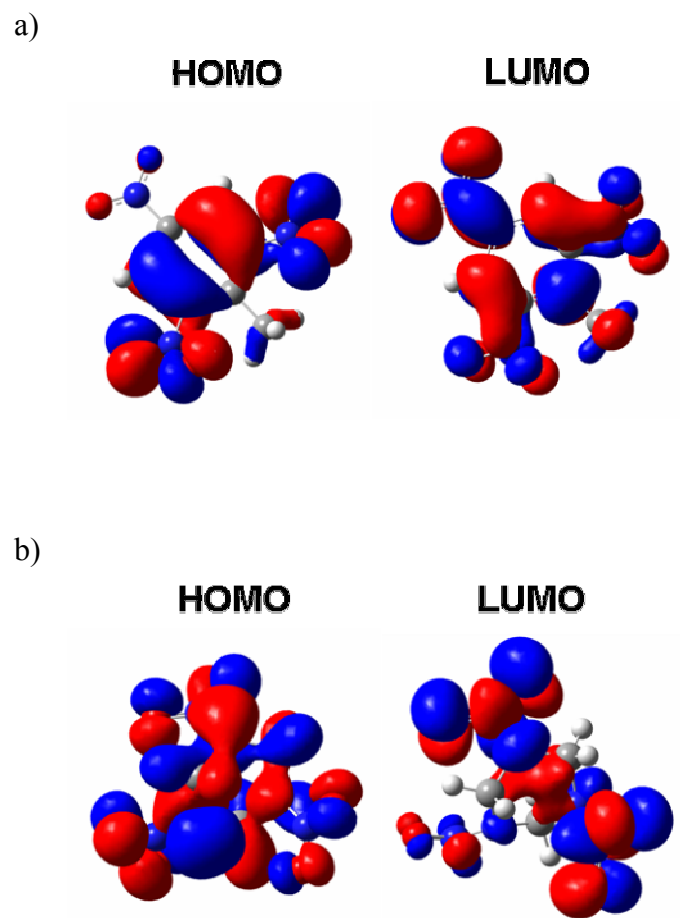


Figure 2-20. Frontier orbital density figures for a) TNT and b) RDX.

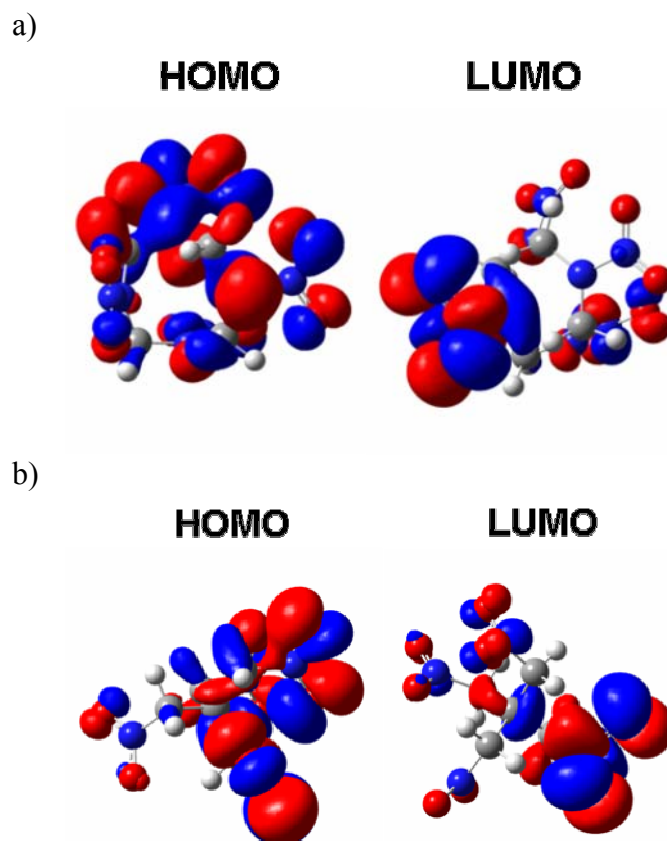


Figure 2-21. Frontier orbital density figures for a) HMX and b) PETN.

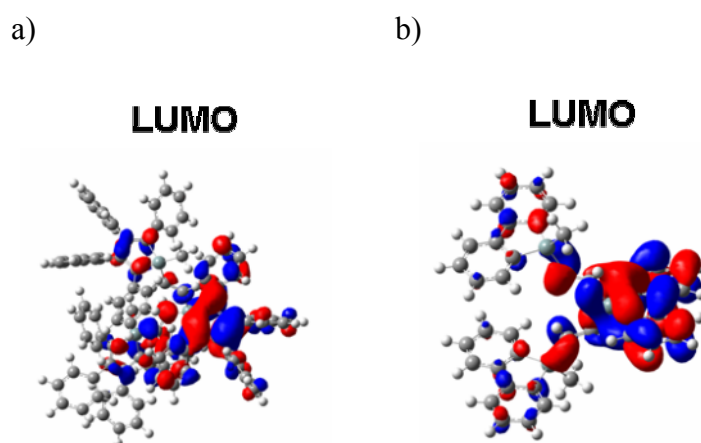


Figure 2-22. Lowest unoccupied molecular orbital (LUMO) density figures for a) 1 and b) 3.

2.8 REFERENCES

- (1) Steinfeld, J. I.; Wormhoudt, J. *Annu. Rev. Phys. Chem.* **1998**, *49*, 203–232.
- (2) Smith, K. D.; McCord, B. R.; McCrehan, W. A.; Mount, K.; Rowe, W. F. *J. Foren. Sci.* **1999**, *44*, 789–794.
- (3) Rouhi, A. M. *Chem. Eng. News.* **1997**, *75*, 14–22.
- (4) Hakansson, K.; Coorey, R. V.; Zubarev, R. A.; Talrose, V. L.; Hakansson, P. *J. Mass. Spectrom.* **2000**, *35*, 337–346.
- (5) Sylvia, J. M.; Janni, J. A.; Klein, J. D.; Spencer, K. M. *Anal. Chem.* **2000**, *72*, 5834–5840.
- (6) Popov, I. A.; Chen, H.; Kharybin, O. N.; Nikolaev, E. N.; Cooks, R. G. *Chem. Commun.* **2005**, *15*, 1953–1955.
- (7) Kolla, P. *Anal. Chem.* **1995**, *67*, 184A–189A.
- (8) Toal, S. J.; Sanchez, J. C.; Dugan, R. E.; Trogler, W. C. *J. Foren. Sci.* **2007**, *52*, 79–83.
- (9) Trogler, W. C. In *Electronic Noses & Sensors for the Detection of Explosives*; Gardner, J. W., Yinon, J., Eds.; Kluwer Academic Publishers: 2004, p 39.
- (10) Mostak, P. *Vapour and Trace Detection of Explosives for Anti-terrorism Purposes*; Krausa, M., Reznev, A. A., Eds.; Kluwer Academic Publishers: 2004, p 23.
- (11) Committee on Assessment of Security Technologies for Transportation, Opportunities to Improve Airport Passenger Screening with Mass Spectrometry (National Academy of Sciences, Washington, D.C., 2003).
- (12) Plexus Scientific Corporation. <http://www.plexsci.com/expray.shtml> (27 Nov 2006).
- (13) (a) Wampler, S. Lawrence Livermore National Laboratory. <http://www-cms.llnl.gov/s-t/elite.html> (27 Nov 2006). (b) Dynes, R. C. *President's Report*; Report 16(6): May 2006.
- (14) (a) McQuade, D. T.; Pullen, A. E.; Swager, T. M. *Chem. Rev.* **2000**, *100*, 2537–2574. (b) Toal, S. J.; Trogler, W. C. *J. Mater. Chem.* **2006**, *16*, 2871–2883. (c) Liu, Y.; Mills, R.; Boncella, J.; Schanze, K. *Langmuir* **2001**, *17*,

- 7452–7455. (d) Chang, C.; Chao, C.; Huang, J. H.; Li, A.; Hsu, C.; Lin, M.; Hsieh, B.; Su, A. *Synth. Met.* **2004**, *144*, 297–301.
- (15) (a) Toal, S. J.; Jones, K. A.; Magde, D.; Trogler, W. C. *J. Am. Chem. Soc.* **2005**, *127*, 11661–11665. (b) Toal, S. J.; Magde, D.; Trogler, W. C. *Chem. Comm.* **2005**, *43*, 5465–5467. (c) Sohn, H.; Sailor, M. J.; Douglas, M.; Trogler, W. C. *J. Am. Chem. Soc.* **2003**, *123*, 3821–3830. (d) Sohn, H.; Calhoun, R. M.; Sailor, M. J.; Trogler, W. C. *Angew. Chem., Int. Ed. Engl.* **2001**, *40*, 2104–2105.
- (16) (a) Geramita, K.; McBee, J.; Shen, Y.; Radu, N.; Tilley, T. D. *Chem. Mater.* **2006**, *18*, 3261–3269. (b) Tang, B. Z.; Zhan, X.; Yu, G.; Lee, P. P. S.; Liu, Y.; Zhu, D. *J. Mater. Chem.* **2001**, *11*, 2974–2978. (c) Sun, Y.; Giebink, N. C.; Kanno, H.; Ma, B.; Thompson, M. E.; Forrest, S. R. *Nature (London, United Kingdom)* **2006**, *440*, 908–912. (d) Deng, L.; Furuta, P. T.; Garon, S.; Li, J.; Kavulak, D.; Thompson, M. E.; Frechet, J. M. J. *Chem. Mater.* **2006**, *18*, 386–395. (e) D'Andrade, B. W.; Datta, S.; Forrest, S. R.; Djurovich, P.; Polikarpov, E.; Thompson, M. E. *Org. Electr.* **2005**, *6*, 11–20. (f) Ren, X.; Li, J.; Holmes, R. J.; Djurovich, P. I.; Forrest, S. R.; Thompson, M. E. *Chem. Mater.* **2004**, *16*, 4743–4747.
- (17) Tamao, K.; Kawachi, A. *Adv. Organomet. Chem.* **1995**, *38*, 1–58.
- (18) (a) Yamaguchi, Y. *Synthetic Met.* **1996**, *82*, 149–153. (b) Yamaguchi, S.; Tamao, K. *Bull. Chem. Soc. Jpn.* **1996**, *69*, 2327–2334.
- (19) Tamao, K.; Uchida, M.; Izumizawa, T.; Furukawa, K.; Yamaguchi, S. *J. Am. Chem. Soc.* **1996**, *118*, 11974–11975.
- (20) (a) Sohn, H.; Huddleston, R. R.; Powell, D. R.; West, R. *J. Am. Chem. Soc.* **1999**, *121*, 2935–2936. (b) Xu, Y.; Fujino, T.; Naito, H.; Dohmaru, T.; Oka, K.; Sohn, H.; West, R. *Jpn. J. Appl. Phys.* **1999**, *38*, 6915–6918. (c) Yamaguchi, S.; Endo, T.; Uchida, M.; Izumizawa, T.; Furukawa, K.; Tamao, K. *Chem. Eur. J.* **2000**, *6*, 1683–1692. (d) Kim, W.; Palilis, L. C.; Uchida, M.; Kafafi, Z. H. *Chem. Mater.* **2004**, *16*, 4681–4686. (e) Lee, S. H.; Jang, B.-B.; Kafafi, Z. H. *J. Am. Chem. Soc.* **2005**, *127*, 9071–9078.
- (21) (a) Yamaguchi, S.; Jin, R.-Z.; Tamao, K. *J. Organomet. Chem.* **1998**, *559*, 73–80. (b) Chan, K. L.; McKiernan, M. J.; Towns, C. R.; Holmes, A. B. *J. Am. Chem. Soc.* **2005**, *127*, 7662–7663. (c) Wang, E.; Li, C.; Mo, Y.; Zhang, Y.; Ma, G.; Shi, W.; Peng, J.; Yang, W.; Cao, Y. *J. Mater. Chem.* **2006**, *16*, 4133–4140.
- (22) Corriu, R. J. P.; Douglas, W. E.; Yang, Z.-X. *J. Organomet. Chem.* **1993**, *456*,

35–39.

- (23) Toal, S. J.; Sohn, H.; Zakarov, L. N.; Kassel, W. S.; Golen, J. A.; Rheingold, A. L.; Trogler, W. C. *Organometallics* **2005**, *24*, 3081–3087.
- (24) Chauhan, B. P. S.; Shimizu, T.; Tanaka, M. *Chem. Lett.* **1997**, 785–786.
- (25) (a) Burroughes, J. H.; Bradley, D. D. C.; Brown, A. R.; Marks, R. N.; Mackay, K.; Friend, R. H.; Burns, P. L.; Holmes, A. B. *Nature* **1990**, *349*, 539–541. (b) Kim, Y.-H.; Shin, D.-C.; Kwon, S.-K.; Lee, J.-H. *J. Mater. Chem.* **2002**, *12*, 1280–1283. (c) Shim, H.-K.; Jin, J.-I. *Adv. Polym. Sci.* **2002**, *158*, 193–243. (d) Lee, J.-H.; Hwang, D.-H. *Chem. Commun.* **2003**, 2836–2837. (e) Friend, R. H.; Gymer, R. W.; Holmes, A. B.; Burroughes, J. H.; Marks, R. N.; Taliani, C.; Bradley, D. D. C.; dos Santos, D. A.; Bredas, J. L.; Lögdlund, M.; Salaneck, W. R. *Nature* **1999**, *397*, 121–128. (f) Suh, M. C.; Chin, B. D.; Kim, M.-H.; Kang, T. M.; Lee, S. T. *Adv. Mater.* **2003**, *15*, 1254–1258.
- (26) (a) Korshak, V. V.; Sladkov, A. M.; Luneva, L. K. *Izv. Akad. Nau SSSR, Otd. Khim. Nauk* **1962**, 2251–2253. (b) Luneva, L. K.; Sladkov, A. M.; Korshak, V. V. *Vysokomol. Soedin.* **1965**, *7*, 427–431.
- (27) Joo, S.-H.; J., M.-Y.; Ko, D. H.; Park, J.-H.; Kim, K. Y.; Bae, S. J.; Chung, I. *J. Appl. Polym. Sci.* **2006**, *100*, 299–306.
- (28) Sumiya, K.-I.; Kwak, G.; Sanda, F.; Masuda, T. *J. Polym. Sci., Part A: Polym. Chem.* **2004**, *42*, 2774–2783.
- (29) (a) Dong, S. K.; Sang, C. S. *J. Polym. Sci., Part A: Polym. Chem.* **1999**, *37*, 2933–2940. (b) Dong, S. K.; Sang, C. S. *J. Polym. Sci., Part A: Polym. Chem.* **1999**, *37*, 2263–2273.
- (30) (a) Geisa, R.; Schulz, R. C. *Makromol. Chem.* **1990**, *191*, 857–867. (b) Lampert, R. A.; Meech, S. R.; Metcalf, J.; Phillips, D.; Schapp, A. P. *Chem. Phys. Lett.* **1983**, 137–140. (c) Maulding, D. R.; Roberts, B. G. *J. Org. Chem.* **1969**, *34*, 1734–1736. (d) Grem, G.; Leditzky, G.; Ullrich, B.; Leising, G. *Adv. Mater.* **1992**, *1*, 36–37. (e) Swager, T. M.; Gil, C. J.; Wrighton, M. S. *J. Phys. Chem.* **1995**, *99*, 4886–4893.
- (31) Habrard, F.; Ouisse, T.; Stéphan, O.; Aubouy, L.; Gerbier, Ph.; Hirsch, L.; Huby, N.; Van der Lee, A. *Synthetic Metals* **2006**, *156*, 1262–1270.
- (32) Solutions (30 mg mL⁻¹) of **1-6** were spin-cast from toluene for 1 min. at 2000

rpm. The 25 mm × 25 mm quartz substrate plates were cleaned by sonication in acetone and methanol for 10 min. each. Dichloromethane was then spin-cast onto the quartz plate to remove any residual particulate contamination.

- (33) Kraft, A.; Grimsdale, A. C.; Holmes, A. B. *Angew. Chem., Int. Ed.* **1998**, *37*, 403–428.
- (34) Chen, J.; Law, C. C. W.; Lam, J. W. Y.; Dong, Y.; Lo, S. M. F.; Williams, I. D.; Zhu, D.; Tang, B. Z. *Chem. Mat.* **2003**, *15*, 1535–1546.
- (35) (a) Yin, S.; Peng, Q.; Shuai, Z.; Fang, W.; Wang, Y.-H.; Luo, Y. *Phys. Rev. B: Condens. Matter* **2006**, *73*, 205409/1–205409/5. (b) Bhongale, C. J.; Chang, C.-W.; Diao, E. W.-G.; Hsu, C.-S.; Dong, Y.; Tang, B.-Z. *Chem. Phys. Lett.* **2006**, *419*, 444–449. (c) Chen, J.; Xu, B.; Yang, K.; Cao, Y.; Sung, H. H. Y.; Williams, I. D.; Tang, B. Z. *J. Phys. Chem. B* **2005**, *109*, 17086–17093. (d) Ren, Y.; Lam, J. W. Y.; Dong, Y.; Tang, B. Z.; Wong, K. S. *J. Phys. Chem. B* **2005**, *109*, 1135–1140.
- (36) (a) Wolak, M. A.; Delcamp, J.; Landis, C. A.; Lane, P. A.; Anthony, J.; Kafafi, Z. *Adv. Funct. Mat.* **2006**, *16*, 1943–1949. (b) Wolak, M. A.; Melinger, J. S.; Lane, P. A.; Palilis, L. C.; Landis, C. A.; Anthony, J. E.; Kafafi, Z. H. *J. Phys. Chem. B* **2006**, *110*, 10606–10611. (c) Wolak, M. A.; Melinger, J. S.; Lane, P. A.; Palilis, L. C.; Landis, C. A.; Delcamp, J.; Anthony, J. E.; Kafafi, Z. H. *J. Phys. Chem. B* **2006**, *110*, 7928–7937. (d) Jang, B.-B.; Lee, S. H.; Kafafi, Z. H. *Chem. Mater.* **2006**, *18*, 449–457.
- (37) Yang, J.-S.; Swager, T. M. *J. Am. Chem. Soc.* **1998**, *120*, 5321–5322.
- (38) (a) Shirakawa, S.; Lombardi, P. J.; Leighton, J. L. *J. Am. Chem. Soc.* **2005**, *127*, 9974–9975. (b) Kinnaird, J. W. A.; Ng, P. Y.; Kubota, K.; Wang, X.; Leighton, J. L. *J. Am. Chem. Soc.* **2002**, *124*, 7920–7921.
- (39) (a) Fesik, S. W. *J. Biomol. NMR* **1993**, *3*, 261–269. (b) Cheng, J.; Lepre, C. A.; Moore, J. M. *Biochemistry* **1994**, *33*, 4093–4108. (c) Shuker, S. B.; Hajduk, P. J.; Meadows, R. P.; Fesik, S. W. *Science* **1996**, *274*, 1531–1534. (d) Schnur, E.; Turkov, M.; Kahn, R.; Gordon, D.; Gurevitz, M.; Anglister, J. *Biochemistry* **2008**, *47*, 911–921. (e) Kríz, J.; Dybal, J.; Makrlík, E.; Budka, J. *Magn. Reson. Chem.* **2008**, *46*, 235–243.
- (40) Maria, P.-C.; Gal, J.-F. *J. Phys. Chem.* **1985**, *89*, 1296–1304.
- (41) Saxena, A.; Fujiki, M.; Naito, M.; Okoshi, K.; Kwak, G. *Macromolecules* **2004**, *37*, 5873–5879.

- (42) (a) Scatchard, G. *Ann. NY Acad. Sci.* **1949**, *51*, 660–672. (b) Fielding, L. *Tetrahedron* **2000**, *56*, 6151–6170.
- (43) Ngowe, C. O.; Bishop, K. D.; McGuffin, V. L. *Anal. Chim. Acta* **2001**, *427*, 137–142.
- (44) (a) Cernia, E.; Delfini, M.; Di Cocco, M. E.; Palocci, C.; Soro, S. *Bioorg. Chem.* **2002**, *30*, 276–284. (b) Delfini, M.; Bianchetti, C.; Di Cocco, M. E.; Pescosolido, N.; Porcelle, F.; Rosa, R.; Rugo, G. *Bioorg. Chem.* **2003**, *31*, 378–388.
- (45) (a) Zhou, Q.; Swager, T. M. *J. Am. Chem. Soc.* **1995**, *117*, 12593–12602. (b) Zhou, Q.; Swager, T. M. *J. Am. Chem. Soc.* **1995**, *117*, 7017–7018.
- (46) Thomas III, S. W.; Amara, J. P.; Bjork, R. E.; Swager, T. M. *Chem. Commun.* **2005**, 4572–4574.
- (47) (a) Saravanan, N. P.; Venugopalan, S.; Senthilkumar, N.; Santhosh, P.; Kavita, B.; Prabu, H. G. *Talanta* **2006**, *69*, 656–662. (b) Orloff, M. K.; Mullen, P. A.; Rauch, F. C. *J. Phys. Chem.* **1970**, *74*, 2189–2192. (c) Chaloosi, M.; Gholamian, F.; Zarei, M. A. *Propellants, Explosives, Pyrotechnics* **2001**, *26*, 21–25.
- (48) Kawabata, H.; Ishida, K.; Matsushige, K.; Tachikawa, H. In *Proc. Int. Symp. Super-Functionality Organic Devices*; IPAP Conf. Series 6: 2005, pp 42–45.
- (49) (a) Nielsen, A. T.; Chafin, A. P.; Christian, S. L.; Moore, D. W.; Nadler, M. P.; Nissan, R. A.; Vanderah, D. J.; Gilardi, R. D.; George, C. F.; Flippen-Anderson, J. L. *Tetrahedron* **1998**, *54*, 11793–11812. (b) Simpson, R. L.; Urtiew, P. A.; Ornellas, D. L.; Moody, G. L.; Scribner, K. J.; Hoffman, D. M. *Propellants, Explosives, Pyrotechnics* **1997**, *22*, 249–255.
- (50) (a) Zhang, M.-X.; Eaton, P. E.; Gilardi, R. *Angew. Chem., Int. Ed.* **2000**, *39*, 401–404. (b) Eaton, P. E.; Zhang, M.-X.; Gilardi, R.; Gelber, N.; Iyer, S.; Surapaneni, R. *Propellants, Explosives, Pyrotechnics* **2002**, *27*, 1–6.
- (51) Chang, L. S.; Corey, J. Y. *Organometallics* **1989**, *8*, 1885–1893.
- (52) Gilman, H.; Gaj, B. J. *J. Org. Chem.* **1957**, *22*, 447–449.
- (53) Ruhlmann, K. *Z. Chem.* **1965**, *5*, 354.
- (54) Liu, Y.; Stringfellow, T. C.; Ballweg, D.; Guzei, I. A.; West, R. *J. Am. Chem. Soc.* **2002**, *124*, 49–57.

- (55) Dennis, J. W. H.; Rosenblatt, D. H.; Blucher, W. G.; Coon, C. L. *J. Chem. Eng. Data* **1975**, *20*, 202–203.
- (56) Hariharan, P. C.; Pople, J. A. *Theor. Chim. Acta.* **1973**, *28*, 213–222. Several calculations at the B3LYP/6-311+G** level of theory for **1** and **3** show that the extra valence and diffuse functions give similar results to the 6-31G* basis set used in this study.
- (57) Becke, A. D. *J. Chem. Phys.* **1993**, *98*, 5648–5652.
- (58) Lee, C.; Yang, W.; Parr, R. G. *Phys. Rev. B* **1988**, *37*, 785–789.
- (59) (a) Stratmann, R. E.; Scuseria, G. E.; Frisch, M. J. *J. Chem. Phys.* **1998**, *109*, 8218–8224. (b) Bauernschmitt, R.; Ahlrichs, R. *Chem. Phys. Lett.* **1996**, *256*, 454–464. (c) Casida, M. E.; Jamorski, C.; Casida, K. C.; Salahub, D. R. *J. Chem. Phys.* **1998**, *108*, 4439–4449.
- (60) Gaussian 03, Revisions B.05, Frisch, M. J.; Trucks, G. W.; Schlegel, H. B.; Scuseria, G. E.; Robb, M. A.; Cheeseman, J. R.; Montgomery Jr., J. A.; Vreven, T.; Kudin, K. N.; Burant, J. C.; Millam, J. M.; Iyengar, S. S.; Tomasi, J.; Barone, V.; Mennucci, B.; Cossi, M.; Scalmani, G.; Rega, N.; Petersson, G. A.; Nakatsuji, H.; Hada, M.; Ehara, M.; Toyota, K.; Fukuda, R.; Hasegawa, J.; Ishida, M.; Nakajima, T.; Honda, Y.; Kitao, O.; Nakai, H.; Klene, M.; Li, X.; Knox, J. E.; Hratchian, H. P.; Cross, J. B.; Bakken, V.; Adamo, C.; Jaramillo, J.; Gomperts, R.; Stratmann, R. E.; Yazyev, O.; Austin, A. J.; Cammi, R.; Pomelli, C.; Ochterski, J. W.; Ayala, P. Y.; Morokuma, K.; Voth, G. A.; Salvador, P.; Dannenberg, J. J.; Zakrzewski, V. G.; Dapprich, S.; Daniels, A. D.; Strain, M. C.; Farkas, O.; Malick, D. K.; Rabuck, A. D.; Raghavachari, K.; Foresman, J. B.; Ortiz, J. V.; Cui, Q.; Baboul, A. G.; Clifford, S.; Cioslowski, J.; Stefanov, B. B.; Liu, G.; Liashenko, A.; Piskorz, P.; Komaromi, I.; Martin, R. L.; Fox, D. J.; Keith, T.; Al-Laham, M. A.; Peng, C. Y.; Nanayakkara, A.; Challacombe, M.; Gill, P. M. W.; Johnson, B.; Chen, W.; Wong, M. W.; Gonzalez, C.; Pople, J. A. Gaussian, Inc., Wallingford CT, **2004**.
- (61) Balasubramanian, R.; George, M. V. *Tetrahedron* **1973**, *29*, 2395–2404.

CHAPTER III

Divinylbenzene Bridged Silole and Silafluorene Polymers. Improved Applications to Surface Imaging of Explosive Particulates

3.1 ABSTRACT

The syntheses, spectroscopic characterization, and fluorescence quenching efficiencies of 1,1-silole- and 1,1-silafluorene-phenylenedivynylene polymers are reported. Model dimeric metallole compounds containing a phenylenedivynylene bridge have been synthesized to provide detailed structural and spectroscopic insight into conformational effects and electron delocalization. Poly((tetraphenyl)silole-phenylenedivynylene) and poly(silafluorene-phenylenedivynylene) both maintain a regio-regular *trans*-vinylene Si-C backbone with σ^* - π/π^* conjugation. Various hydrosilylation catalysts were screened to evaluate their ability to produce high molecular weight polymers and to direct a strictly *trans*-product. Molecular weights (M_w) for these polymers are in the range of 8400 to 9600. Fluorescence spectroscopy shows a significant bathochromic shift for the silafluorene polymer from solution to the solid-state. A surface detection method for the analysis of solid particulates of TNT, DNT, PA, RDX, HMX, Tetryl, TNG and PETN by fluorescence quenching was explored. The blue-emitting silafluorene polymer exhibited improved sensitivity for detecting explosive particle residues as compared to previously reported metallole polymers. Detection limits as low as 100 pg cm^{-2} for TNT are obtained. The Stern-Volmer equation quantitatively models the fluorescence quenching of these polymers by TNT, RDX, and PETN in thin solid state films.

3.2 INTRODUCTION

The recent rise in global terror threats and the general availability of high explosives and precursors thereof have increased demand for improved explosives screening processes. Current detection methods include but are not limited to gas chromatography coupled with mass spectrometry,¹ gas chromatography-electron capture detection,² surface-enhanced Raman spectroscopy,³ mass spectrometry,⁴ X-ray imaging, nuclear quadrupole resonance, thermal and fast neutron analysis, and ion mobility spectrometry,⁵ colorimetric methods,⁶ and fluorimetric detection.⁷ The recent success of amplified fluorescence quenching with conjugated polymers to detect nitroaromatic⁸ has prompted the development of new polymeric materials for explosives detection. Luminescent polymers offer rapid response times, low detection limits, intuitive interpretation, and cost efficient solutions. The properties of luminescent polymers can be altered through tuning of the HOMO and LUMO energy levels through chemical modification of the polymer backbone and the degree of π -conjugation.⁹ By extending the conjugation length, properties such as electron-hole mobility, emission wavelength, crystal packing (excimer emission) and amplified chemosensor response can be altered. Poly(*p*-phenyleneethynylene)s have been widely studied because of their highly rigid and delocalized structures. The use of acetylenic polymers can be problematic in solid state applications due to self-quenching, so bulky pendent groups are required to prevent the π -stacking that leads to quenching; however, this often requires lengthy syntheses.

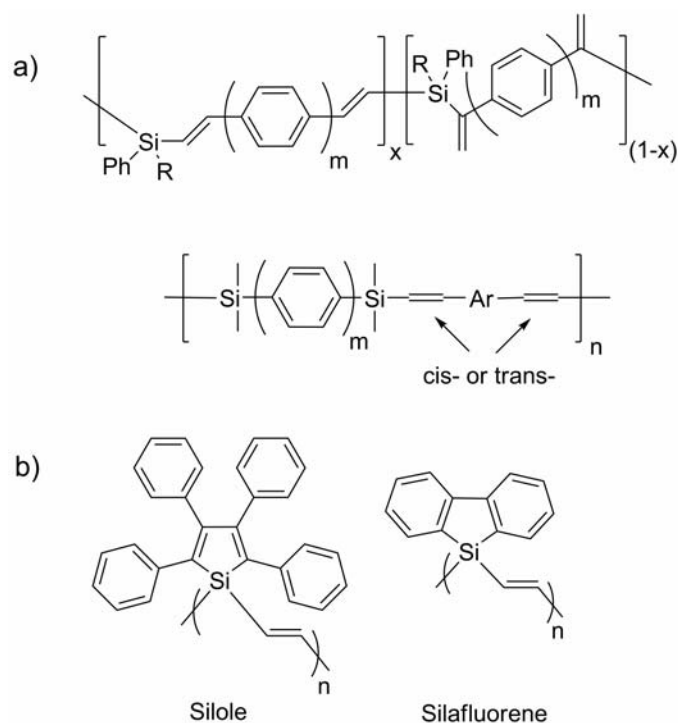


Figure 3-1. Chemical structures of silicon-containing vinylene polymers. a) Silane-phenylenevinylene polymers with irregular stereochemistry about the vinylene moieties. b) Silole- and silafluorene-vinylene polymers with $\sigma^*-\pi/\pi^*$ conjugation through the silicon center.

Another approach is to use a more flexible vinylene framework that maintains orbital conjugation while inhibiting π -stacking in thin-films. Polymers consisting of *p*-vinylene units are among the most popular due to their strong emissive properties.¹⁰ Techniques used to access these vinylic functionalities include Heck coupling,¹¹ Wittig condensation,¹² the Gilch route,¹³ and the Suzuki-Heck cascade.¹⁴ These reactions either require multi-step synthetic procedures, harsh reaction conditions, specific precursors, or are incompatible with various functional groups. To maximize conjugation, a regular *trans*-stereochemical framework is essential. A lack of regio-regularity can shorten the length of the conjugated segments within the polymer and

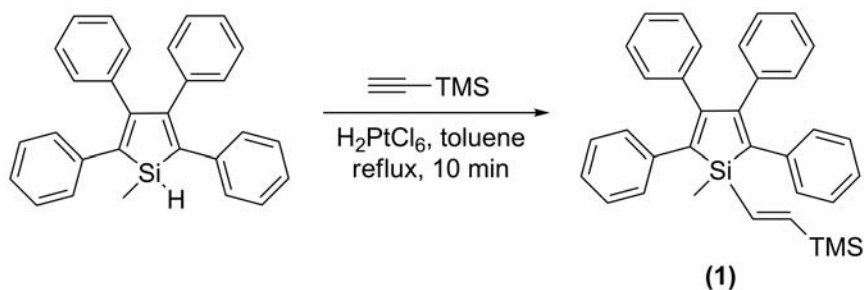
inhibit exciton mobility along the polymer backbone. Characterization of the stereochemistry of the important vinylene bridge is often difficult due to broadening in the aromatic region of the ^1H NMR spectrum of high molecular weight polymers.

Silane-phenylenedivinylene copolymers have recently been synthesized by hydrosilylation and palladium-catalyzed coupling of dihydridosilanes with unsaturated carbon linkers (Figure 3-1a).¹⁵⁻¹⁸ These copolymers are slightly delocalized through σ - π conjugation in the silicon-carbon framework. Silicon-doped poly(vinylenes) are also promising OLED and pre-ceramic materials.¹⁹⁻²³ The inclusion of silicon into the polymer framework stabilizes the structure and creates a more flexible and soluble polymer.²⁴ Delocalization is limited in these polycarbosilanes because of minimal conjugation between π -systems through the silicon atom, and the mixture of geometric isomers often produced during the hydrosilylation reaction (*trans*, *cis*, *gem*). These polymers also lack the visible photoluminescence (PL) properties required for imaging applications as fluorescent chemosensors.

Siloles, or 1-silacyclopentadienes, and poly(tetraphenyl)siloles have attracted attention because of their unique photoluminescent properties.^{25,26} Applications include electron transporting materials²⁷ and inorganic polymer sensors,²⁸⁻³¹ which take advantage of the σ^* - π^* conjugation between the σ^* orbital on the silicon centers of the polymer backbone and the π^* molecular orbital of the butadiene moiety in the metallole ring. Dehydrocoupling³² and Wurtz coupling³³ approaches have been used to prepare these materials, which are short chain oligomers that are susceptible to photobleaching from the weak Si-Si backbone. Hydrosilylation has also been used to

create short polymer chain conjugated silole and silafluorene polymers that incorporate a vinylene-bridged Si-C backbone (Figure 3-1b).³⁴ These polymers have shown promise as a new class of robust, conjugated vinylene polymers for chemical sensor and UV-emitting applications. However, visualization of these polymers is not optimal due to their largely UV-emission properties. Silafluorene is attractive as a fluorophore because of its ability to sense a wide range of explosive analytes.³⁴ It also provides improved thermal stability and eliminates g-band (green emission) defects often seen in fluorene based UV-blue emitting materials.³⁵ The co-polymerization of silafluorene in the 1,1-positions with an unsaturated organic co-monomer offers the possibility of a new type of stable blue-emitting materials.

This chapter focuses on the synthesis of silole and silafluorene copolymers by catalytic hydrosilylation of 1,4-diethynylbenzene (DEB) for use in explosives detection. These materials form a new class of easily synthesized phenylene-divinylene conjugated polymers. Model dimeric complexes were synthesized and characterized by single crystal X-ray diffraction to provide insight into the structural conformation and orbital overlap in these systems. Catalyst and reaction temperatures were varied to optimize formation of the regio-regular *trans*-product. The photoluminescence properties of these materials were characterized both in solution and in thin-films. The blue-emitting silafluorene copolymer exhibits excellent detection for a wide range of common high explosives. The ease of synthesis, processability and enhanced detection limits obtained for a range of explosives, make



Scheme 3-1. Hydrosilylation of trimethylsilylacetylene by 1-hydrido-1-methyl-(tetraphenyl)silole using H_2PtCl_6 .

them attractive alternatives to current particle sensing technology. The thin-film stability, extended conjugation and conformational flexibility also make these polymers promising new materials for blue-emitting photoluminescence and possibly electroluminescence applications.

3.3 RESULTS AND DISCUSSION

3.3.1 Model Compounds

To test whether hindered siloles would undergo catalytic hydrosilylation, 1-methyl-1-*trans*(2-trimethylsilyl)ethenyl-2,3,4,5-(tetraphenyl)silole (**1**) was synthesized by the H_2PtCl_6 (CPA) catalyzed hydrosilylation of trimethylsilylacetylene with 1-methyl-1-hydrido(tetraphenyl)silole (Scheme 3-1). The starting material is consumed within 10 min, as indicated by the disappearance of the Si-H proton resonance and appearance of vinylic protons in the ^1H NMR spectrum. The crystal structure reveals exclusive *cis*- β -addition (yielding the *trans* product) to the trimethylsilylacetylene group, which is promoted by steric crowding between the metalloid center and the 2,5-phenyl groups on the silole unit (Figure 3-2). With β -

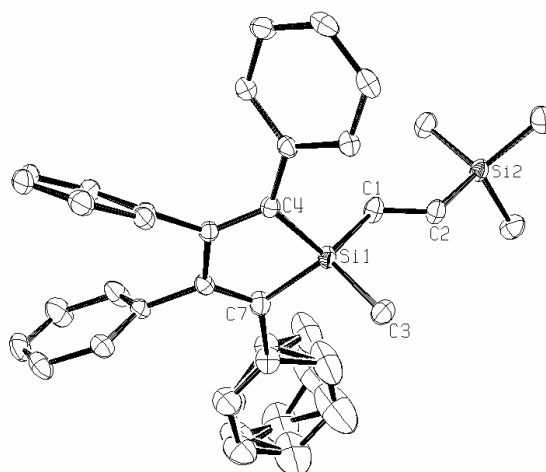
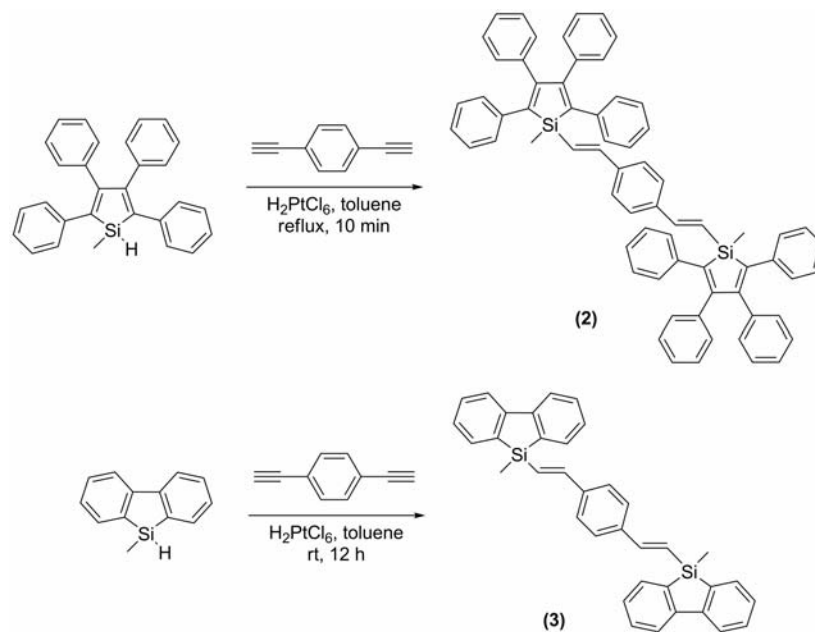


Figure 3-2. Thermal ellipsoid plot of **1** at the 50% probability level. Selected bond lengths, (Å): Si1-C1 1.856(2), C1-C2 1.866(1), Si2-C2 1.358(2); and angles, (deg): Si1-C1-C2 93.21(6), C1-C2-Si2 107.4(1), C3-Si1-C1 107.0(1), C4-Si1-C7 116.1(1). The phenyl ring bound to C7 was modeled with a disorder model using two conformations.

addition favored, this approach held promise for the stereospecific synthesis of regular copolymers by catalytic hydrosilylation.

Model dimeric complexes were then synthesized to aid structural characterization of new phenylenedivinylene polymers (Scheme 3-2). Synthesis of 1,4-di(1-methyl-1-*trans*-ethenyl-2,3,4,5-(tetraphenyl)silole)benzene (**2**) produced a regio-regular structure using CPA catalyst in toluene at temperatures ranging from 25 °C to its boiling point (Scheme 3-2). A strictly *trans*-product was confirmed by X-ray diffraction (Figure 3-3). The synthesis of 1,4-di(1-methyl-1-*trans*-ethenyl-silafluorene)benzene (**3**) was first attempted by refluxing the starting materials in toluene; however, the ¹H NMR spectrum revealed a mixture of *cis*- (doublet at 6.41 ppm, J: 19 Hz), *gem*- (two doublets at 6.03 and 5.83 ppm, J: 2.4 and 2.4 Hz), and



Scheme 3-2. Synthesis of **2** and **3** by catalytic hydrosilylation.

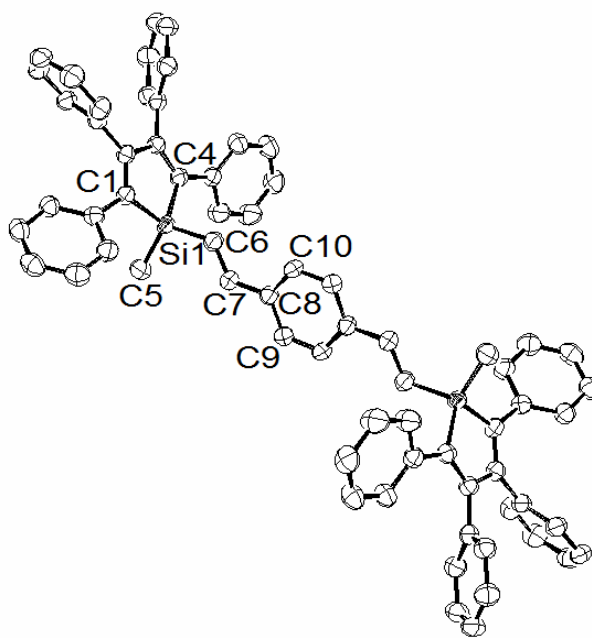


Figure 3-3. Thermal ellipsoid plot of **2** at the 50% probability level. Hydrogen atoms and solvent molecules omitted for clarity. Selected bond lengths, (Å): Si1-C6 1.8461(18), C6-C7 1.325(2), C7-C8 1.473(2); and angles, (deg): C1-Si1-C4 92.57(8), Si1-C6-C7 125.69(15), C6-C7-C8 127.13(18).

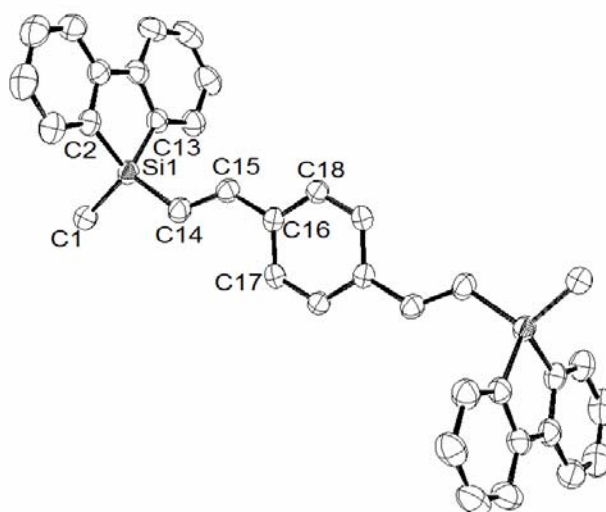


Figure 3-4. Thermal ellipsoid plot of **3** at the 50% probability level. Hydrogen atoms omitted for clarity. Selected bond lengths, (Å): Si1-C14 1.848(2), C14-C15 1.337(3), C15-C16 1.476(3); and angles, (deg): C2-Si1-C13 91.08(9), Si1-C14-C15 123.14(16), C14-C15-C16 126.13(18).

trans-vinyl (two doublets at 7.07 and 6.51 ppm, J: 19.2 and 19.2 Hz) isomeric products. However, by stirring the starting materials at room temperature for 12 hours, the *trans*-only product **3** was obtained in 79% yield. X-ray quality crystals were obtained by slow evaporation of a hexane solution and the structure was found to adopt a regio-regular *trans*-structure for both vinylene functionalities (Figure 3-4). The effect of reaction temperature on the stereochemistry of **3** is explained by the sterically less demanding environment at silicon for the silafluorene moiety as compared with the (tetraphenyl)silole. On oxidative addition to the platinum center, 1,2-insertion of the Si-H bond across the coordinated triple bond of DEB exhibits reduced steric control in the case of the silafluorene. Therefore, a reduced temperature is necessary to select the kinetically favored *trans*-product.

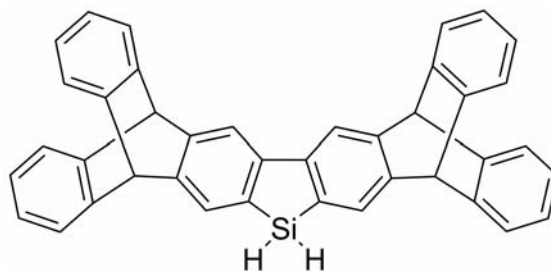


Figure 3-5. Chemical structure of 1,1-dihydrido-4,5,8,9-bis(triptycene)silafluorene (siliptycene). The experimental procedure for its synthesis is provided in the supporting information.

To test the importance of steric crowding, we synthesized an iptycene-substituted silafluorene (Figure 3-5). The iptycene functionality provides a bulky framework around the silafluorene core unit. Attempts to polymerize this siliptycene monomer by both dehydrocoupling and catalytic hydrosilylation of 1,4-diethynylbenzene failed over a range of temperatures and catalysts. The lack of reactivity observed at the silicon center supports the notion that catalytic hydrosilylation in these systems is susceptible to control by steric effects.

The *trans*-vinylene bond lengths of 1.325(2) Å in **2** are typical carbon-carbon bond lengths. The torsion angles for Si1-C6-C7 (silole-vinyl) and C6-C7-C8 (vinyl-phenyl) are 125.69(15)° and 127.13(18)°, respectively. The out-of-plane angle between the vinylene groups and the bridging phenylene functionality is only 7.0°. However, the vinylene unit plane for **2** lies at 84.8° with respect to the face of the silole unit. This near orthogonal alignment suggests minimal orbital overlap between the vinylene unit and the σ^* orbital of the silicon center. The poor alignment at the silicon center should reduce exciton delocalization along the chain in the polymer if a similar structure is adopted as for the dimer.

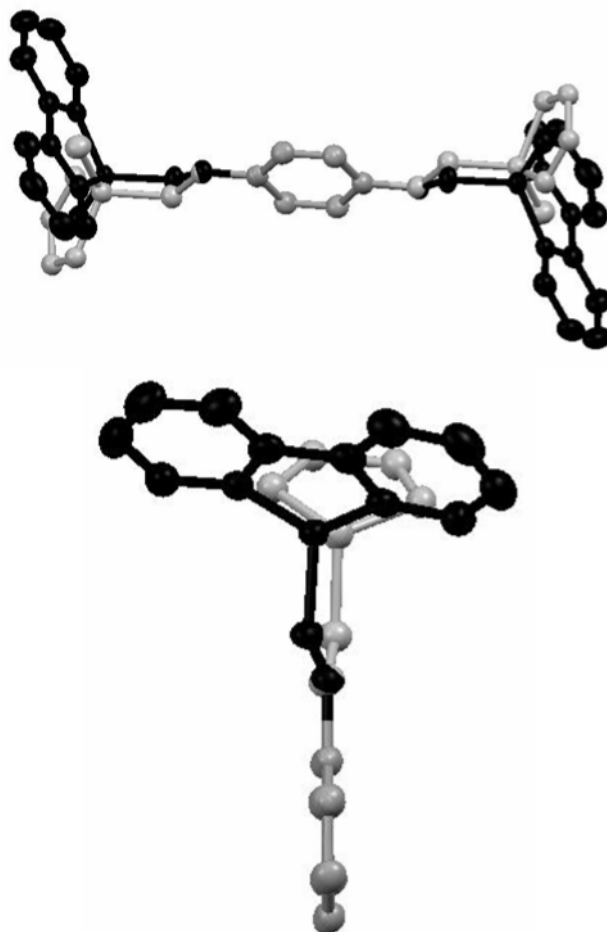
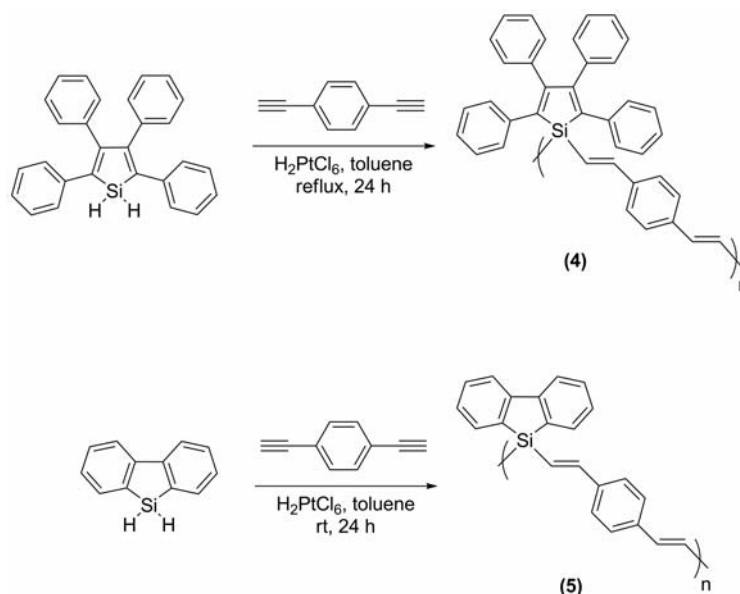


Figure 3-6. Superimposed crystal structures of **2** (grey atoms) and **3** (black atoms). Structures were aligned according to the phenylene subunit. Top: a side view of the structures. Hydrogen atoms and phenyl rings for **2** were omitted for clarity. Bottom: a view down the plane of the phenylene ring with half of the structures omitted for clarity. The large out-of-plane angle for **3** as compared to **2** allows for better orbital overlap between the vinylene group (π/π^*) and the silicon center (σ^*).

Dimer **3** shows a similar structure as **2** with a *trans*-vinylene bond length of 1.337(3) Å and torsion angles of 123.14(16)° and 126.13(18)° for Si1-C14-C15 (silafluorene-vinyl) and C14-C15-C16 (vinyl-phenyl), respectively. The torsion angles are slightly smaller than the ones observed in **2** due to the less sterically



Scheme 3-3. Synthesis of **4** and **5** by catalytic hydrosilylation.

demanding silafluorene moiety. The out-of-plane angle between the vinylene groups and the bridging phenylene functionality is 20.9° . The plane of the vinylene unit in **3** is at 71.0° with respect to the plane of the silafluorene unit. This allows the π -orbitals of the vinylene unit to better face the silacyclopentadiene, creating partial overlap with the σ^* orbitals of the silicon center. Since the σ^* orbitals at silicon have a major contribution to the LUMO of this photoluminescent monomer, conjugation in the silafluorene polymers is expected to be better than in the (tetraphenyl)silole analogue. Figure 3-6 contains the superimposed structures of the dimers.

3.3.2 Catalyst Optimization and Polymerization

With the stereochemical regularity of the hydrosilylation reaction optimized through kinetic control, poly((tetraphenyl)silole-phenylenedivinylene) (**4**) and

Table 3-1. Polymerization results for **4** and **5** prepared by catalytic hydrosilylation with various catalysts in toluene for 24 h.

Entry	Conditions	Catalyst ^a	Yield ^b (%)	M_w (GPC)	$(M_w/M_N)^c$
4_a	reflux	H ₂ PtCl ₆	51	8400	1.8
4_b	reflux	Wilkinson's catalyst	49	6000	1.8
4_c	reflux	Karstedt's catalyst	67	5600	1.5
4_d	reflux	Pd(PPh ₃) ₄	75	5500	1.3
5_a	room temperature	H ₂ PtCl ₆	68	9600	2.0
5_b	room temperature	Wilkinson's catalyst	63	4400	1.7
5_c	room temperature	Karstedt's catalyst	69	3700	2.1
5_d	room temperature	Pd(PPh ₃) ₄	51	5300	1.8

^a Reactions performed with following quantity of catalyst (mol %): H₂PtCl₆ (0.2), Wilkinson's (2.0), Karstedt's (1.0), Pd(PPh₃)₄ (1.0). ^b Calculated after three precipitations from methanol. ^c Calculated by GPC.

poly(silafluorene-phenylenedivinylene) (**5**) were synthesized in good yield (>80%) with the CPA catalyst (Scheme 3-3). Isolated yields are lower than the spectroscopic yields due to the removal of low molecular weight oligomers through multiple precipitations. Although CPA is a commonly used heterogenous catalyst for hydrosilylation reactions, several other catalysts were screened for the copolymerization of 1,1-dihydrido(tetraphenyl)silole (H₂silole) and 1,1-

dihydridosilafluorene (H_2SF) with DEB in an attempt to improve polymer yields and to increase molecular weights. The catalysts screened include Wilkinson's catalyst ($RhCl(PPh_3)_3$), $Pd(PPh_3)_4$ and Karstedt's catalyst (platinum-divinyltetramethyldisiloxane) (Table 3-1). All polymers were analyzed using 1H NMR and GPC to characterize polymer stereoregularity and molecular weights, respectively. Although the $Pd(PPh_3)_4$ catalyst forms **4** and **5** in high yields, and with comparable molecular weights (Table 3-1), the removal of the homogeneous catalyst presents a purification challenge. Wilkinson's catalyst produces slightly lower molecular weights with lower yields. This could be due to competitive polymerization pathways as it is also an effective catalyst for dehydrocoupling.³² Karstedt's catalyst produces the lowest molecular weights and yields of the four catalysts studied. This liquid platinum disiloxane catalyst is inconvenient and separation from the product is problematic. Overall, CPA produces the highest molecular weights and yields, and it is separated easily from the polymer by filtration. Polymers **4_a** and **5_a** seen in Table 3-1 were chosen for all the photoluminescence and explosives detection studies and will hereafter be referred to as **4** and **5**, respectively.

3.3.3 Photoluminescence

3.3.3.1 Solution-phase Photoluminescence and Quantum Efficiencies

Photoluminescence (PL) data for all the compounds synthesized in this study are listed in Table 3-2. For the silole-containing materials, there is no shift in the fluorescence emission from monomer ($H_2silole$) to dimer **2** (Figure 3-7). There is

Table 3-2. Summary of photoluminescence data for monomers, dimers, and polymers.

Entry	λ_{abs} (nm) ^a	ϵ_{max} (L mol ⁻¹ cm ⁻¹)	Solution λ_{flu} (nm) ^a	Thin-film λ_{flu} (nm) ^c	Φ_{flu} (%) ^d
H ₂ silole	305	7500	482	485	0.13
H ₂ SF	288	7700	343	365	24
2	306	14 000	482	482	0.65
3	290	31 000	348	380	17
4	322	7600 ^b	487	478	0.60
5	294	14 000 ^b	359	447	4.0

^a UV-vis and fluorescence taken in toluene. ^b Absorptivities are calculated per mole of silicon. ^c Emission maximum for thin layer of fluorophore absorbed onto TLC plate. ^d Quantum yield (Φ_{flu}) of fluorescence \pm 30%, relative to 9,10-diphenylanthracene in toluene.

only a slight bathochromic shift of 5 nm (213 cm⁻¹) for the corresponding polymer **4**. These results are consistent with the structural analysis, which revealed an orthogonal alignment of the bridging organic π -system and the Si-C σ^* orbitals in dimer **2**. The flexibility of the phenylene-divinylene units in solution for high molecular weight materials, such as polymer **4**, may allow population in the solution phase of some conformers with improved alignment. In contrast, the silafluorene dimer revealed a better alignment for conjugation of the bridging organic π -system and the Si-C σ^* orbitals. The fluorescence emission of dimer **3** is red-shifted 5 nm (419 cm⁻¹) from the

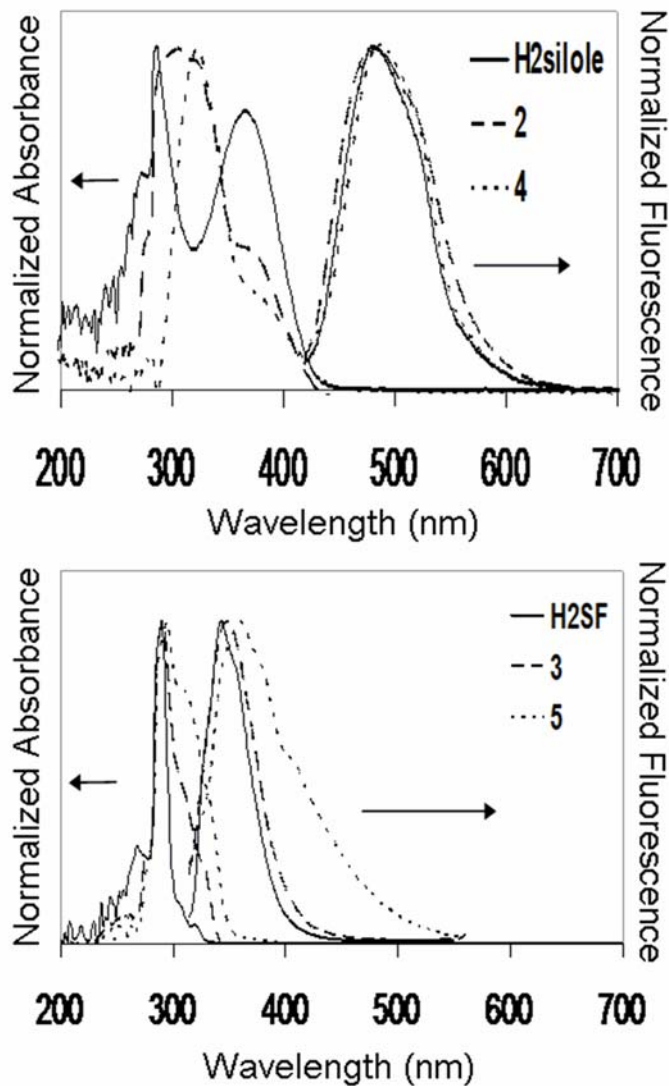


Figure 3-7. UV-vis and fluorescence spectra of siloles (H₂silole, **2**, and **4**) and silafluorenes (H₂SF, **3**, and **5**) showing a bathochromic emission shift for the polymers, and peak broadening of **5**.

H₂SF monomer (Figure 3-7), and polymer **5** is red-shifted another 11 nm (880 cm⁻¹) from dimer **3**. There is also significant peak broadening in the emission spectrum of polymer **5** as compared to H₂SF and **3**. This suggests that polymer **5** has a partially

delocalized structure and is a better candidate for fluorescence detection applications with improved exciton mobility.

Quantum yield measurements show that the silafluorene materials are efficient emitters in solution. Polymer **5** has a fluorescence quantum yield of ~ 4%, which is an order of magnitude greater than polymer **4**. However, polymer **4** has a higher solution fluorescence quantum yield than previously prepared (tetraphenyl)silole polymers.³² Conformational flexibility in solution is known to increase non-radiative decay pathways, lowering the fluorescence quantum yields in solution as compared to the solid state.³⁶ Thus, the rigid siliptycene monomer (Figure 3-5) has the highest solution emission quantum yield (27%). It is well known that solid-state emission intensities of the (tetraphenyl)silole polymers are often 20x to 30x larger than in solution, an effect called aggregation induced emission (attributed to restricted phenyl ring rotation in the solid-state).

3.3.3.2 Solid-state Photoluminescence

Solid-state fluorescence studies were conducted to gain insight into the thin-film PL properties of polymers **4** and **5**. Previous studies with (tetraphenyl)silole and silafluorene containing polymers show that silica thin-layer chromatography (TLC) plates serve as an effective, low cost medium for the analysis of thin-film PL properties.^{34,37} Polymers **4** and **5** were developed onto silica TLC plates (Whatman PE SIL G/UV) using chloroform (4 mg mL⁻¹). The area developed was maintained at 6 cm² for each sample. Dimers **2** and **3** were examined for comparison. Figure 3-8

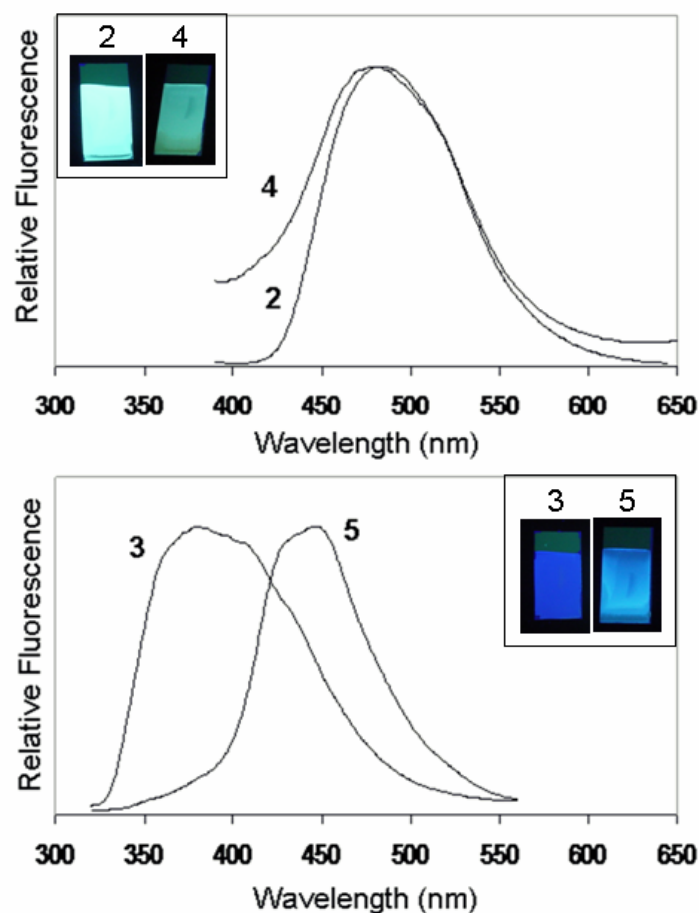


Figure 3-8. Solid-state fluorescence emission spectra for siloles (**2** and **4**) and silafluorenes (**3** and **5**). Inserted figures depict the luminescence observed under a UV lamp (302 nm) for thin-films of **2-5** on silica TLC plates.

shows the fluorescence emission comparison between dimers and polymers in the thin-films. Polymer **4** shows no significant shift in the emission spectrum from its dimer **2**, or from its solution phase emission (Figure 3-7). This supports the conclusion that there is limited conjugation through the backbone of this polymer and that the sterically demanding phenyl substituents prevent interchain stacking and excimer emission.³⁷ In contrast, the thin-film fluorescence spectrum for polymer **5** is shifted 88 nm (5484 cm^{-1}) from its solution phase emission spectrum. This is

consistent with formation of a partially ordered film where π -stacking interactions between polymer chains create a network of overlapping frontier molecular orbitals, facilitating a broadened excimer emission. There is a change from a predominantly high energy UV emission in solution to a blue emission in solid films. This dramatic red-shifted luminescence is an important feature for solid state emitting applications and improves visualization of the polymer film for imaging sensor applications.

3.3.4 Explosives Detection by Fluorescence Quenching

3.3.4.1 Surface Detection of Explosive Particulates

Important high explosives for fluorescence quenching detection applications contain nitroaromatic, nitrate ester, or nitramine functionalities.³⁸ Fluorescence detection takes advantage of the relatively low LUMO energies of these explosive materials, which can accept an excited-state electron from the fluorophore. Fluorescence detection studies were carried out with a range of explosives materials including 2,4,6-trinitrotoluene (TNT), picric acid (PA), 2,4-dinitrotoluene (DNT), cyclotrimethylenetrinitramine (RDX), cyclotetramethylene-tetranitramine (HMX), 2,4,6-trinitrophenyl-N-methylnitramine (Tetryl), trinitroglycerin (TNG), and pentaerythritol tetranitrate (PETN). Detection of explosive particulates and solid film residues were a focus, rather than detection of vapors, since the explosives studied have very low vapor pressures. Vapor pressures of production-line explosive mixtures can be further reduced by a factor 1000 when sealed in plastics.^{38a} The method

explored here focuses on visual imaging of trace explosive particles through a fluorescence quenching process.

Previous investigations using DFT calculations have shown that explosive analytes have a large range of LUMO energies, rendering it difficult to detect the broad class with one fluorescent sensor.³⁴ We recently have had success using UV-emitting silafluorene materials that incorporate a high energy ¹SOMO (singlet singly occupied donor molecular orbital) that lies above the LUMO energy of a larger range of explosives than for previous fluorescence sensors.³⁴ However, visualization of these predominantly UV emitting polymer films was difficult due to the low emission intensity in the visible region of the spectrum. Polymer **5** was designed to maintain a high energy ¹SOMO with a slightly lower energy band-gap for enhanced visible blue emission and easier visualization. Dilute standards of each explosive were prepared in toluene and stored in amber vials to prevent photo-degradation. The explosive solutions were spotted onto Whatman® filter paper or a porcelain tray at the desired concentration level with use of a glass microsyringe. Two surfaces were examined to determine any effect of substrate porosity on the explosive detection process. A solvent blank was included next to each analyte as a control. All solution spots were a 5 μ L volume, producing a spot of ~ 1 cm in diameter. After solvent evaporation, the substrate was airbrushed with a solution of polymer (0.5 mg polymer mL⁻¹ in 2:1 toluene:acetone) at a rate of 0.5 mL s⁻¹. The addition of toluene facilitates dissolution of explosive analytes for effective mixing with the polymers to form a solid solution on drying. Polymers **4** and **5** were visualized using a UV-B ($\lambda_{em} = 302$ nm) light

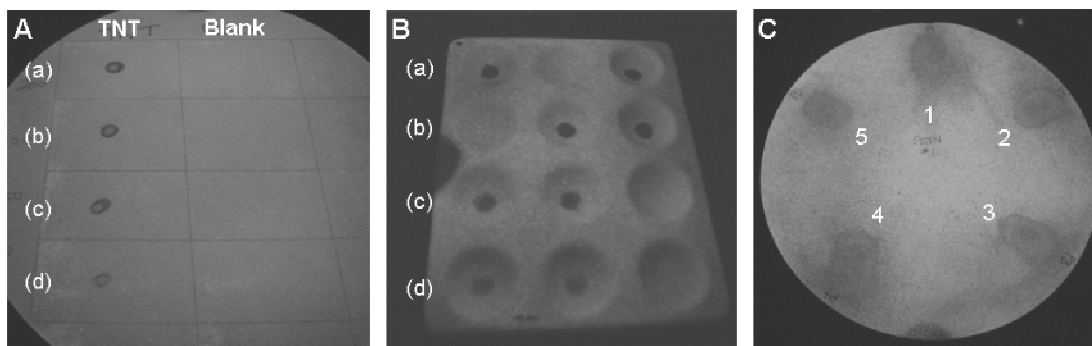
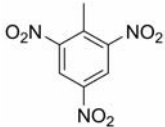
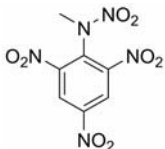
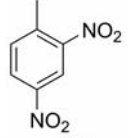
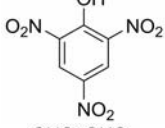
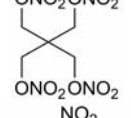
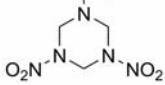
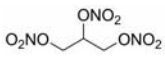
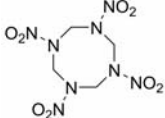


Figure 3-9. Examples of fluorescence quenching of a thin-film of polymer **5** by solid-particulates of various explosives imaged with a Sony 2.0 megapixel digital camera under continuous UV excitation (302 nm). A: Detection of TNT particulates (a) 64 ng cm^{-2} , (b) 32 ng cm^{-2} , (c) 16 ng cm^{-2} , (d) 3 ng cm^{-2} on filter paper. A toluene blank was spotted as a control. B: Detection of Tetryl particulates (a) 64 ng cm^{-2} , (b) 32 ng cm^{-2} , (c) 16 ng cm^{-2} , (d) 3 ng cm^{-2} on a porcelain tray. The analyte was randomly placed in 2 of 3 wells and observed quenching was confirmed by an independent observer. C: Detection of five successive thumbprints on filter paper contaminated with production-line PETN particulates. Successive prints were placed in succession without further handling of the explosive material.

source with a UV-transmitting filter to eliminate background radiation. Polymer **4** exhibits a yellow-green luminescence and polymer **5** emits a bright blue luminescence. To verify that detection also worked for authentic bulk commercial explosives, a series of thumbprints containing production-line PETN (NEWTEC Services Group Inc.) were also examined, so the resultant contamination resembles what one may encounter in the field.

For visual assessment, a double-blind test was carried out using two spots of the explosive material at each concentration, spotted randomly onto three locations along with solvent blanks. Illuminated samples were examined in a double blind process by an independent observer, who judged when quenching was discernible. Dark spots in the luminescent film indicate quenching of the polymer by the analyte

Table 3-3. Summary of solid-state detection limits (ng cm^{-2}) for various explosives by fluorescence quenching of polymers **4** and **5**. Dashed lines represent no detection at 64 ng cm^{-2} or less.

Explosive	Structure	P_{vap} (Torr)	4		5	
			Porcelain	Filter Paper	Porcelain	Filter Paper
TNT		5.8×10^{-6}	3	6	0.1	0.1
Tetryl		5.7×10^{-9}	1	1	0.1	0.2
DNT		1.1×10^{-4}	6	13	0.6	0.3
PA		5.8×10^{-9}	1	1	2	0.3
PETN		1.4×10^{-8}	—	—	0.6	1
RDX		4.6×10^{-9}	—	—	3	2
TNG		4.4×10^{-4}	—	—	6	2
HMX		8.0×10^{-11}	—	—	6	3

(Figure 3-9). Detection limits are reported as the lowest amount of explosive necessary for the independent observer to discern quenching visually and accurately (> 95% accuracy) in the correct locations. A summary of the detection limits is provided in Table 3-3. Lower detection limits for polymer **4** were obtained on the

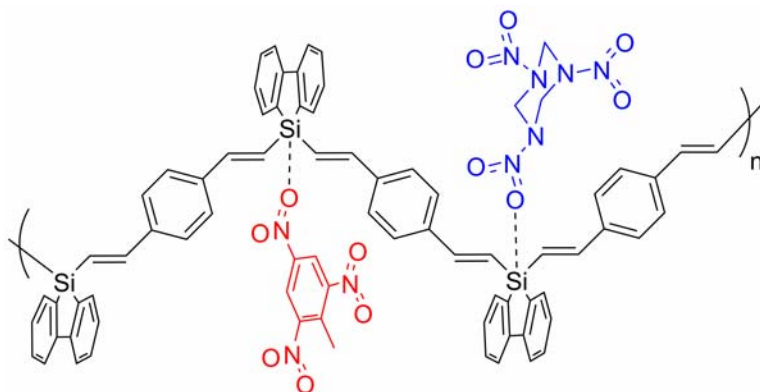


Figure 3-10. Schematic representation of explosive analyte binding events with polymer **5**. Planar aromatic molecules such as TNT (red) as well as aliphatic explosive molecules such as RDX (blue) can readily access the silicon centers by Lewis acid/base interactions in part due to the spacing between silicon units created by the phenylene-divinylene framework.

smooth porcelain substrate as compared with the porous filter paper. However, polymer **4** is only able to detect the nitroaromatic explosives TNT, DNT, PA and Tetryl. This is expected due to the unfavorable energy matching between the green emitting (tetraphenyl)silole materials and the non-aromatic explosives with high energy LUMOs.³⁴ Polymer **5** shows better detection limits for the nitroaromatic explosives than polymer **4**. The improved conjugation of **5** over **4** may play a role in the increased exciton migration and the amplified fluorescence quenching effect. Polymer **5** also shows the ability to detect the entire range of nitramine, nitroaromatic, and nitrate ester explosives studied at the same or better detection limits than achieved with previous polymers.^{34,39} Several factors play a role in these results. Polymer **5** is highly luminescent in the visible blue region of the spectrum when placed in thin films. The spacing between silafluorene units in this phenylene-divinylene polymer is also greater than in the vinylene polymers, allowing room for

better analyte-to-polymer interactions (Figure 3-10). These binding interactions take place at the Lewis acidic silicon center; therefore, less steric encumbrance surrounding these centers can lead to better detection limits.³⁴

3.3.4.2 Solid-state Stern-Volmer Analysis

Surface detection of explosives particulates is inherently difficult to quantify. The human eye detection approach provides a practical, but qualitative forensic test. To better quantify quenching efficiency at the molecular level, Stern-Volmer quenching constants (K_{SV}) were determined for solid-state detection (Equation 1).

$$I_0/I = 1 + K_{SV}[Q] \quad (1)$$

$$\ln(\Phi_0/\Phi) = VN_A[Q] \quad (2)$$

Silica TLC plates were chosen as the substrate due to the consistency and reliability of the thin-film PL results. This method offers a good imitation of a porous sampling substrate, such as filter paper, often used for the collection of unknown particulates. The analytes chosen for this solid-state study include TNT, RDX, and PETN, each representing a different class of nitrogen-based explosives. Solutions containing a dissolved explosive and either polymer **4** or **5** (4 mg mL^{-1} in CHCl_3) were individually developed onto the TLC plate with varying explosive concentrations. This creates a thin-film solid solution of polymer containing uniformly distributed explosive analytes. While the Stern-Volmer equation is usually applied to model a

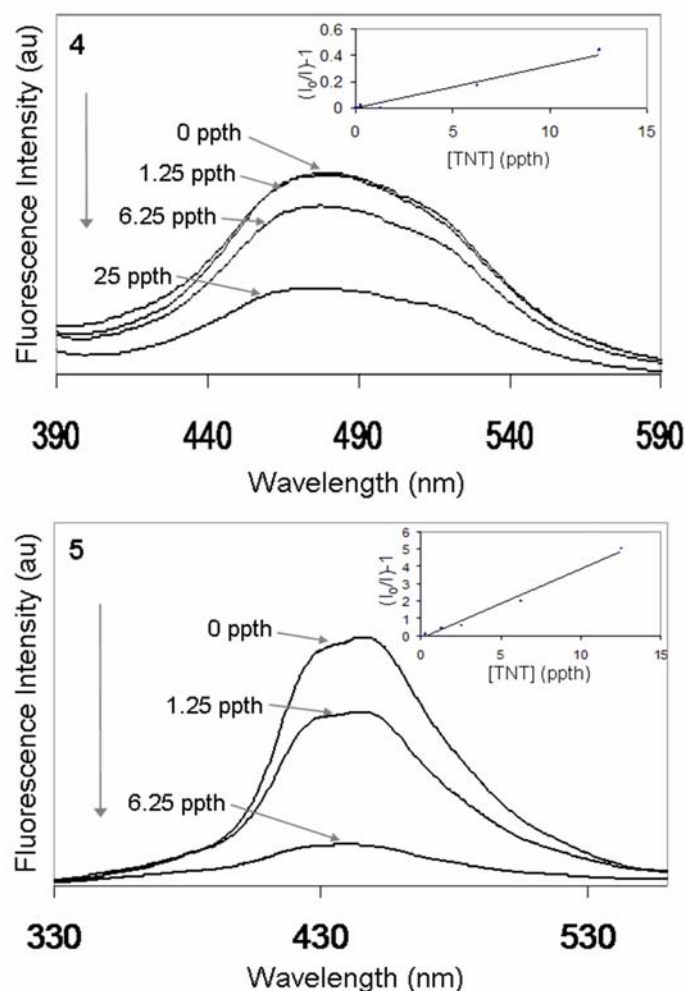


Figure 3-11. Solid-state fluorescence quenching of **4** (top) and **5** (bottom) by TNT on silica TLC plates. The concentration of explosive is reported in ppth of explosive-to-polymer (ppth = parts per thousand by weight). The insert in the upper right of each plot represents the linear regression analysis of the Stern-Volmer equation.

diffusing emitter and quencher, it also applies to static quenching where the emitting species binds the quencher. The latter situation effectively applies in a solid solution. Another quantitative technique to measure the efficiency of a static fluorescence quenching process is the Perrin formulation (Equation 2). However, this method requires the measurement of absolute fluorescence quantum efficiencies in the bound

Table 3-4. Summary of solid-state Stern-Volmer constants (K_{SV}) for the fluorescence quenching of polymers **4** and **5** by TNT, RDX and PETN on silica TLC plates. Values reported in ppth^{-1} (ppth = parts per thousand by weight of the explosive dissolved in the polymer film). No quenching was observed for polymer **4** with RDX and PETN.

Explosive	K_{SV} (ppth^{-1})	
	4	5
TNT	3.5×10^{-2}	4.0×10^{-1}
RDX	—	5.6×10^{-2}
PETN	—	5.0×10^{-2}

and unbound states. These quantities are difficult to obtain for solid-state, thin-film analyses due to the lack of reliable reference materials. Therefore, the Perrin formulation is usually applied to highly concentrated solutions where the donor and acceptor moieties are covalently linked. To our knowledge, the Stern-Volmer analysis has not been used previously to model quenching efficiencies in solid solutions. A typical graph of the fluorescence from each film is provided in Figure 3-11, showing increasingly reduced emission in films containing increasing amounts of explosives. By plotting the change in fluorescence intensity versus the concentration of analyte in the solid solution, the Stern-Volmer constant is obtained for solid state quenching from the slope of the line.

The observed quenching by TNT, RDX, and PETN reveals good agreement with the Stern-Volmer equation with R^2 values > 0.98 . A summary of the Stern-Volmer constants (K_{SV}) is given in Table 3-4. As expected, TNT is detected by both **4** and **5** with K_{SV} of $3.5 \times 10^{-2} \text{ ppth}^{-1}$ and $4.0 \times 10^{-1} \text{ ppth}^{-1}$ (ppth = parts per thousand by

weight of the explosive dissolved in the polymer film), respectively. Since as little as 6 ppth of explosive can quench about 90% of the emission in polymer **5**, exciton delocalization (both inter and intra polymer chain) in the solid state must be significant. Polymer **4** failed to demonstrate fluorescence quenching in the presence of either RDX or PETN, consistent with the results from filter paper and porcelain solid-state detection studies. The fluorescence from polymer **5** is quenched in the presence of both PETN and RDX. However, the K_{SV} for these non-aromatic explosives are an order of magnitude lower than observed for TNT, similar to the visual filter paper and porcelain solid-state detection studies. Thus, the process of depositing solid solution films by evaporation of solutions of both analyte and fluorophore proved to be a simple and advantageous method of quantifying quenching efficiencies in the solid-state. It also suggests possible algorithms for the estimation of explosive particles from the spray-on imaging method.

3.3.4.3 Detection Interferents

Insensitivity to common interferents is another important consideration when developing an explosive sensing polymer. Interference arises when fluorescence quenching arises from a substance other than the targeted analyte. Polymers **4** and **5** show no change in luminescence when the polymer films are exposed to common organic solvents such as THF, toluene, benzene, acetonitrile, acetone, and methanol. There is some interference from spotted benzophenone and benzoquinone, but only at quantities exceeding 16 ng cm^{-2} . These oxidizing aromatic organic molecules, though

not typically found in nature, are typical interferents for other fluorescence quenching polymers.⁴⁰

3.4 CONCLUSIONS

Overall, detection of the targeted explosive analytes was achieved with excellent sensitivity. The strained silacycle of both the (tetraphenyl)silole and silafluorene co-monomers act as a Lewis acid center that promotes binding of nitro- and nitrate-containing explosive analytes.³⁴ The incorporation of flexible phenylene-divinylene units prevents self-quenching processes in the thin films and maintains delocalization for fluorescence quenching. Polymer **5** shows a large bathochromic shift in the solid-state creating a bright blue emission at low surface concentrations. These new conjugated polymers show promise as stable and efficient fluorescing materials for chemosensor, photoluminescent, and possibly electroluminescent applications.

3.5 EXPERIMENTAL

3.5.1 General Synthetic Techniques

Caution: TNT and picric acid are high explosives and should be handled only in small quantities. Picric acid also forms shock sensitive compounds with heavy metals. Purchased explosive standards were handled as dilute solutions to eliminate their explosion hazard. All synthetic manipulations were carried out under an atmosphere of dry argon gas using standard Schlenk techniques. Dry solvents were

purchased from Aldrich Chemical Co. Inc. and used after purification with an MBraun Auto Solvent Purification System. Spectroscopic grade toluene from Fisher Scientific was used for the fluorescence measurements. Trimethylsilylacetylene and 1,4-diethynylbenzene (97%) were purchased from Aldrich Chemical Co. Inc. 1,4-diethynylbenzene was sublimed before use (30 °C at 0.5 Torr). The following were prepared by literature methods: 1-hydrido-1-methyl(tetraphenyl)silole,⁴¹ 1,1-dihydrido(tetraphenyl)silole,³² 1-hydrido-1-methylsilafluorene,⁴² and 1,1-dihydridosilafluorene.⁴³ NMR data were taken on 300, 400, and 500 MHz spectrometers. UV-vis spectra were obtained with the use of a Hewlett-Packard 8452A diode array spectrometer. A Perkin-Elmer LS 45 luminescence spectrometer was used to record fluorescence emission and excitation spectra. IR spectra were obtained on a Nicolet Magna-IR 550 spectrometer. GPC data was obtained with the use of a Viscotek GPCmax VE 2001 GPC; molecular weights were recorded relative to polystyrene standards and low molecular weight silole monomers and dimers.

3.5.2 X-ray Crystal Structure Determination

Diffraction intensity data were collected with a Bruker P4/CCD Smart Apex CCD diffractometer at 100 K for **1** and 203 K for **2** and **3**. Crystal, data collection, and refinement parameters are given in the Table 3-5, Appendix. The space groups were chosen based on the systematic absences. The structures were solved by direct methods, completed by subsequent difference Fourier syntheses, and refined by full matrix least-squares procedures on F^2 . The data were integrated using the Bruker

SAINT software program and scaled using the SADABS software program. Solution by direct methods (SIR-2004) produced a complete heavy-atom phasing model consistent with the proposed structure. All non-hydrogen atoms were refined anisotropically by full-matrix least-squares (SHELXL-97). All hydrogen atoms were placed using a riding model. Their positions were constrained relative to their parent atom using the appropriate HFIX command in SHELXL-97. All software and sources of scattering factors are contained in the SHELXTL (5.10) program package (G. Sheldrick, Bruker XRD, Madison, WI).

3.5.3 Synthesis of 1-methyl-1-*trans*(2-trimethylsilyl)ethenyl-2,3,4,5-(tetraphenyl)silole (1)

1-hydrido-1-methyl(tetraphenyl)silole (500 mg, 1.25 mmol), trimethylsilylacetylene (1 mL, 7 mmol), and 0.1-0.5 mol % H_2PtCl_6 were vigorously refluxed in toluene (5 mL), under argon for 10 min. The dark orange solution was filtered through a sintered glass frit and evaporated to dryness. The remaining solid was dissolved in 1 mL of THF, precipitated with 10 mL of methanol, and the yellow powder was obtained by vacuum filtration on a sintered glass frit. The product was recrystallized from hot pentane, yielding yellow crystals (0.43 g, 68%). ^1H NMR (400.053 MHz, CDCl_3): δ 6.71-7.09 (m, 22H, silole Ph, and =CH-Si), 0.55 (s, 3H, CH_3), 0.065 (s, 9H, CH_3 -Si); $^{13}\text{C}\{^1\text{H}\}$ NMR (100.59 MHz, CDCl_3): δ 157.4, 143.0 (t, =CH-Si), 154.9, 140.3, 139.6, 138.9 (q, carbons on silole ring and Ph), 130.0, 129.0, 127.8, 127.43, 126.2, 125.5 (q, Ph), -1.1 (s, $(\text{CH}_3)_3$ -Si), -6.2 (s, CH_3); $^{29}\text{Si}\{^1\text{H}\}$ NMR

(99.37 MHz, INEPT, CDCl₃, TMS (δ 0.00)): δ -2.96, -7.33; UV: $\lambda_{\text{abs}} = 286, 366$ nm; Fluorescence: $\lambda_{\text{em}} = 478$ nm, at $\lambda_{\text{ex}} = 360$ nm; mp = 118-119 °C; Calcd for C₃₄H₃₄Si₂: C 81.8, H 6.87; Found: C 81.2, H 6.95.

3.5.4 Synthesis of 1,4-di(1-methyl-1-*trans*-ethenyl-2,3,4,5-(tetraphenyl)silole)benzene (2)

1-hydrido-1-methyl(tetraphenyl)silole (500 mg, 2.6 mmol), 1,4-diethynylbenzene (170 mg, 1.3 mmol), and 0.1-0.5 mol % H₂PtCl₆ were vigorously refluxed in toluene (10 mL), under argon for 10 min. The dark orange solution was filtered through a sintered glass frit and evaporated to dryness. The remaining solid was dissolved in 1 mL of THF, precipitated with 10 mL of methanol, and the yellow powder was obtained by filtration on a sintered glass frit. The product was recrystallized from hot benzene, yielding yellow crystals (0.26 g, 72%). ¹H NMR (400.053 MHz, CDCl₃): δ 7.40 (s, 4H, benzyl), 6.83-7.10 (m, 42H, silole Ph, and =CH-Si), 6.64 (dd, 2H, =CH-Ph), 0.65 (s, 6H, CH₃); ¹³C{¹H} NMR (100.59 MHz, CDCl₃): δ 155.1, 147.4, 140.1, 139.5, 138.8, 138.1, 129.9, 129.0, 127.9, 127.5, 126.9, 126.3, 125.7, 122.8, -5.5; ²⁹Si{¹H} NMR (99.37 MHz, INEPT, CDCl₃, TMS (δ 0.00)) δ -1.40; Calcd for C₆₈H₅₄Si₂: C 88.1, H 5.87; Found: C 87.7, H 6.89.

3.5.5 Synthesis of 1,4-di(1-methyl-1-*trans*-ethenyl-silafluorene)benzene (3)

1-hydrido-1-methylsilafluorene (311 mg, 1.6 mmol), 1,4-diethynylbenzene (311 mg, 0.8 mmol), and 0.1-0.5 mol % H₂PtCl₆ were stirred in toluene (5 mL) at

room temperature, under argon for 12 h. The light yellow solution was passed through a sintered glass frit and evaporated to dryness. The remaining solid was purified by flash chromatography on silica gel using hexanes-dichloromethane as the eluent. Colorless crystals were collected from hexanes (0.325 g, 79%). ^1H NMR (400.053 MHz, CDCl_3): δ 7.86 (d, 4H, silafluorene-Ph), 7.57 (d, 4H, silafluorene-Ph), 7.44 (t, 4H, silafluorene-Ph), 7.36 (s, 4H, Ph), 7.29 (t, 4H, silafluorene-Ph), 7.07 (d, 2H, C=CH), 5.51 (d, 2H, C=CH), 0.60 (s, 6H, CH_3); $^{13}\text{C}\{^1\text{H}\}$ NMR (100.59 MHz, CDCl_3): δ 148.5, 147.0, 137.6, 133.5, 130.7, 127.8, 127.1, 126.8, 123.5, 121.2, 111.6, -5.08; $^{29}\text{Si}\{^1\text{H}\}$ NMR (99.37 MHz, INEPT, CDCl_3 , TMS (δ 0.00)) δ -8.8; Calcd for $\text{C}_{36}\text{H}_{30}\text{Si}_2$: C 83.3, H 5.90; Found: C 82.9, H 6.25.

3.5.6 Synthesis of poly((tetraphenyl)silole-phenylenedivinylene) (**4**)

1,1-dihydrido(tetraphenyl)silole (100 mg, 0.26 mmol), 1,4-diethynylbenzene (36 mg, 0.28 mmol), and 0.2 mol % H_2PtCl_6 (**4_a**) or 2% Wilkinson's catalyst (**4_b**) or 1% Karstedt's catalyst (**4_c**) or 1% $\text{Pd}(\text{PPh}_3)_4$ (**4_d**) were vigorously refluxed in toluene (5 mL), under argon for 24 h. The dark orange solution was filtered through a sintered glass frit and evaporated to dryness. The remaining solid was dissolved in 2 mL of THF and a yellow solid was precipitated with 22 mL of methanol. The precipitation procedure was repeated three times to remove low molecular weight oligomers. A yellow powder was collected by vacuum filtration (69 mg, 51%). Polymer **4_a** was used for the detailed characterization. ^1H NMR (300.075 MHz, CDCl_3): δ 6.60-7.20 (br, 24H, silole Ph, =CH-Si, and =CH-Ph), 7.40 (br, 4H, phenylene Ph); IR (KBr):

$\nu_{\text{C}\equiv\text{C}}$, $\nu_{\text{Si-H}}$ 2142 cm^{-1} , $\nu_{\text{C}\equiv\text{C-H}}$ 3290 cm^{-1} (acetylinic hydrogen suggests polymer end groups are terminal $\text{C}\equiv\text{CH}$); Calcd for $\text{C}_{38}\text{H}_{28}\text{Si}\cdot 2\text{H}_2\text{O}$: C 83.2, H 5.88; Found: C 83.2, H 5.80.

3.5.7 Synthesis of poly(silafluorene-phenylenedivinylene) (**5**)

1,1-dihydridosilafluorene (100 mg, 0.55 mmol), 1,4-diethynylbenzene (79 mg, 0.62 mmol), and 0.2 mol % H_2PtCl_6 (**5_a**) or 2% Wilkinson's catalyst (**5_b**) or 1% Karstedt's catalyst (**5_c**) or 1% $\text{Pd}(\text{PPh}_3)_4$ (**5_d**) were stirred at room temperature in toluene (4 mL), under argon for 24 h. The orange solution was filtered and evaporated to dryness. The remaining solid was dissolved in 4 mL of THF, precipitated with 40 mL of methanol. The precipitation procedure was repeated three times to remove low molecular weight oligomers. A white powder was collected by vacuum filtration (122 mg, 68%). Polymer **5_a** was used for the detailed characterization. ^1H NMR (300.075 MHz, CDCl_3): δ 7.20-8.00 (br, 12H, silafluorene H-Ph), 7.00 (br, dd, *trans*-vinyl); IR (KBr): $\nu_{\text{C}\equiv\text{C}}$, $\nu_{\text{Si-H}}$ 2077 cm^{-1} (no $\text{C}\equiv\text{CH}$ stretch indicates endgroups are terminal Si-H); Calcd for $\text{C}_{22}\text{H}_{18}\text{Si}\cdot\text{H}_2\text{O}$: C 81.0, H 5.56; Found: C 80.8, H 5.47.

3.5.8 Synthesis of 1,1-dihydrido-4,5,8,9-bis(triptycene)silafluorene (siliptycene)

To a stirring solution of 2,3-dibromotriptycene⁴⁴ (1.0 g, 2.4 mmol) in dry THF at -78 °C was added n-BuLi (0.8 mL, 1.25 mmol) over 20 min. Upon addition, the reaction was slowly warmed to 0 °C and quenched with 5% HCl. The product was extracted with diethylether, dried over MgSO_4 and evaporated to dryness. A light

yellow powder was obtained (600 mg, 97%). The powder was dried under vacuum and dry diethylether (20 mL) was added. To the reaction was added n-BuLi (1.7 mL, 2.4 mmol) at -78 °C and stirred at room temperature for 5 h. Dichlorosilane (0.3 mL, 3.0 mmol) was slowly added and the reaction was stirred overnight. The yellow solution was quenched with sat. NH_4Cl , extracted with diethylether, dried over MgSO_4 and evaporated to dryness. The product was purified by column chromatography (dichloromethane:hexanes) to yield a white powder (310 mg, 70%). ^1H NMR (400.053 MHz, CDCl_3): δ 7.86 (s, 2H, silafluorene Ph), 7.53 (s, H, silafluorene Ph), 7.436.94 (m, 16H, Ph), 5.43 (s, 4H, $\square\text{CH}$), 5.18 (s, 2H, $\text{Si}\square\text{H}$); $^{13}\text{C}\{^1\text{H}\}$ NMR (100.59 MHz, CDCl_3): δ 148.5, 147.9, 145.2, 145.1, 144.4, 129.8, 129.3, 125.3, 125.2, 124.2, 123.7, 116.5, 54.8, 53.7; $^{29}\text{Si}\{^1\text{H}\}$ NMR (99.37 MHz, INEPT, CDCl_3 , TMS (δ 0.00)): δ \square 22.4; UV: $\lambda_{\text{abs}} = 286, 314$ nm, $\epsilon = 13000$ $\text{L}\cdot\text{cm}^{-1}\cdot\text{mol}^{-1}$; Fluorescence: $\lambda_{\text{em}} = 388$ nm at $\lambda_{\text{ex}} = 315$ nm, $\Phi_{\text{flu}} = 0.27$; CH calcd for $\text{C}_{40}\text{H}_{26}\text{Si}$: C 89.9, H 4.90; Found: C 89.1, H 4.89.

3.6 ACKNOWLEDGEMENTS

This chapter, in part, is a reprint of the material as it appears in the following paper: Sanchez, J. C.; Urbas, S. A.; Toal, S. J.; DiPasquale, A. G.; Rheingold, A. L.; Trogler, W. C. “Catalytic Hydrosilylation Routes to Divinylbenzene Bridged Silole and Silafluorene Polymers. Applications to Surface Imaging of Explosive Particulates” *Macromolecules* **2008**, *41*, 1237-1245. The crystallographic information file (CIF) for compounds **1-3** is available on the internet at pubs.acs.org as “Supporting Information” to this publication.

3.7 APPENDIX

Table 3-5. Summary of X-ray crystallographic data for compounds **1-3**.

	1	2	3
Formula	C ₃₄ H ₃₄ Si ₂	C ₉₂ H ₇₈ Si ₂	C ₃₆ H ₃₀ Si ₂
Formula weight	498.81	1239.72	518.78
Space group	<i>P2₁/n</i>	<i>P-1</i>	<i>Pbca</i>
<i>a</i> , Å	6.0014(4)	11.500(3)	14.3625(12)
<i>b</i> , Å	15.5685(11)	13.326(3)	13.0470(11)
<i>c</i> , Å	30.818(2)	13.958(3)	15.3108(13)
α , deg	90	62.081(4)	90
β , deg	93.6220(10)	74.553(4)	90
γ , deg	90	72.412(4)	90
<i>V</i> , Å ³	2873.6(3)	1781.7(7)	2869.1(4)
<i>Z</i>	4	1	4
Crystal color, habit	colorless, block	yellow, block	colorless, prism
ρ (calc), g cm ⁻³	1.153	1.155	1.201
μ (MoK α), mm ⁻¹	0.144	0.097	0.147
Temp, K	100(2)	203(2)	203(2)
Reflections measured	24815	12819	7100
Reflections ind.	6505 [R _{int} =0.0269]	8187 [R _{int} =0.0252]	3288 [R _{int} =0.0336]
R(F) (<i>I</i> > 2 σ (<i>I</i>)) ^a	0.0493	0.0596	0.0524
R(ω F ²) (<i>I</i> > 2 σ (<i>I</i>)) ^b	0.1310	0.1563	0.1350

^a $R = \sum ||F_o| - |F_c|| / \sum |F_o|$. ^b $R(\omega F^2) = \{ \sum [\omega(F_o^2 - F_c^2)^2] / \sum [\omega(F_o^2)^2] \}^{1/2}$;
 $\omega = 1 / [\sigma^2(F_o^2) + (aP)^2 + bP]$, $P = [2F_c^2 + \max(F_o, 0)] / 3$

3.8 REFERENCES

- (1) Hakansson, K.; Coorey, R. V.; Zubarev, R. A.; Talrose, V. L.; Hakansson, P. *J. Mass. Spectrom.* **2000**, *35*, 337–346.
- (2) Smith, K. D.; McCord, B. R.; McCrehan, W. A.; Mount, K.; Rowe, W. F. *J. Foren. Sci.* **1999**, *44*, 789–794.
- (3) Sylvia, J. M.; Janni, J. A.; Klein, J. D.; Spencer, K. M. *Anal. Chem.* **2000**, *72*, 5834–5840.
- (4) Popov, I. A.; Chen, H.; Kharybin, O. N.; Nikolaev, E. N.; Cooks, R. G. *Chem. Commun.* **2005**, *15*, 1953–1955.
- (5) Kolla, P. *Anal. Chem.* **1995**, *67*, 184A–189A.
- (6) XPRAY Field Test Kit available from Mistral Group, Web URL: http://www.mistralgroup.com/SEC_explosives.asp
- (7) (a) McQuade, D. T.; Pullen, A. E.; Swager, T. M. *Chem. Rev.* **2000**, *100*, 2537–2574. (b) Toal, S. J.; Trogler, W. C. *J. Mater. Chem.* **2006**, *16*, 2871–2883.
- (8) La Grone, M.; Cumming, C.; Fisher, M.; Fox, M.; Jacob, S.; Reust, D.; Rockley, M.; Towers, E. www.nomadics.com/EM_aerosense_fluor.pdf (2 Sept 2007).
- (9) Seki, K.; Furuyama, T.; Kawasumi, T.; Sakurai, Y.; Ishii, H.; Kajikawa, K.; Ouchi, Y.; Masuda, T. *J. Phys. Chem. B* **1997**, *101*, 9165–9169.
- (10) (a) Johansson, D. M.; Theander, M.; Srdanov, G.; Yu, G.; Inganäs, O.; Andersson, M. R. *Macromolecules* **2001**, *34*, 3716–3719. (b) Fan, C.; Plaxico, K. W.; Heeger, A. J. *J. Am. Chem. Soc.* **2002**, *124*, 5642–5643.
- (11) Lee, Y.; Liang, Y.; Yu, L. *Synlett* **2006**, *18*, 2879–2893.
- (12) (a) Ahn, T.; Song, S.-Y.; Shim, H.-K. *Macromolecules* **2000**, *33*, 6764–6771. (b) Kim, J. K.; Yu, J. W.; Hong, J. M.; Cho, H. N.; Kim, D. Y.; Kim, C. Y. *J. Mater. Chem.* **1999**, *9*, 2171–2176. (c) Kim, J. K.; Hong, S. I.; Cho, H. N.; Kim, D. Y.; Kim, C. Y. *Polym. Bull. (Berlin)* **1997**, *38*, 169–176.
- (13) (a) Jin, S. H.; Kang, S. Y.; Kim, M. Y.; Chan, Y. U.; Kim, J. Y.; Lee, K.; Gal, Y. S. *Macromolecules* **2003**, *36*, 3841–3847. (b) Jin, S. H.; Park, H. J.; Kim, J.

- Y.; Lee, K.; Lee, S. P.; Moon, D. K.; Lee, H. J.; Gal, Y. S. *Macromolecules* **2002**, *35*, 7532–7534.
- (14) Grisorio, R.; Mastrorilli, P.; Nobile, C. F.; Romanazzi, G.; Suranna, G. P. *Tetrahedron Lett.* **2005**, *46*, 2555–2558.
- (15) Kim, D. S.; Shim, S. C. *J. Polym. Sci. Polym. Chem.* **1999**, *37*, 2263–2273.
- (16) Kim, D. S.; Shim, S. C. *J. Polym. Sci. Polym. Chem.* **1999**, *37*, 2933–2940.
- (17) Pang, Y.; Ijadi-Maghsoodi, S.; Barton, T. J. *Macromolecules* **1993**, *26*, 5671–5675.
- (18) Sumiya, K.-I.; Kwak, G.; Sanda, F.; Masuda, T. *J. Polym. Sci. Polym. Chem.* **2004**, *42*, 2774–2783.
- (19) Benfaremo, N.; Sandman, D. J.; Tripathy, S.; Kumar, J.; Yang, K.; Rubner, M. F.; Lyons, C. *Macromolecules* **1998**, *31*, 3595–3599.
- (20) Kim, D.-J.; Kim, S.-H.; Zyung, T.; Kim, J.-J.; Cho, I.; Choi, S. K. *Macromolecules* **1996**, *29*, 3657–3660.
- (21) Kim, H. K.; Ryu, M.-K.; Kim, K.-D.; Lee, S.-M.; Cho, S.-W.; Park, J.-W. *Macromolecules* **1998**, *31*, 1114–1123.
- (22) Rickle, G. K. *J. Appl. Polym. Sci.* **1994**, *51*, 605–612.
- (23) Son, D. Y.; Bucca, D.; Keller, T. M. *Tetrahedron Lett.* **1996**, *37*, 1579–1582.
- (24) Ohshita, J.; Kunai, A. *Acta Polym.* **1998**, *49*, 379–403.
- (25) West, R.; Sohn, H.; Bankwitz, U.; Calabrese, J.; Apeloig, Y.; Mueller, T. *J. Am. Chem. Soc.* **1995**, *117*, 11608–11609.
- (26) Yu, G.; Yin, S.; Liu, Y.; Chen, J.; Xu, X.; Sun, X.; Ma, D.; Zhan, X.; Peng, Q.; Shuai, Z.; Tang, B.; Zhu, D.; Fang, W.; Luo, Y. *J. Am. Chem. Soc.* **2005**, *127*, 6335–6346.
- (27) Tamao, K.; Uchida, M.; Izumizawa, T.; Kenji, F.; Yamaguchi, S. *J. Am. Chem. Soc.* **1996**, *118*, 11974–11975.
- (28) Sohn, H.; Calhoun, R. M.; Sailor, M. J.; Trogler, W. C. *Angew. Chem. Int. Ed.* **2001**, *40*, 2104–2105.

- (29) Sohn, H.; Sailor, M. J.; Magde, D.; Trogler, W. C. *J. Am. Chem. Soc.* **2003**, *125*, 3821–3830.
- (30) Toal, S. J.; Trogler, W. C. In *Nanotechnology and the Environment*; Karn, B., Masciangioli, T., Zheng, W., Colvin, V., Alivasatos, P., Eds.; Oxford University Press: 2004.
- (31) Trogler, W. C. In *Electronic Noses & Sensors for the Detection of Explosives*; Gardner, J. W., Yinon, J. Eds.; Kluwer Academic Publishers: 2004, p 39–52.
- (32) Toal, S. J.; Sohn, H.; Zakarov, L. N.; Kassel, W. S.; Golen, J. A.; Rheingold, A. L.; Trogler, W. C. *Organometallics* **2005**, *24*, 3081–3087.
- (33) Sohn, H.; Huddleston, R. R.; Powell, D. R.; West, R.; Oka, K.; Yonghua, X. *J. Am. Chem. Soc.* **1999**, *121*, 2935–2936.
- (34) Sanchez, J. C.; DiPasquale, A. G.; Rheingold, A. L.; Trogler, W. C. *Chem. Mater.* **2007**, *19*, 6459–6470.
- (35) Chen, R.-F.; Fan, Q.-L.; Liu, S.-J.; Zhu, R.; Pu, K.-Y.; Huang, W. *Synth. Met.* **2006**, *156*, 1161–1167.
- (36) Luo, J.; Xie, Z.; Lam, W. Y. J.; Cheng, L.; Chen, H.; Qiu, C.; Kwok, H. S.; Zhan, X.; Liu, Y.; Zhu, D.; Tang, B. Z. *Chem. Commun.* **2001**, 1740–1741.
- (37) Chen, J.; Law, C. C. W.; Lam, J. W. Y.; Dong, Y.; Lo, S. M. F.; Williams, I. D.; Zhu, D.; Tang, B. Z. *Chem. Mater.* **2003**, *15*, 1535–1546.
- (38) (a) Moore, D. S. *Rev. Sci. Instrum.* **2004**, *75*, 2499–2512. (b) Singh, S. *J. Hazard. Mater.* **2007**, *144*, 15–28.
- (39) Toal, S. J.; Sanchez, J. C.; Dugan, R. E.; Trogler, W. C. *J. Forensic Sci.* **2007**, *52*, 79–83.
- (40) Yang, J.-S.; Swager, T. M. *J. Am. Chem. Soc.* **1998**, *120*, 5321–5322.
- (41) Ruehlmann, K. *Z. Chem.* **1965**, *5*, 354.
- (42) Becker, B.; Corriu, R. J. P.; Henner, B. J. L.; Wojnowski, W.; Peters, K.; von Schnering, H. G. *J. Organomet. Chem.* **1986**, *312*, 305–311.
- (43) Chang, L. S.; Corey, J. Y. *Organometallics* **1989**, *8*, 1885–1893.

- (44) Hart, H.; Bashir-Hashemi, A.; Luo, J.; Meador, M. A. *Tetrahedron* **1986**, *42*, 1641–1654.

CHAPTER IV

Efficient Blue Emitting Silafluorene-fluorene Conjugated Copolymers for Increased Explosives Detection Sensitivity

4.1 ABSTRACT

The synthesis and spectroscopic characterization of a series of new blue-emitting silafluorene-fluorene copolymers is described. The polymers are synthesized using kinetically controlled hydrosilylation copolymerization of 1,1-dihydrosilafluorene with a series of 9-substituted 2,7-diethynylfluorenes. The polymers contain a *trans*-only framework with molecular weights in the range of 13 000–20 000, as determined by gel permeation chromatography (GPC) using polystyrene standards and by ^1H NMR spectroscopy using dimethylphenylsilane as an end-capping marker group. The three stereoregular polymers synthesized include a 9,9-dihydrofluorene (**PSF1**), a 9,9-dimethyl-9*H*-fluorene (**PSF2**), and a 9,9'-spirobifluorene (**PSF3**) comonomer with the frameworks. These fluorenyl units are conjugated through the silicon center of the silafluorene moiety by bridging vinylene groups. Quantum yields of fluorescence range from 20 to 100% with **PSF3** having the highest quantum efficiency. Polymers **PSF1-3** emit in the blue region of the spectrum (~ 475 nm), showing good color purity with little change in luminescence properties between the solution and solid-state phases. The polymers were tested for explosives detection properties by a fluorescence quenching mechanism. Targeted explosives include laboratory prepared TNT, DNT, picric acid, RDX, HMX, PETN, TNG, and Tetryl, as well as production line PETN and C-4. All three polymers exhibit detection of explosive particulates with limits as low as 1 pg cm^{-2} for Tetryl.

4.2 INTRODUCTION

The increased use of high explosives in terrorism has created a demand for improved explosives detection and screening technology. Advances are needed in the areas of cost efficiency, sensitivity, selectivity, portability and speed of the signal analysis.¹ Current technology typically addresses one or two of these issues using instrumental spectroscopic methods for vapor phase or bulk detection.² Yet, no single method has incorporated all the features listed above. One promising technology uses conjugated photoluminescent polymers to rapidly detect explosive vapors. Detection limits in the parts-per-trillion (ppt) level and femtogram amounts have been achieved with a fluorescence quenching mechanism.³ This approach has had wide success in the detection of volatile explosives such as TNT. However, packaging may lower effective vapor pressures of explosive materials by a factor of 1000.⁴ Only the highest vapor pressure explosives, or taggants such as dinitroethylene glycol (EDGN) and 2,3-dimethyl-2,3-dinitrobutane (DMNB), respectively, can be reliably detected by vapor methods.⁵

For less volatile explosives, sensitivity has been improved, from a practical standpoint, through particle collection or the direct surface detection of explosive particles.⁶ It is well documented that the handling of explosive materials can leave microgram quantities of explosive residues on subjects and transport vehicles.⁷ By targeting particulate residue rather than explosives in vapor form, pre-concentration issues can be avoided. We have previously shown that the use of blue-emitting silafluorene-vinylene polymers can directly detect explosive particulates at levels as

low as 100 pg cm^{-2} .^{6a} Silole and silafluorene containing polymers have the ability to bind explosives and show sensitivity for nitroaromatics, nitramines, and nitrate esters, including 2,4,6-trinitrotoluene (TNT), picric acid (PA), 2,4-dinitrotoluene (DNT), cyclotrimethylenetrinitramine (RDX), cyclotetramethylene-tetranitramine (HMX), 2,4,6-trinitrophenyl-N-methylnitramine (Tetryl), trinitroglycerin (TNG), and pentaerythritol tetranitrate (PETN). In order to optimize detection sensitivity, new polymers are required with increased fluorescence quantum yields. It is also important to have a high enough energy excited state to promote rapid electron transfer to the broad class of explosives, yet the emission should be of low enough energy to be visible for non-instrumental detection. There is also interest in efficient blue emitting polymers for optoelectronic applications, such as in OLEDs.⁸

Photoluminescent polymers typically include extended aromatic systems with functional groups designed to balance the materials electronic properties, such as conjugation length, frontier molecular orbital energies, and excited-state decay pathways, with physical properties, such as solubility, density, and molecular weight.³ Polymer properties can also be controlled through chemical modifications in the backbone structure. Popular polymerization routes include Heck coupling,⁹ Wittig condensation,¹⁰ the Gilch route,¹¹ the Suzuki-Heck cascade,¹² Sonogashira coupling,¹³ Stille coupling,¹⁴ Suzuki coupling,¹⁵ and Tamao-Kumada coupling.¹⁶ These methods typically create polymers with backbones consisting of vinylene, ethynylene, or phenylene frameworks. Synthetic routes to vinylene-type polymers are better developed than those for synthesizing ethynylene-type frameworks. Polymers

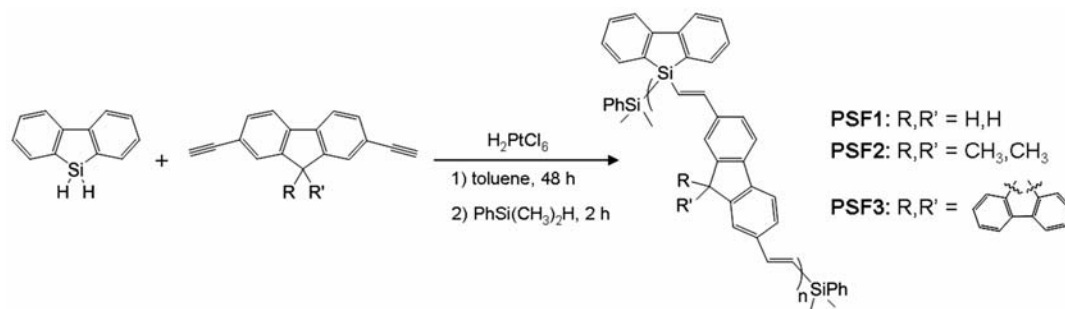
consisting of *p*-vinylene units have been widely studied because of their strong emission properties.¹⁷

We recently developed a series of silafluorene-vinylene and -phenylenedivinylene copolymers as new UV-blue emitting materials for particulate detection of explosive materials.^{6a,18} These polymers show good fluorescence quantum efficiencies, stability in solid film applications, and excellent detection limits for explosives sensing. The inclusion of silafluorene into the polymer framework increases polymer flexibility and thermal stability while maintaining electronic delocalization.¹⁹ Hydrosilylation is an efficient polymerization technique, occurring under mild reaction conditions to yield high molecular weight and stereoregular polymers.¹⁸ Lewis acid-base interactions between the lone-pairs from the nitro groups of explosives and the metallole silicon center assists analyte binding in these polymers.^{6a} These studies suggest that optimum explosive sensing polymers would be blue-emitting polymers with higher quantum efficiencies, better color purity, higher molecular weights, and more porous polymer structures.

The good sensitivity of the silafluorene containing polymers is attributed largely to the orbital energy matching between the excited-state ¹SOMO (singlet singly occupied excited donor molecular orbital) of the polymeric materials and the LUMO of the targeted explosive analyte. Another factor is the ability of the strained Lewis acidic silacycle moiety to bind the basic oxygen atoms of explosive analytes for efficient electron transfer from the polymer donor to the electron accepting analyte. The lack of conjugated polymers that efficiently emit in the blue region (λ_{flu}

= 475 nm) of the spectrum has limited the development of effective sensory materials. Functionalized fluorenes and polyfluorenes have emerged as a favorable class of highly efficient blue-emitting organic materials.²⁰ Fluorene has a high fluorescence quantum efficiency and can be easily modified. However, fluorene-containing materials typically lack good thin-film stability and color purity in photoluminescence applications due to the appearance of a green-emission band (g-band) upon exposure to UV-light or high electrical currents.²¹ Although the source of this g-band is still a subject of debate,^{20c,22} its presence can be reduced by alkyl functionalization in the 9-position. It is thought that this type of functionalization inhibits excimer emission in the solid-state as well as prevents photo- or electro-oxidation of the 9-position on the fluorene unit.²³

This chapter reports the synthesis of a series of poly(1,1-silafluorene-fluorene)s by catalytic hydrosilylation of 2,7-diethynyl functionalized 9-substituted fluorenes. The polymers incorporate alternating silafluorene-fluorene units conjugated through vinylene bridges and are obtained in good yield and with high molecular weights. The incorporation of both the fluorene and silafluorene units is crucial for the photoluminescence properties²⁴ and processability of the polymer.²⁵ The polymers were screened for their effectiveness as fluorescent sensors for the detection of explosives particulates. Properties such as high quantum efficiencies and blue fluorescence color purity improve detection results from previous polymers.



Scheme 4-1. Synthesis of **PSF1–3** by catalytic hydrosilylation. **PSF1–2** were synthesized at 0 °C and **PSF3** was synthesized at room temperature. Subsequent end-capping with dimethylphenylsilane was performed at room temperature to facilitate both hydrosilylation and dehydrocoupling.

4.3 RESULTS AND DISCUSSION

4.3.1 Synthesis and Structural Characterization

In previous studies, we found that catalytic hydrosilylation of diethynyl-aryl groups by 1,1-dihydrosilafluorene yields the kinetically favored *trans*-product at room temperature, but not at higher temperatures. Using H₂PtCl₆ as the catalyst, polymers **PSF1**, **PSF2**, and **PSF3** were synthesized with the appropriately substituted 2,7-diethynylfluorene and 1,1-dihydrosilafluorene (Scheme 4-1). The reactions were run at 0 °C for 48 h to prevent the formation of *cis* and *gem* byproducts. The polymers were end-capped with dimethylphenylsilane to remove both the reactive end-groups and the catalyst. Polymers were isolated by precipitation from methanol and washed with acetone to remove impurities and oligomers. Molecular weights (M_w) range from 13 000–20 000 with polydispersities (PDI) of 1.7–2.6 (Table 4-1). Number averaged molecular weights (M_n) were also calculated from the ¹H NMR spectra using the terminal silane methyl groups as a reference. The molecular weights

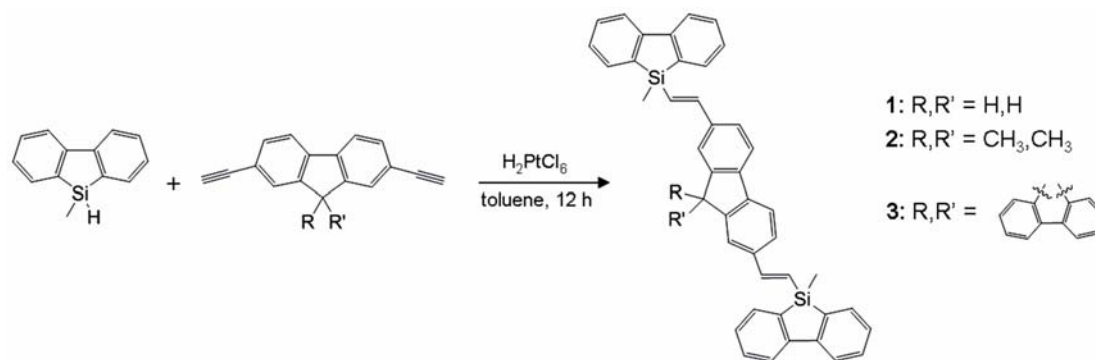
Table 4-1. Molecular weights for **PSF1–3** prepared by catalytic hydrosilylation with H_2PtCl_6 in toluene at 0 °C for 24 h.

Entry	Yield ^a (%)	M_n (NMR)	M_w (GPC)	$(M_w/M_n)^b$	n^c
PSF1	70	15 000	16 000	2.6	40
PSF2	96	17 000	20 000	2.3	47
PSF3	95	9000	13 200	1.7	25

^a Calculated after three precipitations from methanol and acetone wash. ^b PDI Calculated by GPC. ^c Calculated from GPC data.

for **PSF1-3** are higher than those obtained under similar reaction conditions using 1,4-diethynylbenzene instead of fluorene.¹⁸ This may be attributed to greater distance between ethynyl functionalities on a fluorenyl framework as compared to a phenylene framework. Kinetic control was used to synthesize regio-regular *trans*-vinylene polymers of high molecular weights. The *trans*-only stereochemistry is important for maximizing $\sigma^*(\text{Si-C})-\pi/\pi^*(\text{vinylene})$ delocalization through the polymer backbone.¹⁸ The spacing between silafluorene monomer units created by the lengthy divinylfluorene comonomer mitigates steric crowding around the silicon centers, which allows better binding of basic analytes to the Lewis acidic silicon.

A series of model dimeric complexes were synthesized to provide structural models as well as to investigate the extent of delocalization of these systems. Dimers **1-3** were prepared by hydrosilylation of the appropriate diethynyl-functionalized



Scheme 4-2. Synthesis of dimers **1–3** by catalytic hydrosilylation. Reactions for **1–3** were performed at 0 °C.

fluorene with 1-hydro-1-methylsilafluorene (Scheme 4-2). Syntheses were complete after 12 h at 0 °C in every case. Yields were good (70–80%) for the desired *trans*-product after purification by column chromatography. Structural information was obtained through ¹H NMR, ¹³C NMR, and IR spectroscopy. The *trans*-product for dimers **1–3** was confirmed by ¹H NMR spectroscopy. A *trans*-vinylene coupling constant of 20 Hz was observed for each dimer, which is close to 19.2 Hz previously observed for similar silafluorene substituted *trans*-vinylene complexes.¹⁸

4.3.2 Photophysical Properties

Photoluminescence (PL) data were collected for the dimeric and polymeric materials synthesized in this study (Table 4-2). A bathochromic shift was seen in all cases for the absorption λ_{\max} and fluorescence λ_{\max} from the dimer to the polymer (Figure 4-1). The red-shifts increase with increasing steric demand of the functionality at the 9-position of the fluorene moiety. The unsubstituted fluorene unit in **PSF1** shows only a small red shift of 6 nm (431 cm⁻¹) from its model dimer **1**.

Table 4-2. Photoluminescence data for silafluorene-fluorene dimers and copolymers.

Entry	λ_{abs} (nm) ^a	ϵ_{max} (L mol ⁻¹ cm ⁻¹)	Solution λ_{flu} (nm) ^a	Thin-film: TLC λ_{flu} (nm)	Thin-film: Quartz λ_{flu} (nm)	Φ_{flu} ^c
1	292, 340	36 900	370	—	—	0.44
2	292, 330	26 600	370	—	—	0.21
3	290	20 200	372	—	—	0.34
PSF1	346	13 700 ^b	376	446	484	0.52
PSF2	344	26 300 ^b	377	446	456	0.22
PSF3	346	24 800 ^b	392	470	478	1.0

^a UV-vis and fluorescence taken in toluene. ^b Absorptivities are calculated per mole of silicon. ^c Quantum yield (Φ_{flu}) of fluorescence \pm 30%, relative to 9,10-diphenylanthracene in toluene.

PSF2 shows a small bathochromic shift of 7 nm (502 cm⁻¹) from **2**, which is comparable to the shift of 11 nm (880 cm⁻¹) observed in phenylenedivinylene polymers previously reported.¹⁸ A red shift of 20 nm (1372 cm⁻¹) was observed when comparing the spirofluorene containing materials **3** and **PSF3**. This was the largest shift observed for the three polymers. Previous studies have shown that orientation of the bridging vinylene groups are influenced by steric crowding. The alignment of the vinylene groups with respect to the face of the silafluorene moiety has a significant effect on delocalization.^{6a,18} The steric bulk of the spirofluorene comonomer may contribute to the favored alignment of the vinylene π/π^* orbitals with the σ^* orbitals of the silafluorene moiety. This overlap increases conjugation throughout the polymer and shifts the absorption and emission spectra to lower energy. The effect of increased delocalization is even more pronounced in the absorption spectra (Figure 4-

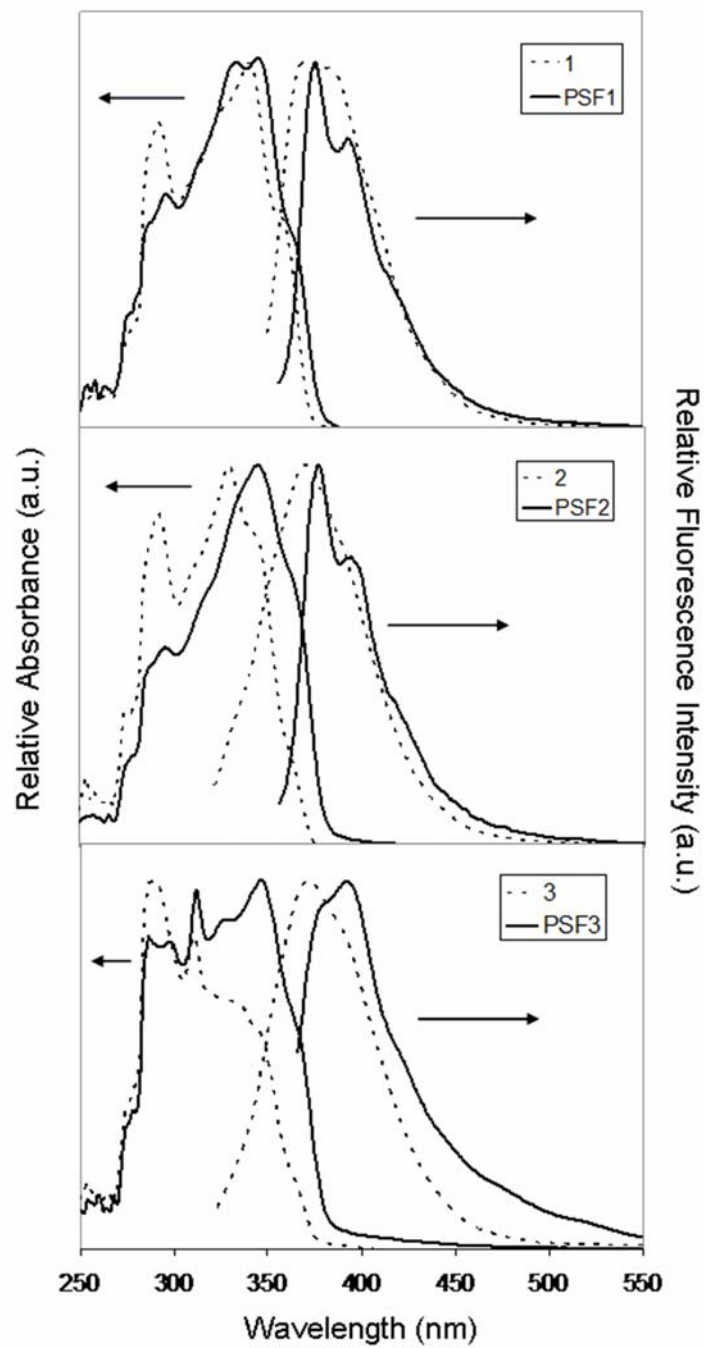


Figure 4-1. Absorption and photoemission spectra of dimers 1-3 and polymers PSF1-3 showing peak broadening in the absorption spectra for PSF2-3 and a bathochromic shift in emission for all three polymers.

1). **PSF1** only shows a 6 nm (510 cm^{-1}) bathochromic shift from its corresponding model dimer **1** while **PSF2** and **PSF3** show red shifts of 14 nm (1233 cm^{-1}) and 56 nm (5581 cm^{-1}), respectively. The solution-phase quantum yields of fluorescence (Φ_{flu}) for **PSF1**, **PSF2**, and **PSF3** are 52%, 21%, and 100%, respectively (Table 4-2). The bulkiness and rigidity of the spirofluorene moiety minimizes solvent interactions and non-radiative decay pathways. The high quantum efficiency along with the blue-shifted solution and solid-state emission properties make **PSF3** a prime candidate for light-emitting device (LED) applications. The fluorescence emission at $\sim 475\text{ nm}$ in the solid state ensures good color purity in the blue region of the spectrum. For explosives detection applications, the brightness of the polymer film permits better visual resolution of quenching events at lower detection limits.

Solid-state PL data were collected to probe the effect of aggregation during thin-film explosives detection studies. Two techniques were chosen to provide insight into the effect of substrate porosity on the fluorescence emission. The first method employs absorption **PSF1-3** (4 mg mL^{-1} in CHCl_3) deposited onto silica TLC plates. This has been shown to be an efficient method for solid-state PL characterization of silafluorene containing materials.^{18,26} The second method involves spin-casting solid solutions of **PSF1-3** (30 mg mL^{-1} in toluene) onto quartz discs. The solid-state PL results are presented in Figure 4-2. Bathochromic shifts in the fluorescence emission of **PSF1-3** are observed, with λ_{max} increasing from solution < TLC plate < quartz disc for all three polymers. **PSF1-3** all show large shifts from solution to TLC plate ranging from 70 nm (4174 cm^{-1}) to 78 nm (4234 cm^{-1}). The shifts in λ_{max} of

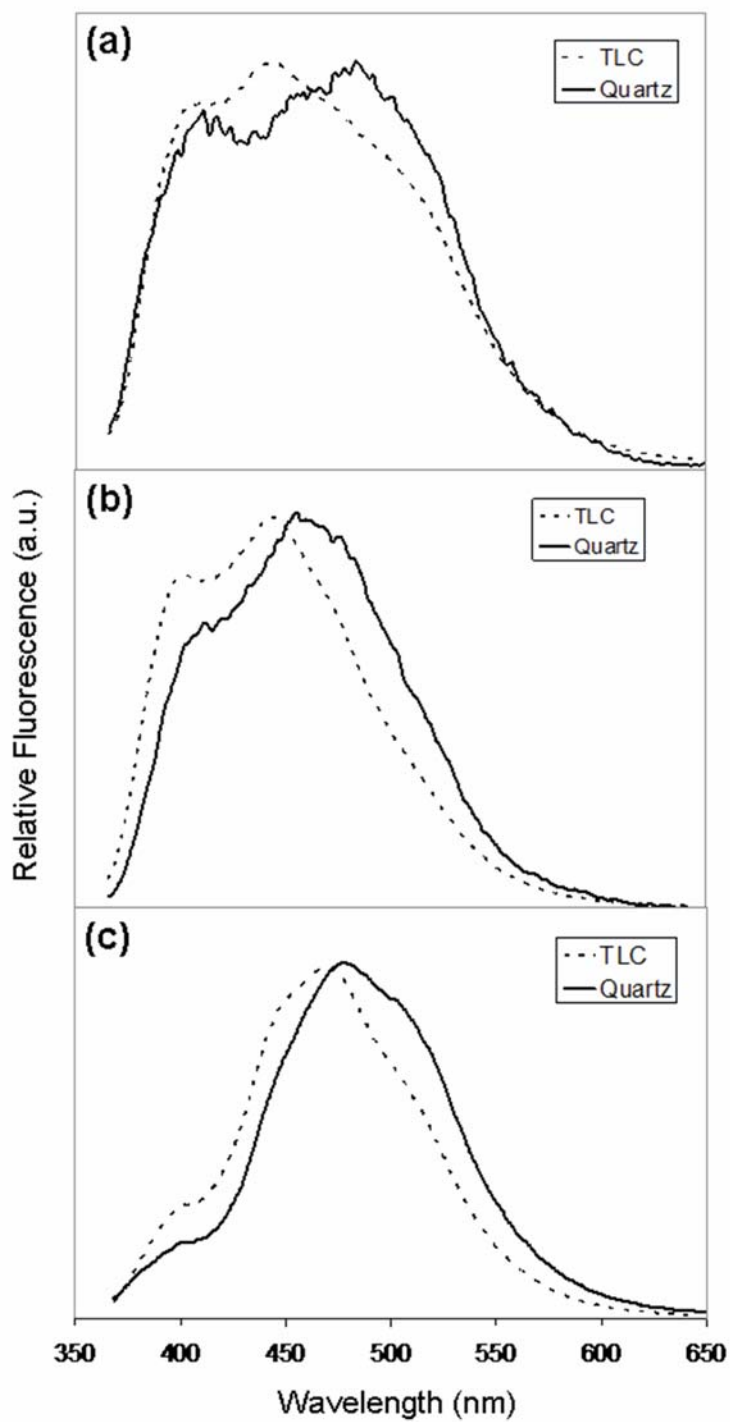


Figure 4-2. Solid-state photoemission spectra on TLC plates (broken line) and quartz plate (solid line). (a) **PSF1**; (b) **PSF2**; (c) **PSF3**.

fluorescence from TLC to quartz are smaller, ranging from 8 nm (356 cm^{-1}) to 38 nm (1760 cm^{-1}). The spectral shifts from the porous TLC substrate to the smooth quartz substrate decrease with increasing steric demand of the functionality at the 9 position of the fluorene group (**PSF1**>**PSF2**>**PSF3**). The quartz substrate appears to allow for maximum ordering between the polymer chains as the solution evaporates. For polymers **PSF1–2**, this interaction leads to a longer wavelength excimer emission in the spin-casted quartz film as compared to the spotting on the TLC film. In the case of **PSF3**, however, there is little change in the fluorescence λ_{max} (8 nm, 356 cm^{-1}) from the TLC film to the quartz film. The bulky spirofluorene comonomer presumably prevents excimer formation in the thin-film spin-cast onto the quartz substrate.

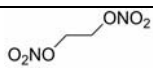
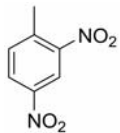
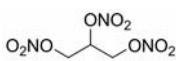
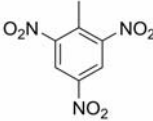
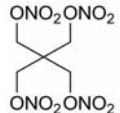
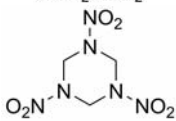
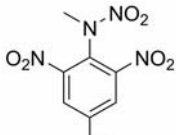
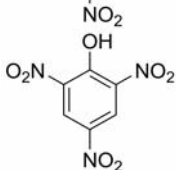
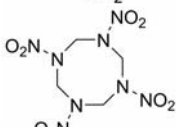
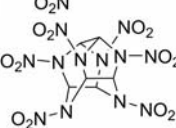
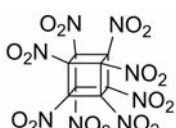
Overall, these polymers show less λ_{max} dependence on substrate than previous polymers with similar structures.¹⁸ This can be attributed to the high molecular weights and flexibility of the vinylene backbone, which prevent the efficient onset of π -stacking in the solid-state. This feature allows these polymers to maintain their thin-film luminescence properties, regardless of the substrate used, providing good color purity, while maintaining high fluorescence quantum efficiencies. Polymers **PSF2–3** show good photo-stability in thin-films. The prominent blue emission band found in these polymers remains after a few weeks on the TLC substrate. **PSF1** shows less photostability, and fades from a bright blue emission to a dull green emission after 10 min exposure to UV light.

4.3.3 Explosives Detection

The PL properties observed for **PSF1–3** are promising for explosives detection applications. The pure blue emission energetically allows electron transfer to a wide range of explosive materials while providing a fully visible blue background luminescence for evaluation by the human eye. The high fluorescence quantum efficiencies minimize sample use, lowering the amount needed for analysis. These polymers also show favorable solid-state emission properties such as good stability (for polymers **PSF2–3**) and the ability to operate on both porous and non-porous surfaces. The unprotected fluorene unit in **PSF1** initially shows good blue-emission properties but is quickly oxidized to a green-yellow emitting material in air. However, photooxidation may be developed into a turn-on emission indicator for selective detection of nitrate ester explosives (See Chapter 5). The rigid, bulky spirofluorene units in **PSF3** assist in the near unity fluorescence quantum yield observed. These groups also prevent stacking in the thin-film, providing a porous polymer layer. This porosity may assist analyte binding at the silicon center. Polymers **PSF1–3** all show some delocalization through the polymer backbone which may allow for an amplified detection process. All of these properties add to the improvement of explosives detection by fluorescing polymers.

High explosives can be classified by their chemical functionality, which includes inorganic nitrates, organic nitrates, nitroaromatics, nitrate esters, nitramines, and peroxide based explosives. Our previous work, using energetic modeling with DFT calculations, has shown that nitroaromatic, nitramine, nitrate ester, and organic

Table 4-3. Summary of chemical structure and selected physical properties of explosive analytes.

Explosive	Structure	Class	P_{vap} (Torr)	Detonation velocity (m s^{-1})
EGDN		Nitrate ester	2.8×10^{-2}	NA
DNT		Nitroaromatic	1.1×10^{-4}	7000
TNG		Nitrate ester	4.4×10^{-4}	7750
TNT		Nitroaromatic	5.8×10^{-6}	6850
PETN		Nitrate ester	1.4×10^{-8}	7920
RDX		Nitramine	4.6×10^{-9}	8440
Tetryl		Nitroaromatic/ Nitramine	5.7×10^{-9}	7080
PA		Nitroaromatic	5.8×10^{-9}	7900
HMX		Nitramine	8.0×10^{-11}	9110
CL-20		Nitramine	<i>na</i>	9650
ONC		Organic nitrate	<i>na</i>	10 100

nitrate based explosives are prime candidates for detection by electron transfer fluorescence quenching by blue emitting polymers.^{6a} Fluorescence quenching involves an excited-state electron transfer process from the polymer fluorophore to the lowest unoccupied molecular orbital (LUMO) of the explosive material. Detection limits are based on the efficiency of this process, which can be improved by increasing analyte–sensor binding interactions and matching the frontier molecular orbital energies of the sensor with the LUMO of the explosives analytes. Chemical and physical properties of some important high explosives are provided in Table 4-3 and these parameters influence detection schemes. For example, the high volatility of EGDN combined with its high energy LUMO makes this explosive difficult to detect by amplified fluorescence quenching. Previous studies have shown that the detection of explosive particulates rather than vapor increases the number of explosive analytes that can be detected.^{6a,18} A detailed description of the quantitative method can be found in the experimental section. Filter paper was used as the substrate for particle detection because it represents the semi-porous materials typically used for particle sample collection in current technology. Laboratory explosives were spotted from dilute solutions at various concentrations with a consistent diameter of 1 cm. Production line explosives PETN and C-4 (NEWTEC Services Group Inc.) were handled and thumbprints were transferred to the substrate. Production line explosives are defined as explosives and mixtures thereof that are application ready. These explosives were used to demonstrate the detection ability of polymers **PSF1–3** on explosives as they would be encountered in the field. Solutions of **PSF1–3** (0.07 mg

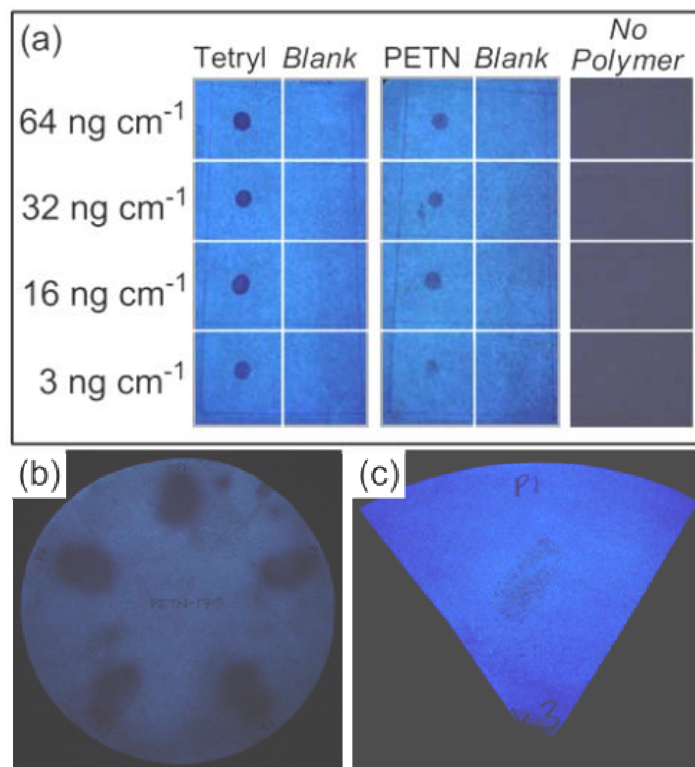


Figure 4-3. Examples of fluorescence quenching of a thin-film of **PSF3** on Whatman2 filter paper by solid-particulates of various explosives under continuous UV excitation (302 nm). (a) Detection of Tetryl and PETN particulates. A toluene blank was spotted next to each explosive as a control. (b) Detection of consecutive thumbprints of production line PETN. (c) Detection of a thumbprint of production line C-4. C-4 is a mixture of RDX (91%), a plasticizer, and a plastic binder.

mL⁻¹ in toluene:acetone) were airbrushed onto the substrate and visualized under a UV lamp (302 nm). Examples of the explosive detection studies using **PSF3** are seen in Figure 4-3. Images of both laboratory and production line test results are included to show the diversity of this approach.

The results of the explosive detection study are seen in Table 4-4. Detection limits are determined based on the observed fluorescence quenching of polymers

Table 4-4. Summary of solid-state detection limits (pg cm^{-2}) for various explosives by fluorescence quenching with **PSF1–3**.

Explosive	PSF1	PSF2	PSF3
Tetryl	1	2	2
TNT	30	60	30
DNT	200	200	200
PA	600	300	100
PETN	300	600	300
TNG	1000	2000	2000
RDX	2000	2000	2000
HMX	2000	2000	2000

PSF1–3 by the explosive analyte. For all three polymers, Tetryl had the lowest detection limits, reaching as low as 1 pg cm^{-2} for **PSF1**. These detection limits are two orders of magnitude lower than previously achieved using a surface detection method.¹⁸ Polymers **PSF2** and **PSF3** are more photo-stable and show comparable detection limits as **PSF1**. The blue luminescence of **PSF1** begins to fade (onset of fading begins after 20 s exposure to UV light) to a dull green and eventually totally disappears after prolonged exposure to UV light ($> 1 \text{ h}$) in air. **PSF2** and **PSF3** maintain their bright blue luminescence for several hours with detection at the lower limits observed over 20 min. Detection limits begin to decrease after 20 min of UV irradiation due to the evaporation of some explosives, rather than deterioration of the polymer. Eventual photooxidation of the silicon centers in polymers **PSF1–3** eliminates the bright blue luminescence. Due to the higher fluorescence quantum

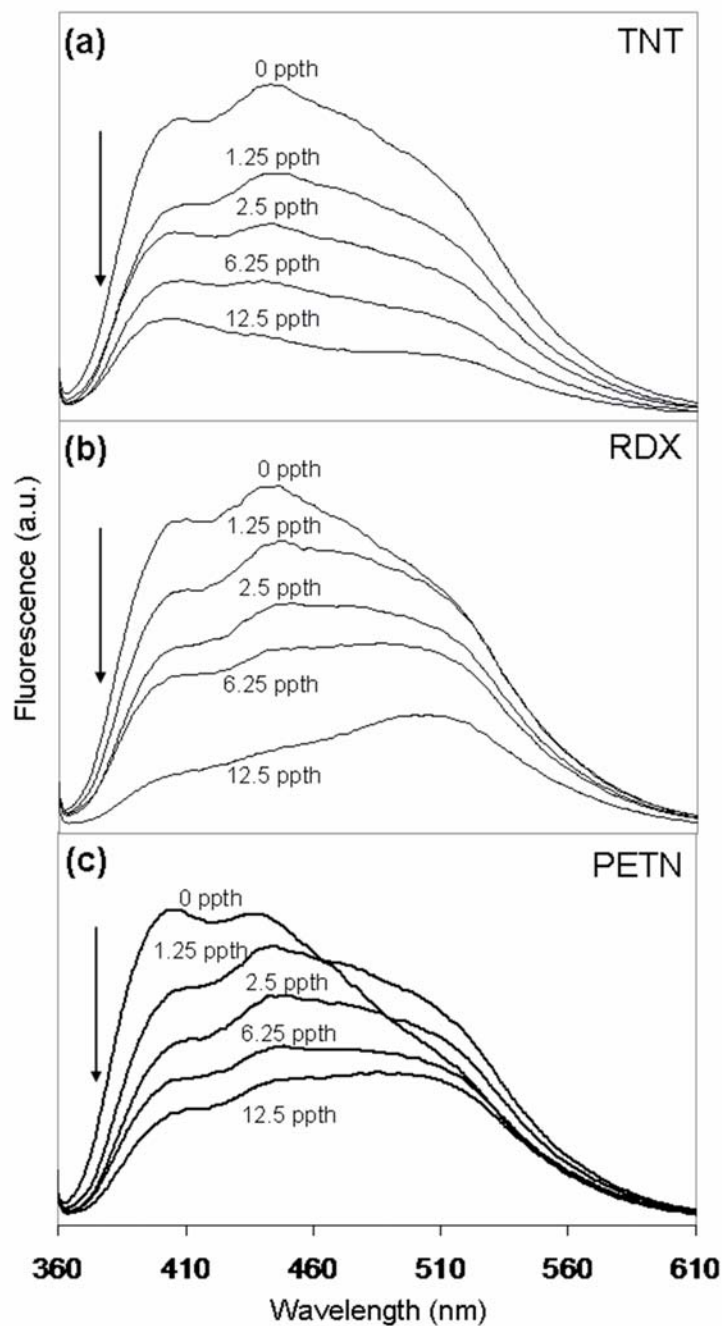


Figure 4-4. Solid-state fluorescence quenching behavior of **PSF1** on silica TLC plates in the presence of (a) TNT, (b) RDX, and (c) PETN. The concentration of explosive is reported in ppth of explosive-to-polymer (ppth = parts per thousand by weight).

efficiencies of **PSF1–3**, the concentration of polymer used for successful detection was 10 times lower than those previously used.

Solid-state detection of explosives particulates can be quantitatively assessed using a Stern–Volmer analysis of solid polymer/analyte solutions.¹⁸ This method was developed to help quantify the detection method at the molecular level. While the Stern–Volmer equation (Equation 1) is usually applied to model a diffusing emitter and quencher, it also applies to static quenching where the emitting species and

$$I_0/I = 1 + K_{SV}[Q] \quad (1)$$

$$\ln(\Phi_0/\Phi) = VN_A[Q] \quad (2)$$

quencher are intimately bound. Another quantitative technique to measure the efficiency of a static fluorescence quenching process is the Perrin formulation (Equation 2). However, this method requires the measurement of absolute fluorescence quantum efficiencies in the bound and unbound state, which are difficult to obtain in thin-film studies using volatile analytes. Therefore, the Perrin formulation is usually applied to highly concentrated solutions where the donor and acceptor moieties are covalently linked and the sample cuvette is sealed. The explosives chosen for the analysis include the three key classes of nitrogen based high explosives: TNT, PETN, and RDX. Solutions containing a dissolved explosive and either polymer **PSF1**, **PSF2**, or **PSF3** (4 mg mL⁻¹ in CHCl₃) were individually developed onto the TLC plate with varying concentrations of explosives. This creates

Table 4-5. Summary of solid-state Stern–Volmer constants (K_{SV}) for the fluorescence quenching of **PSF1–3** by TNT, RDX and PETN, which were measured on silica TLC plates. Values reported in ppth^{-1} (ppth = parts-per-thousand by weight of the explosive dissolved in the polymer film).

Polymer		K_{SV} (ppth^{-1})			
		$\lambda_{\text{flu}} = 400 \text{ nm}$	$\lambda_{\text{flu}} = 445 \text{ nm}$	$\lambda_{\text{flu}} = 500 \text{ nm}$	Average
PSF1	TNT	0.14	0.24	0.23	0.20
	RDX	0.34	0.25	0.097	0.23
	PETN ^a	0.15	0.094	—	0.12 ^b
PSF2	TNT	0.26	0.35	0.32	0.31
	RDX	0.26	0.086	0.021	0.12
	PETN	0.14	0.093	0.051	0.096
PSF3	TNT	0.31	0.24 ^c	0.22	0.26
	RDX	0.041	0.032 ^c	0.035	0.036
	PETN	0.040	0.040 ^c	0.040	0.040

^a Oxidation of the fluorene unit in the presence of PETN limits accuracy of the observed fluorescence quenching at $\lambda_{\text{flu}} > 450 \text{ nm}$. ^b Calculated from $\lambda_{\text{flu}} = 400$ and 445 nm . ^c $\lambda_{\text{flu}} = 470 \text{ nm}$.

a thin-film solid solution of polymer containing uniformly distributed explosive analytes. Representative plots of the spectra taken for **PSF1** are seen in Figure 4-4. A clear decrease in fluorescence is observed with increasing concentrations of dissolved explosives, and the data closely follow the Stern–Volmer equation. The quenching constants (K_{SV}) are given in Table 4-5. Even though the detection of explosives particulates by **PSF1–3** are spectroscopically similar to previous polymers, the visual detection limits by human evaluation are much better because **PSF1–3** are brighter and have better visible color purity than the UV–blue emitting silafluorene-phenylenedivinylene polymers studied previously.¹⁸ The Stern–Volmer plot of **PSF1**, when exposed to PETN, does not show a consistent decrease in fluorescence intensity. While the intensity does decrease, there is also a slight increase in intensity

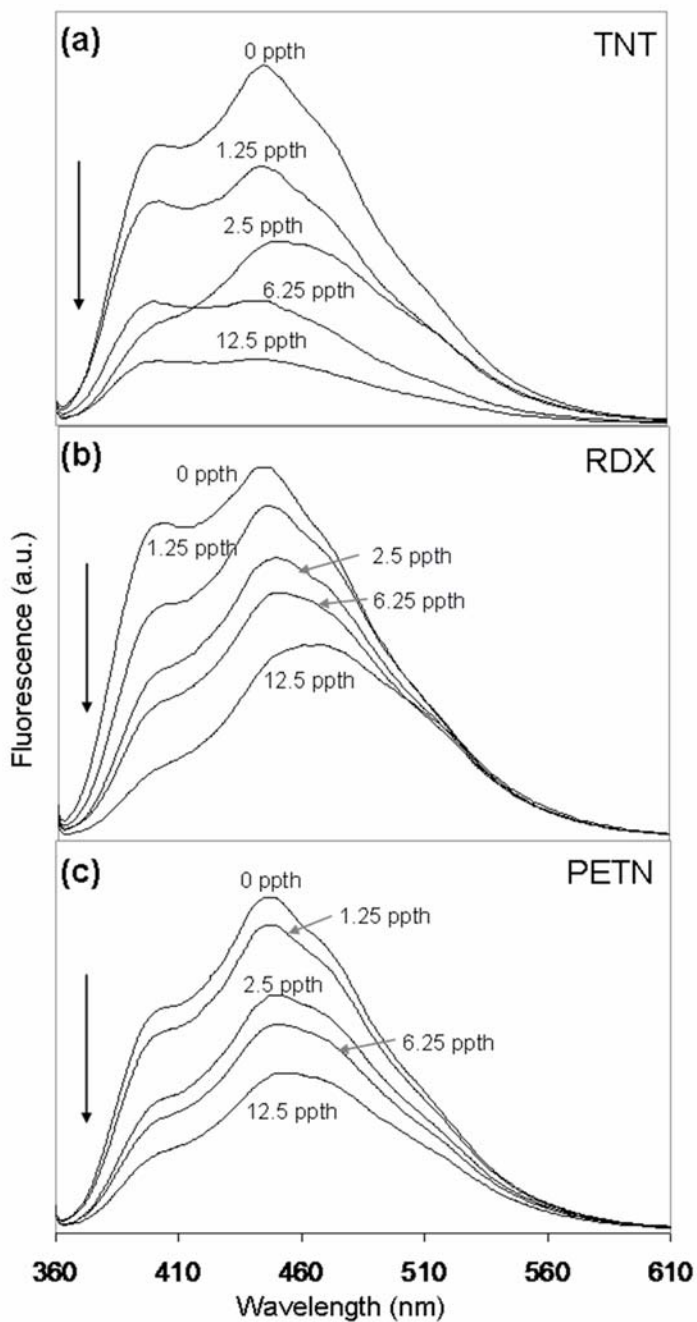


Figure 4-5. Solid-state fluorescence quenching behavior of **PSF2** on silica TLC plates in the presence of (a) TNT, (b) RDX, and (c) PETN. The concentration of explosive is reported in ppth of explosive-to-polymer (ppth = parts per thousand by weight).

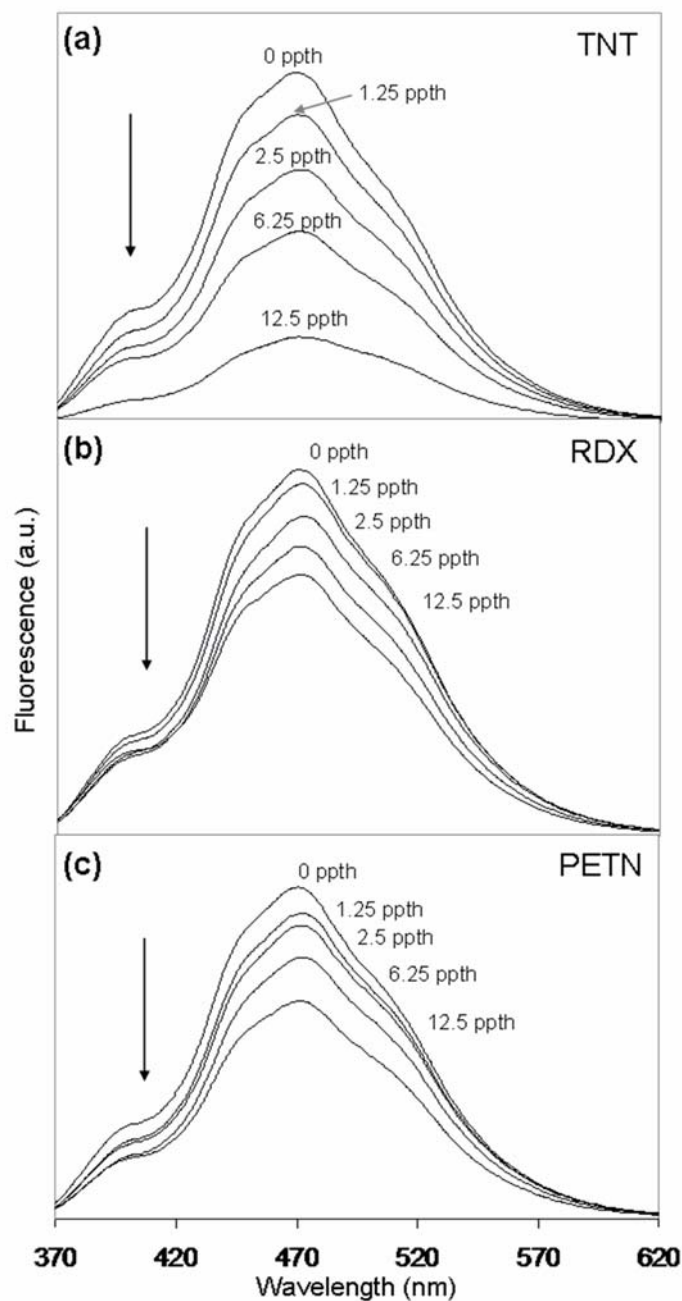


Figure 4-6. Solid-state fluorescence quenching behavior of **PSF3** on silica TLC plates in the presence of (a) TNT, (b) RDX, and (c) PETN. The concentration of explosive is reported in ppth of explosive-to-polymer (ppth = parts per thousand by weight).

at the low energy end of the spectra. This is hypothesized to be a result of oxidation of the fluorene to fluorenone and will be discussed further in Chapter 5. This slight increase has a negative effect on the observed Stern–Volmer behavior.

The Stern–Volmer constant for the detection of PETN by **PSF1** in the solid state is wavelength dependent, which prompted our further analysis of the fluorescence quenching plots of **PSF1–3** (Figure 4-4 for **PSF1** and Figures 4-5 and 4-6 for **PSF2-3**). These plots reveal a correlation between the magnitude of the fluorescence decrease at a given wavelength and the redox potential of the explosive analyte. This correlation is also seen in Table 4-5 with the Stern-Volmer constants at different wavelengths for all three polymers. The nitrate and nitro containing explosives range in LUMO energies from -3.918 eV for Tetryl to -2.122 eV for EGDN. In this case, the LUMO energies of TNT, PETN and RDX are -3.483 eV, -3.075 eV, and -2.531 eV, respectively. Conjugated polymers typically have a distribution of molecular weights that contribute to the polydispersity index (PDI). The varying molecular weights give rise to a combination of conjugation lengths and may be responsible for the broadened emission we observe in the polymers, as compared to monomers and dimers or trimers. This promotes the presence of a broad range of individual excited state energies for the various length polymer chains that can participate in the electron transfer process, from the sensor to analyte, with different relative rates.

In the case of **PSF1** and **PSF2**, it is seen that depending on the explosive analyte, different energies of the spectrum are quenched with more efficiency. For

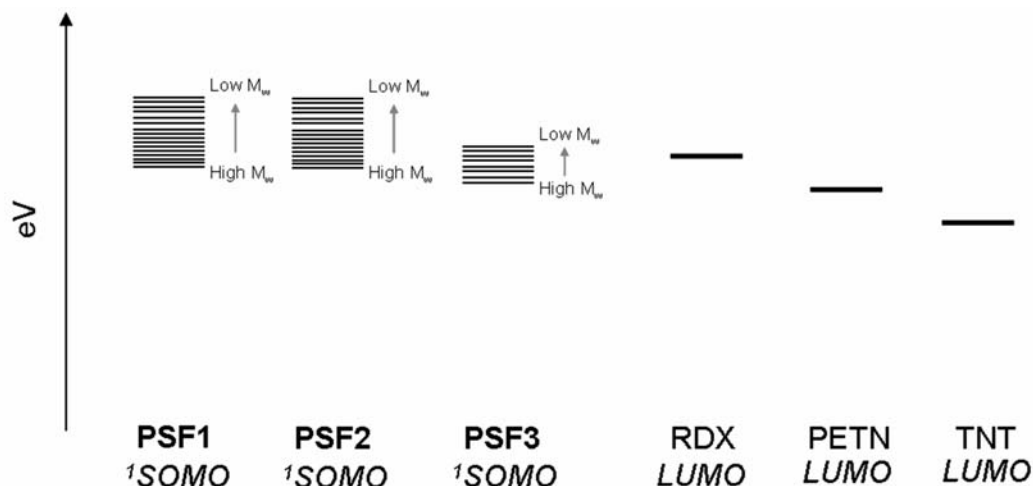


Figure 4-7. Qualitative energy level diagram comparing the emitting state energies of polymers **PSF1–3** with the LUMO energies of RDX, PETN and TNT. The energy distribution of the emitting states for the polymers is postulated to depend on the polydispersity, leading to broader fluorescence emission profiles for polymers with high polydispersities. Good energy matching between the low M_w polymers and RDX leads to better quenching at the high energy part of the spectrum for RDX and vice-versa for TNT for **PSF1** and **PSF2**, which have high polydispersities.

example, the fluorescence quenching spectra of **PSF1** in the presence of TNT shows a larger decrease in intensity at the lower energy part of the spectrum. This is expected based on the LUMO energy of TNT, as polymers at the lower energy part of the spectrum better match the LUMO energy of TNT. For RDX, the fluorescence spectra show a greater decrease in intensity at the higher energy region of the polymer donor emission spectra, which can be rationalized based on a better energy match with the higher LUMO energy of RDX as compared to TNT (Figure 4-7). PETN also shows a greater decrease in the higher energy part of the polymer donor emission spectra; however, results for PETN may also be influenced by competing photooxidation of the fluorene unit which occurs with nitrate ester based explosives. The methyl protected fluorene unit in **PSF2** exhibits similar behavior and confirms this trend for

Table 4-6. Comparison of photoluminescent properties and sensor response of silafluorene based polymers synthesized by catalytic hydrosilylation.

	M_w	Solution λ_{flu} (nm)	Thin-film λ_{flu} (nm)	Φ_{flu}	Detection Limit TNT (ng cm ⁻²)	Detection Limit RDX (ng cm ⁻²)	[Polymer] ($\mu\text{g cm}^{-2}$) ^a
A	4300	362	376	0.04	0.3	2	1.5
B	9600	359	447	0.04	0.1	2	1.5
PSF1	16 000	376	446	0.52	0.03	2	0.15
PSF2	20 000	377	446	0.22	0.06	2	0.2
PSF3	13 200	392	470	1.0	0.03	2	0.1

^a Concentration of polymer in the thin-film used during the solid-state explosives detection studies.

PETN (Figure 4-5). In contrast to the other polymers, **PSF3** shows a uniform quenching behavior at all wavelengths. This polymer has a lower molecular weight and narrower polydispersity than both **PSF1** and **PSF2** (Table 4-1). This presumably reduces the distribution of the number of emitting species of different energies and eliminates the emission band wavelength dependence of the quenching process with varying analytes (Figure 4-7). These results suggest that the solid state Stern–Volmer analysis not only provides information about the detection ability of the polymer sensor but also insight into the dynamics of the excited-state electron transfer process.

Overall, polymers **PSF1-3** show an improvement in increasing molecular weights, photoluminescence efficiencies and detection sensitivities for explosives

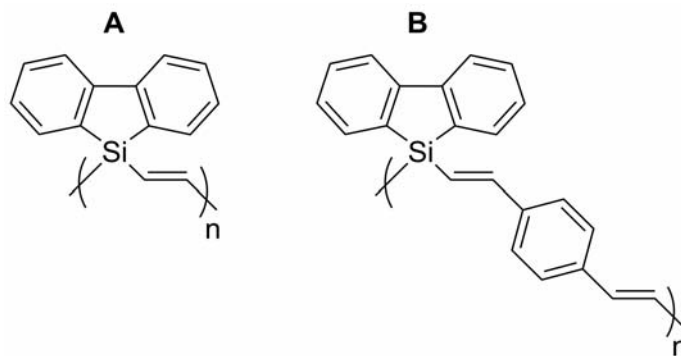


Figure 4-8. Structures of poly(silafluorene-vinylene) (A) and poly(silafluorene-phenylenedivinylene) (B).

over silafluorene-vinylene and phenylenedivinylene polymers previously synthesized (Table 4-6). The molecular weights are improved through the use of a fluorenyl comonomer, which increases the distance between the ethynyl functionalities and relieves the steric hindrance on coordination to the catalyst during polymerization as compared to **A** and **B** (Figure 4-8). The higher molecular weights allow for easier thin-film processing as well as creating a greater red-shift in the emission toward the visible blue region of the spectrum. This delocalization also increases the amplified fluorescence quenching response to explosive analytes, improving sensor sensitivity. The red-shifted emission of polymers **PSF1-3**, as compared to polymers **A** and **B**, enables better visualization of the polymers during detection. The near unity quantum efficiencies for fluorescence also provide an enhanced signal-to-noise ratio and reduce the amount of polymer needed for spray-on detection of surface particulates by nearly an order of magnitude. All these factors lead to a significant improvement in the detection of explosive particulates as demonstrated by detection limits for TNT (Table 4-6). Detection limits for explosives with lower reduction potentials such as

RDX, are on the same order of magnitude as the previous polymers. By red-shifting the emission of polymers **PSF1-3** to provide better visualization of the polymer films, and minimize the amount of material needed for detection, the reduced excited state energy limited the improvement in sensitivity for explosives with high energy acceptor orbitals, such as RDX. In addition to their use as sensory materials, these highly emissive, blue fluorescent polymers may prove useful in other photoluminescence applications.

4.4 CONCLUSIONS

A series of silafluorene-fluorene conjugated polymers **PSF1-3** have been synthesized as new highly efficient blue-emitting materials. These polymers show promise as chemosensors for explosives detection applications. The high quantum efficiencies of fluorescence, ranging from 20-100%, and good color purity in the blue region of the spectrum make these materials attractive as blue fluorophores. High solid-state Stern-Volmer quenching constants were obtained for the fluorescence quenching detection of TNT, RDX and PETN. Detection results also show a correlation between the redox potential of the explosive and the wavelength dependence seen in the quenching process, which is attributed to the molecular weight distribution of emitting species. The larger intramolecular distances between silafluorene units allow for good Lewis acid-base interactions between the silacycle ring and the explosives analytes. Solid-state detection of explosives particulates was successful for a range of explosive analytes including TNT, DNT, picric acid, RDX,

HMX, PETN, TNG, and Tetryl with detection limits as low as 1 pg cm^{-2} . The polymers also show the ability to detect production line explosives such as PETN and C-4, which contain added plasticizers. The unprotected fluorene in **PSF1** shows tandem turn-off/turn-on fluorescence sensing, which is selective for the nitrate ester based explosives PETN and TNG. This illustrates how time dependent photochemistry can be used for increased selectivity in solid state fluorescent sensors.

4.5 EXPERIMENTAL

4.5.1 General Synthetic Techniques

Caution: TNT and picric acid are high explosives and should be handled only in small quantities. Picric acid also forms shock sensitive compounds with heavy metals. Purchased explosive standards were handled as dilute solutions to eliminate their explosion hazard. All synthetic manipulations were carried out under an atmosphere of dry argon gas using standard Schlenk techniques. Dry solvents were purchased from Aldrich Chemical Co. Inc. and used after purification with an MBraun Auto Solvent Purification System. Spectroscopic grade toluene from Fisher Scientific was used for the fluorescence measurements. Trimethylsilylacetylene and 1,4-diethynylbenzene (97%) were purchased from Aldrich Chemical Co. Inc. 1,4-diethynylbenzene was sublimed before use ($30 \text{ }^{\circ}\text{C}$ at 0.5 Torr). The following were prepared by literature methods: 1-hydrido-1-methylsilafluorene,²⁷ 1,1-dihydridosilafluorene,²⁸ 2,7-diethynyl-9,9-dihydridofluorene,²⁹ 2,7-diethynyl-9,9-dimethyl-9H-fluorene,³⁰ 2,7-diethynyl-9,9'-spirobifluorene,³¹ and 2,7-

diethynylfluorenone.³¹ Picric acid and DNT were purchased from Aldrich Chemical Co. and recrystallized from ethanol and methanol, respectively. TNT was prepared from DNT³² and recrystallized from toluene. RDX, HMX, Tetryl, TNG and PETN were purchased as 1 mg mL⁻¹ analytical standards in acetonitrile from Cerilliant®.

NMR data were taken on 300, 400, and 500 MHz spectrometers. UV-vis spectra were obtained with the use of a Hewlett-Packard 8452A diode array spectrometer. A Perkin-Elmer LS 45 luminescence spectrometer was used to record fluorescence emission and excitation spectra. For anaerobic and anhydrous studies, spectral grade toluene was first redistilled over a sodium/benzophenone ketyl. The anhydrous solution was then degassed 3 times using a freeze-pump-thaw method. The final solutions were then further degassed by bubbling argon through the sample for 10 min. The quartz cuvettes were sealed to prevent exposure of the sample solution to the atmosphere. IR spectra were obtained on a Nicolet Magna-IR 550 spectrometer. GPC data were obtained with the use of a Viscotek GPCmax VE 2001 GPC; molecular weights were recorded relative to polystyrene standards and low molecular weight silole monomers and dimers.

4.5.2 Solid-state Explosives Detection

Solutions of explosives were prepared as serial dilutions in toluene and stored in amber vials at 0 °C to prevent degradation. The solutions were spotted onto Whatman® filter paper at the desired concentration level using a glass microsyringe. A solvent control was spotted next to each explosive. All depositions were prepared

from a 5 μL volume, producing a spot of ~ 1 cm in diameter, to ensure consistent analysis. Upon solvent evaporation, the substrate is airbrushed at a rate of 0.5 mL s^{-1} with a 0.07 mg mL^{-1} solution (1:1, toluene:acetone) of the desired polymer. Addition of toluene aids the transient dissolution of explosive analytes and plasticizers, insuring efficient mixing with the polymers on drying. Blue photoluminescent **PSF1–3** were visualized using a UV-B lamp ($\lambda_{\text{em}} = 302 \text{ nm}$) as the excitation source with a UV transmitting filter (U34, HOYA Optics) attached to prevent backscattered visible light. Detection studies were performed for each explosive at trace contamination levels beginning at 64 ng cm^{-2} and ending at 1 pg cm^{-2} until a detection limit was reached.

Illuminated samples were examined by an independent observer to determine if quenching was discernible for polymers **PSF1–3** immediately after exposure to explosive analytes. A double-blind test was carried out at the detection limit using two spots of the explosive material at each concentration, which were spotted randomly onto three locations. In each case a solvent blank was used as the control. The independent observer was unaware where the solvent control and explosive spots were distributed. Dark spots in the luminescent film indicate quenching of the polymer by the analyte. Detection limits are reported as the lowest amount of explosive necessary for the independent observer to observe quenching visually and accurately ($>95\%$) in the correct locations. For **PSF1**, detection limits for PETN and TNG were reported as the lowest amount of explosive necessary to observe

fluorescence quenching and the subsequent green-yellow luminescent turn-on sensing. This required continuous exposure of the substrate to UV light for 1-2 min.

Production line explosives PETN and C-4 were analyzed as thumbprints after handling of the solid explosive materials with nitrile gloves. Explosive particulates were not visible to the human eye before prints were taken. Five prints were consecutively laid down without further handling of the explosive. This study was included to provide real world applicability and exact concentration of explosive material within each print was unknown.

4.5.3 Synthesis of 2,7-di(1-methyl-1-*trans*-ethenyl-silafluorene)-9*H*-fluorene (1)

1-hydrido-1-methylsilafluorene (275 mg, 1.4 mmol), 2,7-diethynyl-9,9-dihydrofluorene (150 mg, 0.7 mmol), and 0.5 mol % H_2PtCl_6 were stirred in toluene (4 mL), under argon for 12 h at 0 °C. The light brown solution was filtered through a sintered glass frit and evaporated to dryness. The remaining solid was purified by column chromatography (silica gel) using dichloromethane:hexanes as the eluent, yielding a white crystalline solid (0.32 g, 76%). mp = 83 °C (decomp.); ^1H NMR (400.053 MHz, CDCl_3): δ 7.87 (m, 4H, PhH), 7.67 (m, 6H, PhH), 7.48 (m, 6H, PhH), 7.32 (m, 6H, PhH), 7.20 (d, 2H, C=CH), 6.55 (d, 2H, C=CH), 3.83 (s, 2H, CCH₂), 0.61 (s, 6H, SiCH₃); $^{13}\text{C}\{^1\text{H}\}$ NMR (100.59 MHz, CDCl_3): δ 148.5, 147.8, 144.3, 142.0, 137.7, 136.9, 133.6, 130.7, 127.6, 126.3, 123.3, 122.4, 121.2, 120.3, 36.9, -5.01; $^{29}\text{Si}\{^1\text{H}\}$ NMR (99.37 MHz, INEPT, CDCl_3 , TMS (δ 0.00)) δ -8.1; Elemental analysis calcd for $\text{C}_{43}\text{H}_{34}\text{Si}_2\cdot\text{H}_2\text{O}$: C 82.6, H 5.80; Found: C 82.5, H 6.28.

4.5.4 Synthesis of 2,7-di(1-methyl-1-trans-ethenyl-silafluorene)-9,9-dimethyl-9H-fluorene (2)

1-hydrido-1-methylsilafluorene (243 mg, 1.2 mmol), 2,7-diethynyl-9,9-dimethyl-9H-fluorene (150 mg, 0.6 mmol), and 0.5 mol % H_2PtCl_6 were stirred in toluene (4 mL), under argon for 12 h at 0 °C. The light brown solution was filtered through a sintered glass frit and evaporated to dryness. The remaining solid was purified by column chromatography (silica gel) using dichloromethane:hexanes as the eluent, yielding a white crystalline solid (0.27 g, 69%). mp = 81 °C (decomp.); ^1H NMR (400.053 MHz, CDCl_3): δ 6.77–8.01 (br, 24H, PhH and C=CH), 6.63 (d, 2H, C=CH), 1.50 (s, 6H, C(CH₃)₂), 0.70 (s, 6H, Si(CH₃)); $^{13}\text{C}\{^1\text{H}\}$ NMR (100.59 MHz, CDCl_3): δ 148.6, 138.9, 137.9, 133.6, 130.8, 127.9, 126.8, 122.5, 121.3, 35.0, 27.2, –5.05; $^{29}\text{Si}\{^1\text{H}\}$ NMR (99.37 MHz, INEPT, CDCl_3 , TMS (δ 0.00)) δ –8.3; Elemental analysis calcd for $\text{C}_{45}\text{H}_{38}\text{Si}_2\cdot\text{H}_2\text{O}$: C 82.8, H 6.17; Found: C 83.6, H 6.25.

4.5.5 Synthesis of 2,7-di(1-methyl-1-trans-ethenyl-silafluorene)-9,9'-spirobifluorene (3)

1-hydrido-1-methylsilafluorene (104 mg, 0.5 mmol), 2,7-diethynyl-9,9'-spirobifluorene (100 mg, 0.26 mmol), and 0.5 mol % H_2PtCl_6 were stirred in toluene (5 mL), under argon for 12 h at 0 °C. The light yellow solution was filtered through a sintered glass frit and evaporated to dryness. The remaining solid was purified by column chromatography (silica gel) using dichloromethane–hexanes as the eluent,

yielding light yellow powder (0.15 g, 75%). mp = 125 °C (decomp.); ^1H NMR (300.075 MHz, CDCl_3): δ 7.95–6.55 (br, 36H, PhH and C=CH), 6.30 (d, 2H, C=CH), 0.50 (s, 6H, Si(CH₃)); $^{13}\text{C}\{^1\text{H}\}$ NMR (100.59 MHz, CDCl_3): δ 148.4, 146.5, 142.0, 137.7, 133.5, 130.6, 130.4, 128.1, 127.7, 124.4, 121.2, 120.5, 22.8, -2.00; $^{29}\text{Si}\{^1\text{H}\}$ NMR (99.37 MHz, INEPT, CDCl_3 , TMS (δ 0.00)) δ -7.7; Elemental analysis calcd for $\text{C}_{55}\text{H}_{40}\text{Si}\cdot 2\text{H}_2\text{O}$: C 83.3, H 5.59; Found: C 83.3, H 5.47.

4.5.6 Synthesis of poly(silafluorene-(9H-fluorene)divinylene) (PSF1)

1,1-dihydridosilafluorene (200 mg, 1.1 mmol), 2,7-diethynyl-9,9-dihydridofluorene (235 mg, 1.1 mmol), and 0.5 mol % H_2PtCl_6 were stirred at 0 °C in toluene (6 mL), under argon for 48 h. The solution was warmed to room temperature and dimethylphenylsilane (0.1 mL, 0.6 mmol) was added and the reaction was stirred for 2 h. The orange solution was filtered and evaporated to dryness. The remaining solid was dissolved in 3 mL of THF, precipitated with 30 mL of methanol. The precipitation procedure was repeated three times to remove low molecular weight oligomers. The off-white solid was washed with acetone and a white powder was collected by vacuum filtration (285 mg, 66%). ^1H NMR (300.075 MHz, CDCl_3): δ 6.60–7.89 (br, 18H, PhH and C=CH), 3.87 (s, 2H, CCH₂), 0.38 (s, terminal PhSi(CH₃)₂).

4.5.7 Synthesis of poly(silafluorene-(9,9-dimethyl-9H-fluorene)divinylene) (PSF2)

1,1-dihydridosilafluorene (200 mg, 1.1 mmol), 2,7-diethynyl-9,9-dimethyl-9H-fluorene (267 mg, 1.1 mmol), and 0.5 mol % H_2PtCl_6 were stirred at 0 °C in toluene (6 mL), under argon for 48 h. The solution was warmed to room temperature and dimethylphenylsilane (0.1 mL, 0.6 mmol) was added and the reaction was stirred for 2 h. The orange solution was filtered and evaporated to dryness. The remaining solid was dissolved in 3 mL of THF, precipitated with 30 mL of methanol. The precipitation procedure was repeated three times to remove low molecular weight oligomers. The off-white solid was washed with acetone and a white powder was collected by vacuum filtration (460 mg, 98%). ^1H NMR (300.075 MHz, CDCl_3): δ 6.55–8.23 (br, 16H, PhH and C=CH), 1.47 (s, 6H, C(CH₃)₂), 0.46 (s, terminal PhSi(CH₃)₂).

4.5.8 Synthesis of poly(silafluorene-(9,9'-spirobifluorene)divinylene) (PSF3)

1,1-dihydridosilafluorene (100 mg, 0.55 mmol), 2,7-diethynyl-9,9'-spirobifluorene (207 mg, 0.55 mmol), and 0.5 mol % H_2PtCl_6 were stirred at room temperature in toluene (7 mL), under argon for 48 h. To the orange solution was added dimethylphenylsilane (0.1 mL, 0.6 mmol) and the reaction was stirred for 2 h. The orange solution was filtered and evaporated to dryness. The remaining solid was dissolved in 3 mL of THF, precipitated with 30 mL of methanol. The precipitation procedure was repeated three times to remove low molecular weight oligomers. The

yellow solid was washed with acetone and collected by vacuum filtration (290 mg, 94%). ^1H NMR (300.075 MHz, CDCl_3): δ 5.95–8.09 (br, 24H, PhH and $\text{C}=\text{CH}$), 0.33 (s, terminal $\text{PhSi}(\text{CH}_3)_2$).

4.6 ACKNOWLEDGEMENTS

This chapter, in part, is a reprint of the material as it appears in the following paper: Sanchez, J. C.; Trogler, W. C. "Efficient Blue Emitting Silafluorene-fluorene Conjugated Copolymers: Selective Turn-off/turn-on Detection of Explosives" *J. Mater. Chem.* **2008**, DOI: 10.1039/b802623h.

4.7 REFERENCES

- (1) Singh, S. *J. Hazard. Mater.* **2007**, *144*, 15–28.
- (2) (a) Hakansson, K.; Coorey, R. V.; Zubarev, R. A.; Talrose, V. L.; Hakansson, P. *J. Mass. Spectrom.* **2000**, *35*, 337–346. (b) Smith, K. D.; McCord, B. R.; McCrehan, W. A.; Mount, K.; Rowe, W. F. *J. Foren. Sci.* **1999**, *44*, 789–794. (c) Sylvia, J. M.; Janni, J. A.; Klein, J. D.; Spencer, K. M. *Anal. Chem.* **2000**, *72*, 5834–5840. (d) Popov, I. A.; Chen, H.; Kharybin, O. N.; Nikolaev, E. N.; Cooks, R. G. *Chem. Commun.* **2005**, *15*, 1953–1955. (e) Kolla, P. *Anal. Chem.* **1995**, *67*, 184A–189A. (f) XPRAY Field Test Kit available from Mistral Group, Web URL: http://www.mistralgroup.com/SEC_explosives.asp.
- (3) (a) McQuade, D. T.; Pullen, A. E.; Swager, T. M. *Chem. Rev.* **2000**, *100*, 2537–2574. (b) Toal, S. J.; Trogler, W. C. *J. Mater. Chem.* **2006**, *16*, 2871–2883.
- (4) (a) Moore, D. S. *Rev. Sci. Instrum.* **2004**, *75*, 2499–2512. (b) Steinfeld, J. I.; Wormhoudt, J. *Annu. Rev. Phys. Chem.* **1998**, *49*, 203–232.
- (5) Davidson, W. R.; Stott, W. R.; Sleeman, R.; Akery, A. K. *Proc. SPIE* **1994**, *2092*, 108–119.
- (6) (a) Sanchez, J. C.; DiPasquale, A. G.; Rheingold, A. L.; Trogler, W. C. *Chem. Mater.* **2007**, *19*, 6459–6470. (b) Toal, S. J.; Sanchez, J. C.; Dugan, R. E.; Trogler, W. C. *J. Forensic Sci.* **2007**, *52*, 79–83.
- (7) (a) Yinon, J.; Zitrin, S. In *Modern Methods and Applications in Analysis of Explosives*; Wiley: Chichester, 1993. (b) Gresham, G. L.; Davies, J. P.; Goodrich, L. D.; Blackwood, L.G.; Liu, B. Y.; Thimsen, D.; Yoo, S. H. *Proc. SPIE* **1994**, *2276*, 34–44.
- (8) (a) Ma, B.; Lauterwasser, F.; Deng, L.; Zonte, C. S.; Kim, B. J.; Fréchet, J. M. J.; Borek, C.; Thompson, M. E. *Chem. Mater.* **2007**, *19*, 4827–4832. (b) Yu, G.; Yin, S.; Liu, Y.; Chen, J.; Xu, X.; Sun, X.; Ma, D.; Zhan, X.; Peng, Q.; Shuai, Z.; Tang, B.; Zhu, D.; Fang, W.; Luo, Y. *J. Am. Chem. Soc.* **2005**, *127*, 6335–6346. (c) Li, Z.; Dong, Y.; Mi, B.; Tang, Y.; Häußler, M.; Tong, H.; Dong, Y.; Lam, J. W. Y.; Ren, Y.; Sung, H. H. Y.; Wong, K. S.; Gao, P.; Williams, I. D.; Kwok, H. S.; Tang, B. Z. *J. Phys. Chem. B* **2005**, *109*, 10061–10066. (d) Mi, B.; Dong, Y.; Li, Z.; Lam, J. W. Y.; Häußler, M.; Sung, H. H. Y.; Kwok, H. S.; Dong, Y.; Williams, I. D.; Liu, Y.; Luo, Y.; Shuai, Z.; Zhu, D.; Tang, B. Z. *Chem. Commun.* **2005**, *28*, 3583–3585. (e) Ren, X.; Li, J.; Holmes, R. J.; Djurovich, P. I.; Forrest, S. R.; Thompson, M. E. *Chem. Mater.* **2004**, *16*, 4743–4747.

- (9) Lee, Y.; Liang, Y.; Yu, L. *Synlett* **2006**, *18*, 2879–2893.
- (10) (a) Ahn, T.; Song, S.-Y.; Shim, H.-K. *Macromolecules* **2000**, *33*, 6764–6771. (b) Kim, J. K.; Yu, J. W.; Hong, J. M.; Cho, H. N.; Kim, D. Y.; Kim, C. Y. *J. Mater. Chem.* **1999**, *9*, 2171–2176. (c) Kim, J. K.; Hong, S. I.; Cho, H. N.; Kim, D. Y.; Kim, C. Y. *Polym. Bull. (Berlin)* **1997**, *38*, 169–176.
- (11) (a) Jin, S. H.; Kang, S. Y.; Kim, M. Y.; Chan, Y. U.; Kim, J. Y.; Lee, K.; Gal, Y. S. *Macromolecules* **2003**, *36*, 3841–3847. (b) Jin, S. H.; Park, H. J.; Kim, J. Y.; Lee, K.; Lee, S. P.; Moon, D. K.; Lee, H. J.; Gal, Y. S. *Macromolecules* **2002**, *35*, 7532–7534.
- (12) Grisorio, R.; Mastroilli, P.; Nobile, C. F.; Romanazzi, G.; Suranna, G. P. *Tetrahedron Lett.* **2005**, *46*, 2555–2558.
- (13) (a) Sonogashira, K.; Tohda, Y.; Hagihara, N. *Tetrahedron Lett.* **1975**, *16*, 4467–4470. (b) Sonogashira, K. In *Comprehensive Organic Synthesis*; Trost, B. M., Fleming, I., Eds.; Pergamon Press: New York, 1991; Vol. 3, p 521. (c) Marsden, J. A.; Haley, M. M. In *Metal-Catalyzed Cross-Coupling Reactions*, 2nd ed.; de Meijere, A., Diederich, F., Eds.; Wiley-VCH: Weinheim, 2004, p 319.
- (14) (a) Stille, J. K. *Angew. Chem. Int. Ed. Engl.* **1986**, *98*, 504–519. (b) Farina, V.; Krishnamurthy, V.; Scott, W. J. *Org. React.* **1997**, *50*, 1–652. (c) Farina, V.; Kapadia, S.; Krishnan, B.; Wang, C.; Liebeskind, L. S. *J. Org. Chem.* **1994**, *59*, 5905–5911. (d) Bao, Z. N.; Chan, W. K.; Yu, L. P. *J. Am. Chem. Soc.* **1995**, *117*, 12426–12435. (e) Lere-Porte, J. P.; Moreau, J. J. E.; Serein-Spirau, F.; Torreilles, C.; Righi, A.; Sauvajol, J. L. *J. Mater. Chem.* **2000**, *10*, 927–932. (f) Bouachrine, M.; Lere-Porte, J. P.; Moreau, J. J. E.; Serein-Spirau, F.; Torreilles, C. *J. Mater. Chem.* **2000**, *10*, 263–268.
- (15) (a) Sinclair, D.; Sherburn, M. S. *J. Org. Chem.* **2005**, *70*, 3730–3733. (b) Dong, C.-G.; Hu, Q.-S. *J. Am. Chem. Soc.* **2005**, *127*, 10006–10007. (c) Weber, S. K.; Galbrecht, F.; Scherf, U. *Org. Lett.* **2006**, *8*, 4039–4041. (d) Miyaura, N.; Suzuki, A. *Chem. Rev.* **1995**, *95*, 2457–2483. (e) Suzuki, A. *J. Organomet. Chem.* **1999**, *576*, 147–168.
- (16) (a) Miyakoshi, R.; Shimono, K.; Yokoyama, A.; Yokozawa, T. *J. Am. Chem. Soc.* **2006**, *128*, 16012–16013. (b) Miyakoshi, R.; Yokoyama, A.; Yokozawa, T. *J. Am. Chem. Soc.* **2005**, *127*, 17542–17547.

- (17) (a) Johansson, D. M.; Theander, M.; Srdanov, G.; Yu, G.; Inganäs, O.; Andersson, M. R. *Macromolecules* **2001**, *34*, 3716–3719. (b) Fan, C.; Plaxico, K. W.; Heeger, A. J. *J. Am. Chem. Soc.* **2002**, *124*, 5642–5643.
- (18) Sanchez, J. C.; Urbas, S. A.; Toal, S. J.; DiPasquale, A. G.; Rheingold, A. L.; Trogler, W. C. *Macromolecules* **2008**, *41*, 1237–1245.
- (19) Ohshita, J.; Kunai, A. *Acta Polym.* **1998**, *49*, 379–403.
- (20) (a) Leclerc, M. *J. Polym. Sci., Part A: Polym. Chem.* **2001**, *39*, 2867–2873. (b) Neher, D. *Macromol. Rapid Commun.* **2001**, *22*, 1365–1385. (c) Scherf, U.; List, E. J. W. *Adv. Mater.* **2002**, *14*, 477–487.
- (21) Bliznyuk, V. N.; Carter, S. A.; Scott, J. C.; Klärner, G.; Miller, R. D.; Miller, C. *Macromolecules* **1999**, *32*, 361–369.
- (22) (a) Uckert, F.; Tak, Y. H.; Müllen, K.; Bässler, H. *Adv. Mater.* **2000**, *12*, 905–908. (b) Lemmer, U.; Heun, S.; Mahrt, R. F.; Scherf, U.; Hopmeier, M.; Siegner, U.; Göbel, E. O.; Müllen, K.; Bässler, H. *Chem. Phys. Lett.* **1995**, *240*, 373–378.
- (23) (a) Gong, X.; Iyer, P. K.; Moses, D.; Bazan, G. C.; Heeger, A. J.; Xiao, S. S. *Adv. Funct. Mater.* **2003**, *13*, 325–330. (b) Sims, M.; Bradley, D. D. C.; Ariu, M.; Koeberg, M.; Asimakis, A.; Grell, M.; Lidzey, D. G. *Adv. Funct. Mater.* **2004**, *14*, 765–781.
- (24) (a) Becker, S.; Ego, C.; Grimsdale, A. C.; List, E. J. W.; Marsitzky, D.; Pogantsch, A.; Setayesh, S.; Leising, G.; Müllen, K. *Synth. Met.* **2001**, *125*, 73–80. (b) Xia, Z.; Heliotis, G.; Hou, Y.; Bradley, D. D. C. *Org. Electron.* **2003**, *4*, 165–177.
- (25) Ohshita, J.; Kunai, A. *Acta Polym.* **1998**, *49*, 379–403.
- (26) Chen, J.; Law, C. C. W.; Lam, J. W. Y.; Dong, Y.; Lo, S. M. F.; Williams, I. D.; Zhu, D.; Tang, B. Z. *Chem. Mater.* **2003**, *15*, 1535–1546.
- (27) Becker, B.; Corriu, R. J. P.; Henner, B. J. L.; Wojnowski, W.; Peters, K.; von Schnering, H. G. *J. Organomet. Chem.* **1986**, *312*, 305–311.
- (28) Chang, L. S.; Corey, J. Y. *Organometallics* **1989**, *8*, 1885–1893.
- (29) Matsumi, N.; Naka, K.; Chujo, Y. *J. Am. Chem. Soc.* **1998**, *120*, 5112–5113.

- (30) Lee, T.; Jung, I.; Song, K. H.; Baik, C.; Kim, S.; Kim, D.; Kang, S. O.; Ko, J. *Organometallics* **2004**, *23*, 4184–4191.
- (31) Rodríguez, J. G.; Tejedor, J. L.; La Parra, T.; Díaz, C. *Tetrahedron* **2006**, *62*, 3355–3361.
- (32) Dennis, W. H.; Rosenblatt, D. H.; Blucher, W. G.; Coon, C. L. *J. Chem. Eng. Data* **1975**, *20*, 202–203.

CHAPTER V

Selective Detection of Explosives Using a “Turn-on” Fluorescence Mechanism

5.1 ABSTRACT

Two methods for the selective detection of explosive particulates are described. In the first method, detection of common explosives including TNT, RDX, HMX, PETN, Tetryl, and TNG may be carried out using a three-step process combining “turn-off” and “turn-on” fluorimetric sensing. This process first detects nitroaromatic explosives by their quenching of green luminescence of polysilole-vinylenes ($\lambda_{\text{flu}} \approx 400 - 510 \text{ nm}$). The second step places down a thin film of 2,3-diaminonaphthalene (DAN) while “erasing” the polysilole-vinylene luminescence. The final step completes the reaction of the nitramines (e.g. RDX) and/or nitrate esters (e.g. PETN) with DAN resulting in the formation of a blue luminescent naphthotriazole complex ($\lambda_{\text{flu}} = 450 \text{ nm}$) providing a “turn-on” response for nitramine and nitrate ester based explosives. Detection limits as low as 0.6 ng cm^{-2} are observed.

The second method introduces simultaneous selective fluorimetric detection of explosives. Polymer **PSF1**, from a series of silafluorene-fluorene polymers introduced in Chapter 4, shows selective fluorescence “turn-on” sensing for nitrate ester based explosives, when irradiated with UV light, while remaining a highly sensitive fluorescence “turn-off” sensor for all three major classes of explosives. This unique simultaneous fluorescence response allows for both sensitive analysis of suspicious materials as well as determination of the explosive’s chemical class. In the presence of nitrate ester based explosives such as PETN or TNG, **PSF1** initially exhibits fluorescence quenching, but continued exposure to UV-light (302 nm),

promotes a photochemical reaction forming a luminescent green fluorenone copolymer. This is the first example of a single material acting as both a turn-off and turn-on selective fluorescent sensor for an explosive material. Solid-state detection of production line explosives demonstrates the applicability of these two methods to real world situations. These sensors offer sensitive and selective detection processes for a diverse group of the most common high explosives used in military and terrorist applications today.

5.2 INTRODUCTION

Explosives detection plays a key role in areas such as minefield remediation,¹ crime scene investigations,² and counter-terrorism applications such as personnel or baggage screening, facility protection and cargo screening.³ Techniques at the forefront of the detection industry include gas chromatography coupled with mass spectrometry,⁴ gas chromatography-electron capture detection,² surface-enhanced Raman spectroscopy,⁵ mass spectrometry,⁶ X-ray imaging, nuclear quadrupole resonance, thermal neutron analysis, and ion mobility spectrometry.⁷ These approaches use both bulk and trace detection methods to analyze suspect materials. Though these have been found to be effective for the applications mentioned above, they may prove inadequate in the area of counter-terrorism.

The recent rise in global terrorism has required that methods for explosives detection be sensitive and at the same time low cost. The most important requirements for successful sensors are early detection, elimination of false positives and efficient sampling methods for a variety of substrates. Conventional spectroscopic and imaging techniques, such as those mentioned above, are available in some airports and other high traffic areas. These large, stationary instruments perform bulk or vapor phase sampling in most cases. As described in a previous report,⁸ vapor sampling may be problematic due to the low volatility of most explosives at room temperature. Nitroaromatic explosives, such as TNT, have moderate vapor pressures (7×10^{-6} Torr at room temperature for TNT), but at low surface concentrations, the vapor concentration of TNT molecules is significantly

lower than its equilibrium vapor pressure.⁹ Explosives such as RDX and HMX have substantially lower vapor pressures (5×10^{-9} and 8×10^{-11} Torr, respectively) than TNT, which makes vapor detection of these compounds challenging.¹⁰

An alternative method is to sample solid particulates that remain after the handling of explosive materials. It is known that widespread contamination results from the manufacturing and handling of explosives, and that trace contamination remains present and detectable, even after extensive cleaning of the contaminated areas.¹¹ The advantage of solid-state detection is the ability to analyze samples even if concentration levels are too low to produce noticeable vapor concentrations. Sampling solid particulates directly rather than vapor may pave the way for low cost, portable devices with low detection limits for rapid on-site evaluation of suspicious materials.

Two low cost, portable technologies currently exist in the field of explosives detection. They are colorimetric detection (e.g. ExPray from Plexus Scientific) and fluorimetric detection (e.g. Fido from Nomadics, Inc.). Fluorescence detection methods have been widely regarded as the more sensitive approach;^{12,13} however, they typically require a liquid or vapor sampling matrix. It has been previously demonstrated that trace explosives detection by solid-state fluorescence quenching provides sensing with low detection limits.⁸ However, this “turn-off” method, which relies on the electron-accepting ability of the explosive analytes, has historically been limited to the more easily oxidized nitroaromatic explosives. In contrast, “turn-on” methods may be preferred because they eliminate the need for background

Table 5-1. A list of some common explosive mixtures and their components.

Mixture	Explosive components
Composition A	RDX, plasticizer
Composition B	RDX, TNT, wax
H-6	RDX, TNT, aluminum, wax
Pentolites	PETN, TNT
Picratol	Picric Acid, TNT
PTX-1	RDX, Tetryl, TNT
PTX-2	RDX, PETN, TNT
Tetrytols	Tetryl, TNT
Torpex	RDX, TNT, aluminum
C-2	RDX, TNT, DNT, NC, MNT
C-3	RDX, TNT, DNT, Tetryl, NC
C-4	RDX, Fuel Oil
DBX	TNT, RDX, AN, aluminum
HTA-3	HMX, TNT, aluminum
Dynamite 3	TNG, NC, SN
Semtex-H	PETN, RDX, plasticizer
Red Diamond	TNG, EGDN, SN, AN, Chalk

fluorescence that may lead to false positives and may improve signal-to-noise in detection. In an engineered system, sensor sensitivity may be optimized because it is possible to amplify single photons against a dark background. In fact, “turn-on” fluorescent immunoassays are frequently used in enzyme detection systems to eliminate background fluorescence that may decrease sensitivity and produce false positives.¹⁴ They may also be more sensitive, and have the potential to be applied to a wider variety of explosive classes.

Nitramine and nitrate ester based compounds make up a large portion of explosive formulations, such as Composition C-4 and Semtex-H (Table 5-1).¹⁵⁻¹⁷ These compounds, which include cyclotrimethylenetrinitramine (RDX), pentaerythritol tetranitrate (PETN), cyclotetramethylene-tetranitramine (HMX), 2,4,6-trinitrophenyl-N-methylnitramine (Tetryl) and trinitroglycerin (TNG), can be used pure or as mixtures. Many improvised explosive devices (IEDs) used by terrorists include such explosive materials.^{10,17} In fact, 42 kilograms of RDX was recovered in multiple sting operations in India in July 2006.¹⁸ These explosives are found in military munitions, which are the primary type used in IEDs in the Iraq terrorist conflict. Nitramine based explosives (e.g. RDX, HMX, Tetryl) are of particular concern because they require almost no confinement,¹⁹ can be mixed and molded without loss of reactivity,²⁰ have high energy yield per unit weight,^{21,22} and are readily available.²³ Nitrate ester based explosives (e.g. PETN, TNG) vary in their properties depending on their chemical structure. A high detonation velocity is one common feature, making them attractive materials to terrorists.¹⁷

Colorimetric explosives detection techniques, such as ExPray, have proven effective in detecting nitramine- and nitrate ester-based explosives and have the ability to distinguish them from nitroaromatics. ExPray induces the chemical release of nitrite from the explosives upon exposure to a basic matrix followed by a reaction of nitrite with a colorimetric reagent in an acidic medium. Detection of nitramine and nitrate esters based on the detection of nitrite gives the sensor its chemical specificity.

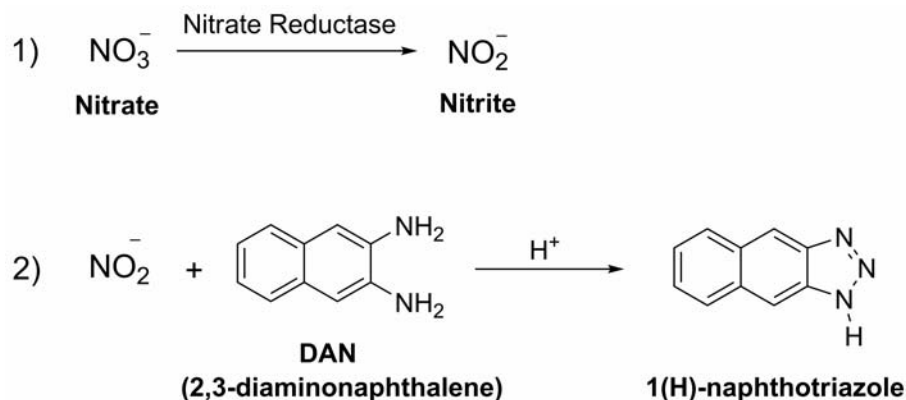


Figure 5-1. Pathway for fluorimetric detection of nitrate and nitrite in biological systems using 2,3-diaminonaphthalene (DAN).

There are biological assays which are also specific for nitrite sensing. These assays are performed to detect nitrate, but do so by reducing the nitrate to nitrite, and further reacting the nitrite with 2,3-diaminonaphthalene (DAN) in an acidic environment to form the fluorescent 1(H)-naphthotriazole (Figure 5-1).²⁴⁻²⁶ These assays are most commonly performed in solution. Detection is observed by monitoring a shift in the fluorescence spectra from $\lambda_{\text{em}} = 375 \text{ nm}$ (DAN) to $\lambda_{\text{em}} = 450 \text{ nm}$ (triazole).

This chapter reports the application of two new fluorimetric sensing methods for the selective detection of explosive particulates. The first method targets the unique nitro functionalities of nitramine and nitrate ester based explosives. A two-step fluorimetric detection process can be carried out using DAN. Detection limits as low as 0.6 ng cm^{-2} are observed for this turn-on luminescent sensor. This process may also be combined with fluorescence quenching technology^{8,27} to establish a three-step fluorimetric sensing system to include the detection of nitroaromatic based explosives. The second method builds upon the concept of a tandem fluorescence

“turn-off” and “turn-on” mechanism. This method uses a silafluorene-fluorene based polymer, introduced in Chapter 4 as **PSF1**, to provide a single-step tandem sensor for the initial detection of a large range of explosives particulates by a fluorescence quenching mechanism, followed by the selective detection of nitrate ester based explosives by an oxidative fluorescence “turn-on” mechanism. This sensor is the first example of simultaneous detection methods for sensor selectivity incorporated into a single polymeric material. Sequential determination of the explosive’s class may be a beneficial feature in rapid on-site detection, as it may allow the analyst to quickly evaluate the threat or choose an appropriate disposal procedure.²⁸ The approaches described herein provide low-cost, selective fluorescence sensing methods for a diverse group of the most common explosives used in military and terrorist applications today.

5.3 RESULTS AND DISCUSSION

5.3.1 Detection of Nitramine and Nitrate Esters

5.3.1.1 Two-step Detection System

The five explosives studied included RDX, HMX, Tetryl, PETN, and TNG. The structures of these explosives are shown in Figure 5-2. The common feature seen in these explosives, and in many other highly energetic materials, is an N-NO₂ (for nitramines) or O-NO₂ (for nitrate esters) functionality. These energetic bonds are also the target site for the detection of these classes of explosives. Detection relies on the detection of nitrite (NO₂⁻) and is achieved through the successive application of two

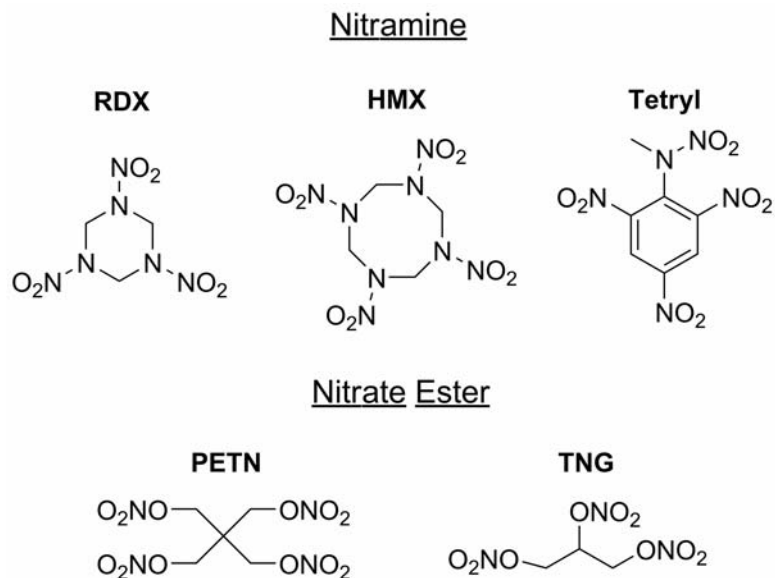


Figure 5-2. Chemical structures of the targeted explosives.

reagents (Reagents B and C). Reagent B, which is applied in the first step in this “two-step” detection process, consists of sodium hydroxide dissolved in organic and protic solvents (see Experimental). The reagent causes the release of nitrite from the explosive through a reaction with base (Figure 5-3). The hydroxide base deprotonates the explosive at a position alpha to the N or O in the nitramine or nitrate ester, respectively. Nitrite is subsequently released as a double bond forms between the carbon and N or O. This reaction is specific for nitramine and nitrate ester based explosives. Reagent B also includes DAN and several organic solvents, which aid in the solvation of both the explosive and DAN to allow for necessary mixing. Heat is applied to provide the energy necessary to promote the reaction, as well as to aid in solvent evaporation. Immediately following the heating process, Reagent C is applied. Reagent C consists of phosphoric acid diluted in a protic organic solvent (see

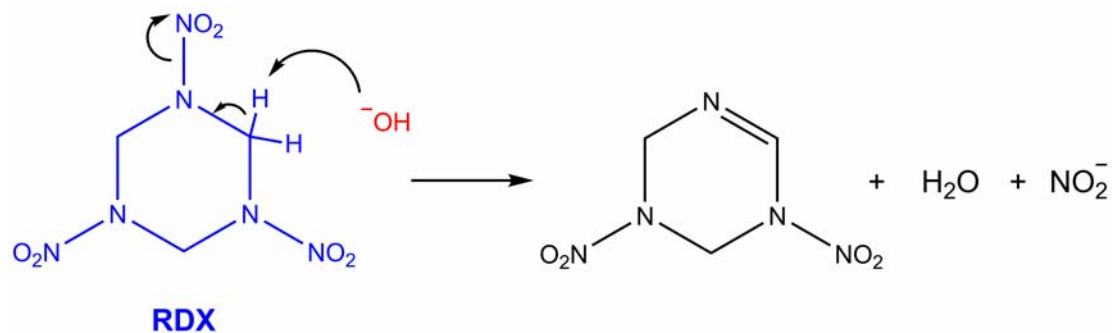


Figure 5-3. Release of nitrite from RDX upon α -hydride extraction by a hydroxide base.

Experimental). The acid in Reagent C reacts with nitrite to form nitrous acid, which then reacts with the DAN applied in Reagent B to form the luminescent 1-[H]-naphthotriazole (Figure 5-2). The luminescent material is visualized by exciting the molecule with an inexpensive blacklight ($\lambda \sim 360$ nm). Slightly better resolution is achieved using a UV-B lamp ($\lambda \sim 302$ nm) coupled with a UV-transmitting filter (HOYA Optics U-340). Detection limits as low as 0.6 ng cm^{-2} are observed with this method. A summary of the detection limits is seen in Table 5-2.

To demonstrate the selectivity of the two-step process for nitramine and nitrate ester based explosives, filter paper samples were prepared with both TNT (nitroaromatic) and RDX spots. Only reagents B and C were applied as described above. While RDX shows “turn-on” fluorescence detection as low as 3 ng cm^{-2} , TNT does not show any “turn-on” fluorescence even for spot loadings as high as 64 ng cm^{-2} (Figure 5-4). The slight darkening at 64 ng cm^{-2} for TNT is actually a red spot from the Meisenheimer complex, which results from the reaction of TNT with the base applied in Reagent B.^{29,30} Detection limits are based primarily on the susceptibility of

Table 5-2. Vapor pressure and detection limits of the different classes of explosives studied with the three-step fluorimetric sensing process.

Explosive	Class	Vapor Pressure (Torr) ^a	Detection Limit (ng cm ⁻²)
RDX	Nitramine	5×10^{-9}	0.6
HMX	Nitramine	8×10^{-11}	3
Tetryl	Nitramine	6×10^{-6}	3
TNG	Nitrate Ester	4×10^{-4}	3
PETN	Nitrate Ester	1×10^{-8}	8

^a Measured at room temperature.¹⁰

each explosive to undergo nucleophilic attack from the strong base and to release nitrite. The low detection limits seen in this study can also be attributed to the resulting “turn-on” fluorescence indicator. Reduction in background noise greatly increases the ability to observe a positive result and provides a reduction in false positives.

This process was also carried out on fingerprints placed on filter paper after contact with production line explosives. Detection of production line explosives in real world applications presents challenges not present in controlled laboratory spot tests. Contaminants in both pre- and post-blast residues mimic what one would find in the field. These may include various plasticizers, by-products of low quality synthetic procedures and common natural residues such as oils and dust. This current detection method can readily visualize the first five successive fingerprints made after direct contact with commercial RDX (Figure 5-5). Fingerprints of the explosives PETN, C-4, and PE-4 are also detected. Contact with the explosives was limited to one touch of the finger or thumb with the material. An example of the detection of PE-4 is seen in

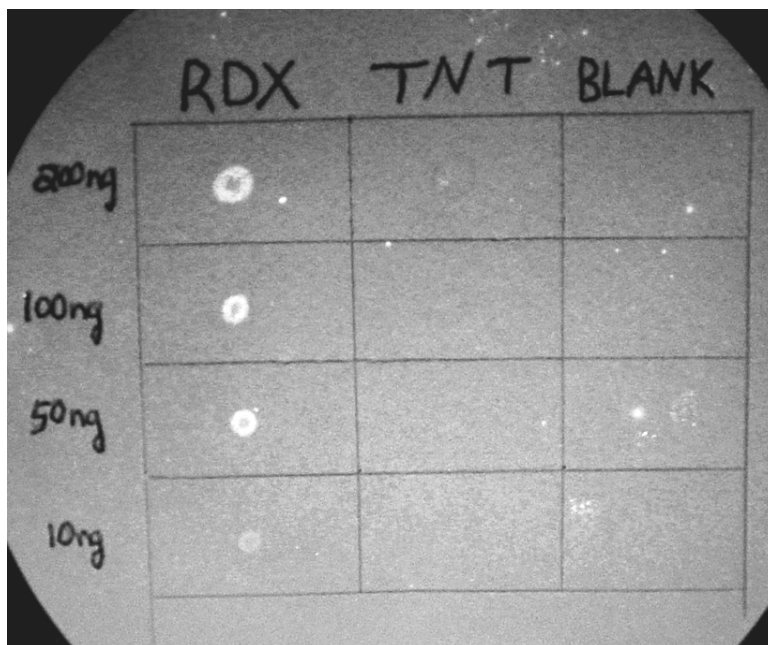


Figure 5-4. Turn-on fluorescence detection of RDX using the two-step process. TNT is detected by colorimetric analysis at a limit of 64 ng cm^{-2} . Blank spots of toluene show no detection.

Figure 5-6. It is important to note that the concentration of explosive materials deposited in these studies remains well above the detection limits determined by the spot tests. These tests indicate that detection of the explosive materials is possible even in the presence of plasticizers and impurities found in the C-4 and PE-4 explosives and with limited handling of the material.

5.3.1.2 Three-step Tandem Sensor

The process of detecting nitramine and nitrate ester based explosives was combined with polysilole-vinylene (Chapter 2) to create a tandem fluorescence sensor that also detects nitroaromatic explosives. Reagent A, consisting of the luminescent polysiloles-vinylene in toluene:acetone, may be airbrushed onto a substrate and the

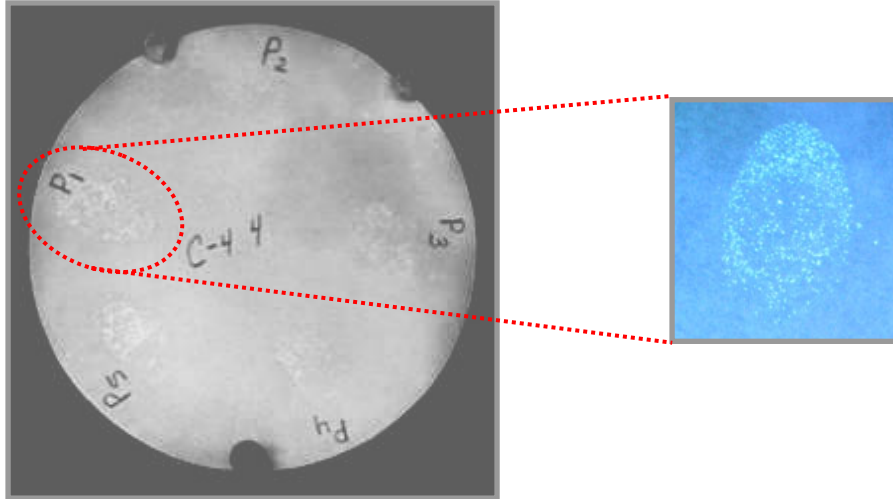


Figure 5-5. Turn-on fluorescence detection of five successive fingerprints of C-4 starting with print 1 (P_1). The color image shows the blue luminescence of triazole complex.

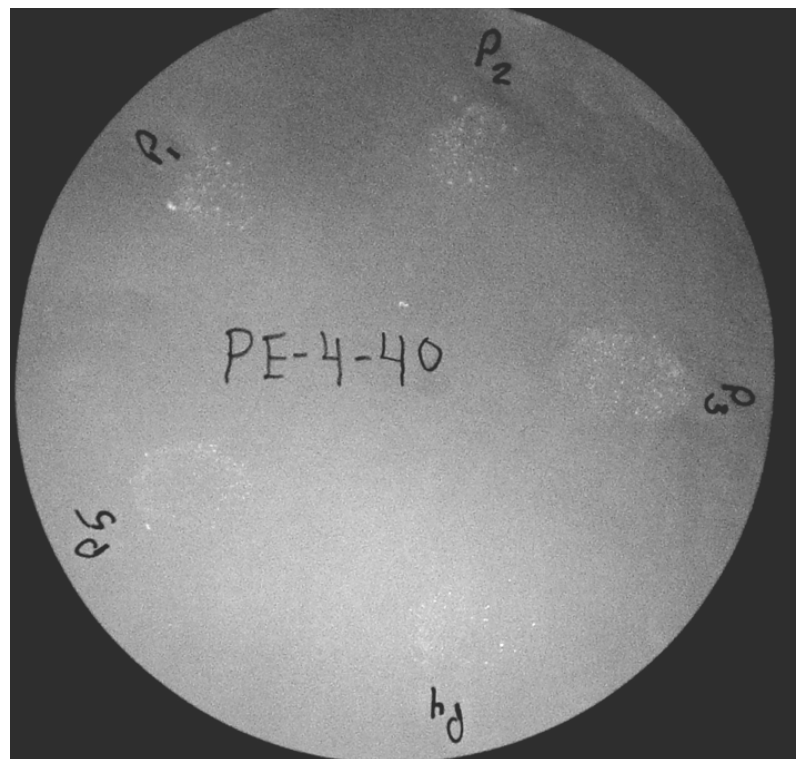


Figure 5-6. Turn-on fluorescence detection of five successive fingerprints of PE-4 starting with print 1 (P_1).

presence of nitroaromatic-based explosives is confirmed under UV light (see Experimental). For selectivity purposes, it is noted that Tetryl (Figure 5-2) is both a nitroaromatic and nitramine explosive and therefore is detected by both the polysiloles-vinylene and the “turn-on” system using DAN. An example of the two technologies side-by-side is seen in Figure 5-7. A handprint of trace particles of tetrabutylammonium nitrite (left) was laid down next to a handprint of trace particles of TNT (right) using nitrile laboratory gloves. RDX was not used directly due to purchasing restrictions. The left portion of the filter paper was exposed to Reagents B and C. The right portion was exposed to Reagent A. This demonstrates how these different detection methods detect the presence of explosive materials.

To demonstrate the effectiveness of the two technologies used in tandem, filter paper samples were prepared onto which TNT and RDX were co-spotted. After application of Reagent A and analysis under UV light, Reagent B is airbrushed onto the substrate. The luminescent polymer in Reagent A is destroyed through degradation of the silicon backbone under basic conditions via a S_n2 ring opening reaction, eliminating its fluorescing properties. This eradicates the background fluorescence that could create interference in the subsequent turn-on detection process. Basic conditions of Reagent B may also cause the appearance of a red spot resulting from the formation of the Meisenheimer complex when nitroaromatics such as TNT are present, which can be viewed in both ambient and UV light (Figure 5-8). This is similar to colorimetric testing of these explosives and will work to confirm the presence of nitroaromatic explosives if there is a sufficient quantity present. It is



Figure 5-7. Side-by-side comparison of two-step turn-on sensor (left) with fluorescence quenching sensor (right). Tetrabutylammonium nitrite was used as the analyte for the turn-on sensor and TNT was used for the fluorescence quenching sensor.

noted that this red spot does not appear at low concentrations (less than 16 ng cm^{-2}) of explosives even when a positive nitroaromatic test result is obtained by the polysilole-vinylene. After the application of Reagent B and subsequent heating, Reagent C, is applied to increase the acidity and cause the formation of the luminescent triazole. The detection limits for the nitramine and nitrate ester explosives are not compromised by the initial use of Reagent A, because polysilole luminescence is completely removed at this point. An example of this fluorescent “on/off” detection series is seen in Figure 5-9.

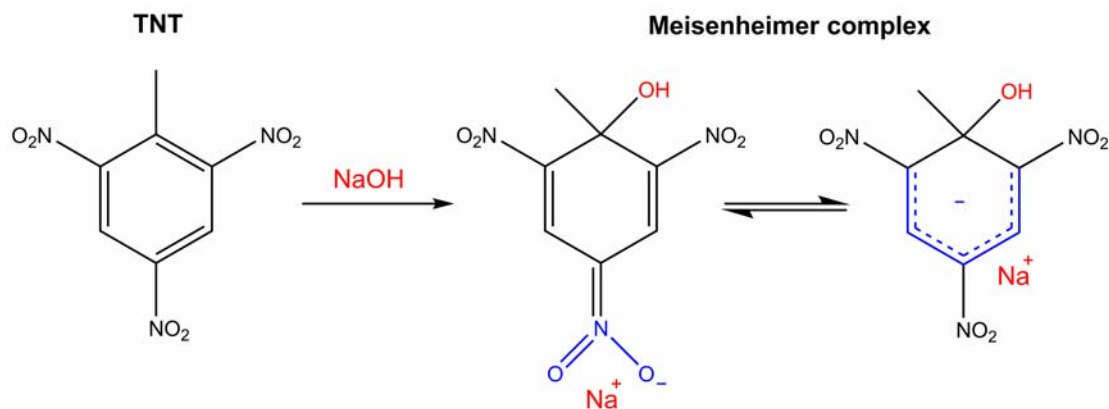


Figure 5-8. Formation of Meisenheimer complex on hydroxide nucleophilic attack of nitroaromatic compounds.

This three-step explosives detection process is effective on production line explosives as well. The first five fingerprints produced after contact with TNT, RDX, PETN, C-4, and PE-4 were all detected in the three-step process with high signal-to-noise, indicating that contaminants, impurities, and plasticizers do not interfere with detection. Possible interferents in the detection of nitroaromatics by polysilole, such as common organic solvents were found to be minimal, while the low abundance of naturally occurring solid-state oxidizers should reduce false-positive results in field tests.⁸ Since the turn-on sensor is based on the specific chemistry of nitramine and nitrate ester based explosives, very few interferents, other than nitrite salts found in some fertilizer products, are known. Even highly oxidizing materials such as benzophenone, TNT, DNT, and picric acid will not quench the luminescence of the triazole complex. Detection of other nitramine (e.g. CL-20) and nitrate ester (e.g. nitrocellulose) based explosives is expected to be achieved using this system.

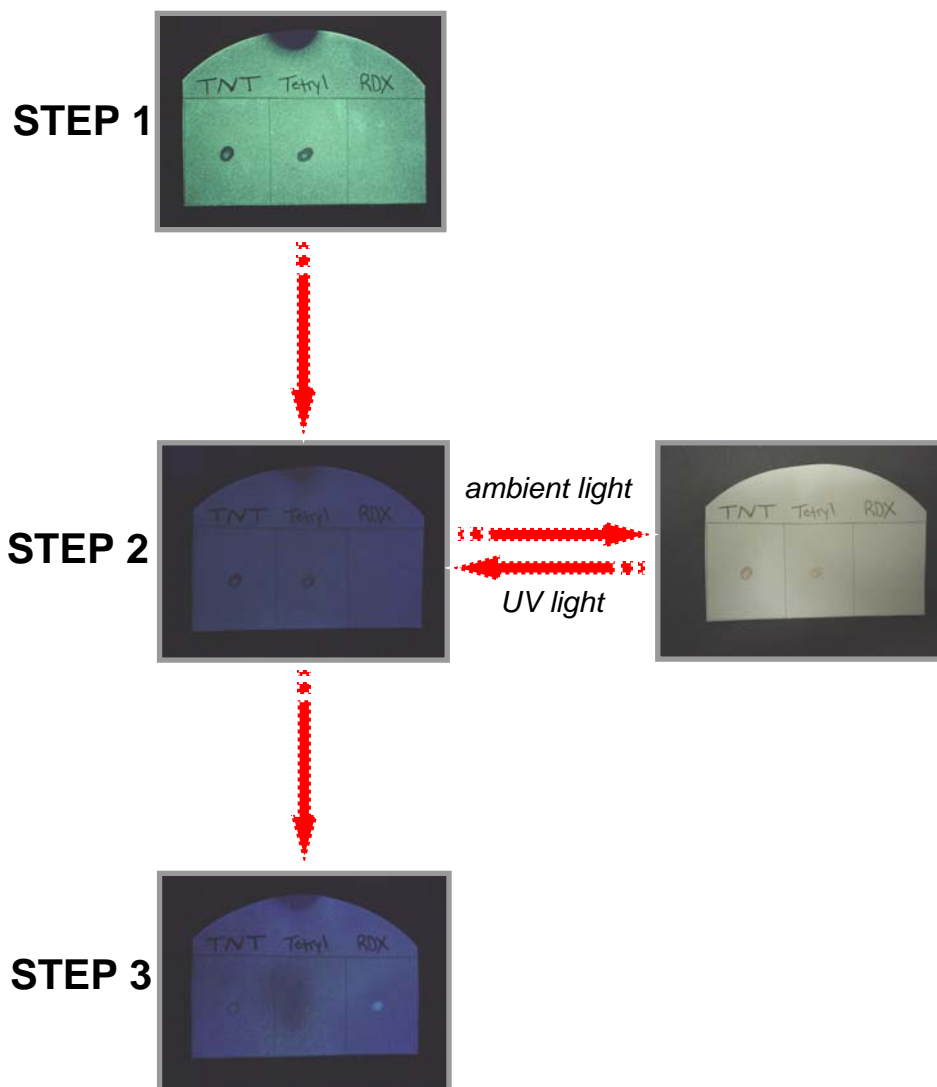


Figure 5-9. Example of three-step sensor for selective explosives detection. The three explosives analyzed were TNT (nitroaromatic), Tetryl (nitroaromatic and nitramine), and RDX (nitramine). Step 1: Detection of nitroaromatic explosives by fluorescence quenching of polysilole-vinylene. Step 2: Polymer degradation and release of nitrite from nitramine and nitrate ester based explosives using Reagent B. Under ambient light, Meisenheimer complex formed with the nitroaromatic explosives confirms their detection at a limit of 16 ng cm^{-2} . Step 3: Formation of the 1(H)-naphthotriazole complex with DAN and nitrite for nitramine and nitrate ester based explosives. Remaining Meisenheimer complex of TNT and Tetryl lowers the detection limit of Tetryl in this step.

5.3.2 Single Step Selective Detection of Nitrate Esters

The highly sensitive, blue-emitting polymer sensors **PSF1-3** from Chapter 4 show promise as the next generation of luminescent polymer sensors. They achieved high sensitivity for a wide range of explosive materials while reducing the amount of polymer needed during the detection process. During those studies, it was observed that polymers **PSF2-3** showed high thin-film stability in both ambient and UV light environments. However, it was noticed that **PSF1** rapidly formed a dull green film when exposed to UV light for more than 30 s. It was also observed that in the presence of nitrate ester based explosives, such as PETN and TNG, **PSF1** showed both a quenching detection mechanism and a turn-on fluorescence detection mechanism. The turn-on mechanism only occurred after prolonged exposure to UV light and was highly selective for nitrate ester based materials. From these observations, further investigation into the validity and application of the simultaneous selective detection of this single polymer sensor was carried out.

5.3.2.1 Model Compound

To assist in the characterization of the turn-on fluorescence sensor observed for **PSF1**, a model dimer (**4**) was synthesized to model the fully oxidized fluorene unit of dimer **1** and subsequently **PSF1** (Figure 5-10). To maintain consistency, the new fluorenone dimer is labeled as dimer **4** to prevent confusion when referring back to Chapter 4 for comparison. Dimer **4** was synthesized at room temperature to insure full dissolution of the starting material.

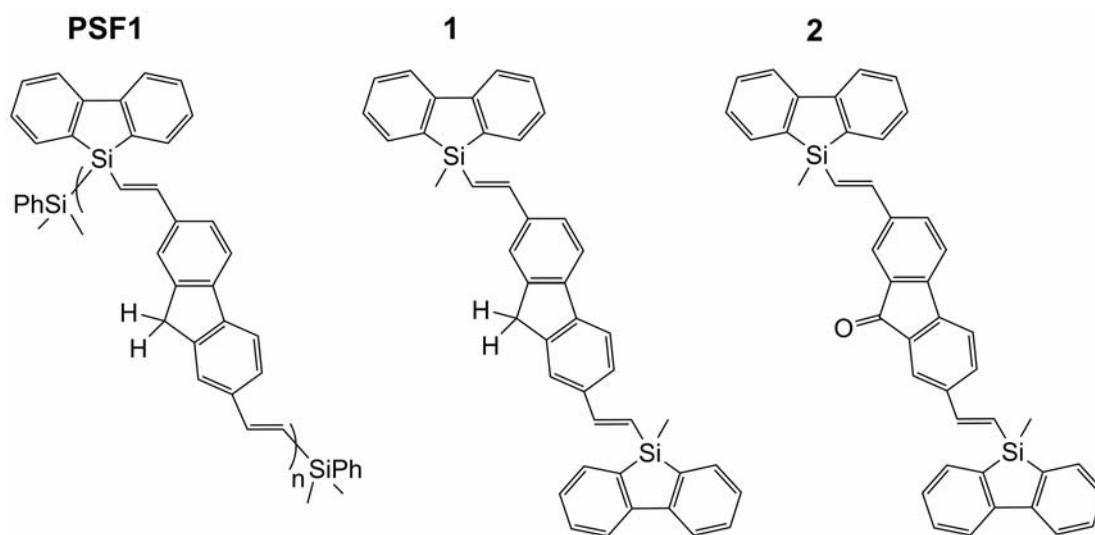


Figure 5-10. Chemical structures of **PSF1** and model dimers **1** and **4**.

The PL properties of a fluorenone model dimer (**4**) were characterized (Figure 5-11) to assist in the determination of oxidized fluorene byproducts during the explosives detection studies. The band-width of the absorption spectrum is narrow compared to dimers **1–3** and is centered at 290 nm. This indicates that the majority of the absorption is taking place on the silafluorene moieties of the polymer. However, the emission band is broad and centered around 520 nm with no observed emission at short wavelengths. The lack of observed emission from the highly emissive silafluorene moiety in **4** implies that efficient energy transfer occurs between the silafluorene and fluorenone chromophores. In addition, the 40 nm (1590 cm^{-1}) bathochromic shift in emission from the fluorenone monomer to **4** shows that there is significant conjugation between the fluorenone and silafluorene moieties through the vinylene subunits.

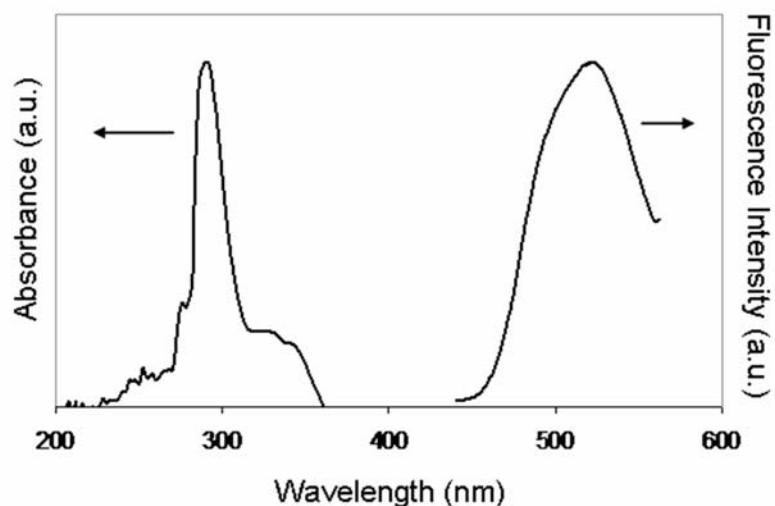


Figure 5-11. Absorption and photoemission spectra of **4**.

5.3.2.2 Explosives Detection

Polymer **PSF1** shows an unusual combination of both fluorescence quenching detection and a photochemically promoted turn-on fluorescence mechanism specific for nitrate ester based explosives, such as PETN. Turn-on fluorescence sensors are attractive, because they provide a detection signal against a dark background. There are only two examples in the literature where turn-on sensors are used for the selective detection of explosives, and none that incorporate a dual quenching-turn on mechanism.³¹ Figure 5-12, for the fluorescence detection of PETN by **PSF1**, illustrates how **PSF1** initially shows fluorescence quenching of the blue emission at amounts as low as 300 pg cm^{-2} when exposed to explosives with nitrate ester functionalities (O-NO_2). Further exposure to UV light causes fading of the all the polymer luminescence, eliminating the dark, quenched spot. This is a result of photooxidation of the silicon-carbon framework in the presence of oxygen,

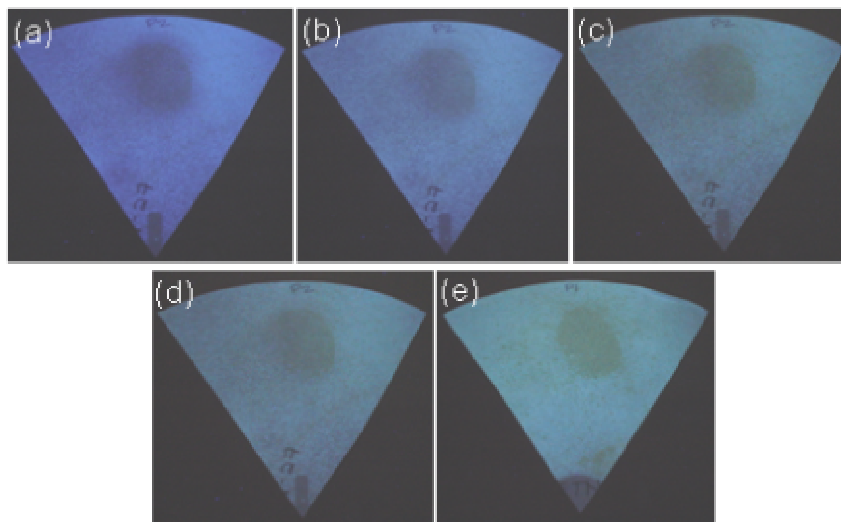


Figure 5-12. Example of the time-dependent turn-off/turn-on selective detection of production line PETN by **PSF1**. (a) Initial detection of PETN by fluorescence quenching at 1 s UV light (302 nm) exposure. (b) Fading of the polymer photoluminescence at 10 s UV light exposure. (c) Onset of the green-yellow turn-on luminescence of the thumbprint at 20 s UV light. (d) Further confirmation of turn-on emission at 30 s UV light. (e) Final stage of luminescence before the onset of photo-degradation at 1 min UV light.

atmospheric water, and UV light. After 20 s of UV light exposure, the previously quenched spot begins to fluoresce in the green-yellow region of the spectrum against the faded background. This luminescence remains for ~30 s and eventually photooxidizes to a dull green color on continued irradiation. This turn-off/turn-on sensing response, due to a specific photochemical process with nitrate ester based explosives, works with production line explosives as shown by the comparison between thumbprints with production line PETN and of TNT (Figure 5-13). Initial detection shows fluorescence quenching by both explosives. On further exposure to UV light, the PETN prints begin to fluoresce green-yellow while the TNT prints remain dark. This unique response is the first example, to our knowledge, of a

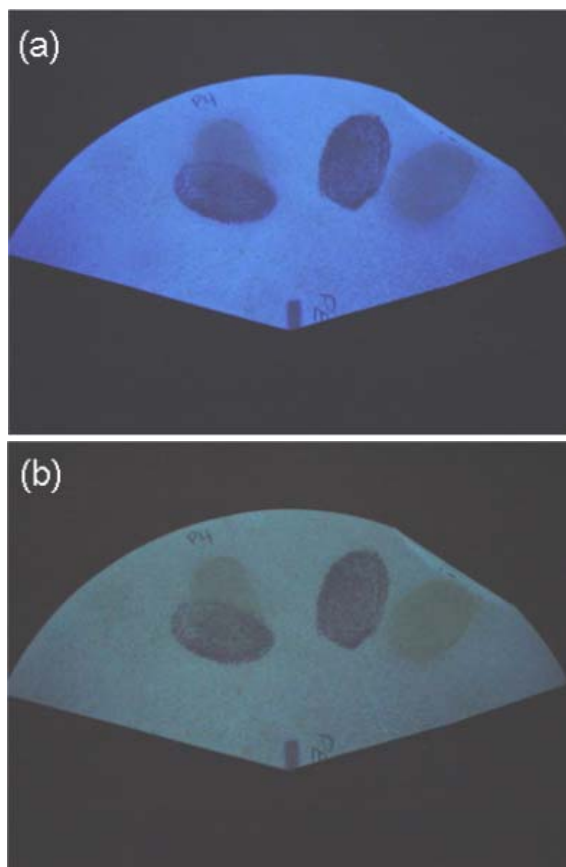


Figure 5-13. Example of detection selectivity for TNT and PETN by **PSF1**. Thumbprints of each explosive were laid down side-by-side and overlapping to emphasize the selective detection process. (a) Initial fluorescence quenching detection of thumbprints of both TNT (dark prints) and PETN (lighter prints). (b) Same thumbprints after exposure to 1 min of UV light (302 nm). The background luminescence has faded to a dull green color. The TNT thumbprints remain dark, quenched spots. The PETN thumbprints now show a green-yellow luminescence providing selectivity for the presence of a nitrate ester explosive.

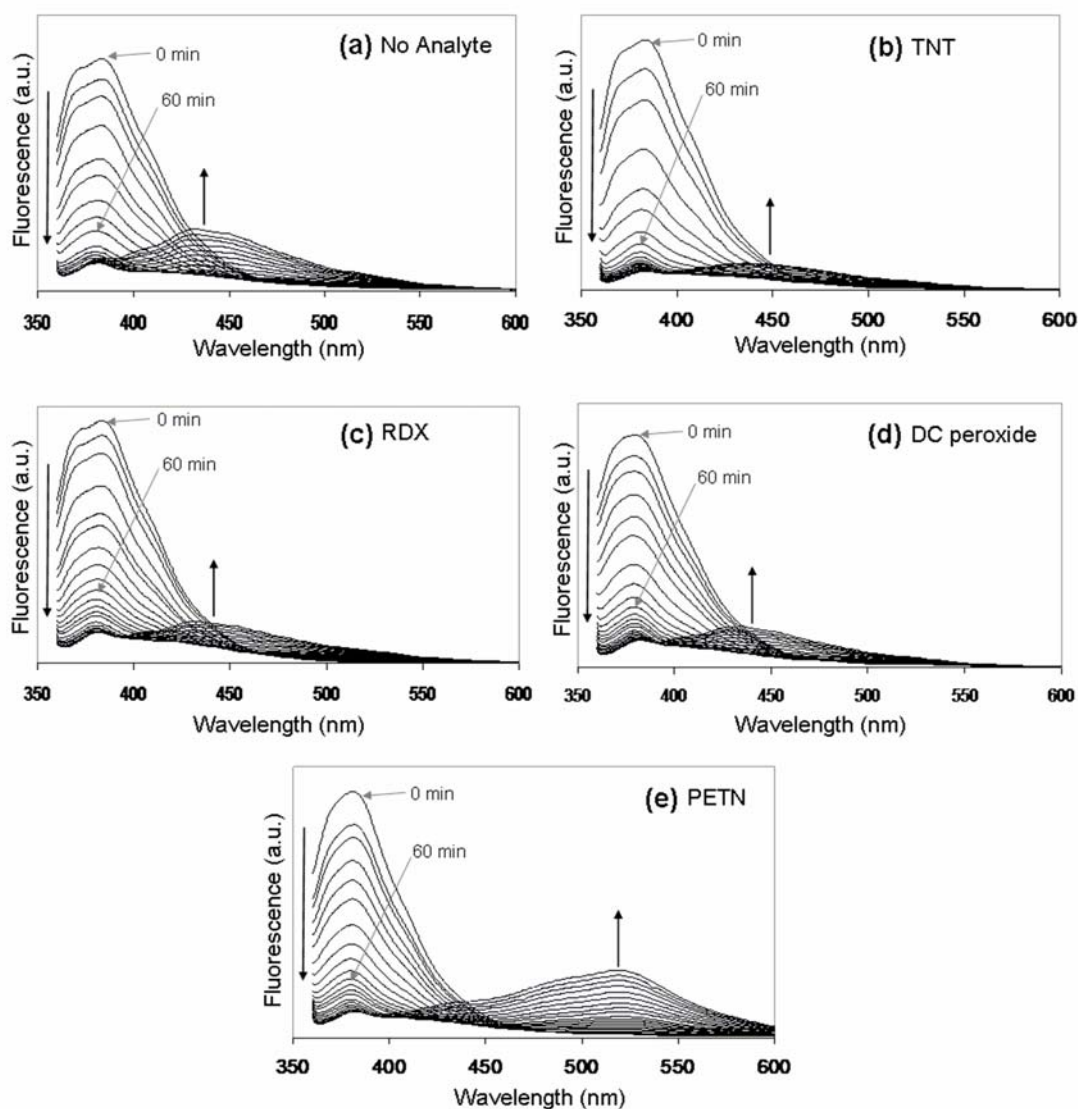


Figure 5-14. Time-dependent solution phase fluorescence quenching behavior of **1** (10 ppb in toluene) upon exposure to UV light in the presence of (a) no analyte, (b) TNT (50 ppm), (c) RDX (50 ppm), (d) dicumyl peroxide (DC peroxide) (50 ppm), and (e) PETN (50 ppm). Spectra taken every 10 min during UV light exposure over 280 min.

simultaneous turn-off/turn-on selective detection of explosives from a single material.

It illustrates how photochemistry can be employed for improved selectivity in the detection of explosive particles. The detection limits reported for PETN and TNG in

Chapter 4 (Table 4) using **PSF1** correspond to the observed quenching and subsequent green-yellow luminescence. These results were repeated several times to ensure their accuracy.

5.3.2.3 Mechanism of Turn-on Fluorescence Response

The hypothesis for the mechanism of detection is that the new green-yellow emission is due to photooxidation of the unprotected fluorenyl units of **PSF1** assisted by the oxygen-rich nitrate ester based explosives. Solution-phase fluorescence spectroscopy experiments support this hypothesis. Model dimer complex **1** was used to provide a well characterized molecular model for the polymer materials. Time-dependent fluorescence spectra of **1** were taken in toluene to observe the spectral effects of different explosive analytes when exposed to UV light. The solutions were not degassed to provide an aerobic environment similar to the one found in the atmospheric thin-film study. Figure 5-14 shows the fluorescence spectra of **1** when exposed to several explosive analytes including TNT (nitroaromatic), RDX (nitramine) and PETN (nitrate ester). A control in the absence of analyte was measured for comparison. Dicumyl peroxide (DC peroxide) was used as an alternative reactive oxygen species (ROS) to determine the selectivity of oxidation towards nitrate ester based explosives. Spectra were taken over the course of 280 min in toluene at concentrations of 10 ppb for **1**. Analytes were added at 50 ppm concentration levels to provide significant spectral changes within the time-frame.

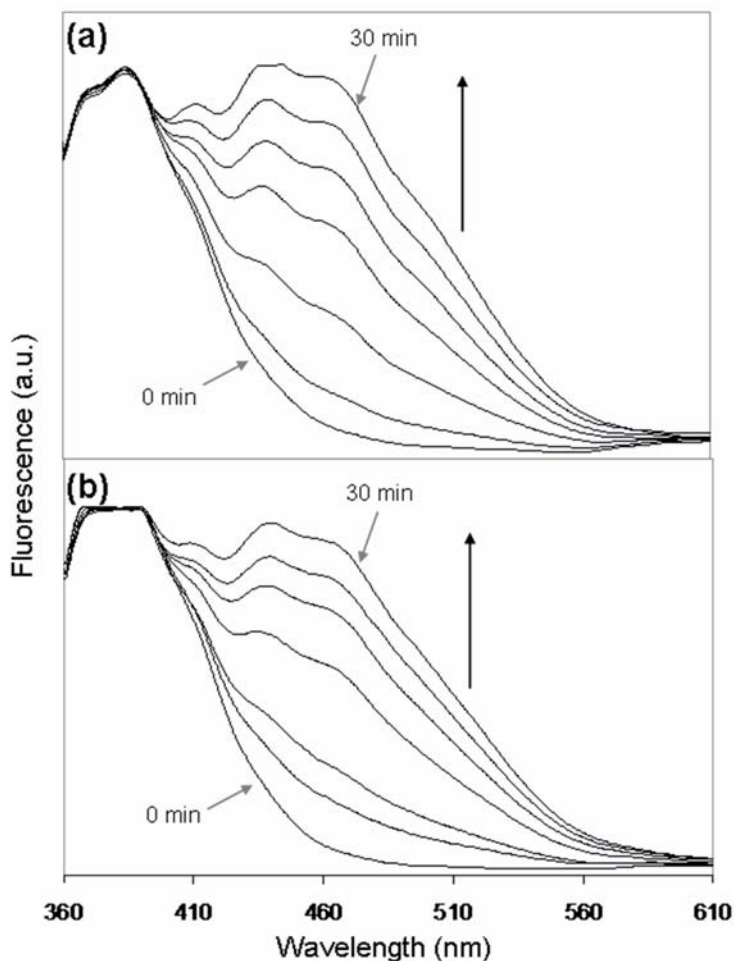


Figure 5-15. Time-dependent solution phase fluorescence quenching behavior of **1** (10 ppb in degassed, anhydrous toluene) on continuous exposure to UV light in the presence of (a) no analyte and (b) PETN (50 ppm). Spectra were taken every 10 min of UV light exposure for 280 min. The oxygen-free environment prevents gross photooxidation of the polymer as indicated by the intact 370 nm emission characteristic of the silafluorene moiety, and photodimerization of the fluorene units is indicated by appearance of the 432 nm feature.

The spectra of **1**, when exposed to UV light with no analyte present, reveals a decrease in fluorescence intensity at 370 nm over the course of 1 h. This decrease in fluorescence intensity is due to the photooxidation of the silafluorene moiety, which can be prevented by using thoroughly dried and degassed solvents (Figure 5-15). At

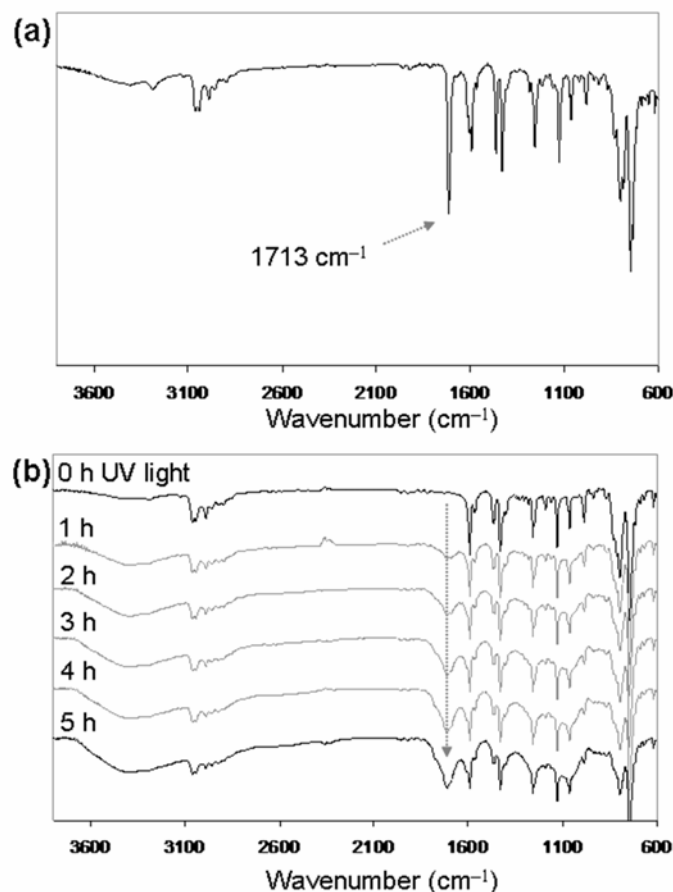


Figure 5-16. IR data showing the thin-film photooxidation of **1** under UV light in the presence of oxygen. (a) IR of authentic silafluorene-fluorenone dimer **4**. (b) Time dependent IR spectra of a thin-film of silafluorene-fluorene dimer **1** on a NaCl plate. Red arrows show the appearance of the ketone stretching frequency characteristic of fluorene to fluorenone conversion as **4** forms.

approximately 2 h, a small emission peak centered at 432 nm begins to appear. This peak further increases in intensity over the course of the experiment. The appearance of the dull green emission was hypothesized to be a result of radical dimerization between the fluorene units. This conclusion was supported by molecular weight analysis (GPC) of **PSF1** after exposure of a thin-film to UV light (302 nm). After 1 h, the polymer's molecular weight increased from 16 000 to 21 100. A control film spin-

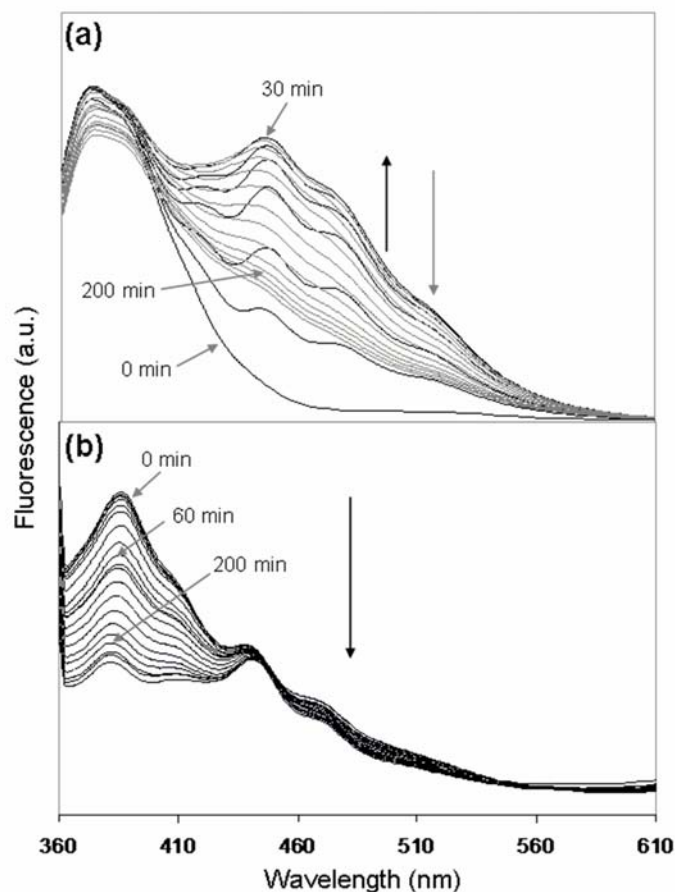


Figure 5-17. Time-dependent solution phase fluorescence quenching plots of (a) **1** and (b) **2** (10 ppb in degassed, anhydrous benzene) upon exposure to UV light (302 nm). Spectra taken every 10 min of UV light exposure over 280 min time frame. Benzene solutions behave similar to toluene, suggesting that the solvent is not responsible for the appearance of the peak at 432 nm. The peak at 432 nm is not observed for dimer **2**, giving further evidence for the dimerization of the fluorene unit for dimer **1**.

cast onto quartz that was not exposed to UV light did not show any such increase. The increase in molecular weight suggests that intermolecular photo-crosslinking of the polymer chains. Since the molecular weight did not increase dramatically, it is likely that radical crosslinking event competes with photooxidation of the fluorene unit. This was confirmed using a solid-state IR analysis of a thin-film of **1** on a NaCl

plate compared with **4** also confirmed (Figure 5-16). A peak centered at 1713 cm^{-1} , corresponding to the carbonyl stretching frequency of **4**, begins to grow in for **1** after 1 h of UV light exposure. This peak continues to increase over the course of 5 h and never completely sharpens as observed in the IR spectrum of **4**. This clearly shows the oxidation of the fluorene unit to fluorenone upon exposure to UV light. It also demonstrates that the UV light and air will not fully oxidize all of **1** into **4**.

Similar GPC experiments performed under an inert atmosphere show a dramatic increase in molecular weight from 16 000 to 69 000 under UV irradiation. The photo-initiated radical dimerization is much more efficient in an aerobic environment. As expected, control experiments using the methyl substituted fluorene dimer **2** (Chapter 4) show no evidence for dimerization in the fluorescence studies (Figure 5-17). Radical dimerization of unsubstituted fluorenes has been observed in previous reports.³² When left under ambient conditions for a few weeks, the emission of **PSF1** completely fades as the silacycle ring becomes photooxidized. This minor product corresponds to the dull green luminescence from the fluorene dimer product observed in the thin-film detection studies after prolonged exposure to UV light. The dimerization is inhibited by the presence of atmospheric oxygen and water (Figure 5-15) and, to a lesser extent, by the explosive analytes. In the absence of oxygen and water, photodecomposition of the silafluorene units does not occur, resulting in the stabilization of the emission at 370 nm when **1** is exposed to UV light. The concomitant rapid appearance of the emission peak at 432 nm supports the fact that oxygen and moisture can inhibit the dimerization of the fluorene units. Nonetheless,

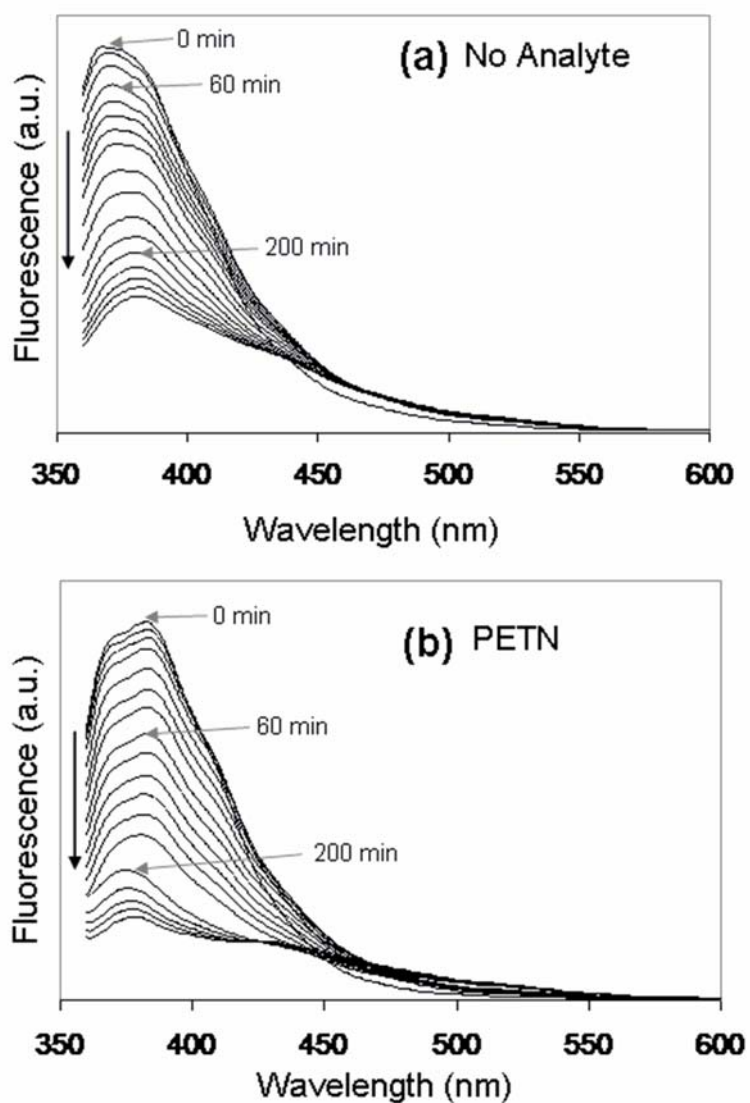


Figure 5-18. Time-dependent solution phase fluorescence quenching plots of **1** (10 ppb in degassed toluene) upon exposure to UV light in the presence of (a) no analyte and (b) PETN. Analytes added at a concentration of 50 ppm. Spectra were taken every 10 min of UV light exposure over 280 min time frame. The oxygen-free environment prevents the onset of oxidation to the polymer (370 nm) and prevents oxidation of the fluorene unit to fluorenone in the presence of PETN (523 nm). The presence of trace quantities of water prevents the onset of dimerization between fluorene units (appearance of the 432 nm).

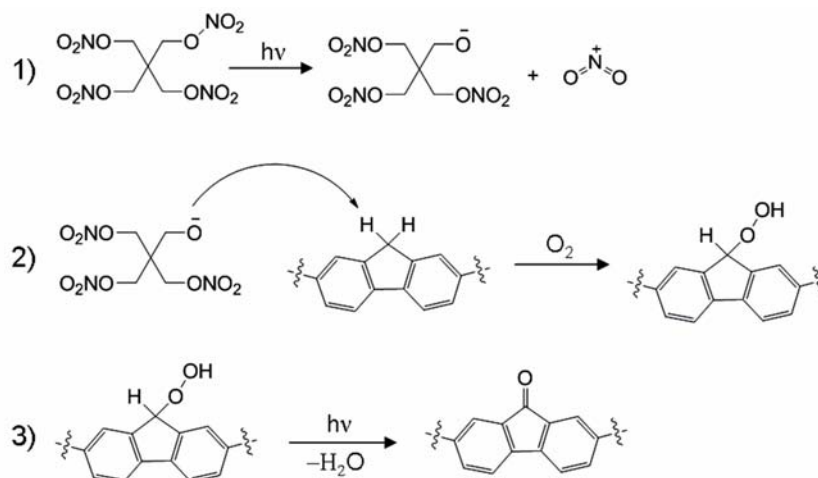


Figure 5-19. Proposed mechanism for the selective oxidation of fluorene by PETN.

this new emitting species remains a minor product. Complete oxidation of the fluorene to fluorenone was not observed in the time-frame of the experiment.

The initial decrease of the 370 nm emission peak for **1** is enhanced by TNT and RDX due to a fluorescence quenching pathway (Figure 5-14). DC peroxide show little or not effect when compared to the control experiment. When exposed to PETN, the spectrum of **1** shows the initial decrease at 370 nm; however, a peak at 523 nm appears at 40 min of UV light exposure. This peak continues to grow in over the course of the 280 min time period. The fluorescence λ_{\max} of 523 nm corresponds exactly with that of dimer **4** (Figure 5-11). The presence of PETN selectively facilitates the rapid formation of the oxidized product **4** in comparison to the other analytes. This oxidation process is suppressed in the absence of oxygen (Figure 5-15 and Figure 5-18). Based on the results of this study, we have proposed a mechanism for the selective oxidation of **1** and **PSF1** by PETN (Figure 5-19). It has been shown that the predominant initial decomposition product of PETN results in the formation

of an oxoanion.³³ This species can be obtained thermally, chemically, or photochemically. This intermediate is unique to nitrate esters because of the O–NO₂ functionality. The oxidation of fluorene can be achieved through many routes, but is enhanced and most efficient in the presence of a base.³⁴ The base facilitates hydride extraction which assists in the full oxidation of fluorene to fluorenone in the presence of oxygen. Synthesis of the fluorenone product can be obtained without a base, however, the formation of the carbanion is much less efficient. These results lead to the selective detection of nitrate ester based explosives by a turn-on fluorescence mechanism through rapid oxidation of the unprotected fluorene in **1** and **PSF1**.

5.4 CONCLUSIONS

It has been demonstrated that selective detection of nitramine and nitrate ester based explosives can be achieved using “turn-on” fluorescence technology. In combination with the fluorescence quenching detection of nitroaromatics using polysiloles-vinylene, a three-step process was established for selective explosives detection at the low nanogram level. Targeting the specific chemical features of the explosive materials has led to the highly selective and sensitive analysis of samples without the need for pre-concentration or pre-treatment of the sampling substrate. The direct in situ analysis of solid particulates gives this method of detection an advantage over conventional sensors. This technology may also be easily integrated into a low power, portable device for low-cost, rapid explosive sensing. The use of fluorescence

as the detection method has allowed for the possibility of much lower detection limits than those typically found in colorimetric methods.

The unprotected fluorene in **PSF1** shows tandem turn-off/turn-on fluorescence sensing, which is selective for the nitrate ester based explosives PETN and TNG. This illustrates how time dependent photochemistry can be used for increased selectivity in solid state fluorescent sensors.

5.5 EXPERIMENTAL

5.5.1 General Synthetic Techniques

Caution: TNT and picric acid are high explosives and should be handled only in small quantities. Picric acid also forms shock sensitive compounds with heavy metals. Purchased explosive standards were handled as dilute solutions to eliminate their explosion hazard. All synthetic manipulations were carried out under an atmosphere of dry argon gas using standard Schlenk techniques. Dry solvents were purchased from Aldrich Chemical Co. Inc. and used after purification with an MBraun Auto Solvent Purification System. Spectroscopic grade toluene from Fisher Scientific was used for the fluorescence measurements. Trimethylsilylacetylene and 1,4-diethynylbenzene (97%) were purchased from Aldrich Chemical Co. Inc. 1,4-diethynylbenzene was sublimed before use (30 °C at 0.5 Torr). The following were prepared by literature methods: 1-hydrido-1-methylsilafluorene³⁵ and 2,7-diethynylfluorenone.³⁶ DNT was purchased from Aldrich Chemical Co. and recrystallized from ethanol and methanol, respectively. TNT was prepared from

DNT³⁷ and recrystallized from toluene. RDX, HMX, Tetryl, TNG and PETN were purchased as 1 mg mL⁻¹ analytical standards in acetonitrile from Cerilliant®.

NMR data were taken on 300, 400, and 500 MHz spectrometers. UV-vis spectra were obtained with the use of a Hewlett-Packard 8452A diode array spectrometer. A Perkin-Elmer LS 45 luminescence spectrometer was used to recorded fluorescence emission and excitation spectra. For anaerobic and anhydrous studies, spectral grade toluene was first redistilled over a sodium/benzophenone ketyl. The anhydrous solution was then degassed 3 times using a freeze-pump-thaw method. The final solutions were then further degassed by bubbling argon through the sample for 10 min. The quartz cuvettes were sealed to prevent exposure of the sample solution to the atmosphere. IR spectra were obtained on a Nicolet Magna-IR 550 spectrometer.

5.5.2 Methods and Reagents

Polysilole-vinylene (Reagent A): Polysilole-vinylene was prepared by catalytic hydrosilylation of 1,1-dihydrido(tetraphenyl)silole and 1,1-diethynyl(tetraphenyl)silole using H₂PtCl₆ (Chapter 2). Reagent A is a solution of polysilole-vinylene (0.2 mg mL⁻¹) in acetone. Polymer solutions are made fresh prior to use.

2,3-Diaminonaphthalene (DAN) (Reagent B): DAN was purchased from Aldrich (97% purity) and used as received. Reagent B is a solution of DAN (4.0 mM) and KOH (0.75 M) in a 2:9:9 ratio of DMSO:acetone:ethanol respectively. The light brown reagent is made fresh prior to use.

Acidic Solution (Reagent C): Reagent C is a 2:1 solution of ethanol and phosphoric acid.

5.5.3 Solid-state Explosives Detection

5.5.3.1 Turn-on Fluorescence Detection with 2,3-diaminonaphthalene

Initial visual detection studies of nitramines and nitrate esters (RDX, HMX, TNG, PETN and Tetryl) were performed by preparing substrates spotted with explosive solutions, prepared from diluted analytical standards purchased from Cerilliant®, using acetonitrile as the solvent. The explosive solutions were spotted onto Whatman® 2 filter paper at the desired concentration level using a glass microsyringe. A solvent blank was spotted next to each explosive. All depositions were prepared from a 5 μL volume, producing a spot of ~ 1 cm in diameter, to insure consistent analysis. Upon evaporation of the acetonitrile, the substrate is airbrushed at a rate of 0.5 mL s^{-1} with Reagent B for ~ 2 s. Heat is applied with a heat gun, followed by application of Reagent C. Upon a final heating process, an independent observer (randomly ordering samples and solvent blanks) identified the appearance of the blue/green luminescent product when illuminated with a black light ($\lambda = 360$ or 302 nm). Whatman filter paper was selected for these studies because of its low background fluorescence. Detection studies were performed for each explosive at contamination levels of 64, 32, 16, 2, 1 and 0.6 ng cm^{-2} . Detection limits were noted as the lowest concentration of explosive that enabled the independent observer to notice luminescence.

Detection of nitroaromatics, as well as nitramines and nitrate esters, was carried out in a three-step process. Whatman filter paper samples were prepared as stated above, but with an additional spots of TNT at concentrations equal to the nitramine and nitrate ester explosives. The sample was then airbrushed with Reagent A and analyzed for TNT by monitoring the quenching of luminescence under a black light ($\lambda = 360$ or 302 nm). Subsequent analysis of nitramine and nitrate ester based explosives was carried out by applying Reagents B-C as described above.

Thumbprint samples of production line explosives were prepared at a Department of Defense approved explosives testing range operated by Newtec Services Group, Inc. Contaminated filter paper samples were prepared by contacting a hand with an explosive (TNT, RDX, PETN, C-4, or PE-4), removing the excess, and then contacting Whatman® 2 filter paper 5 successive times to prepare 5 generations of prints. C-4 is a mixture of RDX (91% by weight) and plasticizer (9% by weight). PE-4 is the British equivalent of C-4 with the only difference being the type and composition of plasticizer used. Detection using Reagents A-C is performed directly on these samples, as described above for the laboratory explosives.

5.5.3.2 Turn-on Fluorescence Detection with PSF1

Solutions of explosives were prepared as serial dilutions in toluene and stored in amber vials at 0 °C to prevent degradation. The solutions were spotted onto Whatman® filter paper at the desired concentration level using a glass microsyringe. A solvent control was spotted next to each explosive. All depositions were prepared

from a 5 μL volume, producing a spot of ~ 1 cm in diameter, to ensure consistent analysis. Upon solvent evaporation, the substrate is airbrushed at a rate of 0.5 mL s^{-1} with a 0.07 mg mL^{-1} solution (1:1, toluene:acetone) of the desired polymer. Addition of toluene aids the transient dissolution of explosive analytes and plasticizers, insuring efficient mixing with the polymers on drying. Blue photoluminescent **PSF1** was visualized using a UV-B lamp ($\lambda_{\text{em}} = 302 \text{ nm}$) as the excitation source with a UV transmitting filter (U34, HOYA Optics) attached to prevent backscattered visible light. Detection studies were performed for each explosive at trace contamination levels beginning at 64 ng cm^{-2} and ending at 1 pg cm^{-2} until a detection limit was reached.

Illuminated samples were examined by an independent observer to determine if quenching was discernible for **PSF1** immediately after exposure to explosive analytes. A double-blind test was carried out at the detection limit using two spots of the explosive material at each concentration, which were spotted randomly onto three locations. In each case a solvent blank was used as the control. The independent observer was unaware where the solvent control and explosive spots were distributed. Dark spots in the luminescent film indicate quenching of the polymer by the analyte. Detection limits are reported as the lowest amount of explosive necessary for the independent observer to observe quenching visually and accurately ($>95\%$) in the correct locations. For **PSF1**, detection limits for PETN and TNG were reported as the lowest amount of explosive necessary to observe fluorescence quenching and the

subsequent green-yellow luminescent turn-on sensing. This required continuous exposure of the substrate to UV light for 1-2 min.

Production line explosives PETN and C-4 were analyzed as thumbprints after handling of the solid explosive materials with nitrile gloves. Explosive particulates were not visible to the human eye before prints were taken. Five prints were consecutively laid down without further handling of the explosive. This study was included to provide real world applicability and exact concentration of explosive material within each print was unknown.

5.5.4 Synthesis of 2,7-di(1-methyl-1-*trans*-ethenyl-silafluorene)fluorenone (4)

1,1-dihydridosilafluorene (258 mg, 1.3 mmol), 2,7-diethynylfluorenone (150 mg, 0.66 mmol), and 0.5 mol % H_2PtCl_6 were stirred in toluene (10 mL), under argon for 12 h at room temperature. The orange solution was filtered through a sintered glass frit and evaporated to dryness. The remaining solid was purified by column chromatography (silica gel) using dichloromethane–hexanes as the eluent, yielding an orange crystalline (0.29 g, 71%). mp = 105 °C (decomp.); ^1H NMR (300.075 MHz, CDCl_3): δ 7.93–6.80 (br, 24H, PhH and C=CH), 6.60 (d, 2H, C=CH), 0.62 (s, 6H, Si(CH₃)); $^{13}\text{C}\{^1\text{H}\}$ NMR (100.59 MHz, CDCl_3): δ 198.3, 148.5, 146.0, 139.3, 137.3, 133.5, 130.8, 127.8, 121.4, -4.99; IR (neat solid): $\nu_{\text{C=O}}$ 1713 cm^{-1} ; $^{29}\text{Si}\{^1\text{H}\}$ NMR (99.37 MHz, INEPT, CDCl_3 , TMS (δ 0.00)) δ -8.5; Elemental analysis calcd for $\text{C}_{43}\text{H}_{32}\text{OSi}_2\cdot\text{H}_2\text{O}$: C 80.8, H 5.36; Found: C 81.1, H 5.72.

5.6 ACKNOWLEDGEMENTS

This chapter, in part, is a reprint of the material as it appears in the following papers: Sanchez, J. C.; Toal, S. J.; Wang, Z.; Dugan, R. E.; Trogler, W. C. “Selective Detection of Trace Nitroaromatic, Nitramine and Nitrate Ester Explosive Residues Using a Three-step Fluorimetric Sensing Process: A Tandem Turn-off, Turn-on Sensor” *J. Foren. Sci.* **2007**, *52*, 1308–1313 and Sanchez, J. C.; Trogler, W. C. “Efficient Blue Emitting Silafluorene-fluorene Conjugated Copolymers: Selective Turn-off/Turn-on Detection of Explosives” *J. Mater. Chem.* **2008**, DOI: 10.1039/b802623h.

5.7 REFERENCES

- (1) Steinfeld, J. I.; Wormhoudt, J. *Annu. Rev. Phys. Chem.* **1998**, *49*, 203–232.
- (2) Smith, K. D.; McCord, B. R.; McCrehan, W. A.; Mount, K.; Rowe, W. F. *J. Foren. Sci.* **1999**, *44*, 789–794.
- (3) Rouhi, A. M. *Chem. Eng. News* **1997**, *75*, 14–22.
- (4) Hakansson, K.; Coorey, R. V.; Zubarev, R. A.; Talrose, V. L.; Hakansson, P. *J. Mass. Spectrom.* **2000**, *35*, 337–346.
- (5) Sylvia, J. M.; Janni, J. A.; Klein, J. D.; Spencer, K. M. *Anal. Chem.* **2000**, *72*, 5834–5840.
- (6) Popov, I. A.; Chen, H.; Kharybin, O. N.; Nikolaev, E. N.; Cooks, R. G. *Chem. Commun.* **2005**, *15*, 1953–1955.
- (7) Kolla, P. *Anal. Chem.* **1995**, *67*, 184A–189A.
- (8) Toal, S. J.; Sanchez, J. C.; Dugan, R. E.; Trogler, W. C. *J. Foren. Sci.* **2007**, *52*, 79–83.
- (9) Trogler, W. C. In *Electronic Noses & Sensors for the Detection of Explosives*; Gardner, J. W., Yinon, J. Eds.; Kluwer Academic Publishers: 2004; p 39–52.
- (10) Mostak, P. In *Vapour and Trace Detection of Explosives for Anti-terrorism Purposes*; Krausa, M., Reznev, A. A., Eds.; NATO Science Series 167, Kluwer Academic Publishers: Boston, 2004; p 23–30.
- (11) Committee on Assessment of Security Technologies for Transportation, National Research Council. Opportunities to improve airport passenger screening with mass spectrometry. Washington, D. C.: The National Academies Press, 2004.
- (12) Agbaria, R. A.; Oldham, P. B.; McCarroll, M.; McGown, L. B.; Warner, I. M. *Anal. Chem.* **2002**, *74*, 3952–3962.
- (13) Boute, N.; Jockers, R.; Issad, T. *Trends Pharmacol. Sci.* **2002**, *23*, 351–354.
- (14) Gibbs, J. Selecting the detection system – colorimetric, fluorescent, luminescent methods; ELISA Technical Bulletin No. 5. Corning Life Sciences: Acton, MA; 2001.

- (15) Daniel, N. W.; Lewis, I. R.; Griffiths, P. R. *Appl. Spectrosc.* **1997**, *51*, 1868–1879.
- (16) Cotte-Rodriguez, I.; Takats, Z.; Talaty, N.; Chen, H.; Cooks, R. G. *Anal. Chem.* **2005**, *77*, 6755–6764.
- (17) GlobalSecurity.org, Military Explosives. <http://www.globalsecurity.org/military/systems/munitions/explosives.htm> (accessed Sept 2006)
- (18) Doane, S.; Ramgopal, R. India PM: Pakistan ties threatened, in *cnn.com* (Cable News Network). 2006 Jul 14.
- (19) Committee on Commercial Aviation Security, National Materials Advisory Board, Commission on Engineering and Technical Systems, National Research Council. Detection of explosives for commercial aviation security. Washington, D. C.: National Academy Press, 1993.
- (20) Rouhi, A. M. *Chem. Eng. News* **1995**, *73*, 10–22.
- (21) Meyer, R. In *Explosives*, 3rd ed; New York: VCH Publishers, 1987.
- (22) Fainberg, A. *Science* **1992**, *255*, 1531–1537.
- (23) Polski, P. A. *J. Testing and Evaluation* **1994**, *22*, 267–274.
- (24) Carre, M. C.; Mahieux, B.; Andre, J. C.; Viriot, M. L. *Analisis* **1999**, *27*, 835–838.
- (25) Misko, T. P.; Schilling, R. J.; Salvemini, D.; Moore, W. M.; Currie, M. G. *Anal. Biochem.* **1993**, *214*, 11–16.
- (26) Damiani, P.; Burini, G. *Talanta* **1986**, *33*, 649–652.
- (27) Sohn, H.; Sailor, M. J.; Magde, D.; Trogler, W. C. *J. Am. Chem. Soc.* **2003**, *125*, 3821–3830.
- (28) Toal, S. J.; Sohn, H.; Zakarov, L. N.; Kassel, W. S.; Golen, J. A.; Rheingold, A. L.; Trogler, W. C. *Organometallics* **2005**, *24*, 3081–3087.
- (29) Meisenheimer, J. *Justus Liebigs Ann. Chem.* **1902**, *323*, 205–226.
- (30) Terrier, F. *Chem. Rev.* **1982**, *82*, 77–152.

- (31) (a) Sanchez, J. C.; Toal, S. J.; Wang, Z.; Dugan, R. E.; Trogler, W. C. *J. Forensic Sci.* **2007**, *52*, 1308–1313. (b) Andrew, T. L.; Swager, T. M. *J. Am. Chem. Soc.* **2007**, *129*, 7254–7255.
- (32) Harrington, L. E.; Britten, J. F.; McGlinchey, J. *Tetrahedron Lett.* **2003**, *44*, 8057–8060.
- (33) Roos, B. D.; Brill, T. B. *Combust. Flame* **2002**, *128*, 181–190.
- (34) (a) Harvey, R. G.; Abu-shqara, E.; Yang, C. *J. Org. Chem.* **1992**, *57*, 6313–6317. (b) Park, K. K.; Tsou, L. K.; Hamilton, A. D. *Synthesis* **2006**, *21*, 3617–3620.
- (35) Becker, B.; Corriu, R. J. P.; Henner, B. J. L.; Wojnowski, W.; Peters, K.; von Schnering, H. G. *J. Organomet. Chem.* **1986**, *312*, 305–311.
- (36) Rodríguez, J. G.; Tejedor, J. L.; La Parra, T.; Díaz, C. *Tetrahedron* **2006**, *62*, 3355–3361.
- (37) Dennis, W. H.; Rosenblatt, D. H.; Blucher, W. G.; Coon, C. L. *J. Chem. Eng. Data* **1975**, *20*, 202–203.

CHAPTER VI

**Synthesis of Polyfluoran for the Detection of Vapor Phase Hydrogen Peroxide.
Application as a Turn-on Fluorescence Sensor for Organic Peroxide Explosives**

6.1 ABSTRACT

The double transesterification polymerization of 3,6-bis(pinacolatoboron)fluoran and pentaerythritol is reported. A model dimeric compound was synthesized to demonstrate the effectiveness of bis-diols to undergo a double transesterification, which is driven by formation of the energetically favored six-member di-ester ring from a monomer containing a five-member di-ester ring. This synthetic procedure provides a new route to boronate based polymers, avoiding unstable boronic acid monomers. Formation of poly-3,6-bis(1,3,2-dioxaborinane)fluoran, with a molecular weight of 10 000, is complete after 48 h at 50 °C. The thermodynamic stability of the six-member boronic ester rings present in the polymer backbone also improves the stability of the polymer and its resistance to oxidation under ambient and UV light conditions. A surface detection method for the analysis of H₂O₂ vapor by a fluorescence turn-on response was explored. The fluorescent response results from oxidative deprotection of the boronate functionalities forming green luminescent fluorescein. Detection limits as low as 3 ppb were observed for H₂O₂ over an 8 h period. Detection of H₂O₂ in liquids can also be carried out through spot tests at concentrations as low as 1 ppm after 5 min. This new vapor phase sensor for H₂O₂ provides a robust, low-cost alternative to current technology for potential applications as a self-integrating sensor for the detection of H₂O₂ as well as the direct monitoring of H₂O₂ levels in areas such as cargo shipments, chemical facilities, and pulp bleaching.

6.2 INTRODUCTION

Detection and analysis of explosive materials and formulations has become an integral part of national and world security.¹ The emergence of improvised explosive devices has challenged standard detection techniques used to screen high throughput civilian and cargo areas. In addition, the quantity of imports into the coastal regions, airports, and border checkpoints in the United States exceeds the manpower capable of screening all the cargo. The lack of robust, low-power, portable detection devices for the rapid on-site screening of both common and suspicious chemicals, materials, cargo, and persons, has driven the need for improved sensor devices.

Advances have been reported for detection devices that target nitro containing organic and inorganic explosives, which include 2,4,6-trinitrotoluene (TNT), cyclotrimethylenetrinitramine (RDX), cyclotetramethylene-tetranitramine (HMX), pentaerythritol tetranitrate (PETN) and trinitroglycerin (TNG).¹ The unique chemical functionalities of these explosives combined with their accessible reduction potentials enable the design of analytical sensors based on electron transfer approaches. Optimization of the sensor properties, including cost efficiency, sensitivity, selectivity, portability and speed of the signal analysis, has been achieved through the use of photoluminescent sensors.² However, several common explosive materials are not detectable by these technologies. One class of improvised explosives widely used by terrorists are organic based peroxides.³ The two most common such materials are triacetone triperoxide (TATP) and hexamethylene triperoxide diamine (HMTD) (Figure 6-1). These chemicals do not contain nitro or aromatic functionalities but

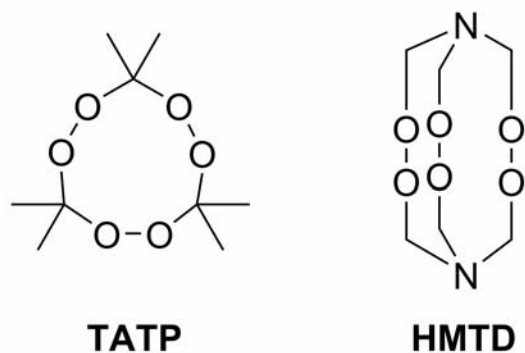


Figure 6-1. Chemical structures of triacetone triperoxide (TATP) and hexamethylene triperoxide diamine (HMTD).

incorporate cyclic peroxides that are stable enough to be transported, but are moderately shock sensitive (Table 6-1).⁴ Their decomposition velocity and explosive power matches those of typical organic nitrates like TNT. Unlike organic nitrates, TATP and HMTD can be synthesized easily with common chemicals, while starting materials do not need to be harvested from munition stockpiles or stolen from chemical factories or institutions.⁵

Current detection methods for TATP and HMTD include separation techniques, ion detection, and UV-vis and fluorescence response to photochemical decomposition.⁶ These methods either involve complex spectroscopic evaluation, multiple steps for detection, or a complex matrix of organic and aqueous solvents. Efforts have focused on targeting hydrogen peroxide (H_2O_2) produced through UV⁷ or acid-catalyzed⁸ decomposition of TATP or HMTD. To eliminate interferences, the samples can be prewashed with catalase. Bulk TATP and HMTD also include residual H_2O_2 left over from their synthesis. While current H_2O_2 detection methods have advanced in sensor sensitivity, they typically involve complex liquid sampling media

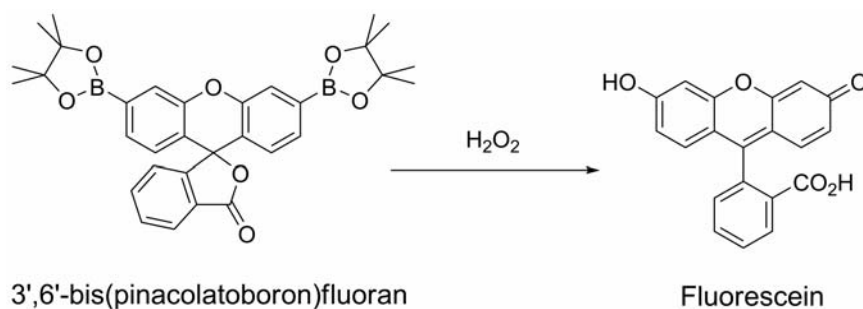
Table 6-1. Properties of organic peroxide based explosives compared with TNT.

Explosive	Type of Explosive	Melting Point (°C)	P_{vap} (Torr)	Detonation Velocity (m s ⁻¹)
TATP	Primary	98	5.3×10^{-2}	5300
HMTD	Primary	148	<i>na</i>	5100
TNT ^a	Secondary	81	5.8×10^{-6}	6850

^a Nitroaromatic based explosive for comparison.

and evaluation.⁹ To overcome these limitations, we have been interested in sensors that target vapor phase H₂O₂. Use of H₂O₂ in paper pulp bleaching, specialty chemical synthesis, and chemical disinfection also require monitoring of H₂O₂ levels¹⁰ due to the acute toxicity inherent in even small doses of H₂O₂ (1 ppm).¹¹ Current methods for the detection of H₂O₂ vapor rely on chemiresistive,¹² electrochemical,¹³ colorimetric,¹⁴ and vibrational spectroscopy analysis.¹⁵

One approach that has shown promise in the field of organic nitrate explosives detection is the use of fluorimetric sensors. This process targets the specific physical or chemical properties of the explosives to produce a detectable change in fluorescence. This change can be evaluated spectroscopically, but can easily be monitored by the naked eye. This allows for rapid analysis, robustness, and lowers the manufacturing and operating cost of the device. Current methods that focus on the use of fluorescence to monitor the presence of H₂O₂ include water soluble FRET-based polyelectrolytes,¹⁶ deprotection of fluorescein derivatives,¹⁷ and benzofurans.¹⁸ These



Scheme 6-1. Selective oxidation of 3,6-bis(pinacolatoboron)fluoran by H_2O_2 forming the fluorescein fluorophore.

methods involve solution-phase determination of H_2O_2 for biological assays. One application that provides high selectivity for H_2O_2 detection is the selective oxidative deprotection of boronic ester substituted fluoran, xanthanone, and phenoxazine derivatives, which have been synthesized in Chang's lab.¹⁹ These functional fluorophores are highly specific for the detection of H_2O_2 in biological systems. The sensors are utilized in a buffered aqueous media, showing good stability toward common interferents. The boronic ester functionalized fluoran shows the greatest fluorescence response due to the high quantum efficiency of fluorescein produced by the H_2O_2 specific oxidation of the two boronic ester functionalities (Scheme 6-1). The simplicity, sensitivity, and selectivity of this system make it an ideal candidate for vapor phase detection of H_2O_2 . However, the thin-film stability and processability of the 3,6'-bis(pinacolatoboron)fluoran monomer limits its use in solid-state sensor technology.

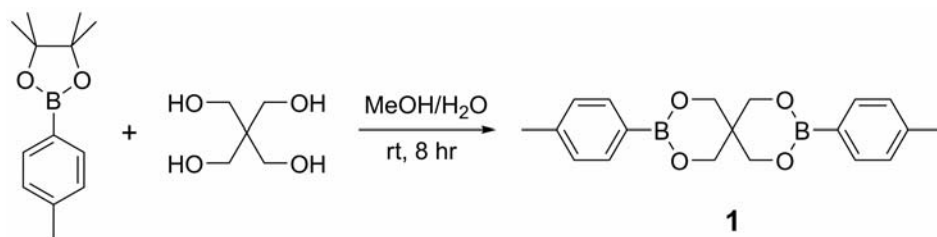
This chapter reports the synthesis of poly-3,6-bis(1,3,2-dioxaborinane)fluoran (**PolyF-1**) by double transesterification polymerization of 3,6-bis(pinacolatoboron)fluoran and pentaerythritol. This is the first synthesis,

which to our knowledge, which uses a double transesterification of boronic esters as a polymerization technique. Similar polymerization routes have used the condensation polymerization of boronic acids with bis-diols. This technique has been employed in the synthesis of oligomers,²⁰ polymers,²¹ and macrocycles²² for use as self-repairing materials and in thermal dehydration crosslinking applications. The drawback is that boronic acids are unstable under ambient conditions and require azeotropic or Dean-Stark removal of water for the reaction to proceed. The instability and complex synthetic issues may be avoided through the use of transesterification. In addition, direct conversion of a five member cyclic boronic ester to a six member cyclic boronic ester yields a highly stable polymer structure.²³ **PolyF-1** was screened for its ability to detect vapor phase H₂O₂ by fluorimetric analysis and it shows promise as a sensitive and selective polymeric sensor film for the detection of trace quantities of H₂O₂ in both solution and vapor phases.

6.3 RESULTS AND DISCUSSION

6.3.1 Synthesis and Characterization

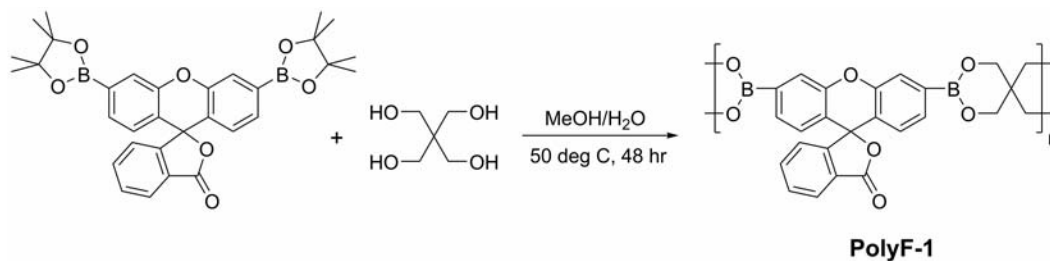
Transesterification of heterocyclic boronic esters is traditionally applied for the functionalization or protection of complex organic frameworks. There is much known about this process and a recent review by Roy and Brown highlights structural effects of both the boronate and diol on the reaction progress.²³ One conclusion drawn from this study was the increased thermodynamic stability observed for six-member ring boronic esters over five-member ring boronic esters. This concept has been used for



Scheme 6-2. Synthesis of model dimer **1** by double transesterification to form six-member rings.

monomer functionalization but has yet to be applied as a route to stabilized boronate polymers.

To demonstrate the viability of boronate double transesterification as a polymerization technique, a model dimer complex (**1**) was synthesized according to Scheme 6-2. The monomer 4-(pinacolboronic ester)toluene was used to mimic common arylboronates that may be used as comonomers for polymerization and pentaerythritol was used as the bis-diol to demonstrate the viability of a double transesterification of two five-member ring boronic esters. The reaction proceeded smoothly at room temperature in MeOH/H₂O over 8 h. The presence of H₂O is important for the solubility of pentaerythritol and its presence as a co-solvent does not hinder the reaction progress as it does during condensation polymerization of boronic acids. The percentage of water was minimized to ensure solubility. Reaction progress was monitored by both TLC and a periodic acid test for the presence of *cis*-diols (see Experimental). The reaction was complete after 8 h with a 65% yield. Dimer **1** was characterized by ¹H NMR and ¹³C NMR analysis. The ¹H NMR shows a singlet (δ 4.05 ppm) representing the methylene groups of the pentaerythritol fragment. This singlet integrates with the methyl resonance of the toluene endgroups (δ 2.37 ppm) at



Scheme 6-3. Synthesis of **PolyF-1** by double transesterification to form six-member boronic ester rings.

a ratio of 4:3, respectively. There is no detectable pinacol, confirming the effectiveness of the purification process. Dimer **1** shows superior thermal stability (mp = 259-261) and shelf life compared to the 4-(pinacolboronic ester)toluene while maintaining its solubility in many common organic solvents.

The promising results seen by the preceding synthesis of dimer **1** led us to consider this technique for polymerization of 3,6-bis(pinacolato)boronfluorene. The double transesterification polymerization of 3,6-bis(pinacolato)boronfluorene and pentaerythritol was carried out in MeOH/H₂O at 50 °C for 48 h (Scheme 6-3). Again, a periodic acid test was used to monitor the formation of pinacol. The polymer (**PolyF-1**) was extracted with methylene chloride and washed with H₂O. The organic solvent was removed under vacuum and the resulting light yellow powder was purified by cold MeOH washings to produce a white solid in good yield (75%). Several washings are required to fully remove the excess pinacol. The molecular weight of **PolyF-1** was determined to be 10 000 by GPC with a polydispersity index (PDI) of 1.5. This polymer is thermally stable and non-luminescent. The ¹H NMR spectrum shows the presence of the pentaerythritol and the absence of the pinacol

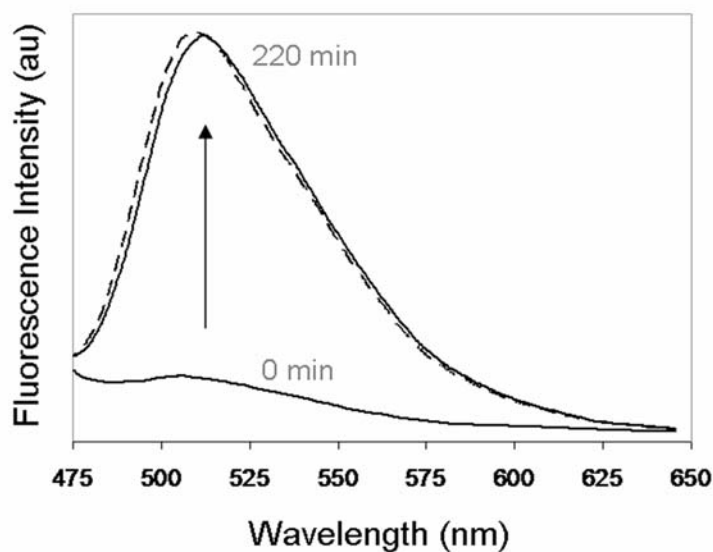


Figure 6-2. Fluorescence response of a $10 \mu\text{g cm}^{-2}$ film of **PolyF-1** to 2.9 ppm of H_2O_2 vapor after 220 min. Solid line at 0 min represents the baseline fluorescence intensity of the **PolyF-1** film. The dashed line represents the fluorescence emission of $100 \mu\text{g cm}^{-2}$ of fluorescein.

protecting group. Both ^1H NMR and ^{13}C NMR show the presence of the fluoran comonomer in the polymer.

6.3.2 Detection of Hydrogen Peroxide

Detection of vapor-phase H_2O_2 was evaluated using thin-films of **PolyF-1** drop-cast onto a Whatman2 porous sampling substrate to increase the surface area for polymer-analyte interactions. Polymer films were maintained at $10 \mu\text{g cm}^{-2}$ throughout the study. Both $2.5 \mu\text{g cm}^{-2}$ and $40 \mu\text{g cm}^{-2}$ films of **PolyF-1** were tested for their sensor effectiveness; however, the $10 \mu\text{g cm}^{-2}$ film shows the best results when considering sensor stability and response while limiting the quantity of polymer used.

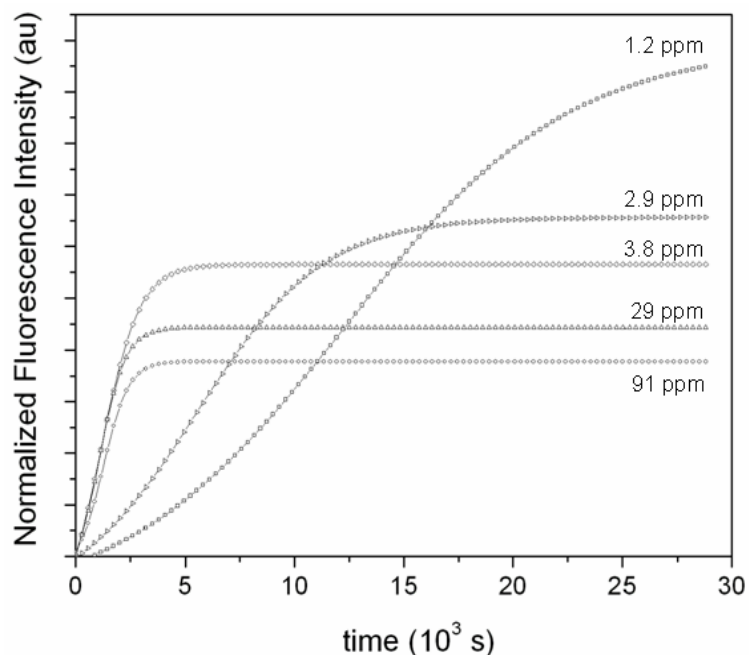


Figure 6-3. Fluorescence trace of $10 \mu\text{g cm}^{-2}$ **PolyF-1** exposed to various vapor concentrations of H_2O_2 .

A modified flow system using an inert carrier gas was used to achieve constant equilibrium vapor concentrations of H_2O_2 (see Experimental). Vapor concentrations of H_2O_2 were calculated using published data.²⁴ Time-dependent fluorescence spectra were taken on exposure of the **PolyF-1** film to H_2O_2 at concentrations of 91, 29, 3.8, 2.9, and 1.2 ppm. A representative fluorescence response plot for exposure of **PolyF-1** to 2.9 ppm H_2O_2 is seen in Figure 6-2. An 8-fold increase in fluorescence intensity (510 nm) is observed over a 3.5 h period for 2.9 ppm H_2O_2 . The fluorescence spectrum observed is nearly identical to the fluorescence emission of a thin-film of fluorescein deposited on the porous substrate. The decomposition of **PolyF-1** upon exposure to H_2O_2 was monitored by GPC, showing the presence of oligomers ($M_w = 700$, PDI = 1.8) after 30 min of H_2O_2 exposure. The sensor reaction proceeds by an

Table 6-2. Summary of **PolyF-1** ($10 \mu\text{g cm}^{-2}$) fluorescence responses on exposure to H_2O_2 vapor.

$[\text{H}_2\text{O}_2]$ (ppm)	k^a (10^{-4} s^{-1})	Flu. Intensity at $\infty (I_\infty)^b$	Time to reach I_∞ (10^3 s)
91	12	18.9	3.0
29	12	22.2	3.6
3.8	10	28.3	4.2
2.9	7.0	32.4	13
1.2	3.0	49.6	24

^a Derived from first order kinetic plots seen in Figure 4. ^b Calculated from the exponential growth fit (Equation 2) of the time dependent fluorescence trace of **PolyF-1** exposed to various concentrations of H_2O_2 (Figure 3).

oxidative deprotection of the boronic ester functionalities, forming fluorescein from fluoran (Scheme 6-1).

The data obtained at varying concentrations of H_2O_2 is summarized in Figure 6-3. At high vapor concentrations of H_2O_2 (>3.8 ppm) there is a rapid initial fluorescence response of the **PolyF-1** film on exposure to H_2O_2 . After ~ 1 h, a maximum fluorescence intensity is reached for each H_2O_2 concentration. At low H_2O_2 vapor concentrations (<2.9 ppm), there is a slow initial fluorescence response followed by a gradual increase in the time required to reach a maximum fluorescence intensity. However, the threshold for the maximum change in fluorescence intensity increases as the concentration of H_2O_2 decreases (Table 6-2). This inverse response is unique to this system. Typical turn-on fluorescence response scales proportionally with the concentration of analyte. In this case, there is an inverse relationship between

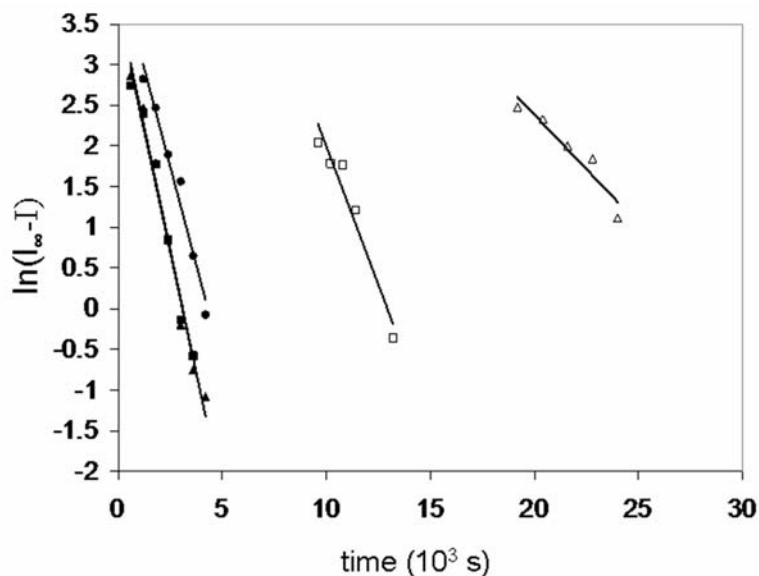


Figure 6-4. First order kinetics plot of the fluorescence response of **PolyF-1** exposed to 91 ppm H₂O₂ (■, R² = 0.98), 29 ppm H₂O₂ (▲, R² = 0.98), 3.8 ppm H₂O₂ (●, R² = 0.97), 2.9 ppm H₂O₂ (□, R² = 0.94), and 1.2 ppm H₂O₂ (△, R² = 0.94). The apparent rate constant (k) is derived from the slope of the linear regression fit. At low concentrations of H₂O₂, the reaction deviates from first order kinetics in H₂O₂.

the maximum fluorescence response and H₂O₂ concentration, which may be explained by the bleaching effect that H₂O₂ has on organic materials, especially at high concentrations. At high vapor concentrations, pseudo first order kinetics in H₂O₂ is expected (Figure 6-4). However, there is also a competitive decomposition of the organic fluorophore with the excess H₂O₂. This competing degradation prevents the maximum fluorescence response from being reached at high concentrations of H₂O₂. While the kinetics at high concentrations of H₂O₂ are pseudo first order, a change in kinetics is observed at around 2.9 ppm H₂O₂. At lower concentrations the reaction begins to slow based on the decrease in the molar ratio of H₂O₂ to **PolyF-1**. At the same time, H₂O₂ is more readily consumed in the more energetically favored oxidative

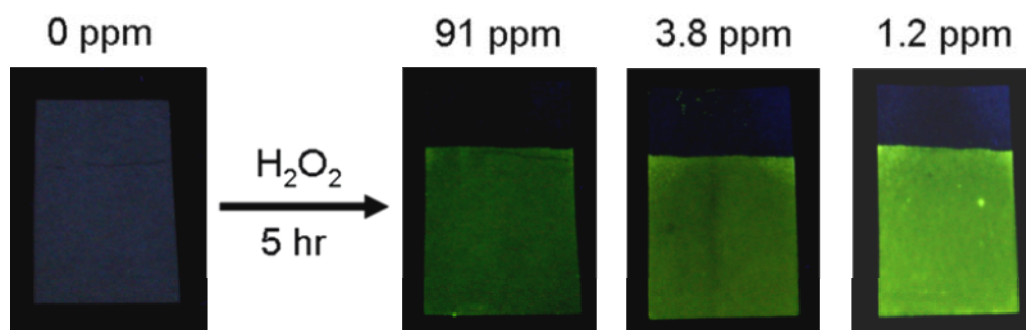


Figure 6-5. Images of the fluorescence response of $10 \mu\text{g cm}^{-2}$ **PolyF-1** to various concentrations of H_2O_2 vapor over a 5 h period. An increase in fluorescence intensity is observed at lower concentrations of H_2O_2 providing a highly sensitive sensor response.

deprotection reaction and oxidative decomposition of the organic fluorophore begins to decrease. This causes a continual increase in the maximum fluorescence intensity (I_∞) at decreasing concentrations of H_2O_2 (Figure 6-5). The reaction is also time-dependent, showing much longer exposure times to reach I_∞ at lower concentrations of H_2O_2 , so there is no problem distinguishing between high and low concentrations of H_2O_2 .

The films of **PolyF-1** were also screened for their stability under ambient and UV light. This is relevant for real world interferents and film stability over time. **PolyF-1** shows a minimal fluorescence response under ambient conditions (0.06%) or UV light exposure (0.5%) over a period of 5 h. This demonstrates the good photostability of the films, as well as their stability to atmospheric oxidizers that may be created in the presence of UV light. The data collected for the UV light control experiment was used to calculate the standard deviation ($\sigma = 0.24$) for the film stability at 0 ppm H_2O_2

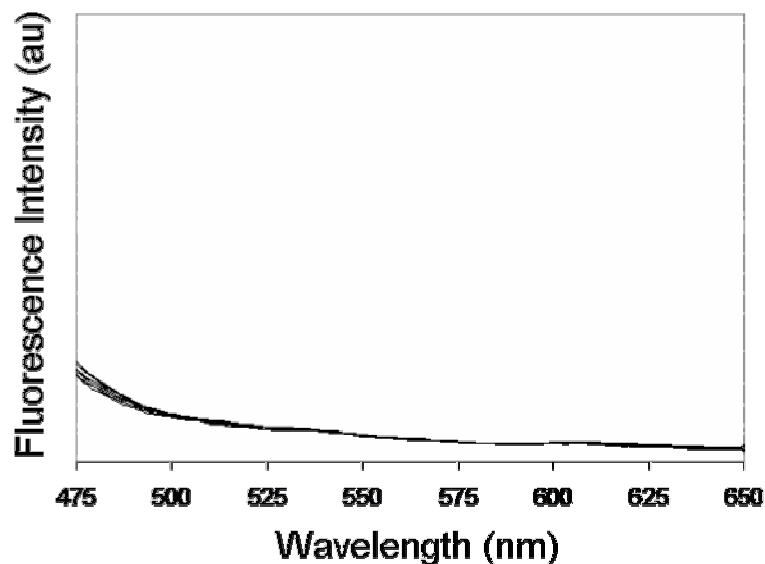


Figure 6-6. Fluorescence response of a $10 \mu\text{g cm}^{-2}$ film of **PolyF-1** to UV light (302 nm) over a 5 h period. An increase in fluorescence intensity at 510 nm is not observed. The fluorescence intensity observed at 510 nm at each time point was used to derived 3σ for the detection limit calculations.

(Figure 6-6). This standard deviation was used to calculate the time at which a detectable signal is achieved for a given concentration of H_2O_2 .

The monomer material 3,6-bis(pinacolatoboron)fluoran was also screened for its ability to detect H_2O_2 . This experiment was performed to determine whether there is an advantage to using the polymeric version of the sensor as **PolyF-1**. The fluoran monomer shows decreased stability when exposed to both ambient conditions (7.4% of the maximum fluorescence intensity) and UV light (3.4%), as compared with **PolyF-1**. The response to H_2O_2 is also weaker, accounting for only a 4-fold increase in

fluorescence intensity on exposure to 2.9 ppm H₂O₂ as compared to an 8-fold increase for **PolyF-1** (Figure 6-7). The stability of the six-member boronic ester functionalities

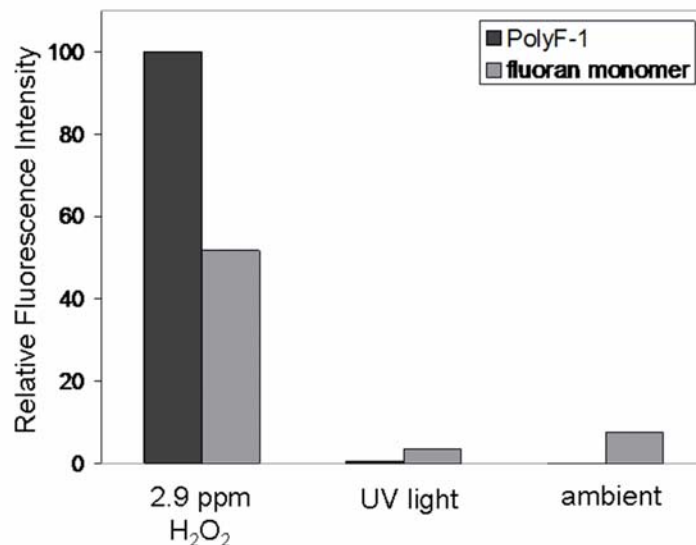


Figure 6-7. Fluorescence responses of a 10 $\mu\text{g cm}^{-2}$ film of **PolyF-1** and the same mass of 3,6-bis(pinacolatoboron)fluoran (fluoran monomer) to 2.9 ppm H₂O₂, UV light, and ambient conditions over a 5 h period. **PolyF-1** shows a greater fluorescence response to H₂O₂ and is more stable as a thin-film than the fluoran monomer.

in **PolyF-1** may assist in directing the peroxide oxidation to deprotection of the boronic ester rather than decomposing the organic framework. In addition, processability of the monomer material for thin-film application is much more difficult than for **PolyF-1**.

Quantifying the detection results of a vapor phase turn-on fluorescence sensor based on the chemical modification of a polymer thin-film presents a unique challenge. The sensor response is proportional to time but inversely proportional to H₂O₂ concentration. The increase in signal response with decreasing concentrations of H₂O₂ prevents typical analysis of the detection response. In order to better quantify

this system, the fluorescence intensity at infinity (I_∞), calculated from a single exponential growth (Equation 1), was fitted to the time-dependent fluorescence

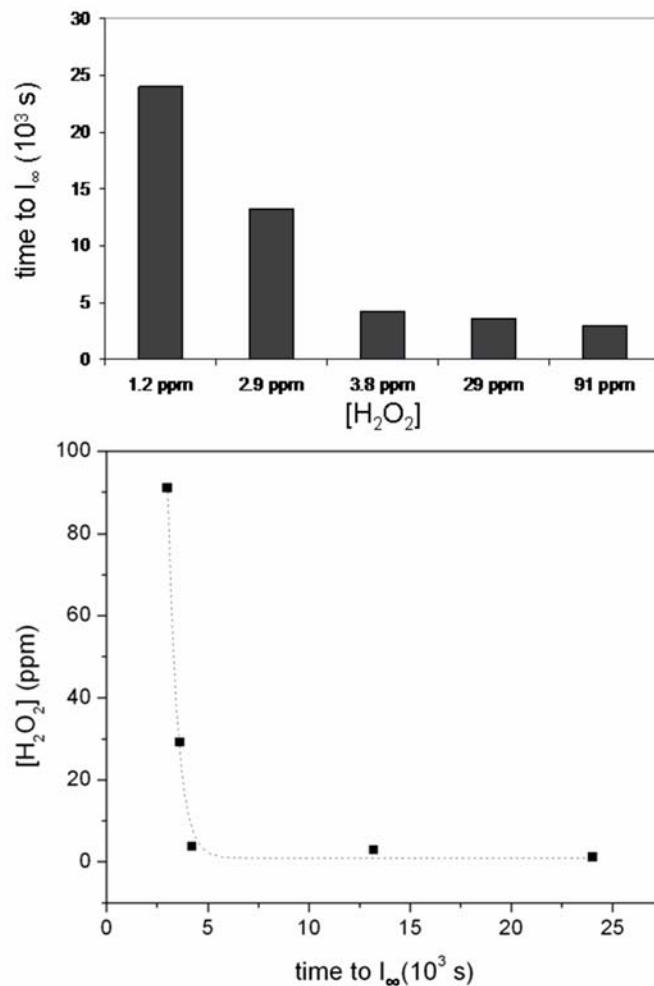


Figure 6-8. Correlation between the concentration of H_2O_2 and the time to reach I_∞ . I_∞ was calculated from the exponential decay fits of the time dependent fluorescence traces at various concentrations of H_2O_2 observed in Figure 6-3. The plot was fit to an exponential decay (Equation 2). A detection limit of 0.7 ppm H_2O_2 is calculated from the threshold reached by Equation 2. This detection limit is based on a maximum fluorescence response of **PolyF-1** to H_2O_2 .

response data (Figure 6-3). Using I_∞ , a correlation between the times required to reach I_∞ and H_2O_2 concentrations can be made (Figure 6-8). The data was fit to an exponential

decay with an R^2 of 0.999 (Equation 2). From this fit a detection limit of 0.7 ppm (at time = ∞) can be determined. This limit is based on the maximum fluorescence

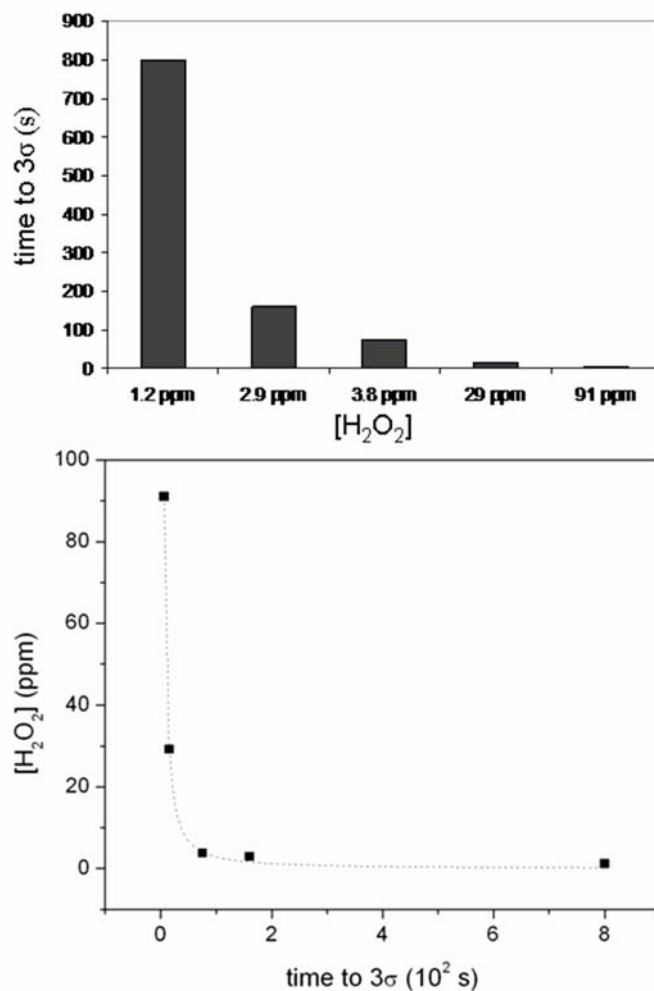


Figure 6-9. Correlation between the concentration of H₂O₂ and the time to reach 3σ of the fluorescence response noise. The noise was calculated from the fluorescence response of **PolyF-1** to UV light over a 5 h period. The data was fit to a power function (Equation 3) providing the ability to calculate the time required to detect a desired concentration of H₂O₂ using a 10 μg cm⁻² film of **PolyF-1**.

response from **PolyF-1** at the film thickness used. However, there are measurable fluorescence responses above the noise limit (3σ) of the spectrophotometer that better quantify the useful detection limit of the sensor. When this response is placed in a time

domain, a correlation can be made between the time and H₂O₂ detection limits (Figure 6-9). This plot correlates the proportional response observed for the fluorescence

Table 6-3. Time-dependent detection limits of H₂O₂ vapor by **PolyF-1** at various exposure times.

time (min)	H ₂ O ₂ Detection Limit (ppb)
10	300
60	30
180	9

intensity at 3σ above the noise of the spectrophotometer with the concentration of H₂O₂. The response is no longer an inverse response and therefore can provide more useful information on the detection capabilities of **PolyF-1**. The noise was calculated to be 0.08 from the fluorescence measurements taken of the **PolyF-1** film on exposure to UV light and ambient conditions (Figure 6-6). The data was fitted to a power function ($R^2 = 0.999$, Equation 3) as opposed to an exponential decay ($R^2 = 0.966$, Equation 2) to prevent a threshold limit from constraining the analysis. Using this equation, the time required to reach a desired detection limit can be calculated (Table 6-3). This plot is not limited by a maximum fluorescence intensity, revealing the low levels of detection that can be achieved with **PolyF-1**. For example, 9 ppb H₂O₂ can be detected after 3 h of exposure according to this analysis. A detection limit of 3 ppb is estimated to be possible after 8 h of exposure, which is two orders of magnitude below the permissible exposure limit (1 ppm) over an 8 h period established by OSHA.²² It is

important to note, that these sensor films are effectively acting as integrating sensors for low levels of H₂O₂. This application may be useful in estimating average

$$y = y_0 + A_1 e^{(x/t)} \quad (1)$$

$$y = y_0 + A e^{(-x/t)} \quad (2)$$

$$y = x^A \quad (3)$$

exposures over, for example, an 8 h working shift or for monitoring the contents of shipping cargo containers for H₂O₂.

The high vapor pressure of H₂O₂ and the specificity that boronic esters show toward H₂O₂ oxidation¹⁹ make **PolyF-1** a highly sensitive and selective sensor for H₂O₂. The films show little response to ambient conditions as well as UV light above the noise limit of the spectrophotometer over a 5 h period, indicating that radical oxygen species (ROS) and other oxidants found in the atmosphere as well as those that may be generated under a UV lamp ($\lambda = 302$ nm) are not interferents. The vapor pressures of most organic peroxides are much lower than for H₂O₂, and thus are not significant interferents during vapor phase detection. Many of these interferents, including various ROS and anionic species, have previously been tested in solution phase studies and show little to no response.¹⁹ Besides its use as a vapor sensor, **PolyF-1** can also be used to screen suspicious liquids. This may be applicable to high throughput screening areas where concealed liquids would not produce a measurable vapor concentration of H₂O₂. To test this application, solutions of H₂O₂ in water at

various concentrations were spotted onto the same $10 \mu\text{g cm}^{-2}$ films of **PolyF-1** used during the vapor phase detection studies. Several common organic peroxides, including di-*t*-butylperoxide and benzoyl peroxide, were also spotted to confirm that

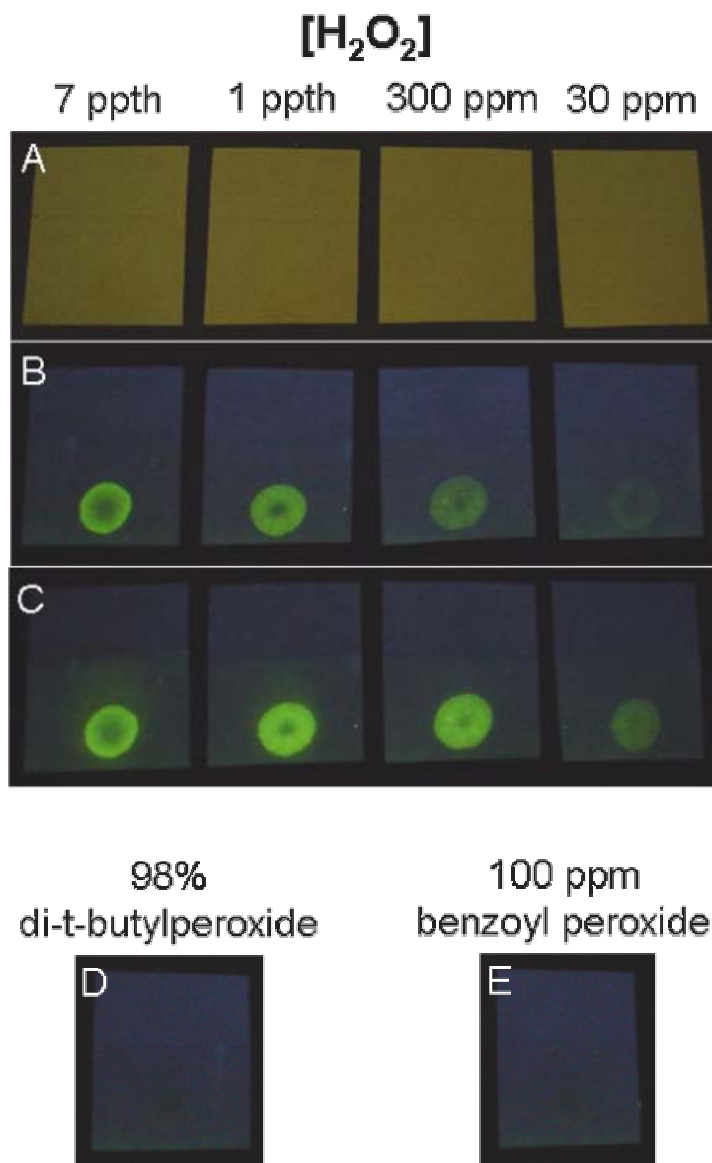


Figure 6-10. Images of the fluorescence response of a $10 \mu\text{g cm}^{-2}$ film of **PolyF-1** to various solution concentrations of H₂O₂ and possible organic peroxide interferents. A) Film appearance under incandescent light. B) Detection of H₂O₂ under UV light (302 nm) after 30 s. C) Detection of H₂O₂ under UV light (302 nm) after 5 min. Detection increases over time. D) No fluorescence response observed for 98% di-*t*-butylperoxide

after 5 min. E) No fluorescence response observed for 100 ppm benzoyl peroxide after 5 min.

the oxidative depolymerization of **PolyF-1** is insensitive to these interferents in spot tests (Figure 6-10). **PolyF-1** easily detects 30 ppm of H₂O₂ during solution spot tests after 30 s. After 5 min, this signal increased further. Benzoyl peroxide (100 ppm) and di-t-butylperoxide (98%) show no detectable response after 5 min when spotted onto the **PolyF-1** film.

6.4 CONCLUSIONS

A new method of polymerization was developed using the double transesterification of arylboronates to synthesize **PolyF-1**. The chemical principle used to favor the polymer structure relies on the formation of six-member boronic ester rings throughout the backbone from a monomer containing a five-member boronic ester ring. This method of polymerization proved facile for the polymerization of fluoran and may be generalized to the polymerization of complex systems that are not compatible with boronic acid monomers. **PolyF-1** was designed and synthesized as a self-integrating sensor for the selective detection of vapor phase H₂O₂ by a fluorescence turn-on mechanism. H₂O₂ is an important by-product produced through thermal and UV degradation of the peroxide based primary high explosives TATP and HMTD and its levels are also an occupational health and safety concern for its increasing use as a disinfectant and bleaching agent. Detection limits on the order of 3 ppb over an 8 h period can be achieved using thin-films of **PolyF-1** on a porous

sampling substrate. The detection process is insensitive to common interferents including organic peroxides and many ROS species. This technology can also be used to screen for H₂O₂ in suspicious liquids. A spot test of 30 ppm H₂O₂ shows visual detection within 30 s, with an increasing fluorescence response over time. The synthetic ease, stability, and processability of **PolyF-1** make it an ideal candidate for H₂O₂ detection applications that require a robust, low cost, sensitive, and selective sensor with rapid qualitative and semi-quantitative signal analysis.

6.5 EXPERIMENTAL

6.5.1 General Synthetic Techniques

All synthetic manipulations were carried out under an atmosphere of dry argon gas using standard Schlenk techniques unless otherwise noted. Dry solvents were purchased from Aldrich Chemical Co. Inc. and used after purification with an MBraun Auto Solvent Purification System. Pentaerythritol (98%) was purchased from Acros Organics and used as received.² For dosing studies, 30 wt% H₂O₂ in water (Acros) was purchased, using a fresh solution for every dosing run. Hydrogen peroxide solutions were assayed via iodometric titration and the average peroxide weight percentage was 27.1% ± 2.0%. Di-*t*-butyl peroxide (Aldrich, 98%) and benzoyl peroxide (Aldrich, 97%) were used as purchased and stored at 2-6 °C under inert gas. The following were prepared by literature methods: 4,4,5,5-tetramethyl-2-*p*-tolyl-1,3,2-dioxaborolane²⁵ and 3,6-bis(pinacolatoboron)fluoran.¹⁹ NMR data were collected using a Varian Mercury Plus spectrometer and 9.4 T superconducting

magnet (399.911 MHz for ^1H and 100.52 MHz for ^{13}C NMR). A Perkin-Elmer LS 45 luminescence spectrometer was used to record fluorescence emission and excitation spectra. GPC data was obtained with the use of a Viscotek GPCmax VE 2001 GPC; molecular weights were recorded relative to polystyrene standards and low molecular weight silole monomers and dimers. The data was fitted using Origin8.

6.5.2 Periodic Acid Test for Cis-diols

The periodic acid test can be used to monitor the presence of 1,2-diols. The transesterification between pinacolatoboron and pentaerythritol produces pinacol as the reaction proceeds. This 1,2-diol can be detected selectively over pentaerythritol through its oxidative cleavage yielding ketone and iodate products. The presence of iodate can then be determined by formation of a white precipitate of AgIO_3 in the presence of Ag^+ . To a periodic acid reagent (2 mL, 0.1 M) was added 1 drop of nitric acid (0.1 M) and 1 drop of solution taken from the reaction mixture. This was stirred for 10 s and 2 drops of AgNO_3 was added. The solution was stirred for 5 s and the resulting white precipitate confirms the presence of pinacol.

6.5.3 Peroxide Detection

Thin-films of **PolyF-1** were prepared by drop-casting the polymer from a CHCl_3 solution onto thin sheets of Whatman2 filter paper (4 cm^2). The filter paper provides a porous sampling substrate that maximizes the surface area of the polymer exposed to the H_2O_2 analyte. Concentrations of 2.5, 10, and $40\text{ }\mu\text{g cm}^{-2}$ were evaluated

for **PolyF-1**. The films are not visible to the naked eye and show no luminescence over a 5 h period after exposure to UV light and ambient air. Detection of H₂O₂ was initially carried out in the vapor phase using a modified inert gas flow system. Argon was bubbled through a dilute solution of H₂O₂ in water and the vapor concentration was calculated based on temperature and mole fraction of H₂O₂ in the solution.²⁴ The inert gas flow was directed into a sealed chamber through a Teflon tube. Cotton was placed inside the chamber to provide a more consistent saturation of H₂O₂. The chamber was purged for 10 min before each film exposure to ensure that an equilibrium vapor concentration was reached. The films were placed into the sealed chamber and fluorescence spectra were recorded upon removal of the film at various time intervals. The film was placed into a solid support scaffold on the fluorimeter to ensure repeatability of the site of photo-excitation on the film. H₂O₂ vapor concentrations of 91, 29, 3.8, 2.9, and 1.2 ppm were evaluated for both **PolyF-1** and the fluoran monomer at a film concentration of 10 µg cm⁻². Solutions of H₂O₂ also examined at concentration of 7 ppt, 1 ppt, 300 ppm, and 30 ppm to show application of **PolyF-1** as both a vapor phase sensor for H₂O₂ and a qualitative screening test for the presence of H₂O₂ in suspicious solutions.

6.5.4 Synthesis of 3,9-dip-tolyl-2,4,8,10-tetraoxa-3,9-diborospiro[5.5]undecane (1)

To a stirring methanol solution of 4,4,5,5-tetramethyl-2-p-tolyl-1,3,2-dioxaborolane (4 mL, 115 mM) was added an aqueous solution of pentaerythritol (1 mL, 0.23 mM). The mixture was stirred at room temperature for 12 h. Reaction

progress was monitored by both TLC and a periodic acid test. After 8 h the solution became cloudy and a white precipitate formed. The solid was extracted with methylene chloride, washed with brine and water, and evaporated to dryness yielding a white powder (50 mg, 65%). ^1H NMR (CDCl_3 , ppm): δ 7.69 (d, 4H, Ph-H), 7.18 (d, 4H, Ph-H), 4.05 (s, 8H, CH_2), 2.37 (s, 6H, CH_3); $^{13}\text{C}\{^1\text{H}\}$ NMR (CDCl_3 , ppm): δ 141.4, 134.1, 128.6, 65.0, 36.8, 21.9; mp = 259-261 °C; Calcd for $\text{C}_{19}\text{H}_{22}\text{O}_4\text{B}_2$: C 67.9, H 6.60; Found: C 68.2, H 6.84.

6.5.5 Synthesis of poly-3,6-bis(1,3,2-dioxaborinane)fluoran (PolyF-1)

To a stirring methanol solution of 3,6-bis(pinacolatoboron)fluoran (4 mL, 45 mM) under ambient conditions was added an aqueous solution of pentaerythritol (1 mL, 0.18 mM). The mixture was stirred at 50 °C for 48 h. Reaction progress was monitored by TLC and a periodic acid test. The colorless solution was extracted with methylene chloride, washed with brine and water, and the organic extract was evaporated to dryness. The resulting off-white solid was washed with cold methanol, yielding a white powder (61 mg, 75%). ^1H NMR (400.053 MHz, CDCl_3): δ 8.03 (m, 1H, Ph-H), 7.73 (br-d, 2H, Ph-H), 7.60 (m, 2H, Ph-H), 7.43 (m, 2H, Ph-H), 7.06 (m, 1H, Ph-H), 6.85 (br-d, 2H, Ph-H), 4.07 (br-s, 8H, CH_2); $^{13}\text{C}\{^1\text{H}\}$ NMR (100.59 MHz, CDCl_3): δ 163.4, 135.4, 130.0, 129.6, 127.1, 125.4, 123.9, 84.5, 65.1, 45.9, 30.1; Calcd for $\text{C}_{25}\text{H}_{18}\text{O}_7\text{B}_2$: C 66.4, H 4.01; Found: C 66.5, H 4.4.

6.6 ACKNOWLEDGEMENTS

This chapter, in part, is a reprint of the material as it appears in the following papers: Sanchez, J. C.; Trogler, W. C. “Polymerization of a Boronate Functionalized Fluorophore by Double Transesterification. Applications to Fluorescence Detection of Hydrogen Peroxide Vapor” *J. Mater. Chem.*, submitted 2008.

6.7 APPENDIX

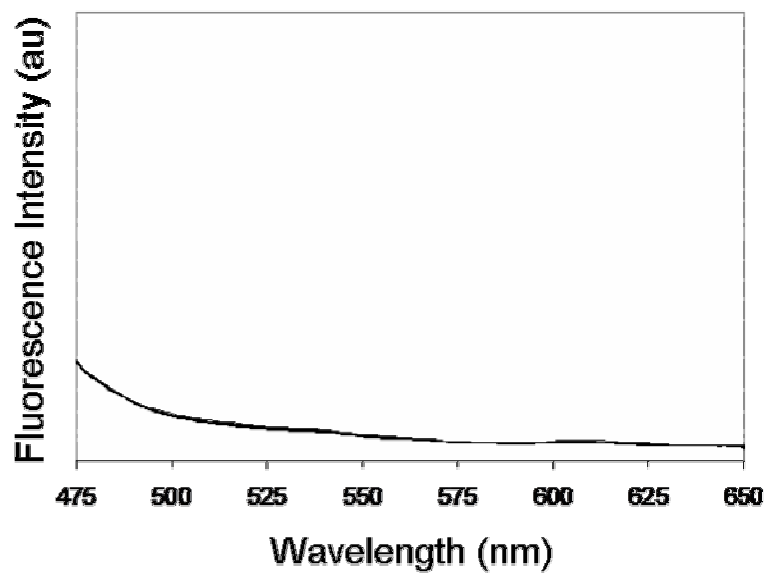


Figure 6-11. Fluorescence response of a $10 \mu\text{g cm}^{-2}$ film of **PolyF-1** to ambient conditions over a 5 h period. An increase in fluorescence intensity at 510 nm is not observed.

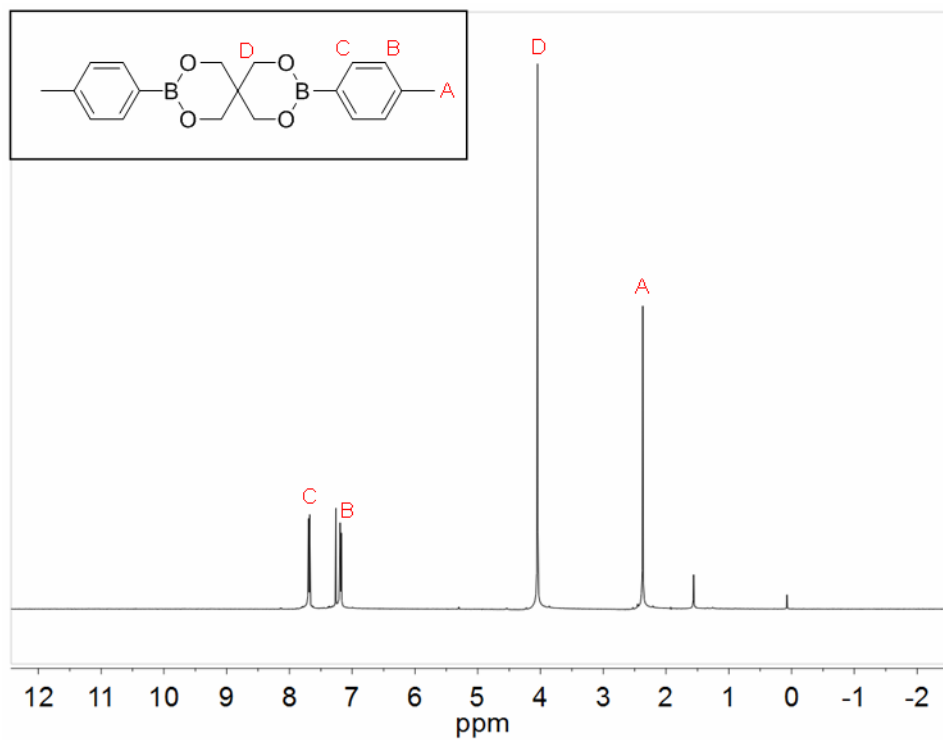


Figure 6-12. ^1H NMR spectrum of dimer 1.

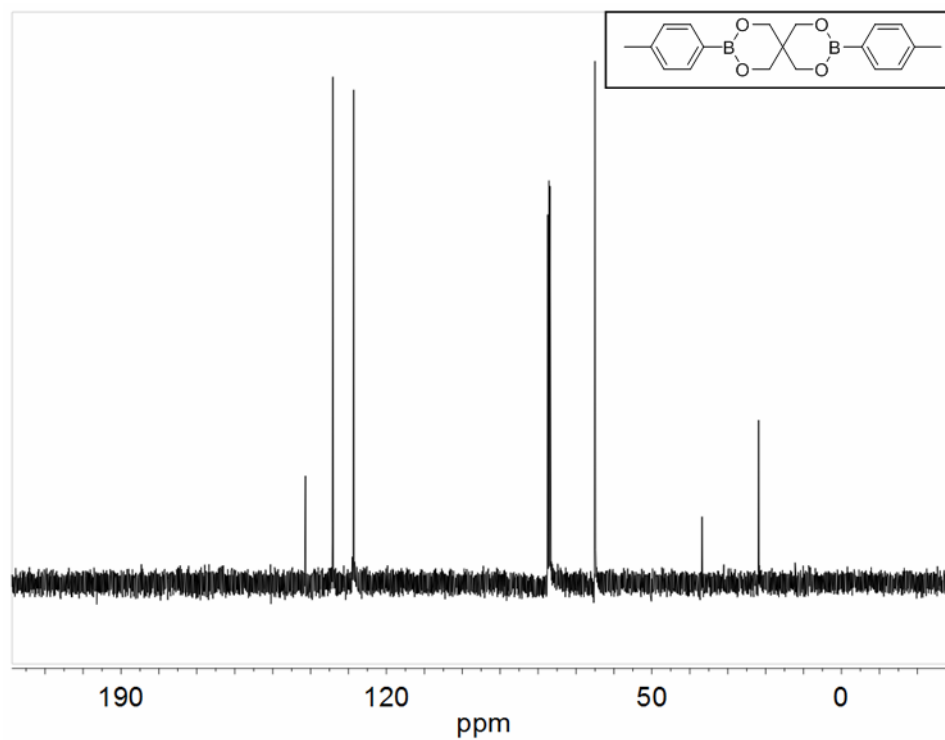


Figure 6-13. ^{13}C NMR spectrum of dimer 1.

6.8 REFERENCES

- (1) (a) Singh, S. *J. Hazard. Mater.* **2007**, *144*, 15–28. (b) Moore, D. S. *Rev. Sci. Instrum.* **2004**, *75*, 2499–2512. (c) Steinfeld, J. I.; Wormhoudt, J. *Annu. Rev. Phys. Chem.* **1998**, *49*, 203–232.
- (2) (a) Toal, S. J.; Trogler, W. C. *J. Mater. Chem.* **2006**, *16*, 2871–2883. (b) McQuade, D. T.; Pullen, A. E.; Swager, T. M. *Chem. Rev.* **2000**, *100*, 2537–2574. (c) Sanchez, J. C.; Trogler, W. C. *J. Mater. Chem.*, in press. (d) Sanchez, J. C.; Urbas, S. A.; Toal, S. J.; DiPasquale, A. G.; Rheingold, A. L.; Trogler, W. C. *Macromolecules* **2008**, *41*, 1237–1245. (e) Sanchez, J. C.; DiPasquale, A. G.; Rheingold, A. L.; Trogler, W. C. *Chem. Mater.* **2007**, *19*, 6459–6470. (f) Sanchez, J. C.; Toal, S. J.; Wang, Z.; Dugan, R. E.; Trogler, W. C. *J. Foren. Sci.* **2007**, *52*, 1308–1313. (g) Toal, S. J.; Sanchez, J. C.; Dugan, R. E.; Trogler, W. C. *J. Foren. Sci.* **2007**, *52*, 79–83.
- (3) (a) McKay, G. J. *Kayaku Gakkaishi* **2002**, *63*, 323–329. (b) White, G. M. *J. Forensic Sci.* **1992**, *37*, 652–656. (c) Evans, H. K.; Tulleners, F. A. J.; Sanchez, B. L.; Rasmussen, C. A. *J. Forensic Sci.* **1986**, *31*, 1119–1125. (d) Ember, L. R. *Chem. Eng. News* **2005**, *83*, 11.
- (4) (a) Federoff, B. T. In *Encyclopedia of Explosives and Related Items*; Picatinny Arsenal: Dover, NJ, 1960; Vol. 1, pp A42–A45. (b) Yinon, J. In *Forensic and Environmental Detection of Explosives*; John Wiley: Chichester, NY, 1999; pp 10–11. (c) Meyer, R.; Köhler, J.; Homburg, A. In *Explosives*, 5th ed.; John Wiley-VCH: Weinheim, 2002; p 346.
- (5) (a) Oxley, J. C.; Smith, J. L.; Chen, H. *Propellants, Explos., Pyrotech.* **2002**, *27*, 209–216. (b) Oxley, J. C.; Smith, J. L.; Shinde, K.; Moran, J. *Propellants, Explos., Pyrotech.* **2005**, *30*, 127–130. (c) Zitrin, S.; Kraus, S.; Glattstein, B. *Proc. Int. Symp. Anal. Detect. Explos., Quantico, VA, 1983*, Fed. Bur. Invest., Washington, DC, 1983, pp 137–141.
- (6) For a recent review on the detection of peroxide-based explosives see: Schulte-Ladbeck, R.; Vogel, M.; Karst, U. *Anal. Bioanal. Chem.* **2006**, *386*, 559–565.
- (7) (a) Hong, J. G.; Maguhn, J.; Freitag, D.; Kettrup, A. *Fresenius J. Anal. Chem.* **1998**, *361*, 124–128. (b) Schulte-Ladbeck, R.; Kolla, P.; Karst, U. *Analyst* **2002**, *127*, 1152–1154.
- (8) Itzhaky, H.; Keinan, E. (2004) United States Patent, US 6,767,717 B1.
- (9) (a) Schulte-Ladbeck, R.; Kolla, P.; Karst, U. *Anal. Chem.* **2003**, *75*, 731–735. (b) Schulte-Ladbeck, R.; Edelmann, A.; Quintas, G.; Lendl, B.; Karst, U. *Anal.*

- Chem.* **2006**, *78*, 8150–8155. (c) van Zoonen, P.; de Herder, I.; Gooijer, C.; Velthorst, N. H.; Frei, R. W.; Kuntzberg, E.; Gubitz, G. *Anal. Lett.* **1986**, *19*, 1949–1961. (d) Li, J.; Dasgupta, P. K. *Anal. Chim. Acta* **2001**, *442*, 63–70. (e) Schulte-Ladbeck, R.; Karst, U. *Anal. Chim. Acta* **2003**, *482*, 183–188. (f) Hong, J.; Maguhn, J.; Freitag, D.; Kettrup, A. *Fresenius J. Anal. Chem.* **1998**, *361*, 124–128. (g) Yamamoto, Y.; Ames, B. N. *Free Radical Biol. Med.* **1987**, *3*, 359–361. (h) Lu, D.; Cagan, A.; Munoz, R. A. A.; Tangkuaram, T.; Wang, J. *Analyst* **2006**, *131*, 1279–1281. (i) Csoregi, E.; Gorton, L.; Marko-Varga, G.; Tudos, A. J.; Kok, W. T. *Anal. Chem.* **1994**, *66*, 3604–3610. (j) Sljukic, B.; Banks, C. E.; Compton, R. G. *Nano Lett.* **2006**, *6*, 1556–1558. (k) Kumar, S. S.; Joseph, J.; Phani, K. L. *Chem. Mater.* **2007**, *19*, 4722–4730. (l) Laine, D. F.; Roske, C. W.; Cheng, I. F. *Anal. Chim. Acta* **2008**, *608*, 56–60.
- (10) Jacobs, P. T.; Lin, S. M. In *Irradiation of Polymers: Fundamentals and Technological Applications*; Clough, R. L., Shalaby, S. W., Eds.; ACS Symposium Series 620, American Chemical Society: Washington, DC, 1996; pp 216–239.
- (11) (a) Occupational Safety and Health Administration Website, Chemical Sampling Information: Hydrogen Peroxide. http://www.osha.gov/dts/chemicalsampling/data/CH_246600.html (accessed May 2007). (b) Dickson, K. F.; Caravati, E. M. *J. Toxicol. Clin. Toxicol.* **1994**, *32*, 705–714. (c) Proud, W. G.; Field, J. E. *AIP Conference Proceedings* **1999**, *505*, 937–940. (d) Maass, O.; Hatcher, W. H. *J. Am. Chem. Soc.* **1920**, *42*, 2548–2569.
- (12) (a) Bohrer, F. I.; Colesniuc, C. N.; Park, J.; Schuller, I. K.; Kummel, A. C.; Trogler, W. C. *J. Mater. Chem.* **2008**, in press. (b) Bohrer, F. I.; Colesniuc, C. N.; Park, J.; Schuller, I. K.; Kummel, A. C.; Trogler, W. C. *J. Am. Chem. Soc.* **2008**, *130*, 3712–3713.
- (13) Dräger Inc. Safety Website, DrägerSensor® H₂O₂ LC Chemical Sensor Data Sheet. http://www.draeger.com/ST/internet/pdf/Master/En/gt/9023492_h2o2lc_d_e.pdf (accessed July 2007).
- (14) (a) AFT International, Inc. Website, Dräger Safety Short Term Detector Tubes: Hydrogen Peroxide. <http://www.afcintl.com/pdf/draeger/8101041.pdf> (accessed July 2007). (b) Centanni, M. A. Visual detector for vaporized hydrogen peroxide. *US Pat.*, 7,186,373, 2003.
- (15) McVey, I. F. Non-dispersive mid-infrared sensor for vaporized hydrogen peroxide. *US Pat.*, 7,157,045, 2002.

- (16) (a) He, F.; Tang, Y.; Yu, M.; Wang, S.; Li, Y.; Zhu, D. *Adv. Funct. Mater.* **2006**, *16*, 91–94. (b) He, F.; Feng, F.; Wang, S.; Li, Y.; Zhu, D. *J. Mater. Chem.* **2007**, *17*, 3702–3707.
- (17) Maeda, H.; Fukuyasu, Y.; Yoshida, S.; Fukuda, M.; Saeki, K.; Matsuno, H.; Yamaguchi, Y.; Yoshida, K.; Hirata, K.; Miyamoto, K. *Angew. Chem. Int. Ed.* **2004**, *43*, 2389–2391.
- (18) (a) Onoda, M.; Uchiyama, T.; Mawatari, K.; Kaneko, K.; Nakagomi, K. *Anal. Sci.* **2006**, *22*, 815–817. (b) Onoda, M.; Tokuyama, H.; Uchiyama, S.; Mawatari, K.; Santa, T.; Kaneko, K.; Imai, K.; Nakagomi, K. *Chem. Commun.* **2005**, 1848–1850.
- (19) (a) Chang, M. C. Y.; Pralle, A.; Isacoff, E. Y.; Chang, C. J. *J. Am. Chem. Soc.* **2004**, *126*, 15392–15393. (b) Miller, E. W.; Albers, A. E.; Pralle, A.; Isacoff, E. Y.; Chang, C. J. *J. Am. Chem. Soc.* **2005**, *127*, 16652–16659.
- (20) (a) Li, Y.; Ding, J.; Day, M.; Tao, Y.; Lu, J.; D'iorio, M. *Chem. Mater.* **2003**, *15*, 4936–4943. (b) Maruyama, S.; Kawanishi, Y. *J. Mater. Chem.* **2002**, *12*, 2245–2249. (c) Chujo, Y.; Tomita, I.; Saegusa, T. *Polym. J.* **1991**, *23*, 743–746.
- (21) (a) Niu, W.; O'Sullivan, C.; Rambo, B. M.; Smith, M. D.; Lavigne, J. J. *Chem. Commun.* **2005**, *34*, 4342–4344. (b) Koumoto, K.; Yamashita, T.; Kimura, T.; Luboradzki, R.; Shinkai, S. *Nanotechnology* **2001**, *12*, 25–31. (c) Nakazawa, I.; Suda, S.; Masuda, M.; Asai, M.; Shimizu, T. *Chem. Commun.* **2000**, 881–882. (d) Musina, E. I.; Litvinov, I. A.; Balueva, A. S.; Nikonov, G. N. *Russ. J. Gen. Chem.* **1999**, *69*, 413–420.
- (22) (a) Barnea, E.; Andrea, T.; Kapon, M.; Eisen, M. S. *J. Am. Chem. Soc.* **2004**, *126*, 5066–5067. (b) Barba, V.; Hoepfl, H.; Farfan, N.; Santillan, R.; Beltran, H. I.; Zamudio Rivera, L. S. *Chem. Commun.* **2004**, 2834–2835. (c) Christinat, N.; Scopelliti, R.; Severin, K. *Chem. Commun.* **2004**, 1158–1159.
- (23) Roy, C. D.; Brown, H. C. *J. Organomet. Chem.* **2007**, *692*, 784–790.
- (24) (a) Scatchard, G.; Kavanagh, G. M.; Ticknor, L. B. *J. Am. Chem. Soc.* **1952**, *74*, 3715–3720. (b) Manatt, S. L.; Manatt, M. R. R. *Chem. Eur. J.* **2004**, *10*, 6540–6557.
- (25) Ishiyama, T.; Ishida, K.; Miyaura, N. *Tetrahedron* **2001**, *57*, 9813–9816.

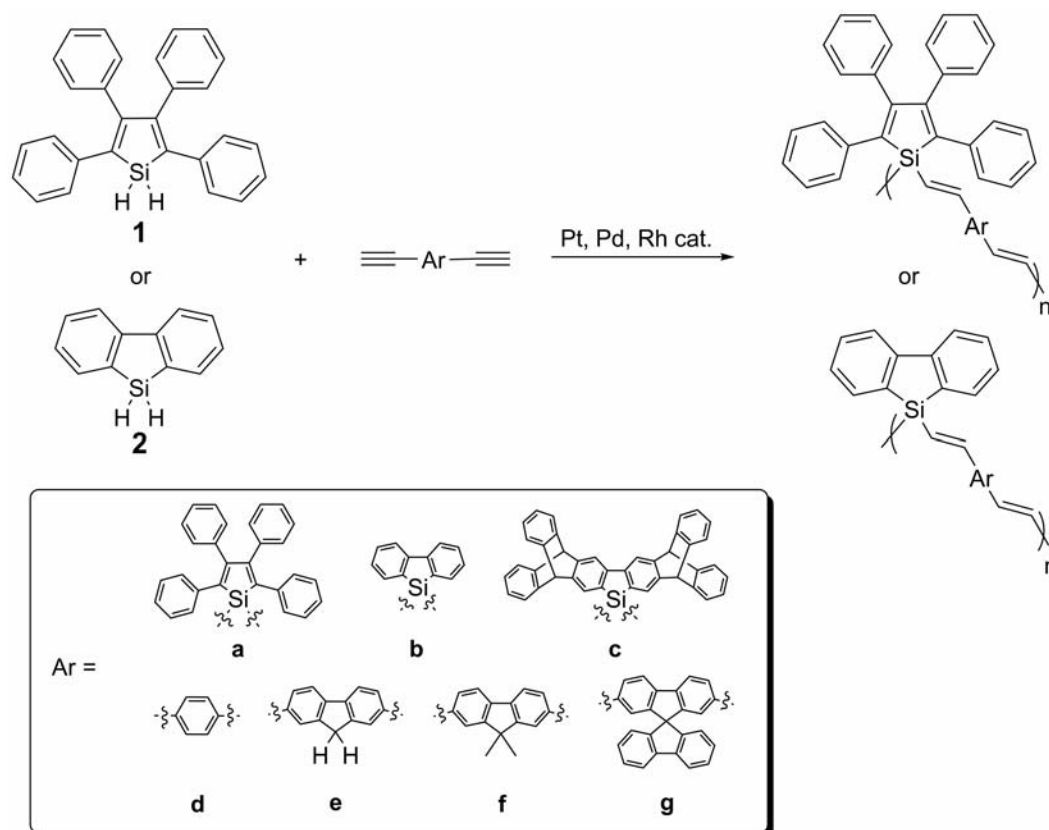
CHAPTER VII

Dissertation Summary, Conclusions and Proposed Future Work

7.1 Summary of Hydrosilylation Polymerization

The polymers synthesized in this dissertation are summarized in Scheme 7-1. Molecular weights and regio-chemistry were seemingly independent of the catalyst used. The more sterically available silafluorene required careful thermal control to achieve the kinetically favored *trans*-product, with α -addition competing at higher reaction temperatures. By placing bulky substituents onto the silafluorene framework, hydrosilylation can be controlled or eliminated completely, as was witnessed using a silyptycene comonomer. Molecular weights increased with the spacing between silole, increasing along the series vinylene < phenylenevinylene < fluorenylenevinylene (Table 7-1). This was expected due to the steric availability to the ethynyl groups offered by the phenylene and fluorenylene comonomers. Similarly, it was also observed that molecular weight and polydispersity can be controlled by placing bulky substitutions on the diethynyl comonomers, such as with the spirofluorene spacer. Stereochemistry and molecular weight can also be monitored by ^1H NMR, making this method of polymerization ideal for reaction optimization.

Silole and silafluorene fluorophores have become an important class of functional materials due to their unique luminescent properties. One key feature in photoluminescent materials is the extent of electronic delocalization. By alternating π -systems and silyl groups in silane chemistry, a unique σ^* - π conjugation is observed by which the σ^* orbital of the silyl group is of sufficient energy and phase to facilitate electron delocalization between vinylene π -systems. This remains valid for 2,3,4,5-



Scheme 7-1. A summary of the catalytic hydrosilylation of 1,1-dihydridometalloles with various diethynylaryl comonomers.

tetraphenylsilole and silafluorene polymers synthesized by catalytic hydrosilylation. Crystal structure analysis as well as DFT calculations on silole- and silafluorene-vinylene based model compounds reveal an overlap in molecular orbitals between the π orbitals of the organic bridge and the Si-C σ^* orbitals involved in forming the metallole π system, silicon centers through the vinylene bridge. This results in delocalization through the metallacyclopentadiene core unit while maintaining conjugating between vinylene and aryl-vinylene comonomers (Figure 7-1). Delocalization is also evidenced by the observed red-shifts in the UV-vis and

Table 7-1. Photoluminescence and molecular weight results from the hydrosilylation polymerization of various 2,3,4,5-tetraphenylsilole and silafluorene copolymers.

Polymer	λ_{abs} (nm)	ϵ_{max} (L mol ⁻¹ cm ⁻¹)	Solution λ_{flu} (nm)	Thin-film: TLC λ_{flu} (nm)	Φ_{flu}	M_w (GPC)	M_w/M_n
1a	304, 389	2900	493	490	0.01	4000	1.15
1b/2a	297, 390	1800	492	486	0.02	4500	1.24
1c	—	—	—	—	—	—	—
1d	322	7600	487	478	0.006	8400	1.8
2b	294	6300	362	376	0.04	4300	1.37
2c	—	—	—	—	—	—	—
2d	294	14 000	359	447	0.04	9600	2.0
2e	346	13 700	376	446	0.52	16 000	2.6
2f	344	26 300	377	446	0.22	20 000	2.3
2g	346	24 800	392	470	1.0	13 200	1.7

fluorescence spectra (Table 7-1). These delocalized structures shift the band-gap 20-70 nm, depending on molecular weight and polydispersity, allowing for fine-tuning of the photoluminescence. The flexible nature of the vinylene backbone also inhibits π - π stacking interactions in thin polymer films. This feature allows for good solid-state quantum emission efficiencies for the silafluorene based polymers. Silole based

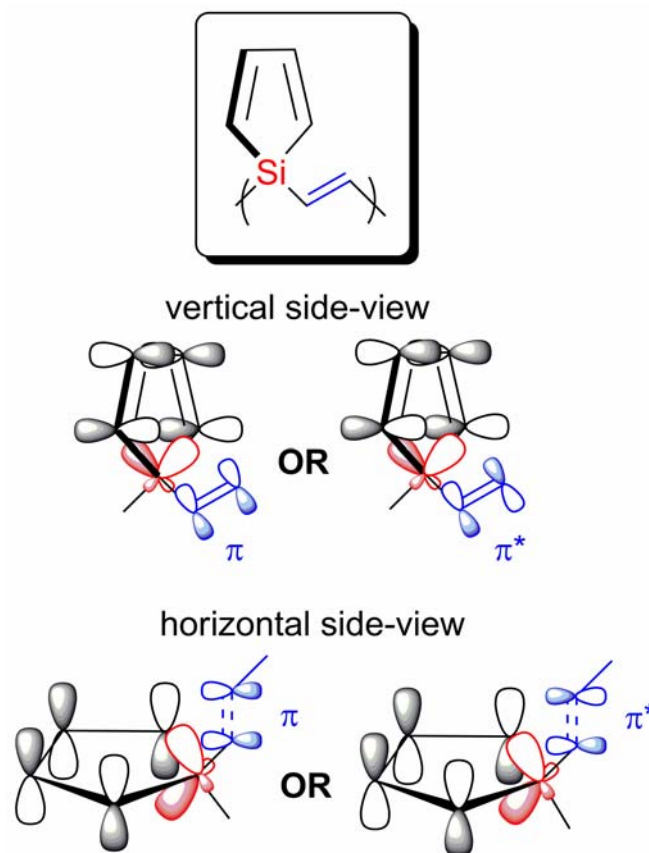


Figure 7-1. Depiction of the orbital overlap between the vinylene spacer and the silicon center along the backbone of polymetallacyclopentadiene-vinylene.

materials containing phenyl substituents on the metallole ring typically show an increase in fluorescence efficiency in their aggregated states based on the restriction of non-radiative decay pathways as phenyl rotation is restricted.^[66] The electronic properties found in polymers synthesized by catalytic hydrosilylation of silacyclopentadiene moieties has led to a series of highly functional photo- and electro-active polymeric materials.

7.2 Summary of Explosives Detection

These new luminescent silole- and silafluorene-based materials were utilized as chemosensors for explosives. There has been substantial progress made in the area of explosives detection over the past decade. Fluorescence based organic polymeric sensors have been introduced as low cost, robust materials for the detection of explosives vapors and particulates. The use of silole and silafluorene fluorophores has allowed for the sensitive detection of a wide range of explosive particulates. The synthetic ease of producing these materials as well as the high solubility and processability created by the silicon-carbon framework enables these polymers to operate with detection limits on the order of 1 pg cm^{-2} (Table 7-2). Inclusion of the ring-strained silacyclopentadiene allows for a new method of analyte binding while maintaining delocalization for an amplified sensor response. This Lewis acid-base binding mechanism can be monitored by spin-lattice relaxation times (T_1) and chemical shift changes ($\sim 0.1 \text{ ppm}$) in the ^{29}Si NMR, showing association constants (K_a) of $\sim 0.12 \text{ M}^{-1}$. In addition, the ability to fine-tune the frontier molecular orbital energies of these materials has allowed for the detection of many different classes of explosives, including those with low vapor pressures (cyclotetramethylene-tetranitramine (HMX) and pentaerythritol tetranitrate (PETN)) and those with low reduction potentials (cyclotrimethylenetrinitramine (RDX) and trinitroglycerin (TNG)).

Selectivity for the detection of explosives was achieved through the design of chemospecific fluorescence turn-on sensors. Nitramine and nitrate ester based

Table 7-2. Summary of explosives detection by fluorescence quenching of silole and silafluorene based polymers. Detection limits reported in ng cm^{-2} .

Explosive	1a	1b/2a	1d	2b	2d	2e	2f	2g
Tetryl	1	1	1	0.2	0.2	0.001	0.002	0.002
TNT	2	0.6	6	0.3	0.1	0.03	0.06	0.03
PA	2	2	1	3	0.3	0.6	0.3	0.1
DNT	3	3	13	2	0.3	0.2	0.2	0.2
PETN	–	–	–	2	1	0.3	0.6	0.3
RDX	–	32	–	2	2	2	2	2
HMX	–	–	–	3	3	2	2	2
TNG	–	–	–	3	2	1	2	2

explosives were selectively targeted through an acid catalyze triazotization reaction, producing a blue luminescent naphthotriazole material. This technology was combined with silole-vinylene polymer sensors to provide a tandem turn-off/turn-on selective fluorescence sensor. This approach was further improved through the use of fluorene as a comonomer to incorporate the turn-off/turn-on mechanism into a single sensory material that detects a range of explosive classes and is selective for nitrate ester based explosives.

Organic peroxide based explosives were targeted by the selective detection of hydrogen peroxide. Hydrogen peroxide is a major component in the production of these explosives as well as being a major byproduct in their decomposition. By using double transesterification polymerization, a stable non-luminescent polymer using fluoran as the pre-fluorophore component was synthesized. Upon selective oxidative deprotection of the boronate functionalities by hydrogen peroxide, a fluorescence response is observed on formation of fluorescein at limits as low as 3 ppb over an 8 h period.

7.3 Conclusions

Hydrosilylation offers a facile synthetic route to 1,1-silole polymerization. The physical and electronic properties are easily manipulated by kinetic and catalytic control. The use of fluorescence quenching as the primary method for the detection of explosive analytes improves the cost efficiency, sensitivity, selectivity, portability, and speed of the signal analysis for the sensory device. Further sensor optimization is accomplished by first tuning the electronic structure of fluorescing silole- and silafluorene-based polymers to better match the energy of the targeted analytes. Detection limits as low as 1 ng cm^{-2} are observed. Improved fluorescence quantum efficiencies provide better signal-to-noise and minimize the material used during detection. Through fine tuning of the polymer's electronic properties, detection limits are improved by 100x, reaching 1 pg ng^{-2} . Sampling of explosive particulates, rather than vapor, reaches a wider range of the low volatility explosives targeted. The use of

silacycles as part of the polymer backbone structure promotes analyte binding through Lewis acid/base interactions. Detection selectivity is advanced through the use of chemo-selective turn-on fluorescence probes in combination with the fluorescence quenching sensors. This tandem sensor approach is implemented into a single sensory material to provide the first example of a selective fluorescent polymer sensor with detection limits as low as 300 pg cm^{-2} . Organic peroxide based explosives are targeted through the direct detection of hydrogen peroxide vapors by an oxidative deprotection of a boronate based polymer. A turn-on fluorescence signal stemming from the formation of fluorescein gives limits as low as 3 ppb over an 8 h period. This offers an integrating sensor with a sensitive and selective turn-on fluorescence response for hydrogen peroxide.

7.4 Future Work

Future work in the area of functionalized silole and silafluorene luminescent polymers may include investigation into applications such as stable blue-emitting polymers for PLED devices, white light applications, and UV emitting materials. Catalyst development for hydrosilylation may provide higher molecular weight polymers with easier control over the regio-chemistry. Further improvements in explosives detection may include the design and synthesis of fluorescent sensors that are selective for the organic peroxides TATP and HMTD. Functionalization of the blue-emitting silafluorene polymers for the selective binding of explosives may also improve their detection capabilities. Improving the luminescence stability of these

materials in the presence of oxygen may also increase their practical application use. An as yet unsolved goal is to target inorganic based explosives using fluorescence detection techniques. This will require selectively detecting nitrate and perchlorate salts, which creates an entirely new set of obstacles to overcome.